A study of the molecular basis of the interaction between AMPARs and their auxiliary subunits

Karolina Anna Krol

Laboratory for Molecular Cell Biology
University College London
2015

Thesis is submitted for the degree of Doctor of Philosophy

Abstract

AMPA receptors (AMPARs) are crucial for fast excitatory synaptic transmission throughout the mammalian central nervous system (CNS). At the molecular level, these receptors are tetramers of GluA1-4 subunits, which can be homomeric or heteromeric, incorporating the Ca^{2+}-impermeable GluA2 subunit. Although the basic tetrameric AMPAR is sufficient for expression of functional channels in a recombinant system, native AMPARs are associated with a number of auxiliary proteins, which modify their trafficking as well as their biophysical and pharmacological properties.

The first AMPAR auxiliary protein discovered was stargazin (γ-2), a transmembrane protein related to the γ-1 subunit of voltage gated Ca^{2+}- channels. The lack of γ-2 in the naturally occurring mouse mutant *stargazer* was found to produce a loss of AMPAR-mediated transmission at the cerebellar mossy fibre to granule cell synapse. This led to the discovery, that γ-2 is crucial for AMPAR trafficking. Subsequent studies focusing on this protein showed that it is also able to modify the functional properties of AMPARs, such as deactivation and desensitization kinetics, single-channel conductance and susceptibility of Ca^{2+}-permeable AMPARs to block by intracellular and extracellular polyamines. In addition, a family of related proteins, known as Transmembrane AMPA Receptor Regulatory Proteins (TARPs) has been identified. As well as γ-2, this includes the subunits γ-3,-4,-5,-7 and -8. All TARPs are related to γ-2 in structure and function, although certain properties vary between the family members.

Since the discovery of TARPs, more proteins modulating AMPAR function have been identified, so that a complex network of AMPAR interacting partners is apparent from the literature in the field. Surprisingly, little focus had been put on how AMPARs interact with auxiliary proteins at the molecular level. Enhancing our knowledge about these interactions could provide insights into the role of AMPARs in synaptic transmission, plasticity and neurological diseases. The aim of my thesis was thus to provide insight into the role of TARPs in modulation of AMPAR complexes and the molecular mechanisms that underlie this modulation. I used a recombinant expression system to identify the physiological relevance of different AMPAR/TARP interaction regions, as well as to investigate the role of TARP stoichiometry on AMPAR/TARP function.

The initial part of my thesis focused on the molecular interactions of AMPARs with their TARP auxiliary subunits. Our experiments showed that various regions of the first extracellular loop (Ex1) of γ-2 play a role in modulation of a number of functional properties of both GluA1 and GluA2(Q) subunits. We also aimed to obtain insight into the corresponding AMPAR regions important for interaction with the TARP. We there-

fore focused on the possible novel role of the AMPAR N-terminal domain (NTD) in TARP-AMPAR interaction and found that, although this domain plays a role in AMPAR function, it has little effect on the modulation of AMPARs by TARPs.

The first two Chapters of my thesis were aimed at answering the question - how do TARPs and AMPARs interact at the molecular level? The work presented in the final Chapter attempted to expand on this question and focused on the role of TARP stoichiometry in AMPAR function. Using tandem TARP-AMPAR constructs expressed in a recombinant system, we have studied the properties of TARP/AMPAR assemblies that contain a known number of γ-2 molecules. This allowed us to identify some of the AMPAR properties that are sensitive to TARP stoichiometry.

As most neurons in the brain express more than one TARP, we also investigated the pharmacological consequences of the simultaneous presence of two TARPs (γ-2 and γ-7) within a single TARP/AMPAR assembly, a possibility that has previously received little attention.

Declaration

I, Karolina Krol confirm that the work presented in this thesis is my own. Where information has been derived from other sources, I confirm that this has been indicated in the thesis.

Signed: _____

Acknowledgements

I would like to thank my supervisor, Professor Stuart Cull-Candy for his kindness, insight and continuous support. I am very grateful for the opportunity to work in his lab.

My thanks to Professor Mark Farrant for his endless patience and for help with all things technical, from the electrophysiological recordings to statistics. His support was most significant.

I have greatly enjoyed my time in the Cull-Candy and Farrant laboratory and could not ask for kinder and more supportive colleagues. I would like to thank Dr Cécile Bats, Dr Jolenta Cheung, Dr Rebecca Jones, Dr Tommy McGee, Dr Elizabeth Needham, Julia Oyrer, Sarah Pearce, Dr Massimiliano Renzi, Dr Mark Rigby, Dr Chris Shelley, Dr David Soto, Dorota Studniarczyk, Dr Steve Sullivan and Dr Marzieh Zonouzi, who have all contributed to my PhD training.

Special thanks go to Dr Ian Coombs for seeing a silver lining in every failed PCR. Thanks to him, the trial and error of molecular biology became less of an error.

Beyond the lab, I would like to thank Dr Ingo Greger, Dr Ondrej Cais and Dr Beatriz Herguedas for their work on collaborative experiments and for helpful discussion on the data.

I would like to thank my family and friends, whose support has been most valuable. Finally, thanks to Piotr, who has been there for me at times good and bad.

My PhD was funded by a 4-year MRC studentship.

Contents

Figures

Tables

Abbreviations

AMPAR α-amino-3-hydroxy-5-methyl-4-isoxazole propionic acid receptor
ADAR2 Adenosine deaminase acting on RNA 2
CaMKII Ca^{2+}/calmodulin-dependent protein kinase II
CKAMP44 Cystine-knot AMPAR modulating protein 44
CMV Cytomegalovirus
CNIH Cornichon homolog
CP-AMPARs Calcium-permeable α-amino-3-hydroxy-5-methyl-4-isoxazole propionic acid receptor
CTD C-terminal domain
EPSC Excitatory postsynaptic current
GFP Green Fluorescent Protein
GRIP Glutamate receptor-interacting protein
GSG1L Germ-cell-specific gene 1-like
IRES Internal ribosome entry site
LBD Ligand binding domain
LTD Long-term depression
LTP Long-term potentiation
Narp Neuronal activity-regulated pentraxin
NP1 Neuronal pentraxin 1
Neto Neuropilin tolloid-like
NMDAR N-methyl-D-aspartate receptor
NSF N-ethylmaleimide-sensitive factor
NSFA Non-stationary fluctuation analysis
NTD N-terminal domain
PDZ Post synaptic density protein, Drosophila disc large tumor suppressor, Zonula occludens-1 protein
PICK1 Protein interacting with PRKCA 1
PKA Protein kinase A
PKC Protein kinase C
PSD-95 Postsynaptic density protein 95
SAP97 Synapse-associated protein 97
SEM Standard error of the mean
stg *stargazer*
TARP Transmembrane amino-3-hydroxy-5-methyl-4-isoxazole propionic acid receptor regulatory protein
TMD Transmembrane domain
wt Wild-type

1

Introduction

Glutamate is the predominant neurotransmitter at the majority of excitatory synapses in the mammalian central nervous system (CNS). Glutamate signalling is mediated by two broad classes of receptors: ionotropic glutamate receptors and metabotropic (G protein-coupled, mGluR) receptors. The latter will not be discussed further in this thesis. Ionotropic glutamate receptors can be divided into three major types, named after their selective synthetic agonists: N-methyl-D-aspartate (NMDA), α-Amino-3-hydroxy-5-methyl-4-isoxazolepropionic acid (AMPA) and kainate receptors. Kainate receptors are often located presynaptically and have been reported to modulate neurotransmitter release (Lerma, 2006). NMDA receptors (NMDARs) are located at both presynaptic (Glitsch and Marty, 1999) and postsynaptic sites. Post-synaptically, they mediate long-lasting excitatory post-synaptic potentials (EPSPs) (Cull-Candy and Leszkiewicz, 2004). However, due to their block by extracellular Mg^{2+}, NMDARs require membrane depolarization to allow ion flow (Nowak et al., 1984; Mayer and Westbrook, 1987; Ascher and Nowak, 1988; Burnashev et al., 1992b). This depolarisation is generally provided by the activation of AMPARs (Collingridge et al., 1988), which mediate the majority of fast glutamatergic transmission in the mammalian brain.

AMPARs across the CNS are thought to associate with auxiliary subunits (Hashimoto et al., 1999; Schwenk et al., 2009; von Engelhardt et al., 2010; Tomita, 2010; Schwenk et al., 2012). Transmembrane AMPA Receptor Regulatory Proteins (TARPs) were the first auxiliary subunits of AMPARs discovered (reviewed in Tomita 2010 and Jackson and Nicoll 2011). TARPs are though to modulate the majority of central AMPARs. Thus, studying AMPAR/TARP interactions at the molecular level could provide insights into AMPAR involvement in excitatory synaptic transmission and related processes, such as synaptic plasticity, neural development and pain perception. This Thesis describes several molecular features of AMPAR/TARP complexes, including the role of interaction regions on both the TARP and on the AMPAR, as well as the effect of TARP

stoichiometry on AMPAR properties. The Introduction aims to provide background information on the relevant molecular biology of AMPARs and TARPs and outline our current understanding of AMPAR/TARP interaction.

1.1 Ionotropic glutamate receptors

Protein subunits of the ionotropic glutamate receptors were identified in the late 1980s and early 1990s by molecular cloning and functional expression techniques (reviewed in Hollmann and Heinemann 1994). All ionotropic glutamate receptors appear to assemble as tetramers of pore-forming subunits. Three NMDAR subunit types have been identified to date (Moriyoshi et al., 1991; Monyer et al., 1992; Kutsuwada et al., 1992), GluN1, GluN2 and GluN3 (Das et al., 1998; Perez-Otano et al., 2001). There are 8 known subtypes of GluN1 (all arising from a single gene), 4 of GluN2 and 2 of GluN3. Most NMDARs appear to be heteromers composed of two GluN1 and two GluN2 subunits (Cull-Candy and Leszkiewicz, 2004). However, Tovar and Westbrook (1999) suggested that in cultured rat hipocampal neurons, two GluN1 and two GluN2B subunits are incorporated at immature synapses, forming diheteromeric receptors; while mature synapses express triheteromeric NMDARs (GluN1/GluN2A/GluN2B). In contrast to GluN1 and GluN2 subiunits, the role of the GluN3 subunits remains unclear (Pachernegg et al., 2012). To date, 5 kainate receptor subunits have been cloned: GluK1-5 (Bettler et al., 1990, 1992; Egebjerg et al., 1991; Herb et al., 1992). However, GluK5 and GluK6 do not form homomeric channels (Herb et al., 1992). NETO (neuropilin (NRP) and tolloid (TLL)-like) proteins have been identified as auxiliary subunits of kainate receptors (Straub et al., 2011; Tang et al., 2011). However, these proteins have also been reported to affect NMDARs (Ng et al., 2009; Tang et al., 2011; Wyeth et al., 2014).

AMPARs are composed of four pore-forming subunits: GluA1-4, each subunit arising from its corresponding gene (GRIA1-4). AMPAR subunits were cloned using the same methods that were later applied to identify NMDAR and kainate receptor subunits (Hollmann et al., 1989; Keinänen et al., 1990; Nakanishi et al., 1990; Boulter et al., 1990) and are described in more detail below. Table 1.1 lists the subunits of ionotropic glutamate receptors and their corresponding genes.

Not included in this Table are the GluD receptors. GluD1-2 are distantly related to both AMPARs and NMDARs (< 25 % sequence similarity with other ionotropic glutamate receptor subunits). However, they do not respond to glutamate (or any other

Receptor	Subunits	Subunit genes
AMPARs	GluA1-4	GRIA1-4
NMDARs	GluN1, GluN2A-D, GluAN3A-B	GRIN1, GRIN2A-D, GRIN3A-B
kainate receptors	GluK1-5	GRIK1-5

Table 1.1: Ionotropic glutamate receptors. Summary of protein subunits of ionotropic glutamate receptors and their corresponding genes (Collingridge et al., 2009).

known ligands) and do not form functional channels when expressed in a recombinant system alone or with other ionotropic glutamate receptor subunits (Lomeli et al., 1993).

1.2 AMPAR pore-forming subunits

Pore-forming subunits of AMPARs (GluA1-4) share about 70 % sequence homology (Keinänen et al., 1990) and are each $\sim$100 kDa in molecular weight (Rogers et al., 1991). The structure of all four pore-forming subunits is broadly similar, with an extracellular N-terminus and intracellular C-terminus. AMPARs have four membrane regions (M1-4), of which M1, M3 and M4 are membrane-spanning helices, while the M2 region is a re-entrant loop, which lines the channel pore (Sobolevsky et al., 2009). An outline of the tertiary structure of an AMPAR subunit is shown in Fig. 1.1 below.

1.3 Domain organisation of AMPARs

As shown in Fig. 1.1, AMPARs are organised into distinct domains. This domain organisation is prevalent both at the level of a single subunit and at the level of the complete tetramer. Each of these domains appears to play a defined role in determining receptor properties. In addition, it is worth noting that despite their tetrameric structure, AMPARs are not simply symmetrical. In comparison to the N-terminal domain (NTD) layer, the ligand-binding domain (LBD) layer is rotated relative to the two-fold symmetry axis of the receptor, so that the two layers are not aligned vertically. The transmembrane domains, on the other hand, show a four-fold rotational symmetry. Thus, the overall tetrameric AMPAR structure is relatively complex (Sobolevsky et al., 2009).

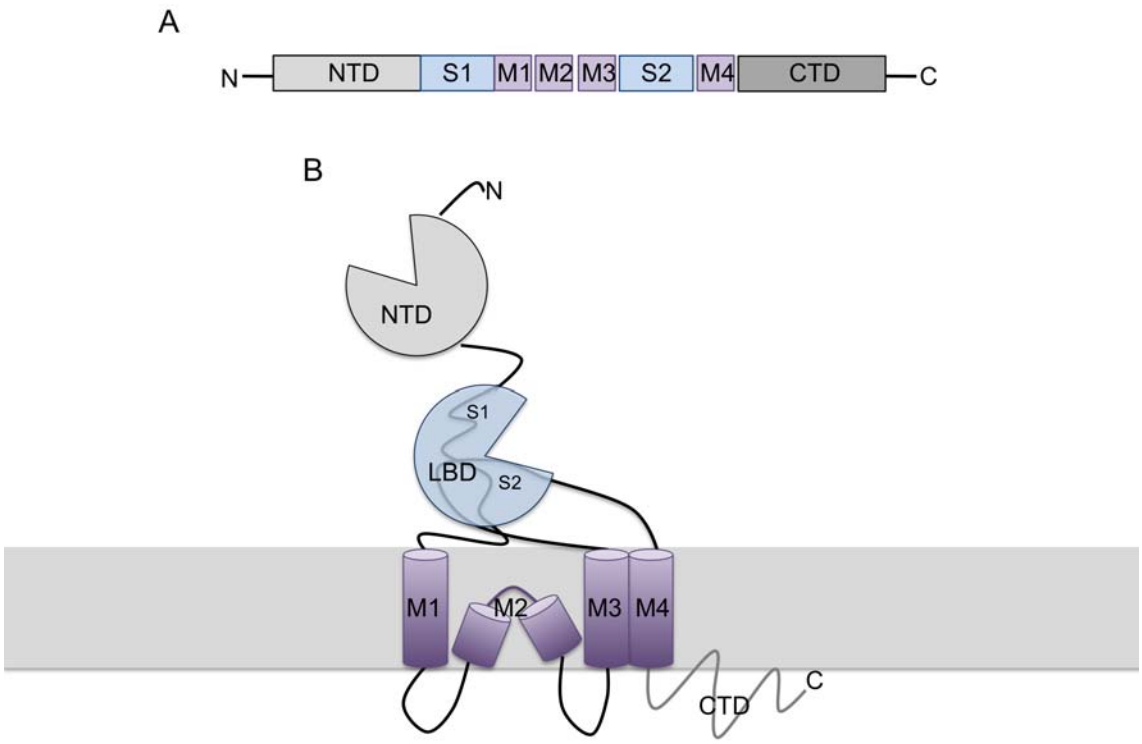

Figure 1.1: Tertiary structure of an AMPAR pore-forming subunit (Traynelis et al., 2010). (**A**) Schematic representation of the primary (polypeptide) structure of an AMPAR subunit showing the different domains. (**B**) Tertiary structure of an AMPAR subunit. Note that two of the domains: NTD and LBD are located extracellularly, while the CTD is intracellular. The two segments: S1 and S2 form the two lobes of the LBD, despite being separated by M1-M3 in the polypeptide chain. NTD (light grey): N-terminal domain, LBD (blue): ligand-binding domain, M1-M4 (purple): membrane domains 1-4, CTD (dark grey): C-terminal domain.

1.3.1 N-terminal domain

The NTD of AMPARs, much like the LBD described below, forms a clamshell-like structure, composed of two distinct lobes (L1 and L2) (Clayton et al., 2009; Jin et al., 2009). GluA4 lacking this domain forms functional channels, albeit with altered properties: prolonged τ desensitization and slightly reduced surface expression. However, binding of both glutamate and the allosteric modulator cyclothiazide (CTZ) remain unchanged in the absence of the NTD (Pasternack et al., 2002). The NTD contains a conserved IQI motif, a trafficking signal important for anterograde trafficking and surface expression in neurons (Xia et al., 2002). This motif is, however, not required for GluA1/2 heteromerization, despite the major role of the AMPAR NTD in AMPAR assembly. Briefly, AMPARs assemble as dimers of dimers and the initial dimerisation process is mediated by tight association of the NTDs (Jin et al., 2009; Rossmann et al., 2011).

In a native environment, the NTD protrudes significantly into the synaptic cleft, which measures approximately only 0.024 μm (Zuber et al., 2005). Thus, the NTD is well-located to bind proteins located within the synapse. GluA2 NTD interaction with N-cadherin promotes formation of dendritic spines and synapses (Saglietti et al., 2007), while the interaction between GluA4 NTD and the neuronal protein pentraxin NP1 is necessary for synaptic clustering of GluA4 (Sia et al., 2007). Another neuronal pentraxin, Narp, interacts with the AMPAR extracellular domain and clusters GluA1-3 (but, interestingly, not GluA4) at the synapse (O'Brien et al., 1999). In addition to these well-defined binding partners, the AMPAR NTD may also bind other synaptic proteins. Nonetheless, the role of the AMPAR NTD is still poorly understood. Our studies designed to further investigate the role of this domain in AMPAR function and TARP interaction are outlined in Experimental Chapter 2 (Chapter 4).

1.3.2 Ligand-binding domain

As outlined in Fig. 1.1, the LBD of AMPARs is composed of two distinct segments, S1 and S2 (Stern-Bach et al., 1994), similar in structure to the bacterial periplasmic amino acid binding proteins and the bacterial glutamate receptor ion channel (GluR0, Chen et al. 1999; Mayer et al. 2001). The two segments form a clamshell-like structure, with two lobes, D1 and D2. Most of the D1 lobe is formed by the S1 segment, immediately proximal to M1, while most of the D2 lobe is formed by the S2 segment, located on the extracellular loop between M3 and M4. The agonist-binding pocket is located between the two lobes (Armstrong et al., 1998). Thus, each of the four AMPAR subunits in the complete receptor forms one glutamate binding site. The number of bound glutamate molecules directly correlates with single-channel conductance levels in both recombinant (Rosenmund et al., 1998) and native (Smith and Howe, 2000; Gebhardt and Cull-Candy, 2006) AMPARs.

Artificial peptide linkers have been used to connect the discontinuous S1 and S2 segments in order to crystallize the LBD. The LBD of AMPARs has been crystallised in complex with both agonists and antagonists (Armstrong et al., 1998; Armstrong and Gouaux, 2000; Hogner et al., 2003; Lunn et al., 2003). Several regions and residues have been reported as important for agonist binding (Jin et al., 2002; Kasper et al., 2002; Hogner et al., 2002; Armstrong et al., 2003), with the specific residues differing slightly, depending on the agonist. The LBD of AMPARs is highly dynamic (Lau and Roux, 2007, 2012), surprisingly, also in the absence of the agonist (Plested and Mayer, 2009). Agonist binding produces closure of the LBD cleft, with the degree of cleft closure being larger for full than for partial agonists (Armstrong and Gouaux, 2000; Jin and Gouaux, 2003; Jin et al., 2003). In other words, full agonists bring the

two lobes of the LBD closer together than do partial agonists. The movement of the LBDs upon agonist binding is translated to the channel pore via linkers (Sobolevsky et al., 2009; Dong and Zhou, 2011). Their corkscrew-like motion produces conformational changes leading to channel opening. These conformational changes seem to be elicited by the M3-S2 linker movement, which repositions the M3 helix, allowing the channel to open (Meyerson et al., 2014).

At the level of the AMPAR tetramer, LBDs form a dimer of dimers structure. LBD dimerisation is thought to follow NTD dimerisation and occur upon transition into the tetrameric state (Shanks et al., 2010). Destabilization of the intradimer interface leads to receptor desensitization: closure of the channel in the presence of glutamate (Sun et al., 2002; Meyerson et al., 2014). Modifications which reduce AMPAR desensitization, such as the L483Y (GluA2) mutation, (Stern-Bach et al., 1998) or the use of CTZ (Yamada and Tang, 1993) stabilise the intradimer interface. The non-desensitising (L483Y) GluA2 mutant shows impaired tetramerization, suggesting that the delayed dimerisation of the LBDs is important for efficient AMPAR expression (Shanks et al., 2010).

By contrast, mutations which promote desensitization, such as S754D (GluA2), destabilise the intradimer interface (Sun et al., 2002). Several detailed desensitization mechanisms have been proposed (see for instance Sun et al. 2002; Sobolevsky et al. 2009). However, it is still unclear how LBD separation is translated into channel closure upon desensitization. Such analysis has proven difficult, as several desensitized AMPAR states appear to exist, differing in the degree of subunit separation, mostly at the NTD level (Meyerson et al., 2014). Previous studies suggest, however, that AMPAR desensitization most likely involves the linkers between the LBD and the transmembrane domains, as mutations in the M3-S2 linker disrupt desensitization (Yelshansky et al., 2004).

1.3.3 Transmembrane domains

Early topology studies (Hollmann et al., 1994) used N-glycosylation sites as a reporters for extracellular localisation. The model for AMPAR structure proposed from these studies was related to the structure of the potassium channel (Doyle et al., 1998; Long et al., 2005) and was later confirmed when the GluA2 cystal structure was obtained (Sobolevsky et al., 2009). The membrane topology of AMPARs is outlined in Fig. 1.1.

Transmembrane domains of the AMPAR show a four-fold rotational symmetry (Sobolevsky

et al., 2009). On the outer face of the plasma membrane, a short helix region preceding M1 (pre-M1) is almost perpendicular to the membrane plane and forms contacts with the extracellular ends of helices M3 and M4. Pre-M1 forms a 'collar' around the transmembrane domain bundle and may contribute to receptor gating. M3 helices are positioned on the inside of the channel domain, while the M2 loop regions line the channel pore, with the central cavity positioned immediately above the Q/R editing site. The M3 helices cross near the extracellular side of the membrane (at the level of pre-M1), forming a gate in the proposed path for ion permeation (Sobolevsky et al., 2009). Disruption of that gate in GluD2 by introducing the A636T mutation produces channels with spontaneous activity, resulting in the neurodegeneration phenotype seen in *Lurcher* mice (Zuo et al., 1997). M1 and M4 helices are positioned on the outside of the channel domain, with the M4 helix forming extensive subunit-subunit contacts (Sobolevsky et al., 2009).

The M4 helix is necessary for AMPAR function (Wollmuth and Sobolevsky, 2004), despite its location on the outside of the channel pore (Sobolevsky et al., 2009). The requirement for the M4 domain is also common to the NMDARs, as these receptors lacking the M4 region and the C terminus are not functional, but some channel activity can be rescued by co-expressing M4 as a separate protein (Schorge and Colquhoun, 2003). The presence of the M4 domain is one of the features distinguishing ionotropic glutamate receptors from the structurally similar K^+ channels (Wollmuth and Sobolevsky, 2004; Sobolevsky et al., 2009).

1.3.4 C-terminal domain

The intracellularly located C-terminus of AMPARs (see Fig. 1.1) contains a PDZ domain, which is responsible for binding to a number of trafficking and synaptic anchorage proteins (reviewed in Malinow and Malenka 2002). The length of the C-tail varies between subunits. The C-terminal domains of GluA3 and the most abundant (short) form of GluA2 are 50 amino acids in length. By contrast, the C-terminal domains of GluA1 and GluA4 are respectively 81 and 68 residues long (Kolleker et al., 2003). Additionally, in certain brain regions alternative splicing generates C-terminal variants of GluA2 and GluA4. The short C-tail of GluA4 (GluA4c) is similar in sequence to that seen in GluA2 and GluA3. This form of the GluA4 subunit is expressed predominantly in cerebellar granule cells (Gallo et al., 1992). In the hippocampus, an alternatively spliced form of GluA2 (GluA2L) possessing a long C tail (Köhler et al., 1994) is thought to contribute to GluA1-independent plasticity mechanisms (Kolleker et al., 2003).

The C-terminal domain of AMPARs is thought to play a key role in receptor trafficking and AMPAR-mediated synaptic plasticity. The role of the C-terminal AMPAR domain is discussed briefly below.

Long-term synaptic plasticity

Changes in synaptic transmission have long been believed to form the molecular basis of learning and memory (see Kandel 1997 for discussion). Long-term potentiation (LTP) describes a prolonged strengthening of synaptic efficacy (Bliss and Collingridge, 1993). Initial studies on the molecular basis of learning and memory formation focused on the hippocampus, following observations on patient HM, whose memory was severely impaired after medial temporal lobe surgery aiming to treat epilepsy. During the surgery, both of his hippocampi, as well as the entorhinal cortex, which forms the major hippocampal input, were removed. The result was a nearly complete anterograde amnesia, with strongest memory loss relating to events in the time preceding the surgery and more distant memories remaining intact (Scoville and Milner, 1957). Thus, the hippocampus emerged as a structure crucial to the formation of memory.

Indeed, initial studies on the hippocampus showed that high-frequency stimulation of the perforant path produced a long-term strengthening of the synaptic response, observed in both anaesthetised (Bliss and Lomo, 1973) and awake (Bliss and Gardner-Medwin, 1973) rabbits. By contrast, low-frequency stimulation was found to produce the opposite phenomenon: a long-term decrease in synaptic efficacy, termed long-term depression (LTD, Barrionuevo et al. 1980). These early findings initiated extensive research on the molecular basis of LTP and LTD. AMPARs emerged as a central element of the post-synaptic plasticity mechanisms, and their role in LTP has been extensively reviewed (Malinow and Malenka, 2002; Barry and Ziff, 2002; Song and Huganir, 2002). Notably, the altered post-synaptic response has been attributed to changes in AMPAR trafficking.

AMPAR trafficking and synaptic plasticity

One of the best understood mechanisms of AMPAR trafficking in plasticity is that present in hippocampal CA1 pyramidal neurons. GluA2/3 heteromeric AMPARs show a continuous cycle of membrane insertion and internalization, while GluA1/2 heteromer insertion into the post-synaptic membrane is activity dependent (Shi et al.,

2001). The constant cycling of GluA2/3 AMPARs is dependent on their interaction with NSF and group II PDZ binding proteins. The activity-dependent insertion of heteromeric GluA1/2 AMPARs also requires binding to PDZ binding proteins (Hayashi et al., 2000; Shi et al., 2001). Thus, the differences in trafficking of distinct AMPAR subtypes relates to their interactions with PDZ binding proteins.

PDZ proteins often bind to the C-terminus of their interacting partners, due to the presence of a carboxylate binding loop (R/K-XXX-GLGF), and are divided into three classes depending on the final 4 amino acids that they recognise in the C-terminal peptide (Sheng and Sala, 2001). The final amino acids of GluA1 (TGL) form a binding site for SAP-97, a Class II PDZ binding protein (Leonard et al., 1998). The similar C-terminal sequences in GluA4 (SDLP) and GuA2L (TDLS) are also proposed PDZ ligands (Barry and Ziff, 2002). On the other hand, the short AMPAR C-tails contain the C-terminal sequence SVKI (GluA2 and GluA3) or SIKI (GluA4c), which form binding sites for GRIP1/2 (Dong et al., 1997, 1999; Osten et al., 2000) and PICK1 (Xia et al., 1999; Dev et al., 1999), also members of Class II of PDZ binding proteins. In addition, the short form subunits GluA2 and GluA4c contain binding sites for NSF (Song et al., 1998). Interaction with NSF may stabilise AMPARs at the synapse by disrupting GluA2-PICK1 complexes (Hanley et al., 2002).

In addition, a number of other proteins have been implicated in AMPAR trafficking and synaptic plasticity, both in the hippocampus and in other brain regions (see for instance Henley et al. 2011 for review). Although the importance of NMDARs in LTP induction was reported early on (Collingridge et al., 1983), CP-AMPARs (see for instance Plant et al. 2006, and the review by Hanley 2014) may provide another mechanism for the postsynaptic Ca^{2+}-entry required forhippocampal LTP induction (Lynch et al., 1983). Their involvement in hippocampal LTP, however, remains controversial, in contrast to other brain regions such as the cerebellum, where CP-AMPARs have been described to contribute to synaptic plasticity (Liu and Cull-Candy, 2005).

1.4 RNA editing and alternative splicing of AMPARs

The mRNA of AMPAR subunits is subject to extensive alternative splicing and RNA editing. The alternative splicing in the C-terminal regions of GluA2 and GluA4 is described above and other sites for these modifications are outlined in this section. The alternative splicing and editing sites are summarised in Fig. 1.2.

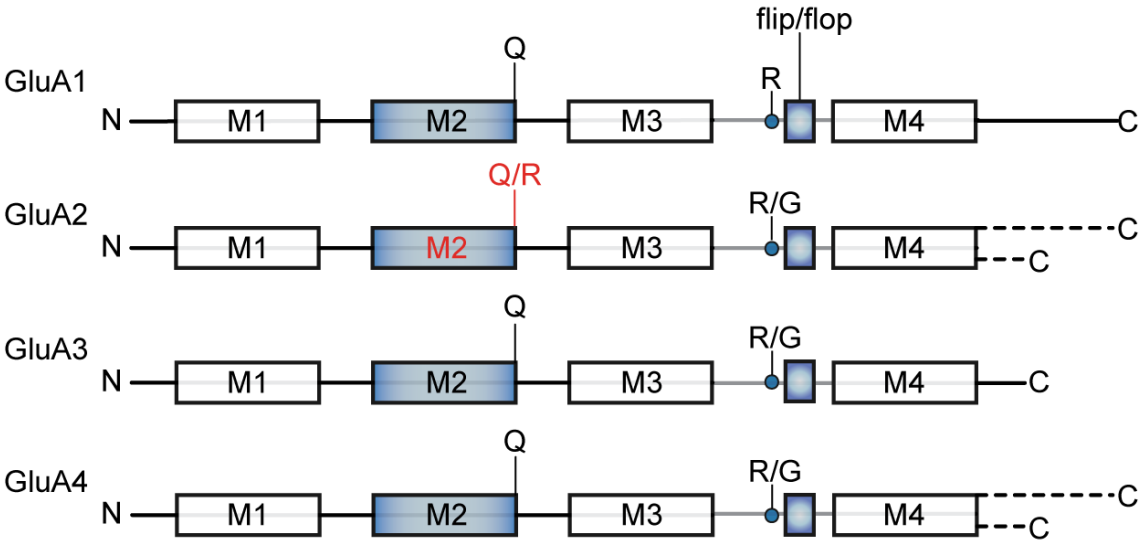

Figure 1.2: Alternative splicing and RNA editing in the pore-forming AMPAR subunits shown in relation to the position of the four membrane regions. The pore-lining M2 helices are shown in light blue. Indicated by the grey line is the S2 region of the LBD, harbouring the flip/flop alternatively spliced region (all subunits, blue rectangle) and the R/G editing site (GluA2-4, blue circle). The flip/flop alternative splicing is a common feature of all AMPAR pore-forming subunits, while the R/G editing occurs in GluA2-4 subunits only. The Q/R RNA editing site of GluA2 is indicated in red. Differential lengths of the C-termini of GluA2 and GluA4 are indicated by dashed lines.

1.4.1 Q/R site

As mentioned above, AMPARs form as homomeric or heteromeric assemblies of GluA1-4. GluA2 subunit co-expression was, early on, found to have profound effects on AMPAR properties. Unlike receptors composed of GluA1, 3 or 4, GluA2-containing heteromeric AMPARs display a linear *I-V* relationship (Boulter et al., 1990; Nakanishi et al., 1990). Heteromeric AMPARs differ from homomers in a number of properties. These crucial differences are determined by a single amino acid (Q586R) switch within the GluA2 subunit, produced by RNA editing in virtually all copies of the GluA2 RNA (Sommer et al., 1991), which renders GluA2-containing AMPARs impermeable to Ca^{2+} (Burnashev et al., 1992a).

This Q/R editing site is located immediately adjecent to the M2 helix, which, as mentioned above, lines the channel pore (Sobolevsky et al., 2009). The mechanism of the RNA editing at this crucial site is quite well defined. The codon CAG, normally coding for glutamine, is edited by adenosine deaminase acting on RNA 2 (ADAR2) to CIG. Inosine is recognised as guanine during translation, which results in an arginine residue being inserted into the polypeptide chain (Yang et al., 1995; Melcher et al., 1996). It is the replacement of the neutral glutamine residue with positively charged

arginine at this site, that defines the lack of GluA2 permeability to Ca^{2+} (Burnashev et al., 1992a; Geiger et al., 1995), and lowers single-channel conductance (Swanson et al., 1997). AMPARs lacking edited GluA2 remain Ca^{2+}-permeable.

Mice which lack GluA2 editing, either due to the introduction of editing-incompatible GluA2 (Brusa et al., 1995), or due to ADAR2 knockout (Higuchi et al., 2000) suffer from epilepsy and die within 3 weeks from birth. This phenotype can be rescued by a point mutation introducing the R form of GluA2 (Higuchi et al., 2000). Underediting of GluA2 is thought to be a major contributor to the pathology of a number of important neurological diseases, including amyotrophic lateral sclerosis (ALS or motor neuron disease, Hideyama et al. 2010) and malignant gliomas (Maas et al., 2001).

Unlike Q/R edited GluA2-containing receptors, Ca^{2+}-permeable AMPARs (CP-AMPARs) are blocked by endogenous intracellular polyamines at positive membrane potentials. Polyamine block is the cause of inwardly rectifying current-voltage relationships (Bowie and Mayer, 1995; Kamboj et al., 1995; Koh et al., 1995) and induces a frequency-dependent facilitation of response at synapses containing these receptors (Bowie et al., 1998; Rozov et al., 1998).

In addition, Q/R editing is a crucial determinant of GluA2 trafficking. The R form of the GluA2 subunit is retained in the ER in hippocampal neurons, although forward trafficking is also regulated by the PDZ domain (Greger et al., 2002). In addition, tetramerization of GluA2R is not favoured. This results in accumulation of GluA2R dimers in the ER, a process which facilitates the formation of heteromeric AMPAR tetramers (Greger et al., 2003). It is, however, worth noting that prominent ER retention of GluA3 also occurs, despite this subunit being Ca^{2+}-permeable (Q form at the Q/R site). Two residues located within the S1 region of the ligand-binding domain: Y454 and R461 have been identified as crucial for ER retention of GluA3. Interestingly, heteromerization facilitates GluA3 surface expression, most likely by masking these residues (Coleman et al., 2010). Indeed, the LBD of GluA2 has also been implicated in receptor export from the ER, since the L483Y mutation, stabilising the LBD dimer interface, inhibits GluA2 surface trafficking (Greger et al., 2006). Thus, despite the role of multiple AMPAR domains in receptor assembly, insertion of the edited GluA2 subunit is a crucial determinant of AMPAR properties, since these receptors tend to preferentially heteromerise (Mansour et al., 2001).

1.4.2 R/G site

The R/G site is located within the LBD of GluA2,3 and 4 (but not GluA1) subunits and immediately precedes the flip/flop alternative splicing region described below (Lomeli et al., 1994). In GluA2 this is the 743 position, where the codon AGA coding for arginine, is converted to IGA. During translation IGA is recognised as GGA coding for glycine. The R/G site is efficiently edited by both ADAR1 and ADAR2 (Melcher et al., 1996). R/G editing affects kinetic properties of AMPARs. Edited receptors, containing a glycine residue at this site, show slower desensitization, faster recovery from desensitization and increased fraction of steady-state current (Lomeli et al., 1994). The proportion of edited transcripts increases during development in a subunit-specific manner (Lomeli et al., 1994) and varies across neuronal cell types (Geiger et al., 1995). The unedited (R form at the R/G site) of GluA2 (R at the Q/R site) appear to exit the ER and express at the cell surface more efficiently than the edited (G form) receptors, while the edited (G) form of the same subunit accumulate in the ER. However, the magnitude of the R/G editing effect on GluA2(R) ER exit depends also on the flip/flop splice variant and is more prominent in the flop form (Greger et al., 2006). In summary, the developmentally regulated R/G editing may result in accumulation of GluA2 in the ER and promote formation of AMPAR heteromers, contributing to the developmental switch from CP-AMPARs to GluA2-containing, Ca^{2+}-impermeable heteromers seen in a number of cell types (see for example Kelly et al. 2009).

1.4.3 Alternative splicing: flip/flop

The diversity of AMPAR subunits is further increased by alternative splicing in the flip/flop region located within the S2 segment of the LBD (Sommer et al., 1990). The flop forms of GluA3 and GluA4, as well as GluA2(flop)-containing heteromers have been shown to desensitize up to 4 times more rapidly than the flip forms. However, no difference in desensitization time constant was observed for the flip and flop forms of homomeric GluA1 (Mosbacher et al., 1994). The relative abundance of mRNA for the two splice forms varies among cell types (Geiger et al., 1995) and can also be developmentally regulated. In cerebellar granule cells, the GluA4 isoform changes from predominantly flip in early development to mostly flop in the adult (Mosbacher et al., 1994).

In GluA2 the alternative flip and flop exons differ in 9 residues, a change sufficient to affect ER retention and surface expression in neurons, as described above (Greger et al., 2006). Indeed, flop forms of AMPARs have been reported to show impaired

ER exit and poor expression compared to flip forms when examined in a recombinant system (Coleman et al., 2006, 2010). In GluA4, the difference in surface trafficking between flip and flop forms appears to be largely determined by a single residue at position 780, valine in the flip form and leucine in the flop form (Coleman et al., 2006). Swapping of this residue between the two isoforms resulted in a $\sim$ 50 % change surface expression (increase in the case of flop form and decrease in the flip form). Importantly, efficient expression of GluA4 flop was observed in transfected mouse cortical neurons in the same study, suggesting that some compensatory mechanism may exist to facilitate flop form trafficking in neurons.

In addition to the effect on AMPAR trafficking, alternative splicing in the flip/flop region also affects the pharmacology of AMPAR allosteric modulators. This is of particular interest as AMPAR allosteric potentiators have been shown to affect hippocampal LTP (Stäubli et al., 1994) and are promising targets for cognitive enhancement therapy in humans (see for example Waegemans et al. 2002). Cyclothiazide (CTZ) is an allosteric potentiator, which increases the amplitude of glutamate-evoked currents and blocks AMPAR desensitization (Yamada and Tang, 1993). The efficacy of CTZ is greater for flip AMPARs than for the flop isoforms (Partin et al., 1994, 1995), a difference which appears to be dependent on a single residue at the position 750 in GluA1: serine in the flip form and asparagine in the flop form (Partin et al., 1995). Indeed, the analogous position in flip GluA2 (754) is also a serine, which, in a crystallography study, has been shown to form part of the CTZ binding site at the LBD dimer interface (Sun et al., 2002). By contrast, another positive allosteric modulator, aniracetam, appears to be more efficacious on the flop forms of AMPARs (Johansen et al., 1995). Its modulation of deactivation and desensitization of GluA1 AMPARs also depends on the 750 residue (asparagine in the case of flop forms), however mutations at this site have a less striking effect on the action of aniracetam than on that of CTZ (Partin et al., 1996). Aniracetam has subsequently been shown to bind at the LBD dimer interface of the non-desensitized receptor (Jin et al., 2005; Ahmed and Oswald, 2010), which stabilises the LBD in an agonist-bound state, resulting in a profound slowing of AMPAR deactivation.

1.5 Post-translational modifications of AMPARs

AMPARs are subject to extensive post-translational modifications, which alter their properties. These include phosphorylation, glycosylation, palmitoylation and ubiquitination.

1.5.1 AMPAR glycosylation

N-linked glycosylation

The extracellular regions of AMPARs are extensively glycosylated. N-linked glycosylation occurs within the ER on asparagine residues located within the consensus sequence NX(S/T) (X in this case stands for any amino acid apart from proline). AMPAR subunits have 4-6 consensus sequences for N-linked glycosylation, localised to the NTD and the signal peptide (Hollmann et al., 1994; Standley and Baudry, 2000). In the case of GluA1 all of the 6 consensus sites appear to be glycosylated, as determined by the shifts in molecular weight upon glycosylation site removal (Hollmann et al., 1994).

Pre-treatment of cells with tunicamycin, which abolishes N-linked glycosylation, suggests that glycosylation is not required for AMPAR function in a recombinant system. However, responses to both glutamate and kainate appear to be affected by loss of glycosylation in a manner specific to subunit and flip/flop splicing state. In addition, the susceptability of AMPARs to current potentiation by the lectin Concanavalin A (ConA) appears to be determined by glycosylation. GluA1 is ConA-sensitive, while GluA2 is not. This difference has been attributed to GluA1 glycosylation at N45 and N239 (Everts et al., 1997).

In addition to the modulation of agonist-evoked currents, glycosylation may prevent degradation of AMPARs. Loss of glycosylation at the N387 site within GluA3 results in degradation by granzyme B and has been implicated in the autoimmune response present in Rasmussen's encephalitis, a form of childhood epilepsy (Gahring et al., 2001).

O-linked glycosylation

O-linked glycosylation occurs within the Golgi apparatus and involves the attachment of sugars (usually O-N-acetylglucosamine) to serine or threonine residues of the target protein. No consensus sequence for this type of glycosylation appears to be established. However, O-linked glycosylation often occurs at the same sites as phosphorylation and the two modifications are mutually exclusive.

Jacalin, a lectin specific for O-linked oligosachcharides, was found to bind to AMPARs, suggesting that these receptors are targets for O-linked glycosylation (Hullebroeck

and Hampson, 1992). Subsequent studies suggested that this form of glycosylation may play a role in AMPAR-mediated plasticity. Abolishing O-linked glycosylation with alloxan (inhibitor of O-linked beta-N-acetylglucosamine transferase) potentiated GluA1-mediated currents. The potentiation was dependent on a single site, S831 (the calcium/calmodulin-dependent protein kinase II (CaMKII) phosphorylation site described below). In addition, alloxan enhanced hippocampal LTP and promoted surface expression of GluA1 and GluA2 subunits (Kanno et al., 2010), suggesting that this bidirectional modification may be important in synaptic plasticity. A similar bidirectional regulation mechanism has been proposed (see Din et al. 2010) for the S880 PKC phosphorylation site on GluA2 (Seidenman et al., 2003).

1.5.2 Palmitoylation

Palmitoylation is the attachment of a fatty acid chain (usually a palmitoyl group), which occurs on cysteine residues, increasing the hydrophobicity of the protein. To date, two conserved palmitoylation sites on AMPARs have been identified, one located within the M2 and one in the C-terminal domain close to M4. Palmitoylation of the cysteine residue within the M2 (C610 in GluA2) catalysed by GODZ palmitoyl transferase produces accumulation of AMPARs in the Golgi and reduces their surface expression. Palmitoylation of the C terminus (C836 in GluA2) disrupts interaction with the cytoskeletal protein 4.1N (Hayashi et al., 2005). This interaction appears to be important for hippocampal LTP and is additionally regulated by protein kinase C (PKC)-mediated phosphorylation (Lin et al., 2009). Activation of glutamate receptors appears to induce AMPAR depalmitoylation (Hayashi et al., 2005), a mechanism likely to be important for synaptic plasticity.

1.5.3 Ubiquitination

Ubiquitination describes the attachment of the small protein ubiquitin, usually via an isopeptide bond, to a lysine residue of the target protein. The addition of K48-linked ubiquitin chains is well studied and known to target proteins for proteasomal degradation. However, other processes such as protein localisation and protein-protein interactions can also be modified by ubiquitination (see Komander and Rape 2012 for review). Prolonged treatment with the $GABA_A$ receptor antagonist bicuculline causes a reduction in the amplitude of miniature excitatory post-synaptic currents (mPSCs). This homeostatic mechanism appears to involve ubiquitination of GluA1 and its subsequent proteasomal degradation, a process mediated by EphA4 signalling (Fu et al.,

2011). Ubiquitination of GluA1 on its C-terminus appears to be involved in GluA1 internalisation and lysosomal degradation following stimulation with AMPA. However, since internalisation was shown to be defective in a GluA1 mutant where all four C-terminal lysine residues were replaced with arginines, it is unclear which residue is the target for ubiquitination (Schwarz et al., 2010).

1.5.4 Phosphorylation

The role of AMPAR phosphorylation has been widely studied, particularly in relation to synaptic plasticity (Malinow and Malenka, 2002). AMPARs are targets for phosphorylation by both serine/threonine kinases and tyrosine kinases.

GluA1 phosphorylation

GluA1 is phosphorylated in its C-terminal domain by PKC and CaMKII at S831 and by protein kinase A (PKA) at S845 (Roche et al., 1996; Mammen et al., 1997). Phosphorylation of S831 by CaMKII increases single-channel conductance (Derkach et al., 1999), by increasing the frequency of opening to the highest conductance level (Kristensen et al., 2011), although this effect is absent in GluA1/2 heteromers (Oh and Derkach, 2005) unless these are associated with a TARP (Kristensen et al., 2011). Phosphorylation of S845 by PKA, on the other hand, has been reported to increase peak open probability of GluA1 (Banke et al., 2000). Phosphorylation of GluA1 by both CaMKII and PKA appears to be required for synaptic trafficking of GluA1, whereas for GluA4 the activity of PKA alone seems sufficient (Esteban et al., 2003). Indeed, CaMKII has been reported to phosphorylate GluA1 on S831 upon LTP induction in naive synapses, while high-frequnency stimulation of a previously depressed synapse results in GluA1 phosphorylation by PKA at S845. Similarly, dephosphorylation of S845 is implicated in LTD induction in naive synapses, while de-potentiation of a previously potentiated synapse appears to require dephosphorylation of S831 (Lee et al., 2000). Thus, a two-step model for synaptic delivery of AMPARs emerged: phosphorylation by PKA appear to target GluA1 to extrasynaptic sites, while their synaptic incorporation requires neuronal activity resulting in CaMKII activation (Oh et al., 2006) and interactions mediated by the C-terminal PDZ domain of GluA1 (Hayashi et al., 2000).

Phosphorylation of GluA1 by PKC at S816 and S818 promotes its interaction with 4.1N, which is important for hippocampal LTP, as described above (Boehm et al.,

2006; Lin et al., 2009). PKC was also found to phosphorylate GluA1 at T840 in an *in vitro* assay (Lee et al., 2007). Another study showed that this site may be a target for phosphorylation by p70S6 kinase and that its dephosphorylation occurs during LTD in the hippocampus (Delgado et al., 2007). Mice lacking the S831, S845 and T840 phosphorylation sites (due to serine to alanine substitutions) showed normal basal synaptic transmission. However, LTP was impaired with the precise effect dependent on age and induction protocol (Lee et al., 2007).

GluA2 phosphorylation

GluA1 phosphorylation and dephosphorylation is an important mechanism in LTP and LTD respectively. GluA2 phosphorylation, on the other hand, appears important for synaptic localisation of AMPARs. S880 is located within the C-terminal PDZ domain of GluA2 and is phosphorylated by PKC. Phosphorylation of this site disrupts GluA2 interaction with GRIP, leading to removal of synaptic AMPARs and LTD (Seidenman et al., 2003). However, PICK1 also binds to the C-terminal domain of GluA2 in a S880 phosphorylation-dependent manner. This interaction has been implicated in hippocampal LTD (Kim et al., 2001). Indeed, disassembly of the GluA2-PICK1 complex by NSF appears to stabilise GluA2 at synapses (Hanley et al., 2002).

Y876 phosphorylation by Src has also been implicated in LTD. Dephosphorylation of this site activates BRAG2, leading to activation of Arf6 GTP-ase and internalisation of GluA2-containing AMPARs during hippocampal LTD (Scholz et al., 2010). In addition, the loss of phosphorylation at this site due to the Y876F mutation causes reduced surface expression and synaptic clustering of GluA2 (Hayashi and Huganir, 2004). Thus, GluA2 phosphorylation at Y876 may stabilise GluA2-containing AMPARs at synapses.

GluA2L is additionally subject to phosphorylation by JNK1 on T912. Increased glutamatergic activity results in dephosphorylation of this site. Conversely, reducing activity with TTX promotes T912 phosphorylation. Although surface and synaptic expression of GluA2L is not affected by altering the T912 phosphorylation state, JNK1 activity is required for membrane re-insertion of internalised GluA2L. A corresponding site (T855) has also been identified on GluA4 and shown to be phosphorylated by JNK1 in response to changes in neuronal activity (Thomas et al., 2008).

1.6 Native AMPARs are associated with TARPs

Early studies on AMPARs expressed in recombinant systems failed to reproduce certain properties of native AMPARs (see for instance Nakanishi et al. 1990). An explanation for this phenomenon emerged following the characterisation of the spontaneous mouse mutant *stargazer* (*stg*). *Stg* mice have absence epilepsy and impaired movement. The phenotype can be attributed to the insertion of the ETn retrotransposon into intron 2 of the CACNG2 gene, coding for γ-2 (Letts et al., 1998), a protein homologous to the γ-1 subunit of voltage-gated Ca^{2+} channels located in skeletal muscle (Jay et al., 1990).

A role for γ-2 different from the modulation of voltage-gated Ca^{2+} channels emerged upon the discovery that *stg* mice lack AMPAR-mediated transmission at the cerebellar mossy fibre-granule cell synapses (Hashimoto et al., 1999). It became evident that γ-2 may modulate AMPARs directly, since transfection of γ-2 into *stg* cerebellar granule cells was sufficient to rescue AMPAR-mediated synaptic currents (Chen et al., 2000). Indeed, subsequent studies defined γ-2 as the prototypical TARP (also known as stargazin), with the complete family comprising 6 functional members in total (Tomita et al., 2003; Kato et al., 2007; Soto et al., 2009). TARPs are often divided into two major groups, depending on their function (Straub and Tomita, 2012): type I (γ-2, -3, -4 and -8) and type II (γ-5 and -7, Kato et al. 2008). Type I TARPs are further subdivided into type Ia (γ-2 and -3) and type Ib (γ-4 and -8, Cho et al. 2007).

Although all 6 members of the TARP family have been shown to modulate multiple properties of AMPAR, as described below, a controversy has arisen with regard to the role of γ-5. Early studies on TARPs often used γ-5 as a negative control, as it was initially thought not to be functional (see for instance Tomita et al. 2005). Subsequently, γ-5 was indentified as a TARP independently by two different labs. However, their results differed profoundly. Kato et al. (2008) suggested that γ-5 specifically modulates GluA2-containing, Ca^{2+}-impermeable AMPARs and shows opposite effects from other TARPs on deactivation and desensitization kinetics and glutamate potency. By contrast, Soto et al. 2009 found that γ-5 selectively modulates AMPAR subunits with long C-tails. The two studies, in fact, agreed only on the point that γ-5 fails to promote AMPAR surface expression. Thus, the precise role of γ-5 in the modulation of distinct AMPAR populations remains uncertain.

TARPs are differentially expressed among cell types and brain regions (Tomita et al., 2003; Fukaya et al., 2005), and are considered vital components of most AMPAR complexes in the brain. TARP proteins and their corresponding genes are listed in Table 1.2 below.

TARP	Gene
γ-2	CACNG2
γ-3	CACNG3
γ-4	CACNG4
γ-5	CACNG5
γ-7	CACNG7
γ-8	CACNG8

Table 1.2: TARP family members and the corresponding genes.

γ-1 and γ-6 are not included in this Table, despite being closely related to TARPs. As mentioned above, γ-1 is a subunit of voltage-gated Ca^{2+} channels. A role in Ca^{2+} channel modulation has also been described for γ-6 (Hansen et al., 2004).

1.7 TARP protein structure

TARPs have 4 transmembrane domains, with intracellular N- and C-termini. The molecular weight of γ-2 is 37 kDa (Kim et al., 2010), but the individual family members vary in size slightly. The length of the C-terminus also varies between TARP family members (Chu et al. 2001, reviewed by Chen et al. 2007).The structure of TARPs is related to that of claudins, a family of tight junction proteins (Morita et al., 1999). The overall structure of the TARP family members is shown in Fig. 1.3 below.

The close structural similarity between TARPs and claudins suggests that TARPs may also play a role in cell adhesion *in vivo*. γ-2, similar to claudin-1, was found to promote aggregation of L-fibroblast cell lines, in a manner dependent upon γ-2 glycosylation at N48 (Price et al., 2005). Indeed, type I TARPs have been implicated in the regulation of dendritic growth (Hamad et al., 2014), suggesting that the effect of TARPs on synaptic transmission may extend beyond direct regulation of AMPAR-mediated currents.

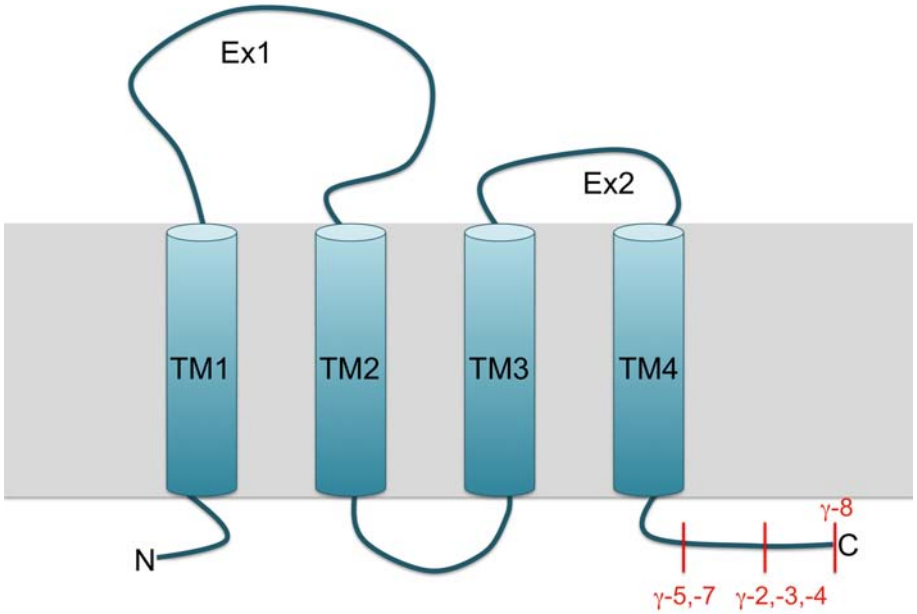

Figure 1.3: Schematic tertiary structure of the TARP family members. TARPs have 4 transmembrane domains (TM1-4). The N and C termini are located intracellularly. The two extracellular loops labelled Ex1 and Ex2 are approximately 70-85 and 30 residues long, respectively, and are important for interaction with AMPARs. The C-terminus of TARPs affects AMPAR trafficking and varies between family members (alternative C-tail lengths are indicated by red lines). Adapted from Deng et al. (2006).

1.8 TARPs modulate the biophysical and pharmacological properties of AMPARs

1.8.1 Modulation of AMPAR deactivation and desensitization

Type I TARPs prolong AMPAR deactivation and desensitization and increase the fraction of steady-state current (Priel et al., 2005; Turetsky et al., 2005; Tomita et al., 2005). In addition, GluA1 recovery from desensitization is accelerated by γ-2 (Priel et al., 2005). However, the magnitude of TARP effect on desensitization and deactivation of AMPARs depends on TARP isoform (Milstein et al., 2007) and the AMPAR subunit present (Kott et al., 2007). Type Ib TARPs, γ-4 and γ-8 appear to be more efficient than type Ia (γ-2 and γ-3) at prolonging GluA1 deactivation and desensitization. A similar difference in modulation of desensitization τ_w between γ-8 and γ-2 has been reported for co-expression with GluA1/2 heteromers (Cho et al., 2007). The sensitivity to TARP-mediated modulation of kinetics varies between AMPAR subunits. Notably, GluA3 appears to be only weakly sensitive to modulation of deactivation and desensitization by γ-2 or γ-3 and is most efficiently modulated by γ-4 and γ-8 (Suzuki et al., 2008).

Type II TARPs differ from type I TARPs in respect to modulation of AMPAR deactivation and desensitization. Deactivation of GluA1 is only weakly prolonged by γ-7 and not prolonged by γ-5. In contrast, desensitization of GluA1 is prolonged to an equal extend by γ-7 and γ-2 and only slightly (and insignificantly) prolonged by γ-5 (Kato et al., 2007). GluA4 desensitization is not prolonged by γ-5 (Soto et al., 2009). Thus, type II TARPs have overall less effect than type I TARPs on AMPAR deactivation and desensitization kinetics.

The TARP-mediated modulation of deactivation and desensitization is also reflected in the effect of TARPs on the decay of AMPAR-mediated mEPSCs. In *stg* neurons, γ-4 was found to slow mEPSC decay to a larger extent than γ-2. On the other hand, γ-3 had less effect than γ-2, while γ-8 and γ-2 did not differ from each other in their effect on mEPSC decay time (Milstein et al., 2007).

1.8.2 TARPs affect polyamine block of AMPARs

.

As described above, GluA2-lacking, Ca^{2+}-permeable AMPARs are blocked by endogenous intracellular polyamines. TARPs partially relieve polyamine block (Soto et al., 2007), resulting in biphasic current-voltage relationships similar to those seen in native AMPARs (see for example Nakanishi et al. 1990). The relief of polyamine block is reflected in the shift of the conductance-voltage relationships to the right, and a positive shift in $V_{0.5}$, the voltage at which spermine block is half-maximal (Soto et al., 2007). However, similar to the effect of TARPs on deactivation and desensitization, the extent to which spermine block is attenuated by TARPs varies amongst the different isoforms. γ-2 and γ-3 were found to relieve GluA4 block by spermine to the largest extend, with γ-4, -8 and -7 having an intermediate effect an γ-5 showing the smallest (although still significant) relief of spermine block (Soto et al., 2009).

It is at present unclear whether the effect of TARPs on AMPAR rectification also involves modulation of Ca^{2+} permeability. Soto et al. (2007) demonstrated that γ-2 lacks an effect on Ca^{2+} permeability of GluA4, while Kott et al. (2009) showed that TARPs γ-2 and γ-4 increase Ca^{2+} permeability of GluA1. It is possible that these discrepancies are caused by differences in the expression system and experimental protocol between the two studies.

AMPARs are also blocked at negative membrance voltages by extracellular polyamines - naturally occurring toxins and their synthetic analogues. The block of GluA2/4 het-

eromeric AMPARs by Philantotoxin-74 (PhTx-74) is increased by TARPs and depends on TARP isoform in a manner which correlates with AMPAR mean-single channel conductance. Similarly, the block of Ca^{2+}-permeable GluA4 AMPARs depends on both TARP co-expression (although not the exact type of TARP present) and on the agonist (glutamate or kainate) used to evoke the current (Jackson et al., 2011). This is most likely caused by the TARP-dependent increase in kainate efficacy described below. However, TARPs have also been reported to reduce the susceptibility of GluA1 to block by NASPM, an effect dependent on TARP subtype (Kott et al., 2009).

It is worth noting that the sensitivity of AMPARs to block by PhTx-74 depends not only on TARP co-expression, but also on the AMPAR subunit present. GluA2-containing heteromeric AMPARs are over 100-fold less sensitive to PhTX-74 than the corresponding Ca^{2+}-permeable homomers, but γ-2 co-expression reduces PhTx-74 block of both receptor types. By contrast, GluA2(R) homomeric AMPARs are almost insensitive to PhTx-74 block, despite the presence of γ-2 (Poulsen et al., 2014a).

1.8.3 TARPs increase single-channel conductance of AMPARs

Prior to the discovery of TARPS, single-channel recording of recombinant AMPARs (Swanson et al., 1997) failed to reproduce results obtained from native receptors (Wyllie et al., 1993). AMPARs are known to display multiple subconductance states (Cull-Candy and Usowicz, 1987), dependent on the number of glutamate molecules bound to the tetrameric receptor (Rosenmund et al., 1998; Smith and Howe, 2000). Direct evidence from single-channel recording showed that TARPs γ-2, -4 and -5 increase single-channel conductance of GluA1. In addition, in the presence of γ-4 a fourth subconductance state was observed, in contrast to the three states seen with the TARPless receptor or with other TARPs. This additional state corresponded to a very high conductance level (>50 pS) (Shelley et al., 2012). Of note, co-expression of TARPs γ-2 or γ-8 is also required for the increase in single-channel conductance of GluA1/2 heteromers upon GluA1 phosphorylation at S831 by CaMKII (Kristensen et al., 2011).

An additional line of evidence for the TARP-mediated increase in AMPAR single-channel conductance comes from studies using non-stationary fluctuation analysis to estimate mean-single channel conductance from macroscopic currents. Mean single-channel conductance of GluA1 is increased by TARPs γ-2, -4 and -8, while peak open probability (P_o) is significantly increased only by γ-2 (Suzuki et al., 2008). GluA4 mean-single channel conductance is increased by all TARPs (γ-2, -3, -4, -5, -7 and -8) (Soto et al., 2009). In the same study, γ-5 was found to reduce P_o of GluA4,

while other TARPs lacked any effect on this measure. In contrast, P_o of GluA2Q was increased by γ-2 but not γ-5.

Thus, all TARPs appear to increase single-channel conductance of Ca^{2+}-permeable AMPARs, but vary in their effect on P_o. Interestingly, when GluA2/4 heteromers are examined, TARPs γ-2, -3, -4 and -8 all increase mean-single channel conductance, but γ-8 appears to do so to a larger extent than γ-2. None of the above TARPs appears to affect P_o of GluA2/4 heteromers (Jackson et al., 2011).

1.8.4 TARPs modify AMPAR pharmacology

In addition to altering the affinity for polyamine channel blockers, TARPs have profound effects on other pharmacological properties of AMPARs.

TARPs increase glutamate potency

γ-2 has been widely reported to increase the potency of glutamate, as determined by a shift of the dose-response curve to glutamate to the left and a reduction in EC50 (Yamazaki et al., 2004; Priel et al., 2005; Tomita et al., 2005). Other type I TARPs have also been reported to increase glutamate potency in a subtype-specific manner. GluA1 dose-response curves to glutamate exhibited a larger leftward shift upon co-expression with γ-2 or -3 than γ-4 or -8 (Kott et al., 2007). Although all Type I TARPs increase glutamate potency, the precise effects of different TARP isoforms appear to vary slightly between AMPAR subunits (Suzuki et al., 2008).

Type II TARPs differ from Type I in their effect on glutamate potency. γ-7 fails to increase GluA1 affinity for glutamate (Kato et al., 2007). γ-5 overexpression has been reported, paradoxically, to reduce the potency of glutamate in cultured rat cortical neurons (Kato et al., 2008).

TARPs alter relative kainate efficacy

Kainate is a partial agonist at AMPARs (Patneau and Mayer, 1991), which, compared to glutamate, causes AMPARs to preferentially occupy lower conductance states (Swanson et al., 1997). The dose-response curve of kainate, much like that of glutamate,

is shifted to the left in the presence of γ-2 (Turetsky et al., 2005). The ratio of responses to kainate and glutamate (KA/Glu ratio) is also increased by co-expression of AMPARs with γ-2 (Tomita et al., 2005; Turetsky et al., 2005). A similar increase in kainate/glutamate ratio has also been reported for γ-3, -4 and -8. The KA/Glu ratio is also affected by the AMPAR subunit present and its flip/flop splicing state. However, overall γ-2 and -3 appear to increase the KA/Glu ratio more than do γ-4 or -8 (Kott et al., 2007; Suzuki et al., 2008).

Kainate efficacy is yet another factor in which type I and II TARPs differ. γ-7 co-expression increases the KA/Glu ratio for GluA1 only weakly, compared to γ-2 (Kato et al., 2007). γ-5, on the other hand, fails to increase the KA/Glu ratio (Turetsky et al., 2005; Tomita et al., 2005).

The KA/Glu ratio is a measure of TARP efficacy sensitive not only to TARP co-assembly as such, but also to TARP stoichiometry. In AMPARs associated with γ-2 or γ-8, the KA/Glu ratio increases with increasing TARP stoichiometry, from 0 to 2 to 4 TARP molecules per AMPAR (Shi et al., 2009). By contrast, AMPARs associated with 2 γ-7 molecules appear to exhibit a higher KA/Glu ratio than those associated with 4 molecules of this TARP (Gill et al., 2011). However, a study by Kim et al. (2010), showed that even co-injection of small amounts of γ-2 is sufficient to enhance kainate efficacy on GluA1 in oocytes (albeit to a smaller level that co-injection of larger γ-2 amounts), suggesting that even a single molecule of γ-2 associated with an AMPAR may enhance kainate efficacy.

CNQX acts as a partial agonist at AMPARs associated with type I TARPs

CNQX (6-cyano-7-nitroquinoxaline-2,3- dione) has been widely used as an AMPAR antagonist. However, studies on native AMPARs suggested that it may, paradoxically, enhance neuronal activity (Brickley et al., 2001; Maccaferri and Dingledine, 2002). Indeed, CNQX has been demonstrated to be a partial agonist at both native and recombinant AMPARs, an action entirely dependent on the presence of γ-2 (Menuz et al., 2007). CNQX-evoked currents can also be detected upon co-assebly of TARPs γ-3,-4 and -8 (Menuz et al., 2007; Kott et al., 2009). However, the amplitude of CNQX-evoked currents seems to vary slightly between the TARP isoforms (Kott et al., 2009). Of note, 6,7-dinitroquinoxaline-2,3-dione (DNQX) also behaves as a partial agonist on AMPARs associated with γ-2, while 2,3-dihydroxy-6-nitro-7-sulfamoyl-benzo[f]quinoxaline-2,3-dione (NBQX) does not (Menuz et al., 2007).

In contrast to γ-2, γ-7 fails to convert CNQX from an antagonist to a partial agonist

(Bats et al., 2012), providing another important means of differentiating pharmacologically between AMPARs associated with Type I and Type II TARPs. It remains undetermined whether AMPARs associated with γ-5 show CNQX-evoked currents. However, since GluA1 co-expressed with a chimera in which the first extracellular loop of γ-2 has been exchanged with that of γ-5 shows no CNQX-evoked current (Cokić and Stein, 2008), it is plausible that γ-5 does not convey CNQX-sensitivity on AMPARs.

TARPs affect AMPAR allosteric modulation

The affinity of GluA1 for the positive allosteric modulator CTZ is enhanced by γ-2. In addition, γ-2 enhances the CTZ-mediated potentiation of Glu-evoked current from GluA1 flop, the splice variant which, in the absence of TARP, is modulated by CTZ to a much lesser extend than flip. In addition, the effect of CTZ on GluA1 flop deactivation is enhanced by γ-2 co-assembly (Tomita et al., 2006). In contrast to CTZ, 4-[2-(phenylsulfonylamino)ethylthio]-2,6-difluorophenoxyacetamide (PEPA) acts preferentially on the flop isoforms of AMPARs (Sekiguchi et al., 1997). Co-expression of γ-2 enhances the potentiation of Glu-evoked currents from both flop and flip GluA1 by PEPA (Tomita et al., 2006).

Another study, however, showed that the potentiation of Glu-evoked currents by CTZ is reduced when GluA1 flip is co-expressed with TARPs γ-2,–3 and -4, but not -8 (Kott et al., 2007). The action of another allosteric potentiator related to CTZ, trichlormethiazide (TCM, Yamada and Tang 1993), also appeared reduced by TARPs, in an isoform-specific manner (Kott et al., 2009). The reason for the discrepancies between these studies remain unclear.

Co-expression with γ-2 increases the affinity of GluA1 for the negative allosteric modulator GYKI 53655, an effect independent of AMPAR desensitization and mediated by the first extracellular loop (Ex1) of γ-2 (Cokić and Stein, 2008). γ-2 also enhances AMPAR affinity of LY450295 and promotes its displacement by the negative allosteric modulators GYKI 53655 and CP-465,022 (Schober et al., 2011). Thus, it appears that γ-2 is important for the formation of the binding site for these drugs.

1.8.5 Other effects of TARPs on AMPAR-mediated currents

Resensitization

Resensitization, a feature of certain TARPs, is an increase in steady-state current following AMPAR desensitization. It was first observed when AMPARs were co-expressed with γ-7 (Kato et al., 2007). Subsequent studies showed that TARPs γ-4, -7 and -8, but not γ-2,-3 or -5 cause GluA1 to resensitize. All AMPAR subunits co-expressed with γ-8 display varying extent of resensitization. However, hippocampal neurons expressing γ-8 do not (Kato et al., 2010a). It was later demonstrated that receptors with low stoichiometry of γ-7 or γ-8 do not show resensitization. In the hippocampus cornichon homolog-2 (CNIH-2), another auxiliary subunit of AMPARs, associates with neuronal AMPARs and promotes low γ-8 stoichiometry, thus conveying a non-resensitizing phenotype on hippocampal AMPARs (Gill et al., 2011). It is thus unclear if resensitization has a physiological relevance.

Autoinactivation

Autoinactivation is the term used to describe the bell-shaped dose-response curves to glutamate obtained in the presence of TARP. Bell-shaped steady-state dose-response relationships to glutamate have been observed in various types of neurons, such as chick spinal chord neurons (Vlachová et al., 1987), cerebellar unipolar brush cells and granule cells (Kinney et al., 1997) and neurons of the avian cochlear nucleus (Raman and Trussell, 1992). This reduction in response to glutamate has been termed autoinactivation and explained by dissociation of TARPs at high glutamate concentrations (Morimoto-Tomita et al., 2009). However, a more recent paper showed that autoinactivation occurs even when γ-2 is covalently linked to the AMPAR in an AMPAR-TARP tandem construct, and thus unable to dissociate. The study suggest that autoinactivation results from conformational changes within the AMPAR/TARP complex, rather than from TARP dissociation, and that the phenomenon depends on the AMPAR subunit and flip/flop splicing (Semenov et al., 2012).

1.9 TARPs affect AMPAR trafficking

As described above, γ-2 has been initially identified as the factor required for synaptic trafficking of AMPARs in cerebellar granule cells. It was subsequently shown that

this trafficking effect depends on the C-terminal domain of γ-2, since a γ-2 construct where the C-terminus was deleted failed to rescue mEPSCs in *stg* granule cells (Chen et al., 2000). γ-2,-3,-4 and -8, but not γ-5 also rescued AMPAR-mediated synaptic transmission in *stg* granule cells (Tomita et al., 2003). γ-7, on the other hand, appears to selectively traffic CP-AMPARs to the cell surface and the synapse (Studniarczyk et al., 2013). Several studies have shown that TARPs are crucial to maturation, surface trafficking and synaptic localisation of AMPARs. Association of AMPARs with TARPs, unlike with other AMPAR trafficking factors, appears to be both abundant and stable (Vandenberghe et al., 2005b), corresponding with the dual role of TARP auxiliary subunits as modulators of both AMPAR trafficking and functional properties. The key findings showing the importance of TARPs for AMPAR trafficking are outlined below.

AMPARs are synthesised in the ER as monomers, which subsequently dimerise. The complete AMPAR is a tetramer (dimer of dimers). γ-2 has been shown to associate predominantly with the AMPAR tetramer (Shanks et al., 2010). Tomita et al. (2003) showed that in *stg* cerebellum GluA2 is highly sensitive to EndoH glycosidase, which selectively removes high-mannose sugars characteristic for immature (ER-localised) receptors. In addition, upregulation of ER chaperones following induction of the unfolded protein response appears to mimic the effects of γ-2 on GluA1 trafficking (Vandenberghe et al., 2005a). Thus, the initial interaction between AMPARs and TARPs occurs in the ER and facilitates maturation and ER export of AMPARs. Subsequent studies in heterologous expression systems showed that TARPs greatly enhance AMPAR surface expression (see for instance Yamazaki et al. 2004; Tomita et al. 2005), but do not affect the trafficking of the closely related kainate receptors (Chen et al., 2003).

TARP association does not appear to inhibit AMPAR endocytosis (Vandenberghe et al., 2005a). In fact, endocytosis in response to agonist stimulation has been reported to involve TARP dissociation from the AMPAR (Tomita et al., 2004).

Similar to the C termini of AMPARs, C-termini of TARPs also contain PDZ ligands. The final four amino acids of Type I TARPs (TTPV) form a type I PDZ ligand, while the four most distal amino acids in the C-tail of γ-5 (SSPC) and γ-7 (TSPC) are atypical PDZ ligands (Kato et al., 2010b). PSD-95 is a synaptic scaffolding protein which interacts with the C-terminus of γ-2 (Chen et al., 2000). The levels of γ-2 appear to control the amount of surface AMPARs, while the amount of PSD-95 available for binding to γ-2 seems to regulate the number of synaptic AMPARs (Schnell et al., 2002). Palmitoylation of PSD-95 has been shown to stabilise AMPARs at the synapse (Schnell et al., 2002; El-Husseini et al., 2002). The crucial role of γ-2 interaction with PSD-

95 was demonstarted by Bats et al. (2007). This study used a γ-2 construct lacking the C terminus to show that the interaction between PSD-95 and the PDZ domain of γ-2 regulates lateral diffusion of AMPARs. Disruption of this interaction prevents AMPAR clustering at synapses. A similar enhancement of AMPAR lateral mobility has been noted when γ-2 interaction with PSD-95 was disrupted using dominant-negative biomimetic ligands (Sainlos et al., 2011). Of note, other synaptic scaffolding proteins, such as SAP-97, PSD-93 and SAP-102 have also been shown to interact with γ-2 (Chen et al., 2000).

1.10 Post-translational modification of TARPs

The C-termini of type I TARPs contain multiple phosphorylation sites. The use of phosphomimetic mutants showed that phosphorylation of T321 (located within the C terminal TTPV PDZ ligand) by PKA disrupts γ-2 binding to PSD-95 and reduces AMPAR-mediated synaptic transmission in hippocampal neurons (Chetkovich et al., 2002; Choi et al., 2002). However, incubation of cultured neurons with forskolin, which increases intracellular cAMP levels, failed to alter synaptic localisation of AMPARs (Chetkovich et al., 2002). It is thus possible that γ-2 is phosphorylated by PKA after reaching the synapse and that other synaptic scaffolding proteins interacting with TARPs (or directly with AMPAR subunits) may be important for retaining AMPARs at the synapse.

The T321 residue is also phosphorylated by mitogen activated protein kinase (MAPK). Mutations of consensus sequences for PKA and MAPK phosphorylation showed that phosphorylation by the two kinases bidirectionally regulates synaptic localisation of γ-2 during plasticity. Phosphorylation of T321 by PKA, but not by MAPK is required for synaptic clustering of γ-2 during chemical LTP in cultured hippocampal neurons. On the other hand, induction of LTD in response to mGluR agonist DHPG appears to require γ-2 phosphorylation by MAPK, but not by PKA (Stein and Chetkovich, 2010).

The C-terminus of type I TARPs contains 9 conserved serine residues, which are targets for phosphorylation by PKC and CaMKII. In hippocampal neurons, a phosphomimetic mutant in which all of these serines are phosphorylated enhances synaptic trafficking of AMPARs, occludes LTP and largely prevents LTD induction. The converse mutant, where all these phosphorylation sites are removed, prevents LTP induction (Tomita et al., 2005). Experiments in knock-in mice showed that in cerebellar granule cells, the phosphomimetic mutant of γ-2 showed increased mEPSC amplitude

reflecting an increase in synaptic AMPAR trafficking. The mechanism of increased synaptic trafficking of γ-2 upon its phosphorylation relies on the regulation of the interactions with lipid bilayers. Dephosphorylated γ-2 interacts with lipid bilayers, which compete for γ-2 interaction with PSD-95 (Sumioka et al., 2010). Indeed, phosphorylation of the γ-2 C-terminus by CaMKII induces synaptic trapping of γ-2-associated AMPARs by promoting interactions of the γ-2 C-terminus with synaptic scaffolding proteins. This appears to reduce the paired-pulse ratio in cultured hippocampal neurons, most likely due to inhibition of replacement of desensitizied AMPARs with functional ones by lateral diffusion (Opazo et al., 2010).

γ-2 has also been shown to be regulated by S-nitrosylation at C302. S-nitrosylation of γ-2 enhances its binding to GluA1 and promotes surface expression of both GluA1 and γ-2. Since NMDA treatment of cerebellar granule cells enhances S-nitrosylation of γ-2, this post-translational modification may play an important role in synaptic plasticity (Selvakumar et al., 2009).

1.11 AMPAR-TARP interaction

The molecular basis for AMPAR-TARP interaction is one of the major questions investigated in this Thesis. To date, several regions of both the TARP and the AMPAR have been identified as important for this interaction.

Interaction regions on the TARP

The Ex1 of γ-2 is one notable domain important for interaction with the AMPAR. Insertion of a HA tag into the C-terminal part of the γ-2 Ex1 loop reduced the amount of co-precipitated GluA2 and the amplitude of Glu-evoked current, suggesting that Ex1 is important for the binding and modulation of AMPARs by this TARP (Tomita et al., 2004). A chimeric construct in which Ex1 of γ-2 was replaced with that of γ-5 showed a greatly reduced KA/Glu ratio compared to wt γ-2, but did not affect GluA1 surface expression (Tomita et al., 2005). Another study showed that the replacement of Ex1 of γ-2 with that of γ-4 prolonged desensitization of GluA1 responses to a level seen with wt γ-4. The converse operation, replacing Ex1 of γ-4 with Ex1 of γ-2, produced responses with desensitization kinetics mimicking that of γ-2 (Cho et al., 2007). In addition, TARP isoform-specific effects on mEPSC amplitude, decay and rise time also appear to be governed by Ex1 (Milstein et al., 2007).

TARPs have been shown to contribute to the membrane density of AMPAR complexes isolated from rat brain (Nakagawa et al., 2005). In addition, the replacement of Ex1 and TM2 of γ-5 with that of γ-2 was sufficient to increase kainate efficacy to levels seen when GluA1 was co-expressed with wt γ-2, suggesting that TM2 may also contribute to modulation of kainate efficacy by TARPs (Tomita et al., 2005).

C-terminal truncations (Tomita et al., 2004) of γ-2 and chimeras with γ-5 (Tomita et al., 2005) showed that the C-terminus of TARPs is important for the enhancement of AMPAR surface trafficking by TARPs. The C-terminal interaction, however, appears not to affect the TARP-mediated increase in KA/Glu ratio (Tomita et al., 2005).

Despite previous studies providing some insight into TARP regions important for AMPAR/TARP interaction, the detailed map of the regions involved remains unresolved. Multiple domains might contribute to the modulation of native receptors by TARPs, as a construct containing the cytoplasmic domain of γ-2 and the transmembrane and extracellular (Ex1 and Ex2) domains of γ-8 increased amplitude and decay time constant of mEPSCs relative to γ-8 alone, when expressed in *stg* cerebellar granule cells (Milstein and Nicoll, 2009).

Interaction regions on the AMPAR

Previous studies suggest that γ-2 can still modulate GluA2 surface trafficking in the absence of the NTD (Bedoukian et al., 2006). Similarly, the γ-2-mediated slowing of GluA2 desensitization (Bedoukian et al., 2006) and enhancement of KA efficacy on GluA1 (Tomita et al., 2007) are retained in the absence of the NTD. However, none of these studies investigated whether the magnitude of γ-2 effect is the same in the absence of the NTD, a question which is addressed in Experimental Chapter 2 (Chapter 4) of this Thesis.

γ-2 has also been reported to interact with the LBD of AMPARs. The L497Y mutant of GluA1 disrupts AMPAR desensitization by altering the LBD conformation, as described above (Sun et al., 2002). When co-expressed with this mutant, γ-2 failed to enhance Glu-evoked current and showed only a small (albeit significant) increase in KA/Glu ratio (Tomita et al., 2007).

Another region implicated in AMPAR-TARP interaction are the linkers connecting AMPAR LBD to the membrane domains. As mentioned above, γ-2 appears to contribute to the binding site for the negative allosteric modulators GYKI 53655 and CP-465,022. These drugs have been shown to bind to the S1-M1 and S2-M4 linkers (Balannik

et al., 2005). The γ-2-mediated enhancement of GYKI 53655 binding to GluA1 is largely mediated by Ex1 of γ-2, since the co-expression of a chimeric TARP in which Ex1 of γ-2 has been replaced with that of γ-5 reduced GYKI 53655 binding compared to wt γ-2 (Cokić and Stein, 2008). Thus, previous studies suggest that Ex1 of γ-2 interacts with the LBD-membrane domain linker region of AMPARs, a finding which appears consistent with the results shown in Experimental Chapter 1 (Chapter 3) of this Thesis.

There is also evidence for involvement of AMPAR transmembrane domains in TARP modulation. The A636T mutation targets a GluA1 residue located in the channel gate formed by the M3 helix, as described above, and is analogous to the mutation found in *Lurcher* mice. The A636T GluA1 mutant showed no enhancement of Glu-evoked current upon γ-2 co-assembly. γ-2 also failed to modulate KA/Glu ratio and surface expression of this mutant, suggesting a critical role of this membrane region in TARP interaction (Tomita et al., 2007). Mutations of the Q/R site also affect γ-2-mediated increase in GluA1 surface trafficking and KA/Glu ratio as well as the slowing of desensitization upon γ-2 co-assembly (Körber et al., 2007).

It is worth noting, that in the study by Körber et al. (2007) γ-2 did not appear to affect GluA1 block by NASPM, irrespective of the amino acid present at the Q/R site. NASPM, like other extracellular polyamines, is though to bind directly to the channel pore in a manner dependent on Q/R editing. Thus, the lack of TARP effect on NASPM block suggests that the effect of the Q/R site on TARP function may arise from an allosteric interaction elsewhere in the AMPAR. Further research would be required to determine the involvement of the AMPAR channel pore in TARP interaction and to explain the conflicting reports on the effect of TARPs on AMPAR block by extracellular polyamines (compare for instance Körber et al. 2007; Kott et al. 2009 and Jackson et al. 2011). Indeed, it appears that there is a complex allosteric interaction between γ-2 and the membrane and LBD regions of the AMPAR, since the effect of γ-2 on extracellular polyamine block is strongly dependent on the efficacy of the agonist used to activate AMPARs (Poulsen et al., 2014b) and thus on the degree of LBD cleft closure.

Finally, as described above, the C-terminus of γ-2 is critical for surface and synaptic trafficking of AMPARs. This interaction appears to be controlled by the C-terminus of AMPARs, since C-terminal truncation mutants of GluA1 or GluA2 showed little enhancement of surface trafficking upon γ-2 co-expression. On the contrary, the γ-2-mediated slowing of GluA1 desensitization was unaffected in the C-terminal GluA1 mutant (Bedoukian et al., 2006). However, the details of γ-2 interaction with the AMPAR C-terminus appear elusive, as the study failed to identify amino acids in the

AMPAR C-terminus responsible for γ-2-mediated increase in surface expression.

1.12 The role of TARPs in disease

Studies employing genetic analysis suggests TARPs may be linked to a variety of neurological diseases. Homozygosity analysis of a family with high incidence of epilepsy, hearing impairment and schizophrenia showed that the disease loci mapped to a region of chromosome 22 where the CACNG2 gene is located. However, no mutations in the exons of CACNG2 were found (Knight et al., 2008). On the other hand, CACNG3 (located on chromosome 16; Everett et al. 2007) but not CACNG2 (Abouda et al., 2010) has been implicated in a specific form of epilepsy, namely childhood absence epilepsy.

Changes in TARP protein levels were found in a rat model of schizophrenia (Drummond et al., 2013). Indeed, genetic analysis showed that the CACNG2 gene may be implicated in a subpopulation of schizophrenia patients (Liu et al., 2008). In addition, post-mortem analysis of brains from schizophrenia patients revealed abnormally increased γ-2 expression in the dorsolateral prefrontal cortex (Beneyto and Meador-Woodruff, 2006).

Polymorphisms in the CACNG2 gene have also been implicated in bipolar disorder and susceptibility to lithium treatment (Silberberg et al., 2008). γ-2 also appears to affect pain processing in mice. Polymorphisms in the CACNG2 gene appear to associate with chronic pain following breast surgery in cancer patients (Nissenbaum et al., 2010).

1.13 Other AMPAR auxiliary subunits

CNIH proteins

TARPs were the first auxiliary AMPAR subunits identified. The proteomic approach, involving mass spectrometry investigation of native AMPAR precipitates, has since been successfully employed to identify other auxiliary subunits of AMPARs. CNIH-2 and CNIH-3 have been shown to form complexes with AMPARs and modulate AMPAR properties, such as deactivation and desensitization kinetics and surface expression (Schwenk et al., 2009; Coombs et al., 2012). However, unlike TARPs, CNIH-2 has

little effect on recovery from desensitization (Schwenk et al., 2009) or KA/Glu ratio (Shi et al., 2010).

In neurons CNIH-2 appears to be restricted to certain cell types. CNIH-2 fails to rescue synaptic currents in *stg* mice, but increases whole-cell currents, consistent with enhancement of surface trafficking of AMPARs. In addition, its expression in cerebellar granule cells from *stg* heterozygotes has no effect on AMPAR kinetics (Shi et al., 2010). Similarly, in cerebellar Purkinje cells CNIH-2 apparently fails to reach the cell surface (Gill et al., 2011). In the hippocampus, on the other hand, γ-8 and CNIH-2 appear to co-assemble in the same complexes to modulate AMPAR responses (Kato et al., 2010a; Gill et al., 2011). Of note, Shi et al. (2010) found no evidence for slowing of AMPAR gating kinetics upon CNIH-2 transfection into CA1 hippocampal pyramidal cells in slice cultures. However, the result could potentially be explained by the use of wt mice, where AMPR stoichiometry was already saturated, so that addition of more CNIH-2 failed to affect AMPAR properties. A recent study showed, that the CNIH-2-mediated slowing of AMPAR deactivation and desensitization, even more pronounced than that seen with TARPs, modulates synaptic currents in the hippocampus in a cell-specific manner (Boudkkazi et al., 2014). The interaction between AMPARs and CNIH-2 is also likely to be subunit-specific, as CNIH-2 knockout mice display a profound loss of synaptic GluA1 (Herring et al., 2013).

CKAMP44

The hippocampus is also the predominant site of expression of another AMPAR auxiliary subunit, CKAMP44 (cystine-knot AMPAR modulating protein, von Engelhardt et al. 2010). Its expression appears to be particularly high in the dentate granule cells. CKAMP44 increases the rate of AMPAR desensitization and slows recovery from it. Overexpresion of this protein also slows deactivation of AMPARs. In addition, CKAMP44 increases the potency of the agonist glutamate and reduces the potency of the allosteric potentiator CTZ, suggest a role in modulation of AMPAR pharmacology. Physiologically, CKAMP44 knock-out results in increased paired-pulse ratio upon stimulation of the lateral or medial perforant path, suggesting a role for this protein in synaptic transmission in the dentate gyrus.

GSG1L

GSG1L is a protein related to claudins and TARPs, which has been recently identified as an auxiliary AMPAR subunit (Shanks et al., 2012). Co-expression of this protein with GluA2Q appears to slow both desensitization and recovery from it. GSG1L seems to efficiently increase AMPAR surface expression in a recombinant system and, transfected into cultured cortical neurons, colocalises with AMPAR subunits at the cell surface and the synapse.

AMPARs form multicomponent complexes

A recent study (Schwenk et al., 2012) employed the proteomics approach to reveal a great diversity of putative AMPAR auxiliary subunits. While some of them, such as TARPs and CNIH proteins, are relatively well studied, very little is known about other candidates. Multiple auxiliary proteins may co-assemble with varying stoichiometry, suggesting a complex regulation of native AMPARs in different brain regions, cell types and developmental stages. The study also suggests that the binding of some AMPAR auxiliary subunits may be mutually exclusive, suggesting additional means for AMPAR regulation by competition for AMPAR binding between different auxiliary proteins.

2

Materials and Methods

2.1 HEK-293 cell culture

HEK-293, HEK-293T or tsA201 cells were cultured in DMEM (Sigma) supplemented with 10% FBS (LifeTechnologies) and 5% penicillin/streptomycin (LifeTechnologies). Cells were maintained at 37°C and 5% CO_2 in a humidified incubator.

2.2 Heterologous expression of AMPARs

Cells were grown in a T-25 flask as described above, until a confluent monolayer was formed. Cells were then washed with PBS (LifeTechnologies), incubated with 0.5 ml of 0.05% trypsin-EDTA (Sigma) at 37°C for approximately 2 minutes, resuspended in 5-6 ml of culture media and mechanically dissociated by pipetting. The cells were then seeded in a 4-well plate (0.5 ml of cell suspension per well) and transfected with the appropriate DNA using Lipofectamine 2000 (LifeTechnologies), according to the protocol provided by the manufacturer. A total of 1 μg of DNA was used per transfection. The medium used for transfection was OptiMEM (LifeTechnologies). Transfection was terminated after 4-14 hours, cells were dissociated with trypsin-EDTA and seeded onto glass cover slips pre-coated with poly-L-lysine (0.02 mg/ml, Sigma). Following transfection, the media was supplemented with 50-200 μM NBQX to avoid AMPAR-mediated toxicity. Cells were used for electrophysiological recordings 24-72 hrs after transfection.

For the whole-cell experiments described in Experimental Chapter 3 (Chapter 5), a slight modification of the transfection procedure was introduced, in order to better

control the final cell density and allow whole-cell recording from isolated cells. The transfection was terminated after 4-10 hrs by replacement of media. The cells remained in the incubator until approximately 12 hours before recording, when they were trypsinised and seeded onto glass cover slips. Reducing the time between seeding the cells and recording limited cell division on the cover slips, providing more single, isolated cells than the approach typically used to prepare cells for outside-out patch recordings.

Although AMPARs posses several trypsin cleavage sites, and trypsin is often used to digest AMPARs into peptides (see for instance Schwenk et al., 2012) trypsinization of cells after transfection was unlikely to affect the experiments described here. Previous studies report turnover half-lives of 18 $\pm$ 5 hrs and 23 $\pm$ 8 hrs for total GluA2/3 and GluA4, respectively, measured in cultured celebellar cells (Huh and Wenthold, 1999). The half-lives of surface receptors were similar at 17 $\pm$ 4 and 21 $\pm$ 5 h for GluR2/3 and GluR4 subunits, respectively (Huh and Wenthold, 1999). Since for the experiments described in this thesis the cells were trypsinised 12 hours or more before recordings, this should have permitted the exchange of a large proportion of trypsin-digested receptors.

2.2.1 DNA constructs

All rat AMPAR subunits used for the recordings were R/G edited and flip. Both the unedited (Q) and edited (R) forms of the GluA2 subunit were used, as indicated in the appropriate Chapters. The GluA3 subunit used (whether alone or in a TARP-containing tandem construct) contained the R461G mutation, which has been reported to facilitate surface expression (Coleman et al., 2010).

To allow visualisation of transfected cells, cDNA of interest was cloned into the pIRES-EGFP vector (Clontech) or co-transfected with GFP at a fixed GFP amount of 60 ng per each 1 μg total DNA tranfection.

Two TARPs were used in the experiments described here: rat γ-2 (including all mutants and tandem contructs) and human γ-7 (used in tandem AMPAR-TARP constructs).

2.2.2 Transfection ratios

AMPAR:TARP ratio

All experiments with TARPed AMPARs were performed at 1:6 AMPAR subunit:TARP ratio. The 6-fold excess of the TARP was used to maximise the fraction of fully-TARPed AMPARs in the transfected cells.

Heteromeric GluA2R-containing AMPARs (whole-cell experiments in Experimental Chapter 3)

In order to facilitate heteromeric AMPAR assembly, both the TARPless GluA2/3 controls and the tandem AMPAR-TARP contructs were transfected at a 2:1 GluA2:GluA3 ratio, so that the GluA2(R) subunit was in excess.

Heteromeric GluA2R-containing AMPARs (outside-out patch experiments in Experimental Chapter 3)

In order to facilitate heteromeric AMPAR assembly, the ratio of GluA2(R) to GluA1 was adjusted for each type of transfection, however, the GluA2(R) subunit was always in excess. The most commonly employed GluA1:GluA2 ratio for each transfection is indicated in bold.

TARPless GluA1/2: **1:2** or 1:5
GluA1-γ-2 tandem + GluA2 (2 TARP) **1:5** or 1:20
GluA1 + GluA2-γ-2 tandem (2 TARP) 1:5 or **1:20**
GluA1-γ-2 tandem + GluA2-γ-2 tandem (4 TARP) 1:2, **1:5**, 1:10 or **1:20**

2.3 Cloning of the GluA3-containing tandem constructs

The whole-cell experiments described in Experimental Chapter 3 (Chapter 5) required cloning of two tandem constructs: GluA3-γ-7 and GluA3-γ-2. Both constructs were cloned into the pIRES-EGFP. Phusion HF Master Mix polymerase (Finnzymes) was used for all PRC reactions and all primers were from Sigma Genosys. The pIRES-EGFP vector was also used by Dr Ian Coombs to clone the GluA1-γ-2 and GluA2(R)-γ-2 constructs used in the experiments described in Experimental Chapter 3. A schematic plasmid map for all tandem constructs is shown in Fig 2.1 A, while the individual restriction sites are listed in Fig 2.1 B.

A

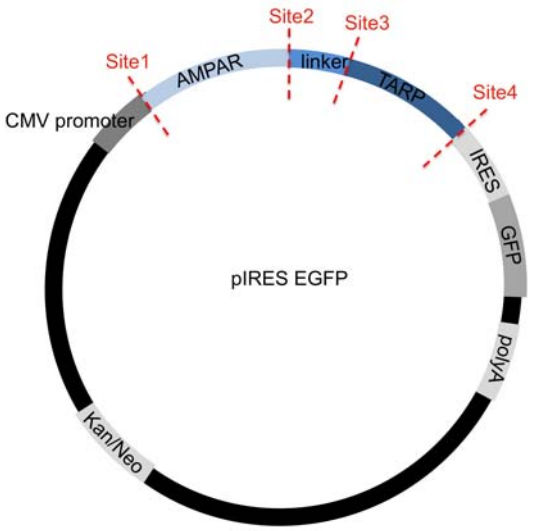

B

AMPAR	TARP	Site 1	Site 2	Site 3	Site 4
GluA1	γ-2	NheI	EcoRI§	EcoRI	SalI
GluA2*	γ-2	NheI	EcoRI§	EcoRI	SalI
GluA3	γ-7	NheI	XhoI	EcoRI	SalI
GluA3$	γ-2	N/A	N/A	N/A	N/A

•GluA2 with endogenous EcoRI site removed by silent mutation

$ Construct created using a blunt-end ligation as described in the text

§ The linker for these constructs is GGGGGEFAT, as described in Chapter 3. The glycines were encoded in the primers, the EF is coded by EcoRI site, while AT is coded by the Kozak sequence (GCCACC) which had already been already present in the TARP construct used. These tandem constructs were made by Dr Ian Coombs.

Figure 2.1: Schematic maps of the AMPAR-TARP tandem constructs used in this thesis. (**A**) Location of the AMPAR and TARP inserts in relation to the selected elements of the pIRES - EGFP vector: 1. the CMV promoter used for expression of the tandem construct in mammalian cells, 2. the AMPAR insert (with endogenous stop codon removed as described below), 3. the linker and 4. the TARP insert. The inserts are followed by 4. IRES (internal ribosome entry site) used for expression of the GFP; 5. GFP and 6. the poly-A tail. The approximate location of the Kan/Neo resistance gene is also indicated. The relative sizes of the individual elements are not drawn to scale. Position of the restriction sites used to create the tandem constructs is indicated by dashed red lines and the sites are numbered 1-4 from N- to C-terminal end of the tandem construct. Please note, that the restriction sites used are all within the multiple cloning site of the vector. (**B**) The identity of the restriction sites used to generate tandem AMPAR-TARP constructs. The sites are numbered 1-4 in consistence with the map in panel A. Please note that no restriction sites were used for the GluA3-γ-2 tandem. This construct was generated by replacing γ-7 with γ-2 in the GluA3-γ-7 tandem, using a blunt-end ligation as described in the text. **Note:** The GluA1-γ-2 and GluA2-γ-2 tandems were made by Dr Ian Coombs.

2.3.1 GluA3-γ-7 tandem

GluA3 was first amplified using the following primers:

- **forward primer:** 5‘ AAAAA**GCTAGC**ATGGGGCAAAGCGTGCTC 3‘
  the NheI restriction site introduced immediately before the start of GluA3 is indicated in bold.

- **reverse primer:** 5‘ AAAAA**CTCGAG**CCGATCTTAACACTTTCTGTTCC 3‘
  the XhoI restriction site introduced immediately after the last codon of GluA3 is indicated in bold. Note that the STOP codon at the end of GluA3 was removed with this primer, which allowed the AMPAR and the TARP to be translated continuously as a single protein.

The PCR product was subsequently digested with NheI and XhoI (both enzymes from New England Biolabs). The γ-7 construct in pIRES-EGFP was also digested with the same enzyme pair. Both the GluA3 insert and the γ-7-containing vector were run on a 1% agarose (Sigma) gel and purified using the PureLink Quick Gel Extraction and PCR Purification Combo kit (LifeTechnologies). The vector was subsequently dephosphorylated using Antarctic Phosphatase (New England Biolabs) and purified using High Pure PCR Cleanup Micro kit (Roche). To generate the tandem GluA3-γ-7 construct, a sticky-end ligation was performed using the Rapid DNA Ligation kit (Roche). Construct was confirmed using DNA sequencing of the linker region, however, the full length of the construct was not sequenced.

The final sequence of the 9 amino acid linker between GluA3 and γ-7 was: GGC TCG AGC TCA AGC TTC GAA TTC GGA, corresponding to G S S S S F E F G.

2.3.2 GluA3-γ-2 tandem

The GluA3-γ-2 tandem construct was cloned by substituting γ-7 in the GluA3-γ-7 tandem with γ-2. This was achieved by amplifying the pIRES-EGFP vector (complete with GluA3 and the linker) in one PCR reaction and separately amplifying γ-2, followed by a blunt-end ligation.

The primers for the GluA3 + linker + vector PCR were as follows:

- **forward primer:** 5‘ GTCGACGGTACCGCGGG 3‘
  This primer was designed to read into the pIRES-EGFP vector after γ-7.

- **reverse primer:** 5‘ TCCGAATTCGAAGCTTGA 3‘
  This primer was designed to amplify the vector from the end of the linker (starting immediately before γ-7).

The primers for the γ-2 (insert) PCR were as follows:

- **forward primer:** 5‘ P -ATGGGGCTGTTTGATCGA 3‘
  Phosphorylated primer amplifying from the start of γ-2.

- **reverse primer:** 5‘ P- TCATACGGGCGTGGTCCG 3‘
  Phosphorylated primer amplifying from the end of γ-2 (including the STOP codon).

Both the vector (pIRES-EGFP + GluA3 + linker) and insert (γ-2) PCR products were treated with DpnI (New England Biolabs) to remove template DNA, run on a 1% agarose gel and purified using the PureLink Quick Gel Extraction and PCR Purification Combo kit, according to the manufacturer instructions. Blunt-end ligation was performed with the Rapid DNA Ligation kit. The sequence of the linker between GluA3 and γ-2 was the same as described above for γ-7. Construct was confirmed using DNA sequencing of the linker region, however, the full length of the construct was not sequenced.

2.4 Drugs and abbreviations

Abbreviation	Full name	Mechanism of action	Manufacturer
CNQX	6-cyano-7-nitroquinoxaline-2,3-dione	competitive antagonist / partial agonist	Abcam or Tocris Bioscience
CTZ	cyclothiazide	allosteric potentiator and desensitization blocker	Abcam or Tocris Bioscience
Glu	L-glutamate	agonist	Sigma
KA	kainate	partial agonist	Abcam or Tocris Bioscience
NBQX	2,3-dihydroxy-6-nitro-7-sulfamoyl-benzo[f]quinoxaline-2,3-dione	competitive antagonist	Abcam or Tocris Bioscience
PhTx-74	philantotoxin-74	channel blocker	Tocris Bioscience
spermine	spermine tetrahydrochloride	channel blocker (CP-AMPARs)	Sigma

Table 2.1: List of drugs and their abbreviations. Abbreviations in the first column are widely used in the text and figures in this Thesis. The mechanism of action (3rd column) refers to AMPARs.

2.5 Electrophysiological recordings

Cells were visualised using a fixed stage upright microscope (Axioskop; Zeiss). Currents were recorded using an Axopatch-1D amplifier and a Digidata 1322A A-to-D interface (both Axon Instruments).

2.5.1 Patch electrodes

Thick walled borosilicate glass (1.5mm o.d., 0.86 mm i.d.; Harvard Apparatus) was used to pull patch electrodes using a two-step vertical puller (Narishige). Electrical capacitance of the electrodes was reduced by coating with Sylgard (Dow Corning 184), which was solidified using a heating coil. The electrodes were heat-polished

to achieve resistance of 6-14 MΩ for outside-out patch experiments and 4-6 MΩ for whole-cell experiments. Electrodes were filled with internal solution, containing 145 mM CsCl, 2.5 mM NaCl, 1 mM EGTA-Cs, 4 mM MgATP, 10 mM HEPES, adjusted to pH 7.3 with CsOH. All chemicals were from Sigma, Fisher or VWR. Internal solution was supplemented with spermine tetrahydrochloride (100 μM) for all experiments apart from those involving the measurement of KA/Glu response ratios.

2.5.2 Fast agonist application to outside-out patches

The bath was perfused with standard external solution (145 mM NaCl, 2.5 mM KCl, 1 mM $CaCl_2$, 1 mM $MgCl_2$, 10 mM glucose and 10 mM HEPES, adjusted to pH 7.3 with NaOH). However, bath perfusion was typically stopped during the recording to minimise noise arising from both the perfusion itself and the suction. Rapid application of agonist solution to outside-out patches pulled from HEK-293, HEK-293T or tsA201 cells was achieved using a fast application tool made from theta glass (2mm o.d.; Hilgenberg GmbH) pulled to a tip diameter of approx. 200 μm. The fast application tool was mounted on a piezoelectric translator (Burleigh PZ-150M). Control and drug solutions flowed continuously through the two barrels of the theta glass. Perfusion was achieved by raising the reservoirs (50 ml syringe tubes) feeding into the fast application tool (gravity perfusion). In addition to standard external solution, drug solution contained L-glutamate (10 mM) and was supplemented with 2.5 mg/ml sucrose to allow visualisation of the solution interface. The control solution was a standard external solution diluted by 5% with distilled water to reduce osmolarity, allowing the liquid junction current to be measured. Currents were low-pass filtered at 10 kHz and digitised at 50 kHz. At the end of each experiment the speed of solution exchange was assessed by destroying the patch and measuring the liquid-junction current at the open pipette tip. Typically, the 20-80% rise time of the liquid-junction current was < 200 μs.

Patches with a seal resistance of <4 GΩ were rejected, as were those in which the current amplitude was small and the holding current amplitude exceeded that of the peak current. Sweeps with external noise were excluded and only epochs with stable current amplitudes and current shapes were analysed. If enough stable sweeps could not be obtained, the records were rejected. The liquid-junction currents were examined for abnormalities of glutamate application, such as additional brief glutamate application following the intended one, and patches where these abnormalities occurred were also rejected. In addition, for the analysis of deactivation, currents with a 20-80% rise time of >300 μs (usually coupled with an aberrant current shape and prolonged decay) were also rejected. The latter selection criterium was established

due to the consistent observation that a very slow rising current was often coupled with a slow decay (despite the solution exchange speed being normal). This could reflect delayed glutamate perfusion onto the patch due to folding of excess membrane at the electrode tip (Ruknudin et al., 1991) or the patch being positioned too far up the electrode (Suchyna et al., 2009).

2.5.3 Whole-cell electrophysiology

The bath was constantly perfused with standard external solution (composition as described above). Local application of agonist solutions to tsA201 cells was achieved using a fast application tool made from theta glass mounted on a piezoelectric translator as described above. However, rapid solution exchange was not performed. Instead, the cell was constantly bathed in control solution (standard external solution), and, when required, the perfusion was switched to the other barrel of the theta glass containing agonist solution. The recordings were performed by repeatedly applying a -5 mV voltage step (10 ms duration) at the rate of 1 Hz. This allowed measurement of the agonist response (by measuring the change in holding current, I_{hold}) and simultaneous monitoring of changes in series (R_s) and input resistances. Currents were low-pass filtered at 10 kHz and digitised at 100 kHz (CNQX/Glu ratio) or 5 kHz (voltage ramps).

Currents were included in the analysis when the change in R_s during the course of the record was < 30%. R_s change was measured as the difference in R_s between the last control sweeps prior to application of CNQX and the last control sweep prior to application of Glu. Cells where the ratio of the initial I_{hold} (average in control prior to CNQX application) to whole-cell capacitance exceeded 15 pA/pF were excluded, as were cells where fluctuations in I_{hold} occluded the measurement of agonist responses.

2.5.4 Application of multiple agonists

To allow switching between multiple agonists a modification of the standard solution delivery system was used. This modified approach was required for the measurement of KA/Glu and CNQX/Glu response ratios, as well as for experiments involving PhTx-74 block.

Instead of connecting the fast-application tool directly to the perfusion system, a di-

vider made from theta glass was introduced between the perfusion tubing and the fast application tool. This allowed two different solutions to be fed into each barrel of the fast application tool, as shown schematically in Fig. 2.2 below. Switching between the solutions was achieved by closing one of the two lines and simultaneously opening the other, allowing the new solution to fill the fast application tool. The completion of the solution exchange was assessed by visualising the response.

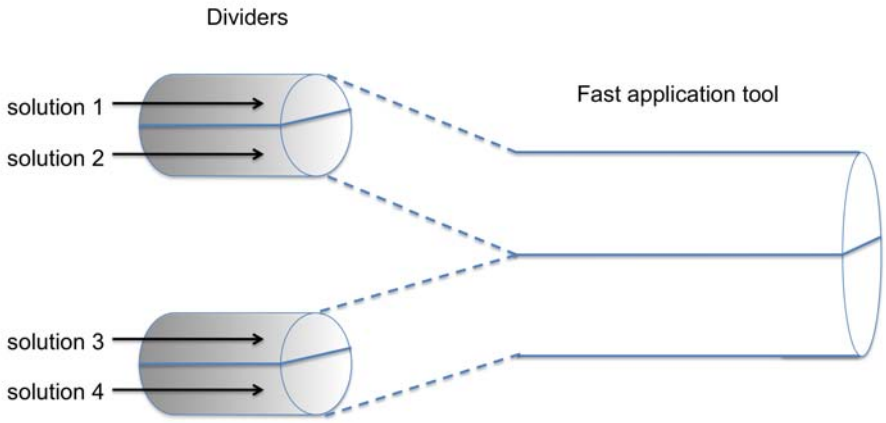

Figure 2.2: Modification of the solution delivery system used for application of multiple agonists. Each barrel of the fast application tool was connected to a divider via a piece of tubing (represented by a dashed line). The divider, made from theta glass itself, was in turn connected to two perfusion lines, allowing the flow in each barrel of the fast application tool to be switched between two solutions. Thus, up to four different soltuions (instead of the standard two) could be used during each experiment.

For KA/Glu response ratios this method was used to switch between Glu and KA (control solution flowed continuously in the other barrel).

For the whole-cell measurements of CNQX/Glu ratio, dividers were connected to both barrels of the theta glass, so that the solution in each barrel could be switched between one of the agonists and control. This allowed rapid onset and offset of both CNQX and Glu current: the cell could be rapidly exposed to agonist or control by switching the perfusion between the two barrels of the theta glass. However, this method required a period of solution exchange in both barrels between the recordings of the currents evoked by the two agonists.

Outside-out patch experiments involving PhTx-74 block were performed in a manner similar to that described above. One barrel of the fast application tool was connected

to two control solutions: standard control solution and control solution supplemented with 100 μM CTZ. The other barrel was connected to two Glu-containing solutions: one containing 10 mM Glu only and the other further supplemented with 100 μM CTZ and 1 mM PhTx-74 . Solutions flowed continuously through both lines of the fast application tool. Rapid exchange between control and Glu-containing solutions was achieved as described above. This method allowed measurement of the Glu response first and subsequent visualisation of PhTx-74 block by switching to solutions also containing CTZ and CTZ + PhTx-74.

2.6 Data analysis

All data were acquired using Clampex 8.2.0.232 (Axon Instruments) and analysed using IGOR Pro (version 6.20, Wavemetrics) and NeuroMatic (version 2.5; http://www.neuromatic.thinkrandom.com).

2.6.1 Deactivation kinetics

Deactivation kinetics was studied using 1 ms applications of 10 mM Glu at -60, -80 or +40 mV as indicated. Selected sweeps were aligned at the 20% current rise (measured at 4 kHz low-pass filtering to obtain accurate rise times regardless of current amplitude). The decay of the average current was typically fitted with a single or double exponential constrained to reach the abscissa. In some cases, a triple exponential fit was required.

Single exponential:

$$I(t) = I_0 + Ae^{\frac{-(x-x_0)}{\tau}} \tag{2.1}$$

Double exponential:

$$I(t) = I_0 + A_{\text{fast}}e^{\frac{-(x-x_0)}{\tau_{\text{fast}}}} + A_{\text{slow}}e^{\frac{-(x-x_0)}{\tau_{\text{slow}}}} \tag{2.2}$$

Triple exponential:

$$I(t) = I_0 + A_1e^{\frac{-(x-x_0)}{\tau_1}} + A_2e^{\frac{-(x-x_0)}{\tau_2}} + A_3e^{\frac{-(x-x_0)}{\tau_3}} \tag{2.3}$$

For the double and triple exponential fits weighted τ (τ_{w}) was calculated as the mathematical average of the τ for each component weighted by their relative amplitudes.

2.6.2 Desensitization kinetics

Desensitization was produced by 100 ms applications of 10 mM Glu at -60, -80 or +40 mV as indicated. Selected sweeps were aligned at the 20% current rise (measured at 4 kHz low-pass filtering). Decay of the current was fitted with a single or double exponential (equations 2.1 and 2.2), as described above for deactivation kinetics, but with no constraints on any of the parameters. The extent of desensitization was quantified by calculating the% of peak current remaining at the end of Glu application (% steady-state current, I_{ss}), according to the equation:

$$\%I_{ss} = \frac{A_0}{(A_{fast} + A_{slow} + A_0)} \times 100 \tag{2.4}$$

2.6.3 Recovery from desensitization

A paired-pulse protocol was used to assess the rate of recovery from desensitization. The patches were held at -80 or +40 mV as indicated. A desensitizing 100 ms pulse of 10 mM Glu was followed by a 10 ms pulse (10 mM Glu). The inter-pulse interval was initially set at 5 ms and increased with every sweep: first in 5 ms increments (10 sweeps), then in 10 ms increments (10 sweeps) and finally in 20 ms intervals (varying the number of sweeps until recovery was complete). For every cell, each inter-pulse interval was repeated (typically 3-5 times) and the the ratios of the 2nd peak to 1st peak amplitudes were averaged for each inter-pulse interval. The currents were low-pass filtered to 1 kHz to minimise the effect of noise on amplitude measurements. For each patch, the average amplitude ratio was plotted (on a linear scale) against the inter-pulse interval (on a logarithmic scale) and the data was fitted to a Hodgkin-Huxley-type function (Carbone and Plested, 2012):

$$N = N_0 + (1 - N_0)(1 - e^{(-k_{rec}\Delta t)})^n \tag{2.5}$$

where N is the fraction of active receptors at the given time difference (Δt) between the first and second pulse, N_0 is the fraction of active receptors at the end of the first pulse, n is a slope factor and k_{rec} is the rate of recovery from desensitization. The time needed for the second peak to recover to 50% of the first peak (t_{50}) was then obtained from the fit.

2.6.4 Kainate/Glutamate ratios

KA/Glu ratios were recorded at -60 mV using 500 μM KA (in standard external solution) and 500 μM Glu (in external solution supplemented with 2.5 mg/ml sucrose). The control solution (diluted with 5% dH_2O) as well as both agonist solutions were supplemented with 100 μM CTZ to limit AMPAR desensitization (Yamada and Tang, 1993) and allow comparison of the steady-state current evoked by the two agonists. Fifteen 100 ms agonist pulses were recorded for each application. The patch was first exposed to Glu before switching to KA and back to Glu. To minimize the influence of any gradual decline in peak response on the estimate of KA/ Glu ratio, the response to Glu used to calculate the ratio was an average of the response to Glu preceding and following the application of KA.

2.6.5 CNQX/Glutamate ratios

Whole-cell responses to CNQX (10 μM) and Glu (50 μM) were measured by locally applying the agonists, as described above, and measuring the changes in I_{hold}. Control, Glu and CNQX solutions were supplemented with 50 μM CTZ to limit AMPAR desensitization. Cells were held at +40 mV in the presence of intracellular spermine (100 μM) to minimise the contribution of Ca^{2+}-permeable GluA3 homomers. CNQX and glutamate were applied for 20 sweeps each. To minimise the effect of small baseline fluctuations on the measurement of CNQX and Glu currents, the response was calculated as the difference between the agonist I_{hold} and the average of the control I_{hold} (before and after the agonist). The CNQX-evoked current was then expressed as a % of the Glu-evoked current.

2.6.6 PhTx-74 block

Patches were held at -80 mV and, initially, rapidly exposed to 10 mM Glu (100 ms) as described above. After the response to Glu alone was obtained, both solutions were replaced. The control solution (diluted with 5% distilled H_2O) was replaced with a solution additionally supplemented with 100 μM CTZ to limit AMPAR desensitization and allow observation of PhTx-74 block (Jackson et al., 2011). The Glu solution (supplemented with sucrose, as described above) was replaced by a solution containing 10 mM Glu, 100 μM CTZ and 1 mM PhTx-74. The patch was then rapidly exposed to the new solution pair (100 ms). PhTx-74 block could thus be observed in every sweep. However the degree of block could not be quantified, since PhTx-74 was applied only

in the Glu solution and not in the control.

2.6.7 Non-stationary fluctuation analysis (NSFA)

Non-stationary fluctuation analysis allows one to deduce single-channel properties from macroscopic responses, such as those seen in outside-out patches. Glutamate (10 mM) was applied to AMPAR-containing outside-out patches (100 ms) and the ensemble variance of all successive pairs of current responses was calculated to minimise the effect of time-dependent changes on current variance estimate (Conti et al., 1980). The mean current was divided into 10 bins of equal amplitude and so was the corresponding enseble variance. The single-channel current (*i*) and the total number of channels in the patch (*N*) were determined by plotting this ensemble variance (σ^2) against mean current ($\bar{I}$) and fitting with a parabolic function (Sigworth, 1980):

$$\sigma^2 = i\bar{I} - \frac{\bar{I}^2}{N} + \sigma^2{}_{\mathrm{B}} \tag{2.6}$$

where $\sigma^2{}_{\mathrm{B}}$ is the background variance.

In addition to the expected variation in current amplitudes due to stochastic channel gating, some patches showed gradual changes in peak amplitude (rundown). Thus, the mean response was calculated from epochs containing a minimum of 30 stable amplitude responses. The mean single-channel conductance was calculated by dividing the single-channel current (*i*) obtained from equation 2.6 by the holding potential (assuming the reversal potential was 0 mV). Peak open probability (P_{o}) was estimated by dividing the mean peak current ($\bar{I}$) by the mean single-channel current (*i*) and the number of channels in the patch (*N*).

To plot the mean parabolic variance-current relationships, current variance for each patch was normalised to the size of the current by dividing it by the mean peak current for that patch. Mean current was also normalised for each bin, by dividing it by the maximum peak current (1$^{\mathrm{st}}$ amplitude bin). NSFA was carried out using a custom macro for IGOR Pro and NeuroMatic, written by Prof. Mark Farrant, which provided an estimate of the fit parameters together with their standard deviation.

2.6.8 Current-voltage plots: homomeric AMPARs

For the experiments described in Experimental Chapters 1 and 2, peak *I-V* plots were generated from responses to 1 ms applications of 10 mM Glu. The voltage was stepped from -100 mV to +60 mV in 10 mV increments and Glu was applied at each voltage. Mean current amplitudes at each voltage (low-pass fitered to 1kHz to allow accurate amplitude measurement) were normalised to the peak current at -100 mV and plotted against the membrane potential. The *I-V* relationships were fitted with 8^{th}-9^{th} order polynomials.

2.6.9 Quantification of rectification: homomeric AMPARs

Rectification index (RI) was determined from current-voltage relationships described above, as the ratio of slope conductance at positive potentials (between +40 mV and +60 mV) and negative potentials (between -60 mV and -40 mV). Slope conductance was calculated by fitting the *I-V* relationships in these two voltage regions to a linear function:

$$y = ax + C \tag{2.7}$$

where a is the slope conductance. Thus, for a completely linear *I-V* relationship, rectification index equaled 1.

2.6.10 Conductance-voltage plots

Current-voltage plots were generated as described above. The average peak current at each voltage was then divided by the holding potential to obtain conductance measurements. The data was fitted to the Boltzmann equation:

$$G(V_{\mathrm{m}}) = G_{\mathrm{max}} \frac{1}{1 + e^{(\frac{V_{\mathrm{m}} + V_{0.5}}{k})}} \tag{2.8}$$

between -100 mV and -10 mV. The data was then normalised by dividing conductance values by the maximal conductance (G_{max}) value obtained from the fit, so that the plots show normalised peak conductance (G) plotted against membrane voltage (V_{m}). The fit allowed to obtain estimation of $V_{1/2}$, which is the voltage at which spermine block is half-maximal and k, which is a slope factor describing the membrane potential shift

necessary to cause an e-fold change in conductance.

2.6.11 Quantification of rectification: heteromeric AMPARs

For the outside-out patch experiments described in Experimental Chapter 3, a less refined method of estimating rectification was used. To assess whether heteromeric assembly (indicated by a linear *I-V* relationship) had been achieved, the patch was first held at -60 mV and a 100 ms pulse of 10 mM Glu was applied. The patch was then stepped to +60 mV and another 100 ms pulse of 10 mM Glu was applied. The ratio of the peak responses at +60 and -60 mV (low-pass filtered to 1 kHz) was used to quantify RI, assuming the reversal potential was 0 mV. Thus, for a completely linear *I-V* relationship, rectification index equaled 1.

2.6.12 Whole-cell measurement of RI

For the whole-cell experiments described in Experimental Chapter 3, RI was determined by ramping V_m from +60 to -60 mV in the presence and absence of Glu (50 μM). Control and Glu solutions were supplemented with 50 μM CTZ. The *I-V* relationship obtained in the absence of Glu was then subtracted from that obtained in Glu. RI was calculated as the ratio of slope conductance at positive potentials (between +40 mV and +20 mV) and negative potentials (between -20 mV and -40 mV). Slope conductance was calculated by fitting the *I-V* relationships in these two voltage regions to a linear function (equation 2.7), as described above. Using this method, for a completely linear *I-V* relationship, rectification index equaled 1.

2.7 Statistics

Summary data are presented in the text as mean $\pm$ standard error (s.e.m.).

All analyses were performed using the R statistical software (The R Foundation for Statistical Computing, http://www.r-project.org/) running in RStudio 0.96.331 (RStudio, Inc.). To test for differences between multiple groups (differing in a single factor), we used Welch heteroscedastic one-way ANOVA, which does not assume equal variances in the test groups. Subsequent pairwise comparisons also used a heteroscedastic test, in this case Welch two-sample *t*-test with Holm's sequential Bon-

ferroni correction.

When the test groups varied in two factors (such as the co-expressed TARP and the presence or absence of the NTD), a Welch heteroscedastic two-way ANOVA was performed. Pairwise comparisons used a Welch two-sample *t*-test with Holm's sequential Bonferroni correction.

The difference between groups was considered significant when $P < 0.05$. In all data figures, a single marker (such as $*$) denotes $P < 0.05$, a double marker ($**$) indicates $P < 0.01$ and a triple one ($***$) $P < 0.001$.

3

Experimental Chapter 1: Mutations in the first extracellular loop of γ-2 affect functional properties of AMPAR/γ-2 complexes

3.1 Summary

The aim of the work described in this Chapter was to investigate the molecular basis of AMPAR/TARP interaction. Some experiments were conducted in collaboration with Ingo Greger and colleagues (MRC LMB Cambridge). Our collaborators used peptide arrays to determine regions of interaction in the first extracellular loop (Ex1) of γ-2 that are responsible for binding to GluA2Q. They generated a range of γ-2 Ex1 mutants corresponding to GluA2Q interaction regions that had been identified by the array. We subjected these Ex1 mutants to functional studies using outside-out patches pulled from HEK cells and employed a number of measures to investigate the role of the Ex1 interactions in AMPAR/TARP complex function. These included deactivation and desensitization kinetics, the fraction of the steady-state current in response to desensitizing glutamate pulses, the mean single-channel conductance (estimated from NSFA), rectification and relative KA efficacy. Ex1 mutants were co-expressed with GluA1 or GluA2Q subunits and compared with TARPless AMPARs as well as with AMPARs co-expressed with wild-type (wt) γ-2.

3.2 Introduction

Previous studies on AMPAR/TARP interactions suggest that three main regions of the TARP protein are important for its regulation of the AMPAR pore-forming subunits. The C terminus of TARPs regulates AMPAR trafficking (Chen et al., 2000; Tomita et al., 2005; Bats et al., 2007; Opazo et al., 2010). The two domains important for modulation of AMPAR functional properties, such as desensitization kinetics and KA/Glu ratio, are the first extracellular loop (Ex1) and the second transmembrane domain (TM2) of TARPs (Tomita et al., 2005; Cho et al., 2007). The evidence for the involvement of TARP Ex1 in modulation of AMPAR properties is particularly strong, as described in the Introduction. Briefly, Ex1 swapping between TARPs appears to largely convey the properties of the Ex1 donor TARP. This has been demonstrated in both recombinant (Cho et al., 2007; Tomita et al., 2005) and native systems (Milstein et al., 2007). Thus, based on the literature available to date, Ex1 emerged as an interesting candidate domain for the more detailed molecular study described in this Chapter.

Our collaborators performed experiments in which GluA2Q interaction sites within the extracellular domain (Ex1 and the second extracellular loop Ex2) of γ-2 and γ-8 were mapped using peptide arrays. They generated γ-2 constructs which contained mutations in Ex1 designed to abolish specific local interactions with the pore-forming subunit. This was achieved by either replacing the naturally occurring amino acid residues with alanine (A) or glycine (G), or by simply deleting the residues important for the interaction. These specific amino acids were chosen for substitution mutations, due to both A and G side-chains being simple in structure (a single hydrogen atom in G and a methyl group in A) and thus unable to mediate complex polar, aromatic or hydrophobic interactions. Where feasible, A residues were used preferentially to G, so as not to allow too much additional flexibility within the protein, which could result from insertion of multiple glycines. Only one Ex1 mutant shown in this Chapter, $HFPE_{82\text{-}85}$ is a deletion, the remaining mutations are all substitutions (see Fig. 3.1). This was deliberate, as any mutation involving a deletion may produce its effects not only by removal of the relevant interaction, but also by disruption of protein structure due to shortened length.

The Ex1 mutants that we investigated in this Chapter were the ones shown by our collaborators to disrupt interaction with both the ligand-binding domain (LBD) and the N-terminal domain (NTD) of the pore-forming GluA2Q subunit. The exception is the $HFPE_{82\text{-}85}$ deletion mutant, as these residues were present in peptides both positive and negative for GluA2Q binding. It was therefore unclear whether the functional effects of this mutation were produced by removing the interaction with GluA2Q or

by shortening the Ex1 loop and thus disrupting its structure. A summary of the γ-2 mutants investigated here is shown in Fig. 3.1.

Since GluA2 pre-mRNA is almost completely edited at the Q/R site (Sommer et al., 1991; Burnashev et al., 1992a), the Q form of GluA2 is not a "physiological" subunit. Despite the fact that GluA2 is not normally expressed in its Q form, this form was chosen to allow analysis of the structural aspects of AMPAR/TARP interaction, since GluA2Q crystal structure is the only complete structure of an AMPAR subunit currently available (Sobolevsky et al., 2009). In order to determine whether the functional consequences of manipulating γ-2-AMPAR interactions were similar when a physiologically expressed subunit was used, we also co-expressed the Ex1 γ-2 mutants with GluA1.

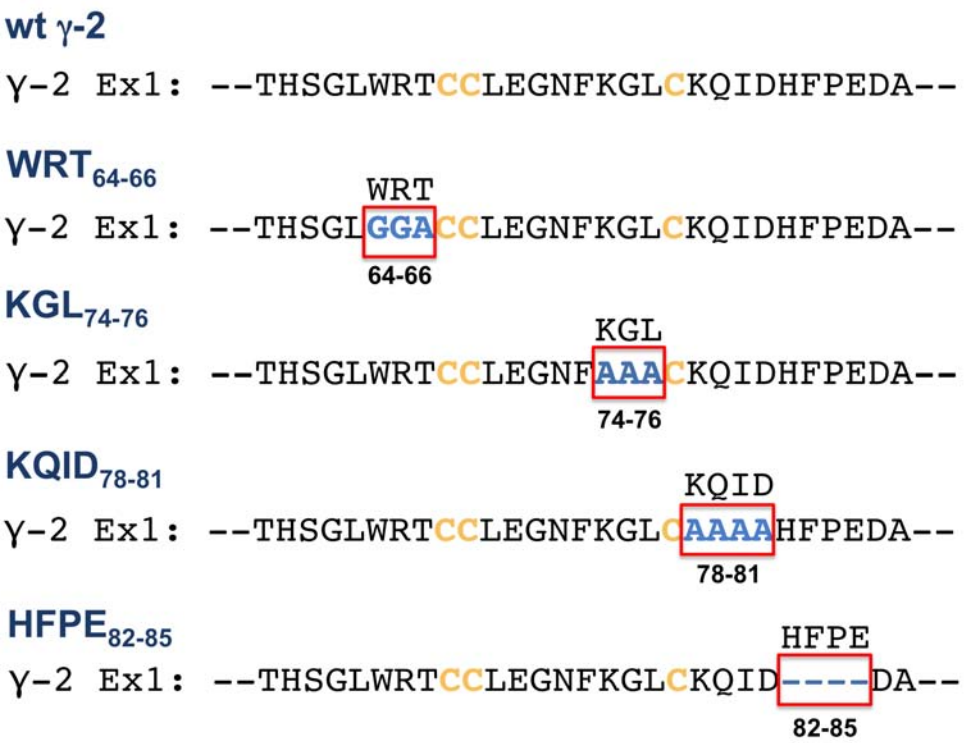

Figure 3.1: Mutations introduced into γ-2 Ex1 to disrupt interactions with GluA2Q. Four mutations were introduced into Ex1 of γ-2 to alter interactions with GluA2Q, as detected using peptide arrays. From the N to C terminal end of the loop these included: $WRT_{64\text{-}66}$ substitued with GGA, $KGL_{74\text{-}76}$ substituted with AAA, $KQID_{78\text{-}81}$ substituted with AAAA and a deletion of four amino acids $HFPE_{82\text{-}85}$. Note that the constructs were generated by members of the Greger lab.

Association with TARPs profoundly affects a number of functional properties of AMPARs. Many of the TARPs slow AMPAR deactivation and desensitization kinetics (Milstein et al., 2007; Cho et al., 2007). The effect of Ex1 mutations on the ability of γ-2 to slow

GluA1 and GluA2Q deactivation and desensitization kinetics was investigated by fitting the decay of responses to 1 ms and 100 ms glutamate (Glu) pulses, respectively. Currents were recorded at -60 mV.

The CP-AMPARs investigated in this Chapter are blocked by endogenous intracellular polyamines at positive membrane potentials, however, γ-2 co-expression has been reported to partially relieve spermine block (Soto et al., 2007). The effect of the mutations in Ex1 of γ-2 on the *I-V* relationship of the co-expressed AMPARs was determined in the presence of 100 μM intracellular spermine by comparing the rectification index (RI) calculated as slope conductance ratio at positive and negative membrane voltages.

TARPs increase the mean single-channel conductance of AMPARs (Tomita et al., 2005; Soto et al., 2009; Jackson et al., 2011; Shelley et al., 2012; Zhang et al., 2014). We used NSFA to estimate mean single-channel conductance of GluA1 and GluA2Q receptors that were TARPless, or co-expressed with wt γ-2 or the Ex1 mutants.

Finally, TARPs modify AMPAR pharmacology, resulting in increased relative efficacy of kainate (Turetsky et al., 2005; Tomita et al., 2005; Shi et al., 2009; Gill et al., 2011). KA/Glu ratios were examined to investigate how the efficacy of KA relative to Glu is affected by the disruption of the γ-2 Ex1 interactions with GluA1 and GluA2Q.

The experiments that lead to the generation of the Ex1 γ-2 mutants were performed by Ingo Greger and colleagues (MRC LMB Cambridge).

3.3 Results

3.3.1 Peptide array indentified residues in Ex1 of γ-2 which are important for binding to the NTD and LBD of GluA2Q

Our collaborators used an array of peptides containing both extracellular loops of TARPs γ-2 and γ-8 to identify residues that contact the NTD and LBD of GluA2. Interactions of GluA2 with γ-8 are shown here as they were part of the same experiment that mapped γ-2 interactions. However, no functional experiments were carried out for γ-8 and this interaction will not be discussed further.

As seen in panel B in Fig. 3.2 there were extensive NTD contacts on both Ex1 and, surprisingly, on the smaller Ex2 loop of γ-2. As this loop is only $\sim$30 residues long, it is not expected to reach far above the plasma membrane. Very little non-specific signal was observed from the antibody alone, when the NTD probe was omitted (Fig. 3.2 B, upper panel). The NTD interaction region on Ex1 spanned not only the center of the loop surrounding the highly conserved GLWRxC67 motif, but also the membrane-proximal N- and C-termini. This suggests that TARP interaction may result in significant conformational changes within the AMPAR, resulting in relative repositioning of the NTD and LBD.

The γ-2 interaction regions of the LBD partially overlapped with those of the NTD. Compared to the NTD interaction, the LBD interactions were shifted towards the N-terminus of Ex1, with a weaker interaction at the center of the loop and very little interaction at the C-terminus (Fig. 3.2 C, upper panel). This suggests that although the Ex1 of γ-2 interacts with both the NTD and LBD of GluA2, the distribution and intensity of the interaction within different parts of the loop varies between those two GluA2 domains. It is worth noting that very little binding of GluK2 LBD to the γ-2 membrane was observed. This further confirms the specificity of the interactions mapped using the peptide arrays, as TARPs are AMPAR auxiliary subunits and are thus expected to show no significant binding to kainate receptor subunits. The sequences of the γ-2 array peptides (Cais et al., 2014) are shown in Table 3.1.

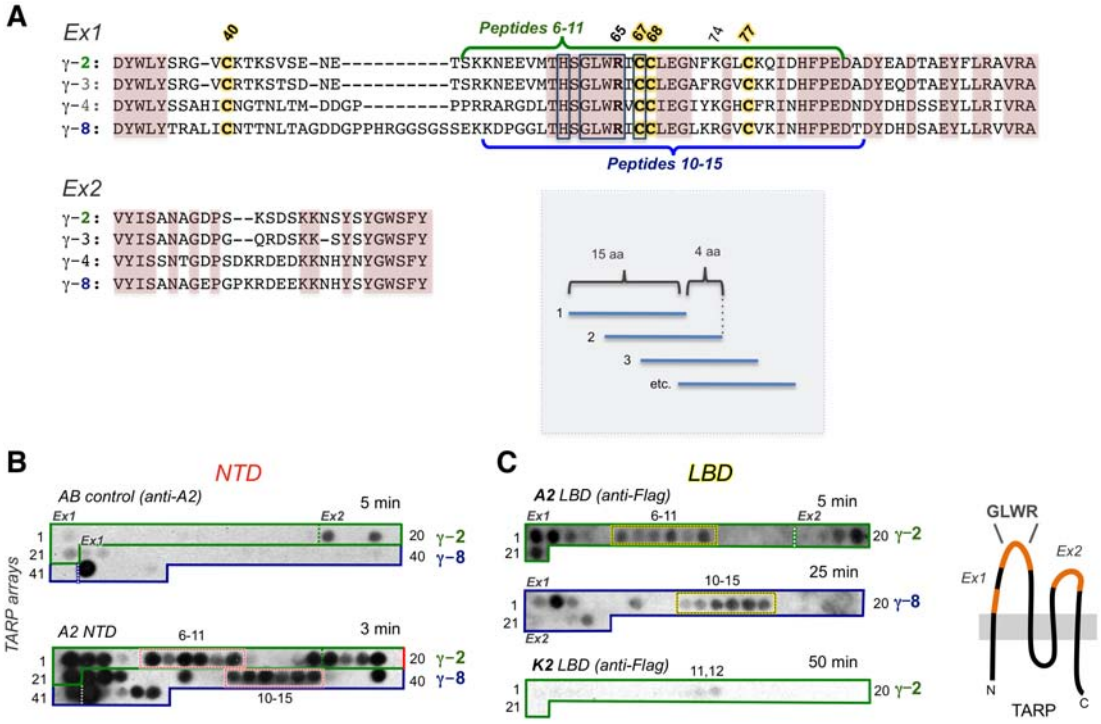

Figure 3.2: Peptide arrays were used to map contacts between the NTD and LBD of GluA2Q and the extracellular domain of TARPs γ-2 and γ-8. (**A**) Alignment of rat TARP extracellular loops (Ex1 and Ex2). Conserved residues are shaded in brown, highly conserved residues are surrounded by a grey box. The four cysteine residues highlighted in yellow are thought to be important for maintaining the secondary structure of Ex1. The R_{65} residue important for NTD binding (see Experimental Chapter 2) is highlighted in bold. Curved brackets above the γ-2 alignment (green) and below the γ-8 alignment (blue) indicate the GluA2Q interaction region located in the center of Ex1, which was mapped functionally in this Chapter. (**B**) TARP array containing Ex1 and Ex2 loops of γ-2 (green box) and γ-8 (blue box) probed with the NTD of GluA2. The array contained 46 15-mer overlapping peptides shifting by 4 residues, as shown in the inset. Top panel: Non-specific signal, resulting from direct anti-GluA2 antibody binding to the membrane. The membrane was exposed for 5 minutes. The dashed line indicates the division between Ex1 and Ex2 peptides. Lower panel: the same membrane was exposed to the rat GluA2 NTD and probed with rabbit anti-GluA2 antibody (Alomone, 1:250) followed by a HRP-conjugated anti-rabbit antibody (Pierce, 1:1500). The membrane was exposed for 3 minutes. (**C**) TARP array probed with the LBD of GluA2. Top panel: LBD interaction with γ-2. The membrane was exposed to Flag-tagged GluA2 LBD and probed with monoclonal anti-Flag M2 antibody (Sigma, 1:1000), followed by a HRP-conjugated anti-mouse antibody (Pierce, 1:1000). Middle panel shows the same experiment with the γ-8 array. Bottom panel shows the control experiment, in which the γ-2 membrane was exposed to Flag-tagged LBD of the kainate receptor subunit GluK2 and probed with the same antibodies as in the top GluA2 panel. The membrane was exposed for 50 minutes. The negative control, probed with monoclonal anti-Flag AB only is not shown, as there was no binding. Bottom right: (**Inset**) Summary of the NTD and LBD interactions with the extracellular domain of γ-2. **Note:** All work that lead to the generation of this figure was conducted by members of the Greger lab. The figure was adapted from Cais et al. (2014).

Peptide number	Peptide sequence
Ex1	
1	**DYWLYSRGVCKTKSV**
2	**YSRGVCKTKSVSENE**
3	**VCKTKSVSENETSKK**
4	KSVSENETSKKNEEV
5	ENETSKKNEEVMTHS
6	**SKKNEEVMTHSGLWR**
7	**EEVMTHSGLWRTCCL**
8	**THSGLWRTCCLEGNF**
9	**LWRTCCLEGNFKGLC**
10	**CCLEGNFKGLCKQID**
11	**GNFKGLCKQIDHFPE**
12	GLCKQIDHFPEDADY
13	QIDHFPEDADYEADT
14	FPEDADYEADTAEYF
15	ADYEADTAEYFLRAV
16	**YEADTAEYFLRAVRA**
Ex2	
17	VYISANAGDPSKSDS
18	**ANAGDPSKSDSKKNS**
19	**DPSKSDSKKNSYSYG**
20	**SDSKKNSYSYGWSFY**
21	**DSKKNSYSYGWSFYF**

Table 3.1: Sequences of the γ-2 peptides immobilised on the array shown in Fig. 3.2, as per Cais et al. (2014), supplementary information. The peptides showing strong binding to GluA2 (NTD and/or LBD) are indicated in bold.

3.3.2 Mutations in Ex1 affected the ability of γ-2 to prolong GluA1 deactivation

We used fast application of glutamate to outside-out patches pulled from transfected HEK cells to determine the effect of the γ-2 Ex1 mutants on AMPAR decay kinetics. 1 ms pulses of 10 mM Glu were used to specifically examine AMPAR deactivation. Currents were recorded at -60 mV.

Compared with GluA1 expressed alone, co-expression of wt γ-2 slowed the time constant of deactivation $\sim$3-fold (from 0.72 $\pm$ 0.11 ms for GluA1 alone to 2.56 $\pm$ 0.33 ms for GluA1 + wt γ-2, P= 0.0031). Ex1 mutants ($KGL_{74\text{-}76}$, $KQID_{78\text{-}81}$ and $HFPE_{82\text{-}85}$) also slowed GluA1 deactivation significantly, but the effect was less pronounced than that of wt γ-2 (τ_w = 1.55 $\pm$ 0.20 ms for $KGL_{74\text{-}76}$, P= 0.016 ; 1.85 $\pm$ 0.21 ms for $KQID_{78\text{-}81}$, P= 0.0042 and 1.30 $\pm$ 0.13 ms for $HFPE_{82\text{-}85}$, P= 0.025). Compared with wt γ-2, mutants $KGL_{74\text{-}76}$ (P= 0.043) and $HFPE_{82\text{-}85}$ (P= 0.021), but not $KQID_{78\text{-}81}$ (P= 0.093) produced currents with significantly faster deactivation when co-expressed with GluA1. This suggests that different regions of Ex1 may play a role in the regulation

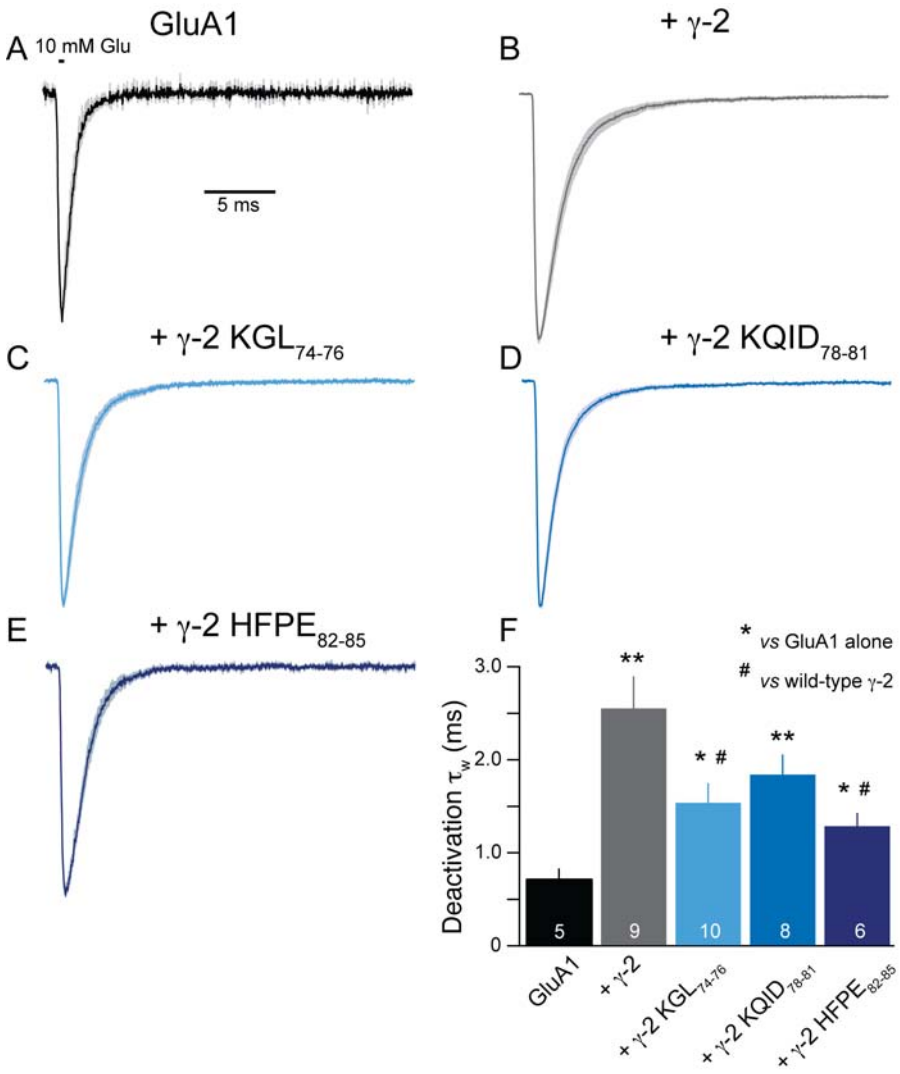

Figure 3.3: Co-expression of GluA1 with the Ex1 mutants resulted in deactivation kinetics intermediate between GluA1 alone and GluA1 + wt γ-2. (**A**) Normalised mean response to 1 ms applications of 10 mM Glu from GluA1-containing patches (black tarce). Grey shading denotes the SEM. The black bar on top of the figure marks the duration of Glu application. Mean currents from individual patches were normalised to the peak and aligned at the 20 % rise time before averaging. (**B-E**) As for A, but for patches expressing GluA1 + wt γ-2, + $KGL_{74\text{-}76}$, + $KQID_{78\text{-}81}$ and + $HFPE_{82\text{-}85}$ respectively. (**F**) Histogram showing τ_w of deactivation for each of the Ex1 mutants as well as GluA1 and GluA1+ wt γ-2 controls. Bars denote the SEM and the *n* numbers for each group are indicated in white at the bottom of the histogram. One-way ANOVA showed a significant effect of γ-2 variants on GluA1 deactivation ($F_{(4,\ 16.19)}$ = 11.15, P= 1.55 $\times$ 10^{-4}). For pairwise tests, asterisks mark significant difference *vs.* GluA1 alone ($*$ P< 0.05, $**$ P< 0.01; Welch *t*-test), while hashes mark significant difference *vs.* GluA1 + wt γ-2 ($\#$ P< 0.05; Welch *t*-test).

of GluA1 deactivation. The effects of Ex1 mutations on GluA1 deactivation are summarised in Fig. 3.3.

3.3.3 The effect of γ-2 on GluA1 desensitization was disrupted by mutations in Ex1

Desensitization time constant (τ_w) was quantified by fitting the decay of current responses to 100 ms pulses of 10 mM Glu, recorded at -60 mV.

As shown in Fig. 3.4, wt γ-2 prolonged GluA1 desensitization τ_w ~2.5-fold (from 2.36 $\pm$ 0.20 ms for GluA1 alone to 5.01 $\pm$ 0.43 ms for GluA1 + wt γ-2, P= 5.04 $\times$ 10^{-5}). All three Ex1 mutants acted as TARPs, in that they associated with AMPARs and significantly prolonged GluA1 desensitization ($KGL_{74\text{-}76}$: 3.22 $\pm$ 0.23 ms P= 0.028, $KQID_{78\text{-}81}$: 3.89 $\pm$ 0.31 ms, P= 0.0025, $HFPE_{82\text{-}85}$: 4.94 $\pm$ 0.50 ms, P= 0.0020). The two most C-terminal mutants, $KQID_{78\text{-}81}$ and $HFPE_{82\text{-}85}$, prolonged GluA1 desensitization to the same extent as wt γ-2 (P= 0.085 and 0.92 for $KQID_{78\text{-}81}$ and $HFPE_{82\text{-}85}$ respectively), suggesting that interactions in these regions of Ex1 do not play a role in modulating GluA1 desensitization. The remaining mutant, $KGL_{74\text{-}76}$ had significantly less effect on GluA1 desensitization than wt γ-2 (P=0.0039).

In addition to desensitization kinetics, the extent of desensitization was also analyzed. We quantified the steady-state current as percentage of the peak current amplitude. The results are summarised in Table 3.2. Overall, there was a significant effect of γ-2 variants on GluA1 steady-state current percentage ($F_{(4,\ 26.4)}$ = 14.39, P= 2.34 $\times$ 10^{-6}). Wt γ-2 (P= 0.0019), as well as $KQID_{78\text{-}81}$ (P= 0.0020) and $HFPE_{82\text{-}85}$ (P= 0.022) significantly increased the steady-state current fraction, while $KGL_{74\text{-}76}$ (P= 0.052) did not. None of the γ-2 mutants differed significantly from wt γ-2 in their action on the percentage of steady-state current (P= 0.16, 0.69 and 0.91 for $KGL_{74\text{-}76}$, $KQID_{78\text{-}81}$ and $HFPE_{82\text{-}85}$ respectively).

	Mean (%)	**SEM**	***n***
GluA1	0.73	0.14	10
wt γ-2	6.41	1.27	20
$KGL_{74\text{-}76}$	3.30	0.89	14
$KQID_{78\text{-}81}$	4.94	0.85	13
$HFPE_{82\text{-}85}$	6.64	1.62	11

Table 3.2: Mutations in Ex1 did not affect γ-2-mediated increase in steady-state current percentage.

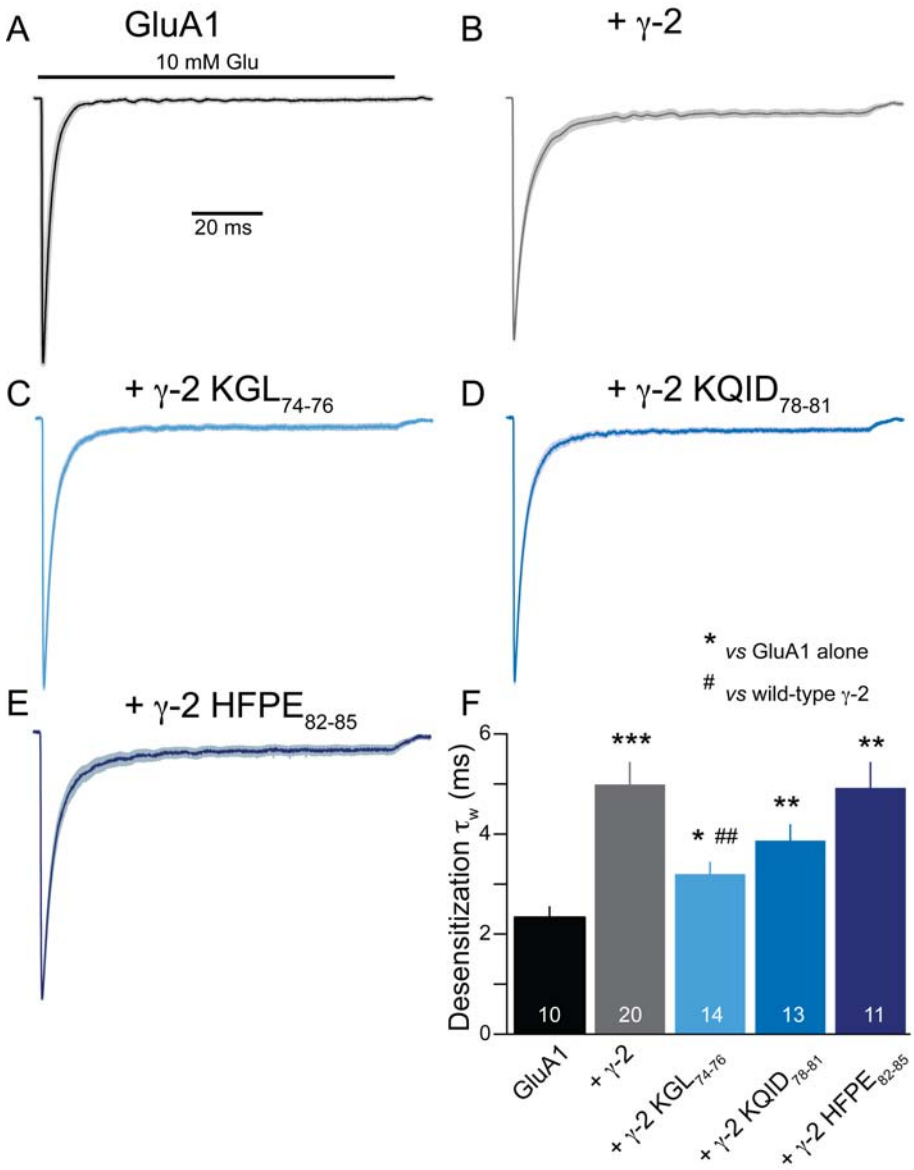

Figure 3.4: Effect of γ-2 Ex1 mutants on GluA1 desensitization. (**A**) Normalised mean response from GluA1-containing patches (black trace) to 100 ms applications of 10 mM Glu. Grey shading denotes the SEM. The black bar on top of the figure marks the duration of Glu application. Mean currents from individual patches were normalised to the peak and aligned at the 20 % rise time before averaging. (**B-E**) As for A, but for patches expressing GluA1 + wt γ-2, + $KGL_{74\text{-}76}$, + $KQID_{78\text{-}81}$ and + $HFPE_{82\text{-}85}$ respectively. (**F**) Histogram showing τ_w of desensitization for each of the Ex1 mutants as well as GluA1 and GluA1+ wt γ-2 controls. Bars denote the SEM and the *n* numbers for each group are indicated in white at the bottom of the histogram. One-way ANOVA showed a significant effect of γ-2 variants on GluA1 desensitization ($F_{(4,\ 29.7)}$ = 12.33, $P = 5 \times 10^{-6}$). Asterisks mark significant difference *vs.* GluA1 alone ($*$ $P < 0.05$, $**$ $P < 0.01$, $***$ $P < 0.001$; Welch *t*-test), while hashes mark significant difference *vs.* GluA1 + wt γ-2 ($\#\#$ $P < 0.01$; Welch *t*-test).

3.3.4 Ex1 γ-2 mutants showed rectification intermediate between GluA1 alone and GluA1 + wt γ-2

The effect of Ex1 mutants on rectification, produced by 100 μM intracellular spermine, was determined by applying 1 ms glutamate pulses at holding potentials from -100 mV to +60 mV, increasing in 10 mV increments. Rectification index was then quantified as slope conductance ratio. Wt γ-2 (RI= 0.365 $\pm$ 0.031) as well as all three Ex1 γ-2 mutants: $KGL_{74\text{-}76}$ (0.238 $\pm$ 0.024), $KQID_{78\text{-}81}$ (0.251 $\pm$ 0.030) and $HFPE_{82\text{-}85}$ (0.214 $\pm$ 0.040) acted as TARPs, partially relieving spermine block of GluA1 homomers at positive membrane potentials, which resulted in a significant increase in RI compared to TARPless GluA1 (0.042 $\pm$ 0.018). However, the relief of block was less pronounced than with wt γ-2. The statistical comparisons between Ex1 mutants and the controls are shown in Table 3.3.

Test No.	Test pair			*P*-value
1	GluA1	*vs.*	GluA1 + wt γ-2	8.31×10^{-6}
2	GluA1	*vs.*	GluA1 + $KGL_{74\text{-}76}$	0.00011
3	GluA1	*vs.*	GluA1 + $KQID_{78\text{-}81}$	0.00085
4	GluA1	*vs.*	GluA1 + $HFPE_{82\text{-}85}$	0.0203
5	GluA1 + wt γ-2	*vs.*	GluA1 + $KGL_{74\text{-}76}$	0.0203
6	GluA1 + wt γ-2	*vs.*	GluA1 + $KQID_{78\text{-}81}$	0.026
7	GluA1 + wt γ-2	*vs.*	GluA1 + $HFPE_{82\text{-}85}$	0.026

Table 3.3: Mutations in Ex1 affected the ability of γ-2 to relieve spermine block of GluA1.

As seen in Fig. 3.5 C, at negative membrane voltages the *I-V* relationship for GluA1 alone was clearly different from that seen when GluA1 was co-expressed with wt γ-2 or any of the Ex1 mutants. This effect of wt γ-2 on the *I-V* relationship of GluA1 is consistent with previous reports (Soto et al., 2007), suggesting that co-expression of γ-2 enhances charge transfer by reducing polyamine affinity. The *I-V* plots for wt γ-2 and all three Ex1 mutants were almost overlaid at negative membrane voltages which is shown more clearly in the conductance-voltage plots (Fig. 3.6). At positive membrane potentials *I-V* relationships of all Ex1 mutants clearly deviated from that of GluA1+ wt γ-2, resulting in a significant difference between the Ex1 mutants and wt γ-2 in the effect on GluA1 rectification. Indeed, all 3 Ex1 mutants relieved polyamine block only to about 70% of the RI value seen with wt γ-2.

Similar to previously published results (Soto et al., 2007), wt γ-2 produced a +28.4 mV shift in the voltage at which spermine block is half-maximal (Fig. 3.6). The Ex1 mutants produced a very similar shift of the *G-V* relationship to that produced by wt γ-2 (Fig. 3.6), which may suggest that the affinity for spermine is unaffected by mutations in Ex1. However, the significant difference in RI (see Fig. 3.5) might imply

that permeation of spermine through the GluA1 channel pore at positive membrane potentials is reduced due to mutations in Ex1 of γ-2.

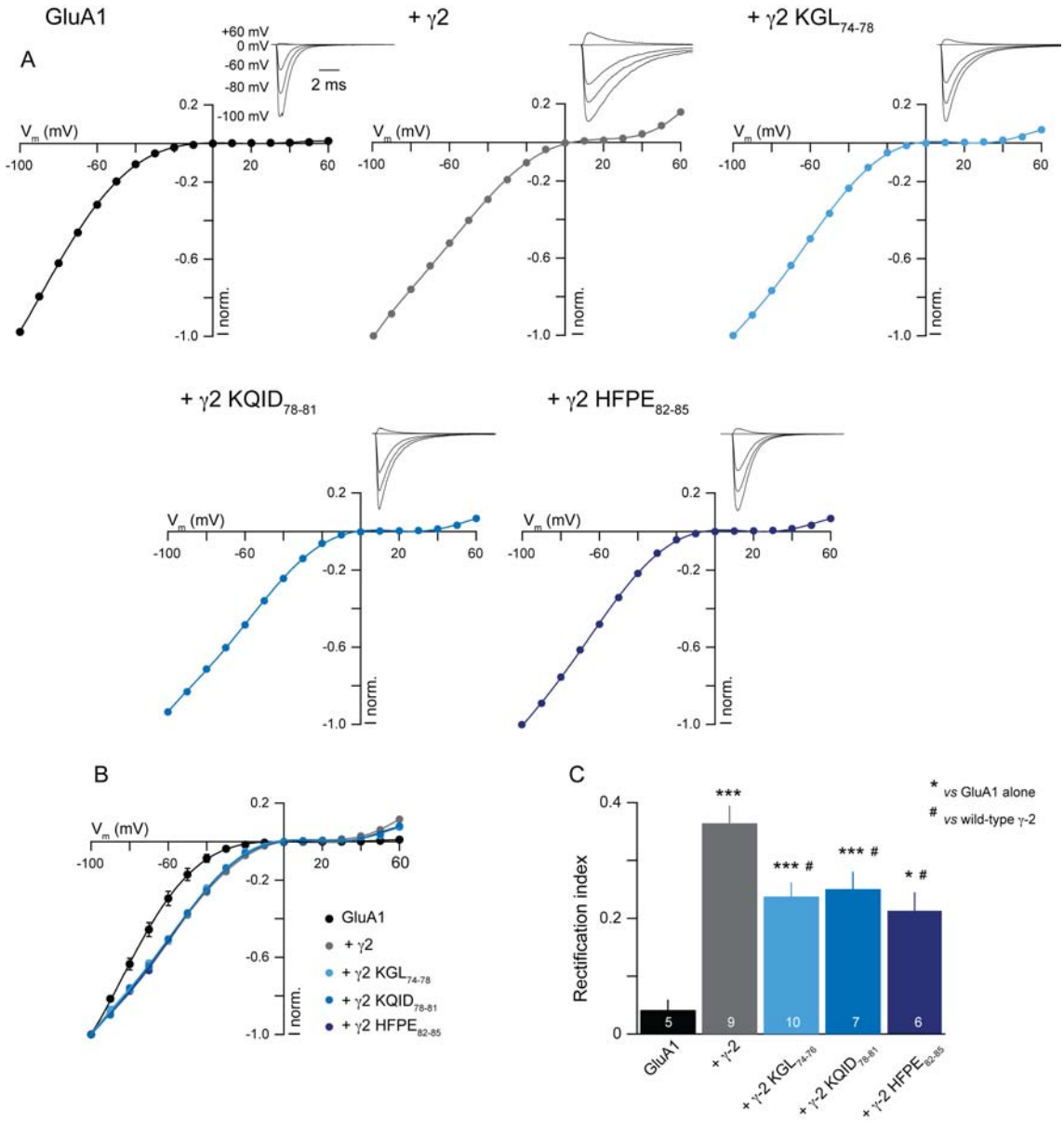

Figure 3.5: Rectification index of Ex1 mutants co-expressed with GluA1 was intermediate between GluA1 alone and GluA1 + wt γ-2.(**A**) Peak *I-V* plots for from individual representative patches for each construct. Note the strong spermine block of GluA1 responses at positive membrane potentials, and a relief of block seen with wt γ-2. Ex1 mutants showed a degree of block that is intermediate between GluA1 alone and GluA1 + wt γ-2. Peak currents at each holding potential were normalised to the peak at -100 mV. Insets show average traces for that patch at -100, -80, -60, 0 and +60 mV as indicated, normalised to the peak at -100 mV. (**B**) Average normalised peak *I-V* plots for GluA1 alone, GluA1 + wt γ-2, GluA1 + KGL_{74-76}, GluA1 + $KQID_{78-81}$ and GluA1 + $HFPE_{82-85}$. Peak currents from each patch were normalised to the peak at -100 mV before averaging.

Figure 3.5 continued: (**C**) Histogram showing rectification index calculated as slope conductance ratio, for GluA1 alone, GluA1 + wt γ-2, GluA1 + $KGL_{74\text{-}76}$, GluA1 + $KQID_{78\text{-}81}$ and GluA1 + $HFPE_{82\text{-}85}$. Bars denote SEM and *n* numbers are indicated at the bottom of the histogram. One-way ANOVA showed a significant overall effect of γ-2 variants on GluA1 rectification ($F_{(4,\ 14.91)} = 24.22$, $P = 2.24 \times 10^{-6}$). Asterisks mark significant difference compared with GluA1 alone ($*$ $P < 0.05$, $***$ $P < 0.001$; Welch *t*-test), while hashes mark significant difference compared with GluA1 + wt γ-2 ($\#$ $P < 0.05$; Welch *t*-test).

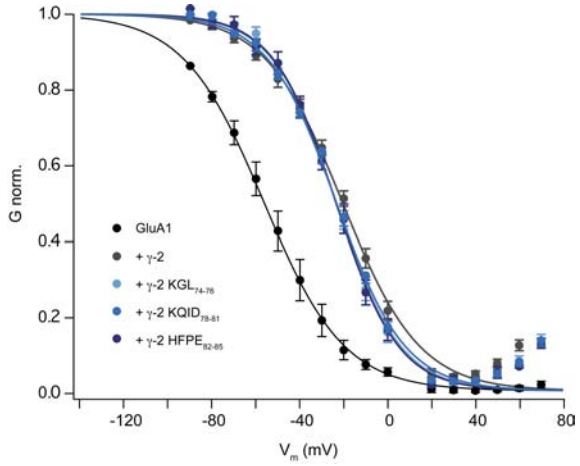

Figure 3.6: The shift in *G-V* relationship at negative membrane potentials was similar when GluA1 was co-expressed with Ex1 mutants and with wt γ-2. Normalised peak conductance was plotted against membrane voltage for GluA1 alone, or GluA1 co-expressed with wt γ-2, $KGL_{74\text{-}76}$, $KQID_{78\text{-}81}$ or $HFPE_{82\text{-}85}$ and fitted to the Boltzmann equation (2.8 on page 62) between -100 mV and -10 mV. Wt γ-2 produced a +35.8 mV shift in the *G-V* relationship for GluA1. The magnitude of the shift was similar for all of the Ex1 mutants. The parameters of the Boltzmann fits are summarized in Table 3.4.

	GluA1	**+ wt γ-2**	**+ $KGL_{74\text{-}76}$**	**+ $KQID_{78\text{-}81}$**	**+ $HFPE_{82\text{-}85}$**
Boltzmann fit	(5)	(9)	(10)	(7)	(6)
$V_{0.5}$ (mV)	-66.4	-30.6	-33.5	-33.5	-33.7
***k* (mV)**	18.3	17.6	14.7	15.7	14.3
$V_{0.5}$ shift (mV)		+35.8	+33.0	+33.0	+32.8

Table 3.4: Parameters of the Boltzmann fits to *G-V* relationships for GluA1 alone and co-expressed with wt γ-2 or Ex1 mutants. Conductance-voltage plots were created from an average *I-V* from (*n*) patches for each condition and fitted to the Boltzmann equation (2.8 on page 62) between -100 mV and -10 mV. $V_{0.5}$ shift is the positive shift from GluA1 alone produced by the different variants of γ-2 (calculated as $V_{0.5}$ for the given γ-2 variant - $V_{0.5}$ for GluA1).

3.3.5 GluA1 mean single-channel conductance was increased by $KGL_{74\text{-}76}$ and $KQID_{78\text{-}81}$ mutants

γ-2 has previously been reported to increase mean single-channel conductance of AMPARs (Soto et al., 2009; Jackson et al., 2011; Shelley et al., 2012), including GluA1 homomers (Coombs et al., 2012). We estimated mean single-channel conductance of GluA1 alone and GluA1 TARPed with wt γ-2 or the Ex1 mutants by fitting the parabolic NSFA equation to the current responses to 100 ms pulses of 10 mM Glu recorded at -60 mV.

Wt γ-2 showed a tendency to increase mean single-channel conductance of GluA1. The increase was $\sim$1.5-fold (from 17.9 $\pm$ 2.0 pS for GluA1 alone to 27.8 $\pm$ 3.2 pS for GluA1 + wt γ-2), but the difference in conductance compared with GluA1 alone was not statistically significant (P= 0.096). This failure of wt γ-2 to significantly increase GluA1 mean single-channel conductance most likely results from the complexity of the statistical analysis performed. Appropriate P-value corrections were applied to the results, due to the need to perform multiple statistical tests within the same data set, so that despite the trend to increase mean-single channel conductance, the effect of γ-2 on this measure was not significant. However, the result may also arise from a biological cause. Out of 16 patches where NSFA was applied, no plausible fit could be obtained in 5, and the remaining patches showed a relatively large scatter in conductance values (from 14.7 pS to 53.1 pS). This could be caused by the presence of multiple channel populations with different conductances, for instance due to the TARP decoupling during glutamate application (Morimoto-Tomita et al., 2009; Semenov et al., 2012).

The $KGL_{74\text{-}76}$ and $KQID_{78\text{-}81}$ mutants significantly increased mean single-channel conductance of GluA1 (to 30.7 $\pm$ 2.1 pS, P= 0.0020 and 31.3 $\pm$ 2.1 pS, P= 0.0015 respectively), as seen in Fig. 3.7F. The mean single-channel conductance for the $HFPE_{82\text{-}85}$ mutant co-expressed with GluA1 was 21.3 $\pm$ 1.8 pS. This mutant was not significantly different from GluA1 alone (P= 0.66). None of the Ex1 mutants differed significantly from wt γ-2 in its effect on GluA1 conductance (P= 0.75, 0.75, and 0.40 for $KGL_{74\text{-}76}$, $KQID_{78\text{-}81}$ and $HFPE_{82\text{-}85}$ respectively).

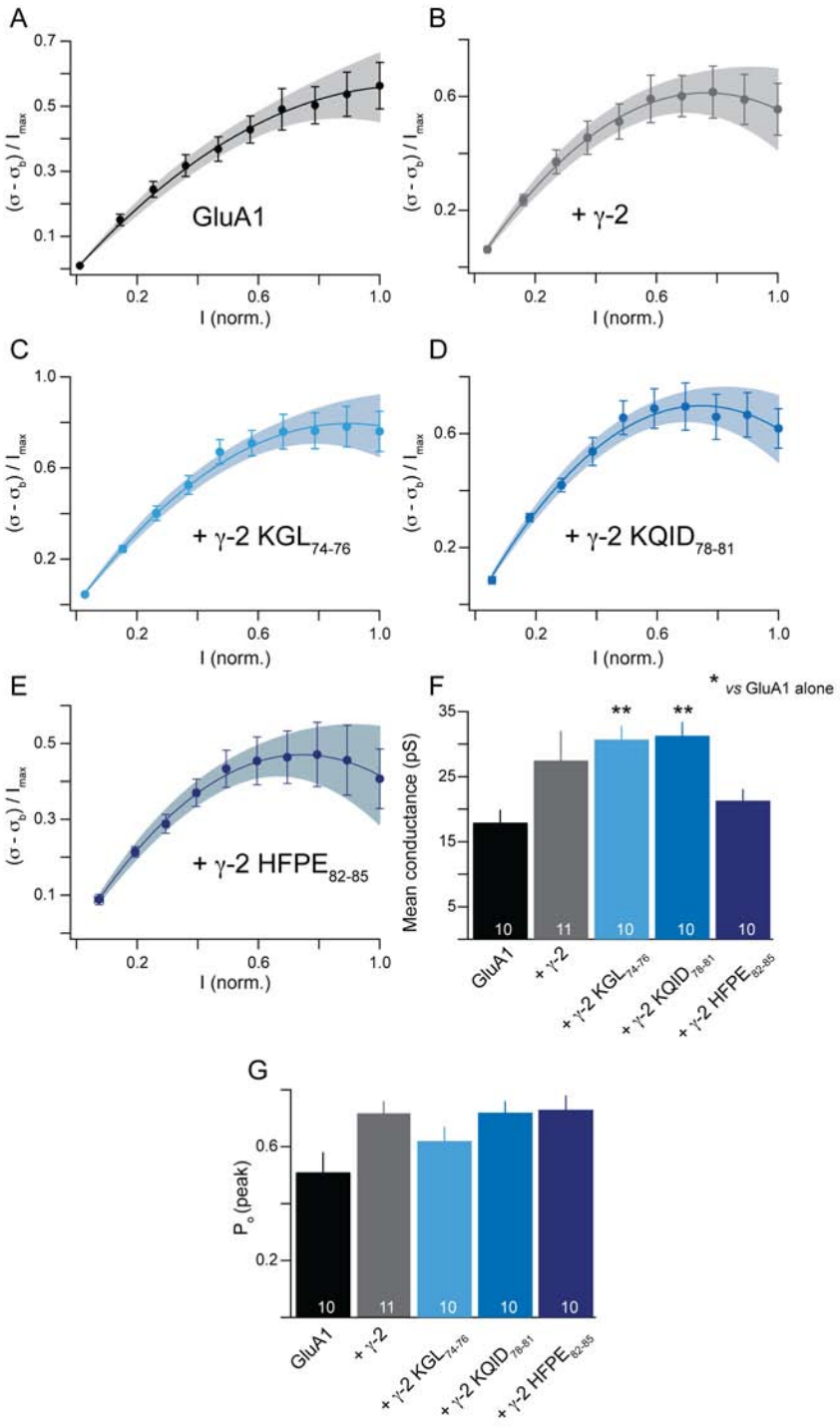

Figure 3.7: γ-2 variants showed differential effects on GluA1 mean single-channel conductance and P_o. (**A**) Average normalised current-variance relationship for GluA1 alone. Mean current (x-axis) was normalised to the peak (1st bin). Variance was also normalised to the peak current after subtracting σ_b. Vertical and horizontal error bars on the data points indicate the variance and mean current SEM respectively. The grey shading covers the area between the 95% confidence interval bands for the parabolic NSFA fit (black line) to equation 2.6 on page 61. The fit was weighted by the SEM and the σ_b parameter was constrained to 0.

Figure 3.7 continued: (**B-E**) As for A, but for GluA1 + wt γ-2, + $KGL_{74\text{-}76}$, + $KQID_{78\text{-}81}$ and + $HFPE_{82\text{-}85}$ respectively. (**F**) Histogram showing mean single-channel conductance for GluA1 alone, GluA1 + wt γ-2, GluA1 + $KGL_{74\text{-}76}$, GluA1 + $KQID_{78\text{-}81}$ and GluA1 + $HFPE_{82\text{-}85}$. Bars denote SEM and *n* numbers are indicated at the bottom of the histogram. One-way ANOVA showed a significant overall effect of γ-2 variants on GluA1 conductance estimates ($F_{(4,\ 22.95)}$= 7.84, P= 3.88 $\times$ 10^{-4}). Asterisks mark significant difference compared with GluA1 alone ($*$ $*$ P<0.01; Welch *t*-test). (**G**) Histogram showing peak open probability for GluA1 alone, or co-expressed with the different γ-2 variants. Bars denote SEM and *n* numbers are indicated at the bottom of the histogram. One-way ANOVA showed no significant overall effect of γ-2 variants on GluA1 P_o ($F_{(4,\ 22.67)}$= 2.58, P= 0.0645).

We also examined the effect of γ-2 variants on the peak open probability (P_o) of GluA1 (Fig. 3.7G), however, no significant overall effect on this measure was detected ($F_{4,\ 22.67}$= 2.58, P= 0.0645). This result differs from that of a previous study, which showed that γ-2 increased P_o of GluA1 (Suzuki et al., 2008). The P_o values for the different GluA1/TARP combinations are shown in Table 3.5.

	Mean (%)	**SEM**	***n***
GluA1	0.51	0.07	10
wt γ-2	0.72	0.04	11
$KGL_{74\text{-}76}$	0.62	0.05	10
$KQID_{78\text{-}81}$	0.72	0.04	10
$HFPE_{82\text{-}85}$	0.73	0.05	10

Table 3.5: P_o values for the different GluA1/TARP combinations.

The results described above suggest that the $KGL_{74\text{-}76}$ and $KQID_{78\text{-}81}$ mutants act as TARPs increasing GluA1 conductance, while the $HFPE_{82\text{-}85}$ mutation may disrupt this property of γ-2. By contast, GluA1 P_o was not affected by mutations in Ex1.

3.3.6 Mutations in Ex1 affect the γ-2 mediated increase in kainate efficacy (relative to glutamate) on GluA1

AMPAR/TARP interaction mediated by Ex1 of γ-2 is known to be important for potentiation of AMPAR responses to kainate (Tomita et al., 2005). We measured the KA/Glu ratio by holding the patch at -60 mV and exposing it to 500 μM Glu then to 500 μM KA and again to Glu, both in the presence of 100 μM CTZ which greatly reduced AMPAR desensitization. The KA/Glu ratio was then quantified as the ratio of the steady-state response to KA and the average of the two responses to Glu.

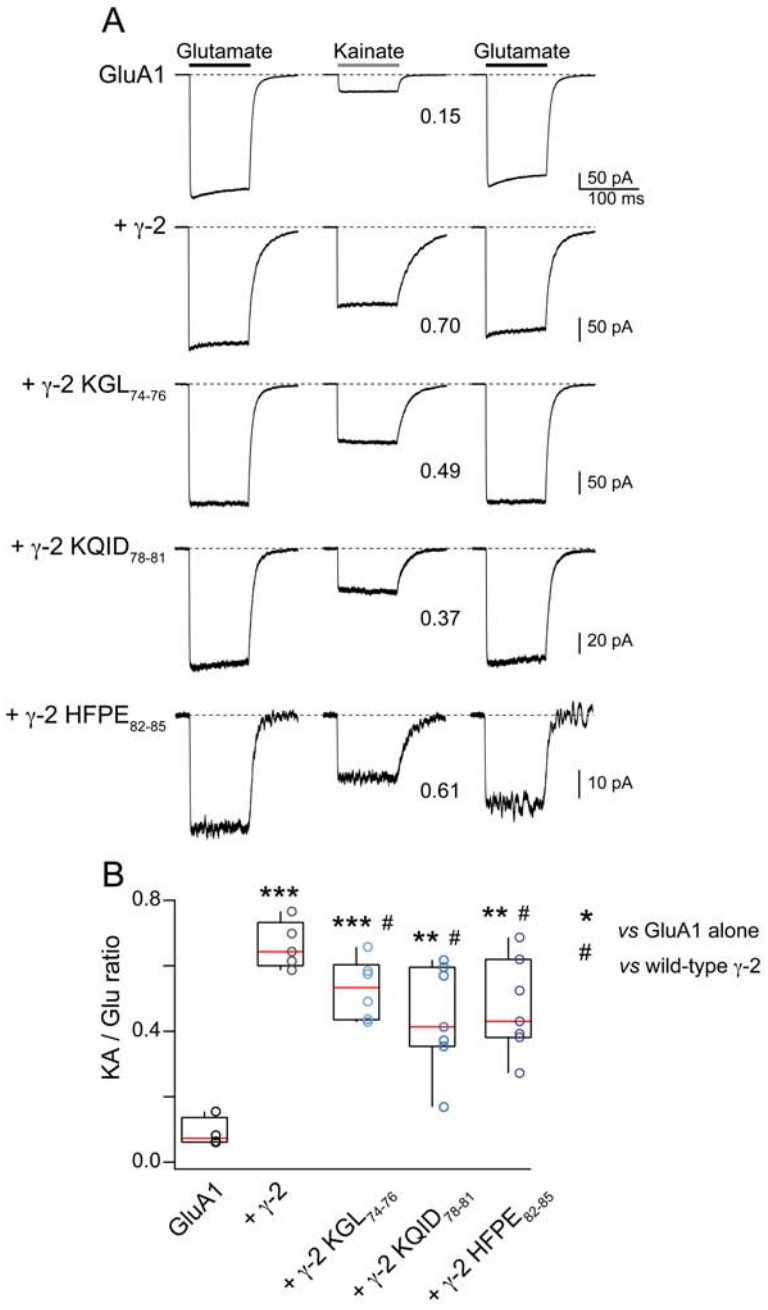

Figure 3.8: Mutations in Ex1 disrupted the γ-2-mediated increase in kainate/glutamate ratio on GluA1. (**A**) Mean responses from representative patches showing the initial response to 500 μM Glu (left), followed by 500 μM KA (middle) and a recovery of response to Glu (right). Control and agonist solutions contained 100 μM CTZ to inhibit desensitization. The KA/Glu ratio for the representative patch is shown next to the trace. (**B**) Box and whisker plot of the KA/Glu ratios (measured as the ratio of the steady-state responses in CTZ). The box shows the 25-75 percentile, while the whiskers are the 10-90 percentile. Individual data points are overlaid on the plot (open circles). One-way ANOVA showed a significant overall effect of γ-2 variants co-expressed with GluA1 ($F_{(4,\ 11.91)}$ = 56.59 , P= 1.18 $\times$ 10^{-7}). Asterisks mark significant difference compared with GluA1 alone ($**$ P< 0.01, $***$ P< 0.001; Welch t-test), while hashes mark significant difference compared with GluA1 + wt γ-2 ($\#$ P< 0.05; Welch t-test).

When wt γ-2 was co-expressed with GluA1, there was a $\sim$6-fold increase in the kainate to glutamate response ratio (KA/Glu ratio= 0.66 $\pm$ 0.03, *n*=5, for wt γ-2 *vs.* 0.09 $\pm$ 0.02, *n*=4, for GluA1 alone, *P*= 1.71 $\times$ 10^{-5}). Ex1 mutants also acted as TARPs judged on this measure, as they increased the efficacy of kainate, albeit to a lesser extent than wt γ-2 ($\sim$5-fold). The KA/Glu ratio was 0.53 $\pm$ 0.04 for $KGL_{74\text{-}76}$ (*n*=6); 0.44 $\pm$ 0.06 for $KQID_{78\text{-}81}$ (*n*=7) and 0.47 $\pm$ 0.06 for $HFPE_{82\text{-}85}$ (*n*=7). Thus, co-expression of these Ex1 mutants resulted in a significant increase in KA/Glu ratio compared to TARPless GluA1 (*P*= 6.93 $\times$ 10^{-5}, 0034 and 0.0012 for $KGL_{74\text{-}76}$, $KQID_{78\text{-}81}$ and $HFPE_{82\text{-}85}$ respectively).

All three γ-2 mutants were significantly less efficient at modulating kainate efficacy than wt γ-2 (*P*= 0.035 for all three mutants). This suggests that the mutations in the Ex1 of γ-2 disrupt AMPAR/TARP interaction in a way that might affect the degree of GluA1 LBD cleft closure, as this is known to determine the efficacy of partial agonists (Jin et al., 2003).

3.3.7 Ex1 mutations affected GluA2Q and GluA1 deactivation kinetics differently

The experiments described above for GluA1 were subsequently repeated with the GluA2Q subunit, in order to elucidate the functional consequences of removing sites of AMPAR/TARP interaction mapped by our collaborators in the peptide array (Fig. 3.2). One additional γ-2 Ex1 mutant was also tested with GluA2Q. This was the $WRT_{64\text{-}66}$ mutant, in which the naturally occurring amino acid residues (WRT) were replaced by GGA. This mutation targets the residues at the very tip of Ex1 which interact with both the NTD and LBD of GluA2Q and which, upon refinement of biochemical data, were considered a good target for functional studies, as it was thought the mutation may alter the positioning of γ-2 Ex1 relative to the NTD and LBD of GluA2Q.

As shown in Fig. 3.9, when compared with GluA2Q alone, wt γ-2 appeared to slow deactivation almost 2-fold, but the effect was not significant (τ_w = 0.71 $\pm$ 0.07 ms, *vs.* 0.41 $\pm$ 0.06 ms for GluA2Q alone). The Ex1 mutants also failed to significantly slow the deactivation of GluA2Q (τ_w = 0.64 $\pm$ 0.04 ms for $KGL_{74\text{-}76}$; 0.62 $\pm$ 0.04 ms for $KQID_{78\text{-}81}$, 0.46 $\pm$ 0.04 ms for $HFPE_{82\text{-}85}$ and 0.54 $\pm$ 0.06 ms for $WRT_{64\text{-}66}$). Indeed, none of the Ex1 mutants different from wt γ-2 in their effect on deactivation. The statistical comparisons are listed in Table 3.6.

Test No.	Test pair			*P*-value
1	GluA2	*vs.*	GluA2 + wt γ-2	0.061
2	GluA2	*vs.*	GluA2 + $KGL_{74\text{-}76}$	0.086
3	GluA2	*vs.*	GluA2 + $KQID_{78\text{-}81}$	0.097
4	GluA2	*vs.*	GluA2 + $HFPE_{82\text{-}85}$	0.79
5	GluA2	*vs.*	GluA2 + $WRT_{64\text{-}66}$	0.66
6	GluA2 + wt γ-2	*vs.*	GluA2 + $KGL_{74\text{-}76}$	0.79
7	GluA2 + wt γ-2	*vs.*	GluA2 + $KQID_{78\text{-}81}$	0.79
8	GluA2 + wt γ-2	*vs.*	GluA2 + $HFPE_{82\text{-}85}$	0.086
9	GluA2 + wt γ-2	*vs.*	GluA2 + $WRT_{64\text{-}66}$	0.40

Table 3.6: Neither wt γ-2 nor the Ex1 mutants significantly prolonged GluA2Q deactivation.

The fact that mutations in Ex1, which disrupt AMPAR/TARP interaction affect deactivation kinetics of GluA1 (see Fig. 3.3) but not GluA2 (Fig. 3.9), suggests that the degree to which TARPs prolong AMPAR deactivation is likely to be AMPAR subunit-specific. Previously, GluA3 deactivation has been found to be unaffected by γ-2 (Suzuki et al., 2008). The same study showed only a weak effect of γ-2 on GluA2Q deactivation, while the prolongation of GluA1 deactivation time constant was much more pronounced. This supports the view that GluA2Q may be less sensitive than

GluA1 to the γ-2-mediated slowing of deactivation kinetics.

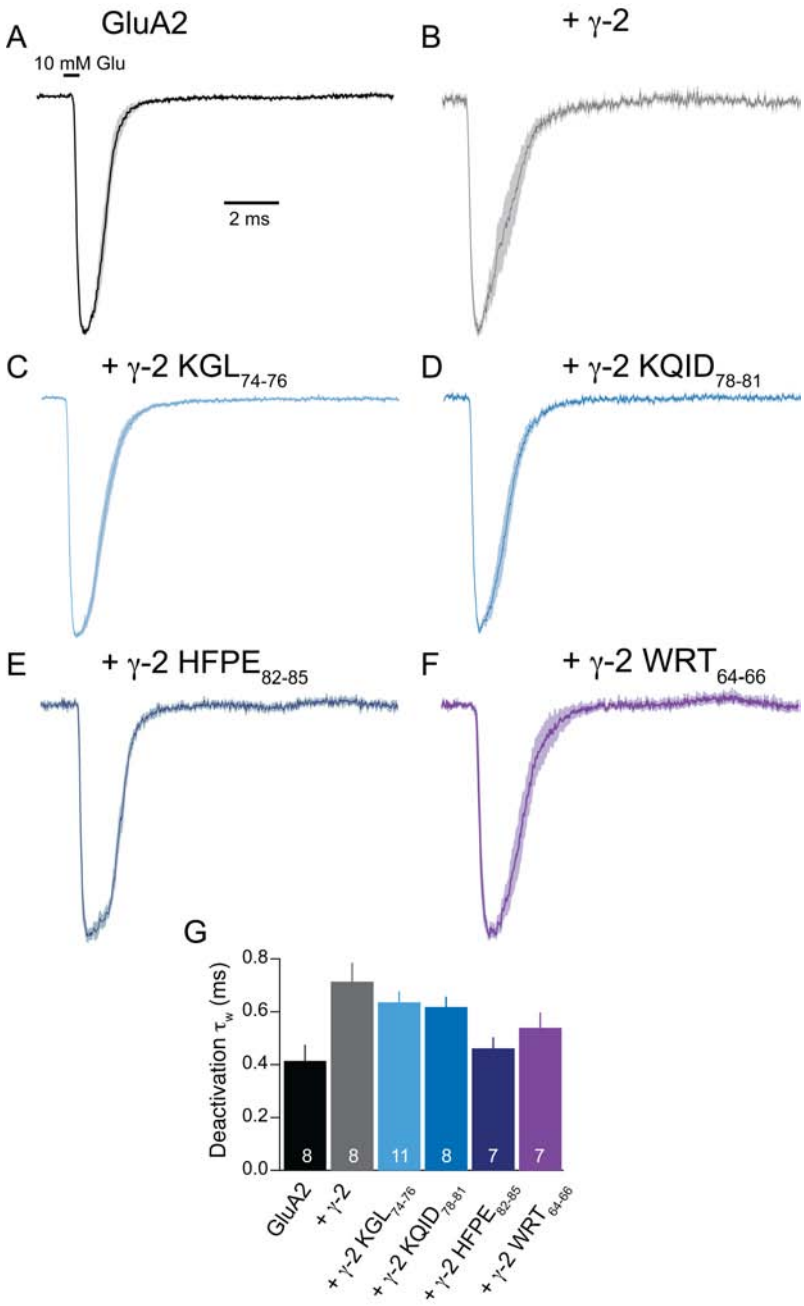

Figure 3.9: γ-2 Ex1 mutants did not affect GluA2 deactivation kinetics. (**A**) Normalised mean response to 1 ms applications of 10 mM Glu from GluA2-containing patches. Grey shading denotes the SEM. The black bar on top of the figure marks the duration of Glu application. Mean currents from individual patches were normalised to the peak and aligned at the 20 % rise time before averaging. (**B-F**) As for A, but for patches expressing GluA2 + wt γ-2, + $KGL_{74\text{-}76}$, + $KQID_{78\text{-}81}$, + $HFPE_{82\text{-}85}$ and + $WRT_{64\text{-}66}$ (**G**) Histogram showing τ_w of deactivation for each of the Ex1 mutants as well as GluA2 and GluA2+ wt γ-2 controls. Bars denote the SEM and the *n* numbers for each group are indicated in white at the bottom of the histogram. Although one-way ANOVA showed that the data did not represent a single population ($F_{(5,\ 19.24)}$ = 3.71, P= 0.0162), the pairwise tests failed to show significant differences between the individual groups.

3.3.8 The $HFPE_{82\text{-}85}$ mutation inhibited the effect of γ-2 on GluA2 desensitization

As shown in Fig. 3.10, wt γ-2 prolonged GluA2 desensitization $\sim$2-fold (τ_w= 9.44 $\pm$ 0.62 ms for wt γ-2 *vs.* 4.84 $\pm$ 0.28 ms for GluA2 alone, P= 4.1 $\times$ 10^{-5}). The $KGL_{74\text{-}76}$ and $KQID_{78\text{-}81}$ mutants had a similar effect on GluA2 desensitization (7.64 $\pm$ 0.25 ms, P= 3.34 $\times$ 10^{-6} for $KGL_{74\text{-}76}$; 10.25 $\pm$ 0.5 ms, P= 1.05 $\times$ 10^{-5} for $KQID_{78\text{-}81}$) and were not significantly different from wt γ-2 (P= 0.051 and P= 0.32 respectively). The $HFPE_{82\text{-}85}$ mutant did not significantly prolong desensitization kinetics compared with GluA2 alone (5.90 $\pm$ 0.35 ms P= 0.066) and differed significantly from wt γ-2 (P= 6.54 $\times$ 10^{-4}). By contrast, the $WRT_{64\text{-}66}$ mutant significantly prolonged GluA2Q desensitization (6.95 $\pm$ 0.27 ms, P= 1.17 $\times$ 10^{-4}) and its effect on desensitization was different from that of wt γ-2 (P= 0.0087).

Two interesting points arise from the above results. First, it appears that compared with GluA1 (see Fig. 3.4), GluA2Q desensitization kinetics is regulated by a more C-terminal part of Ex1, as seen by comparing the effects of $KGL_{74\text{-}76}$ and $HFPE_{82\text{-}85}$ mutants on the two subunits. The γ-2-mediated prolongation of GluA1 desensitization was disrupted by the $KGL_{74\text{-}76}$ but not the more C-terminal $HFPE_{82\text{-}85}$ mutation, while with GluA2Q the reverse pattern was observed. Second, the $WRT_{64\text{-}66}$ mutant upon co-expression with GluA2Q produced receptors with properties intermediate between TARPless GluA2 and GluA2 + wt γ-2. The residues mutated in $WRT_{64\text{-}66}$ are close to the double cysteine (residues 67-68) and are part of a motif highly conserved in the CACNG family, which suggests that these residues may be vital for maintaining the correct structure of the TARP protein. Thus, the effects of this mutation may arise from disruption of the interaction with the pore-forming subunit as well as from changes in Ex1 structure.

	Mean (%)	**SEM**	***n***
GluA2	1.21	0.25	10
wt γ-2	5.03	0.61	12
$KGL_{74\text{-}76}$	3.43	0.30	12
$KQID_{78\text{-}81}$	7.02	1.09	8
$HFPE_{82\text{-}85}$	2.76	0.55	7
$WRT_{64\text{-}66}$	1.51	0.31	14

Table 3.7: $HFPE_{82\text{-}85}$ and $WRT_{64\text{-}66}$ mutants did not increase GluA2 steady-state current fraction.

In addition to desensitization kinetics, the extent of desensitization (quantified as % steady-state current) was also analysed and is summarised in Table 3.7. The regulation of the extent of GluA2 desensitization by Ex1 mutants showed a pattern similar to

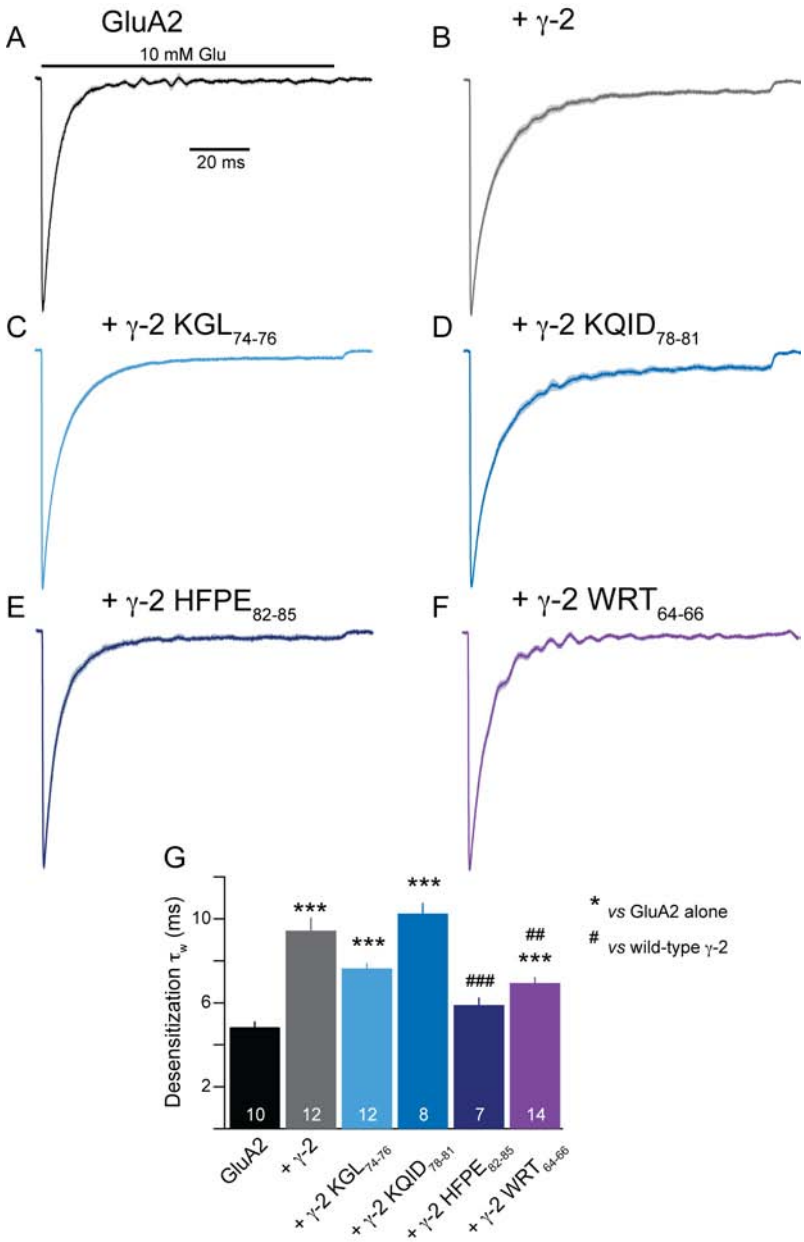

Figure 3.10: Ex1 mutants $HFPE_{82\text{-}85}$ and $WRT_{64\text{-}66}$ differed from wt γ-2 in their effect on GluA2 desensitization. (**A**) Normalised mean response to 100 ms applications of 10 mM Glu to GluA2-containing patches (black trace). Grey shading denotes the SEM. The black bar above the trace marks the duration of Glu application. Mean currents from individual patches were normalised to the peak and aligned at the 20 % rise time before averaging. (**B-F**) As for A, but for patches expressing GluA2 + wt γ-2, + $KGL_{74\text{-}76}$, + $KQID_{78\text{-}81}$, + $HFPE_{82\text{-}85}$ and + $WRT_{64\text{-}66}$ (n=12, 12, 8, 7 and 14 respectively). (**G**) Histogram showing τ_w of desensitization for each of the Ex1 mutants as well as GluA2 and GluA2 + wt γ-2 controls. Bars denote the SEM and the n numbers for each group are indicated in white. One-way ANOVA showed a significant effect of γ-2 variants on GluA2 desensitization ($F_{(5,\ 23.94)}$ = 24.13 , P= 1.26 $\times$ 10^{-8}). Asterisks mark significant difference compared with GluA2 alone ($***$ P<0.001; Welch t-test), while hashes mark significant difference compared with GluA2 + wt γ-2 (## P<0.01, ### P<0.001; Welch t-test).

the regulation of desensitization kinetics. There was an overall significant effect of γ-2 variants on the percentage of GluA2 steady-state current ($F_{(5,\ 23.23)}$ = 14.39 , P= 1.82 $\times$ 10^{-6}). Wt γ-2 significantly increased the % of steady-state current when compared with GluA2 alone as did $KGL_{74\text{-}76}$ and $KQID_{78\text{-}81}$. By contrast, $HFPE_{82\text{-}85}$ and $WRT_{64\text{-}66}$ mutants were ineffective at increasing the steady-state current fraction. The $WRT_{64\text{-}66}$ mutant differed significantly from wt γ-2 in its effect on the extent of GluA2 desensitization, while the remaining mutants did not. The statistical tests are summarised in Table 3.8.

The data shown here suggest that GluA2 steady-state current percentage is affected by Ex1 mutants differently to that of GluA1 (see Fig. 3.4 and Table 3.2), since the $KGL_{74\text{-}76}$, and not the $HFPE_{82\text{-}85}$ mutant, lacked an effect on GluA1 steady-state current fraction.

Test No.	Test pair			*P*-value
1	GluA2	*vs.*	GluA2 + wt γ-2	0.00032
2	GluA2	*vs.*	GluA2 + $KGL_{74\text{-}76}$	0.00012
3	GluA2	*vs.*	GluA2 + $KQID_{78\text{-}81}$	0.0054
4	GluA2	*vs.*	GluA2 + $HFPE_{82\text{-}85}$	0.12
5	GluA2	*vs.*	GluA2 + $WRT_{64\text{-}66}$	0.45
6	GluA2 + wt γ-2	*vs.*	GluA2 + $KGL_{74\text{-}76}$	0.12
7	GluA2 + wt γ-2	*vs.*	GluA2 + $KQID_{78\text{-}81}$	0.27
8	GluA2 + wt γ-2	*vs.*	GluA2 + $HFPE_{82\text{-}85}$	0.066
9	GluA2 + wt γ-2	*vs.*	GluA2 + $WRT_{64\text{-}66}$	0.00061

Table 3.8: $HFPE_{82\text{-}85}$ and $WRT_{64\text{-}66}$ failed to increase the percentage of GluA2 steady-state current.

3.3.9 $HFPE_{82\text{-}85}$ and and $WRT_{64\text{-}66}$ mutations affected the ability of γ-2 to relieve spermine block of GluA2

As seen in Fig. 3.11, wt γ-2 relieved spermine block of GluA2 at positive membrane potentials (RI = 0.383 $\pm$ 0.033 for wt γ-2 *vs.* 0.042 $\pm$ 0.006 for GluA2 alone, P= 3.64 $\times$ 10^{-5}). The $KGL_{74\text{-}76}$ and $KQID_{78\text{-}81}$ mutants were not significantly different from wt γ-2 (P= 0.33 and 0.84 respectively) and showed a large relief of GluA2 spermine block (RI= 0.325 $\pm$ 0.022, P= 1.2 $\times$ 10^{-7} for $KGL_{74\text{-}76}$ and 0.393 $\pm$ 0.037, P= 6.48 $\times$ 10^{-5} for $KQID_{78\text{-}81}$). $HFPE_{82\text{-}85}$ and $WRT_{64\text{-}66}$ mutants relieved GluA2 spermine block to a significant degree (0.179 $\pm$ 0.020, P= 8.64 $\times$ 10^{-4} for $HFPE_{82\text{-}85}$ and 0.182 $\pm$ 0.018, P= 3.58 $\times$ 10^{-4} for $WRT_{64\text{-}66}$). However, the relief of spermine block with these two mutants was $\sim$50 % smaller than that seen with wt γ-2 (P= 7.82 $\times$ 10^{-4} for both $HFPE_{82\text{-}85}$ and $WRT_{64\text{-}66}$).

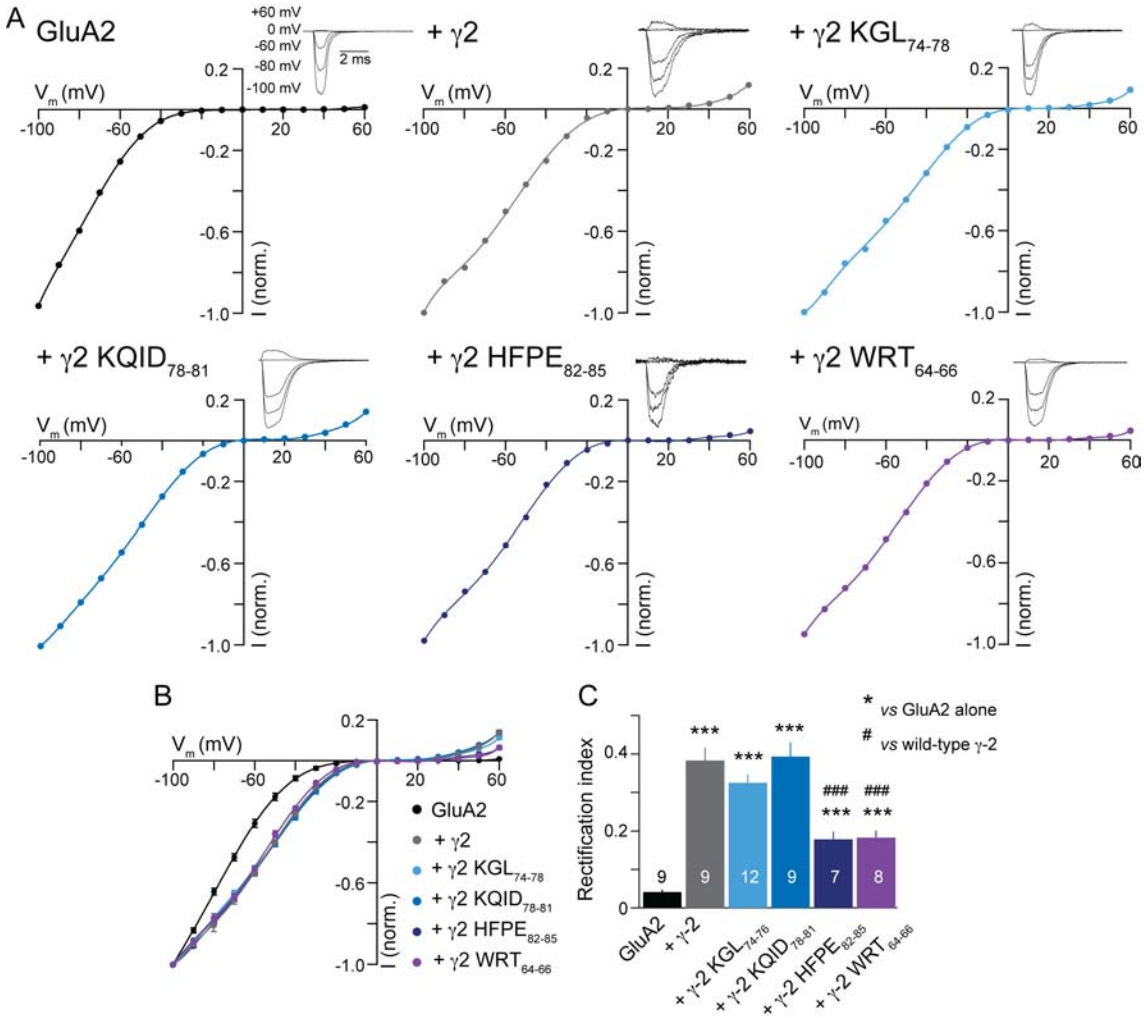

Figure 3.11: $HFPE_{82\text{-}85}$ and $WRT_{64\text{-}66}$, but not other Ex1 mutations, reduced the effect of γ-2 on GluA2 rectification. (**A**) Peak *I-V* plots for from individual representative patches for each construct. Note the strong block of GluA2 responses at positive membrane potentials, and a relief of block seen with wt γ-2. With $KGL_{74\text{-}76}$ and $KQID_{78\text{-}81}$ mutants rectification was similar to γ-2, while $HFPE_{82\text{-}85}$ and $WRT_{64\text{-}66}$ mutants showed an effect on RI that was intermediate between wt γ-2 and TARPless GluA2. Peak currents at each holding potential were normalised to the peak at -100 mV. Insets show average traces for that patch at -100, -80, -60, 0 and +60 mV as indicated, normalised to the peak at -100 mV. (**B**) Average normalised peak *I-V* plots for GluA2 alone, GluA2 + wt γ-2, + $KGL_{74\text{-}76}$, + $KQID_{78\text{-}81}$, + $HFPE_{82\text{-}85}$ and + $WRT_{64\text{-}66}$. Peak currents from each patch were normalised to the peak at -100 mV before averaging. (**C**) Histogram showing rectification index calculated as slope conductance ratio, for GluA2 alone or co-expressed with the different γ-2 variants. Bars denote SEM and *n* numbers are shown on the histogram. One-way ANOVA showed a significant overall effect of γ-2 variants on GluA2 rectification ($F_{(5,\ 19.74)}$ = 65.25 , P= 1.36 $\times$ 10^{-11}). Asterisks mark significant difference compared with GluA2 alone ($***$ P< 0.001; Welch *t*-test), while hashes mark significant difference compared with GluA2 + wt γ-2 (### P< 0.001; Welch *t*-test).

As seen in panel C Fig. 3.11, the *I-V* relationships for $HFPE_{82\text{-}85}$ and $WRT_{64\text{-}66}$ mutants appeared more rectifying at positive membrane potentials compared with either wt γ-2 or the $KGL_{74\text{-}76}$ and $KQID_{78\text{-}81}$ mutants. However, at negative membrane voltages the *I-V* relationships for wt γ-2 and the Ex1 mutants were almost overlaid, which was confirmed by fitting *G-V* plots to the Boltzmann equation (2.8 on page 62) in Fig. 3.12. The difference in *I-V* relationships at positive, but not negative membrane potentials suggest, that as for GluA1 (see Fig. 3.5), mutations in Ex1 may affect permeation of spermine through the channel pore.

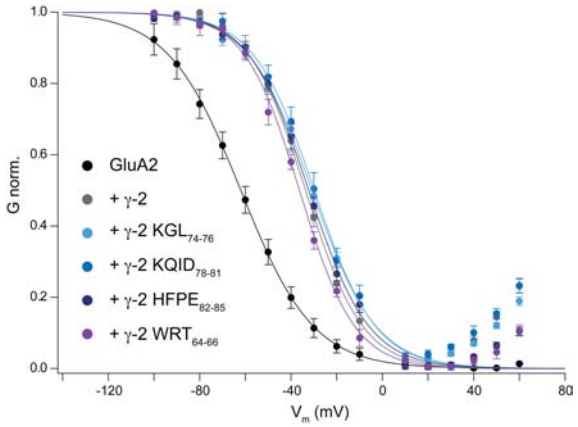

Figure 3.12: When co-expressed with GluA2, the Ex1 mutants and wt γ-2 produced similar shifts in *G-V* relationship at negative membrane potentials. Normalised peak conductance was plotted against membrane voltage for GluA2 alone, or co-expressed with wt γ-2, $KGL_{74\text{-}76}$, $KQID_{78\text{-}81}$, $HFPE_{82\text{-}85}$ or $WRT_{64\text{-}66}$ and fitted to the Boltzmann equation (2.8 on page 62) between -100 mV and -10 mV. Wt γ-2 produced a +28.4 mV shift in the *G-V* relationship for GluA2. The magnitude of the shift was similar for all of the Ex1 mutants. Parameters of the Boltzmann fits are summarized in Table 3.9.

	GluA2	**+ wt γ-2**	**+ $KGL_{74\text{-}76}$**	**+ $KQID_{78\text{-}81}$**	**+ $HFPE_{82\text{-}85}$**	**+ $WRT_{64\text{-}66}$**
Boltzmann fit	(9)	(9)	(12)	(9)	(7)	(8)
$V_{0.5}$ (mV)	-62.0	-33.6	-30.8	-29.8	-32.3	-36.3
***k* (mV)**	15.9	12.5	14.0	13.4	13.2	12.1
$V_{0.5}$ shift (mV)		+28.4	+31.1	+32.2	+29.7	+25.7

Table 3.9: Parameters of the Boltzmann fits to *G-V* relationships for GluA2 alone and co-expressed with wt γ-2 or Ex1 mutants. Conductance-voltage plots were created from an average *I-V* relationship from (*n*) patches for each condition and fitted to the Boltzmann equation (2.8 on page 62) between -100 mV and -10 mV. The parameters of the Bolztmann fits ($V_{0.5}$ and *k*) are shown above.

3.3.10 Ex1 mutants increased GluA2 mean single-channel conductance

Wt γ-2 and all Ex1 mutants increased the mean single-channel conductance of GluA2 receptors (Fig. 3.13G). Wt γ-2 increased mean single-channel conductance $\sim$1.5-fold compared with GluA2 alone (32.6 $\pm$ 2.0 pS for GluA2 + wt γ-2 *vs.* 21.1 $\pm$ 1.8 pS for GluA2 alone. Co-expression of the Ex1 mutants with GluA2Q resulted in a similar increase in mean single-channel conductance. The mean single-channel conductance estimates were 35.3 $\pm$ 1.4 pS for $KGL_{74\text{-}76}$, 38.1 $\pm$ 2.0 pS for $KQID_{78\text{-}81}$, 34.7 $\pm$ 1.4 fro $HFPE_{82\text{-}85}$ and 32.3 $\pm$ 1.6 for $WRT_{64\text{-}66}$. The results of the statistical comparisons are listed in Table 3.10.

Test No.	**Test pair**			***P*-value**
1	GluA2	*vs.*	GluA2 + wt γ-2	0.0023
2	GluA2	*vs.*	GluA2 + $KGL_{74\text{-}76}$	0.00014
3	GluA2	*vs.*	GluA2 + $KQID_{78\text{-}81}$	0.00021
4	GluA2	*vs.*	GluA2 + $HFPE_{82\text{-}85}$	0.00030
5	GluA2	*vs.*	GluA2 + $WRT_{64\text{-}66}$	0.0014
6	GluA2 + wt γ-2	*vs.*	GluA2 + $KGL_{74\text{-}76}$	0.85
7	GluA2 + wt γ-2	*vs.*	GluA2 + $KQID_{78\text{-}81}$	0.28
8	GluA2 + wt γ-2	*vs.*	GluA2 + $HFPE_{82\text{-}85}$	0.85
9	GluA2 + wt γ-2	*vs.*	GluA2 + $WRT_{64\text{-}66}$	0.90

Table 3.10: The Ex1 mutants increased GluA2Q mean single-channel conductance to the same level as wt γ-2.

In addition to increasing GluA2 mean single-channel conductance, wt γ-2 increased peak P_o (Fig. 3.13H) of GluA2 receptors $\sim$1.5-fold (from 0.55 $\pm$ 0.05 for GluA2 alone to 0.82 $\pm$ 0.03 for GluA2 + wt γ-2, P= 0.0073). The $KGL_{74\text{-}76}$ and $KQID_{78\text{-}81}$ mutants also increased GluA2 P_o (to 0.82 $\pm$ 0.01, P= 0.0085 and 0.78 $\pm$ 0.03, P= 0.023, respectively). Those two mutants were not significantly different from wt γ-2 (P= 0.98 and 0.70, respectively). The $HFPE_{82\text{-}85}$ and $WRT_{64\text{-}66}$ mutants did not significantly increase GluA2 P_o (0.70 $\pm$ 0.03, P= 0.087 and 0.72 $\pm$ 0.02, P= 0.073 respectively) and did not differ significantly from wt γ-2 (P= 0.071 and 0.073 for $HFPE_{82\text{-}85}$ and $WRT_{64\text{-}66}$, respectively). This suggests that the Ex1 region of γ-2 may affect peak P_o but GluA2 single-channel conductance is regulated by interactions with TARP regions distinct from Ex1.

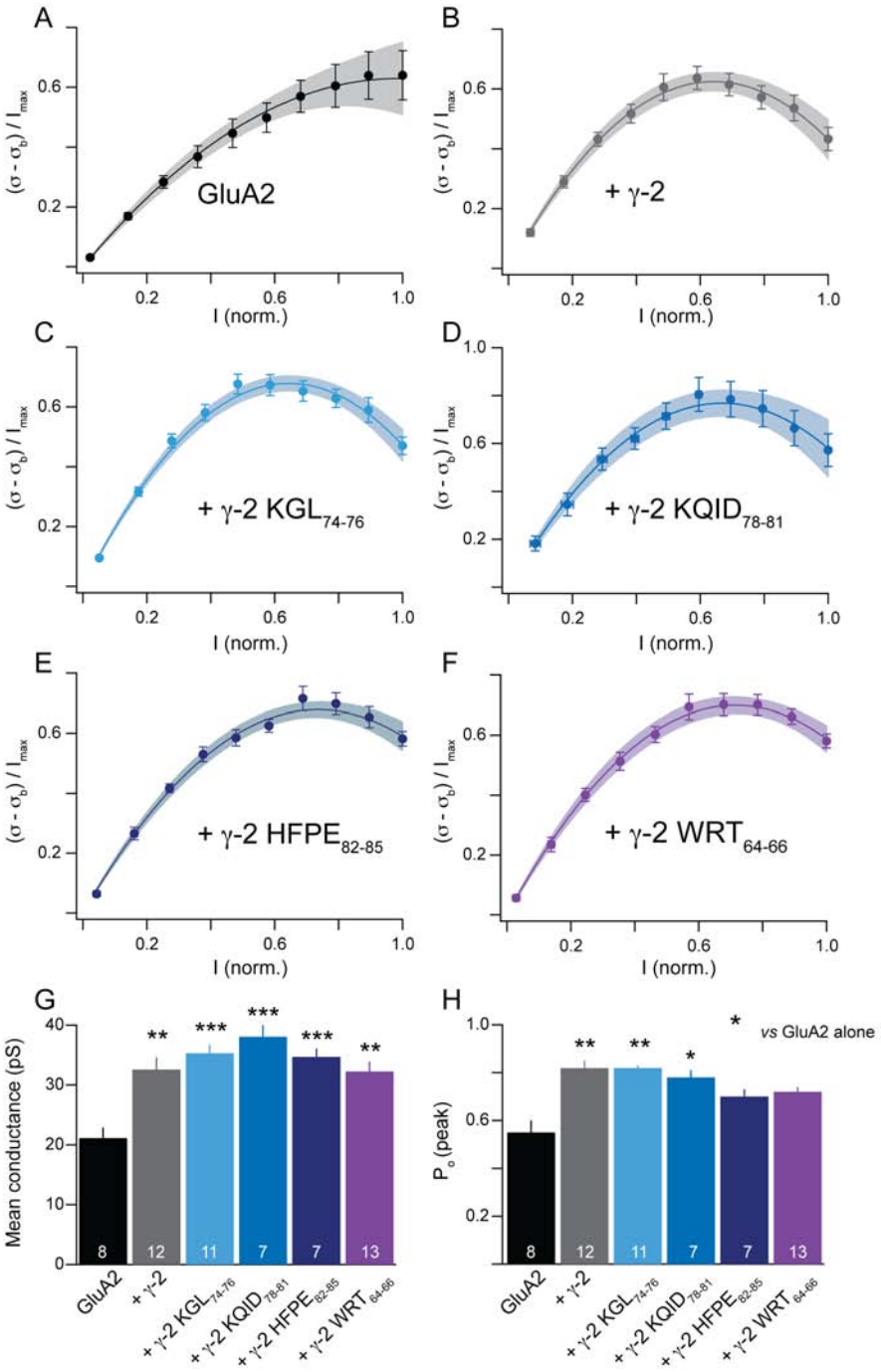

Figure 3.13: All Ex1 mutants increased GluA2Q single-channel conductance but they varied in their effect on P_o. (**A**) Average normalised current-variance relationship for GluA2 alone. Mean current (x-axis) was normalised to the peak (1st bin). Variance was also normalised to the peak current after subtracting σ_b. Vertical and horizontal error bars on the data points indicate the variance and mean current SEM respectively. The grey shading covers the area between the 95% confidence interval bands for the parabolic NSFA fit (black line) to equation 2.6 on page 61. The fit was weighted by the SEM and the σ_b parameter was constrained to 0. (**B-F**) As for A, but for GluA2 + wt γ-2, + KGL_{74-76}, + $KQID_{78-81}$, + $HFPE_{82-85}$ and + WRT_{64-66}, respectively.

Figure 3.13 continued: (**G**) Histogram showing mean single-channel conductance for Ex1 mutants as well as GluA2 alone and GluA2 + wt γ-2 controls. Bars denote SEM and *n* numbers are indicated at the bottom of the histogram. One-way ANOVA showed a significant overall effect of γ-2 variants on GluA2 conductance ($F_{(5,\ 22.37)}$ = 10.13 , P= 3.61 $\times$ 10^{-5}). Asterisks mark significant difference compared with GluA2 alone ($*\ *$ P< 0.01, $*\ *\ *$ P< 0.001; Welch *t*-test). (**H**) Histogram showing peak open probability for Ex1 mutants as well as GluA2 alone and GluA2 + wt γ-2 controls. Bars denote SEM and *n* numbers are indicated at the bottom of the histogram. One-way ANOVA showed a significant overall effect of γ-2 variants on GluA2 P_o ($F_{(5,\ 20.68)}$ = 8.15, P= 2.2 $\times$ 10^{-4}). Asterisks mark significant difference compared with GluA2 alone ($*$ P< 0.05, $*\ *$ P< 0.01; Welch *t*-test).

3.3.11 Ex1 mutants showed effects on kainate efficacy (relative to glutamate) that were intermediate between GluA2 alone and GluA2 + wt γ-2

Co-expression of wt γ-2 resulted in more than 6-fold increase in the KA/Glu ratio compared with GluA2Q alone (0.62 $\pm$ 0.03, *n*=5 for wt γ-2 *vs.* 0.08 $\pm$ 0.03, *n*=4, for GluA2 alone; P= 3.33 $\times$ 10^{-5}). All of the Ex1 mutants significantly increased kainate efficacy when compared with GluA2 alone ($KGL_{74\text{-}76}$: 0.61 $\pm$ 0.07, *n*=7, P= 0.001; $KQID_{78\text{-}81}$: 0.39 $\pm$ 0.06, *n*=5, P= 0.015; $HFPE_{82\text{-}85}$: 0.43 $\pm$ 0.04, *n*=6, P= 0.00038; $WRT_{64\text{-}66}$: 0.21 $\pm$ 0.02, *n*=8, P= 0.026). However, all Ex1 mutants apart from $KGL_{74\text{-}76}$ (P= 0.95) produced changes that differed significantly from that of wt γ-2 (P= 0.028, P= 0.015 and P= 0.00021 for $KQID_{78\text{-}81}$, $HFPE_{82\text{-}85}$ and $WRT_{64\text{-}66}$, respectively).

The results obtained when the γ-2 mutants were co-expressed with GluA2 differed from results obtained when they were co-expressed with GluA1, where the $KGL_{74\text{-}76}$ mutation reduced kainate efficacy compared with wt γ-2 (compare Figs. 3.14 and 3.8). This suggests, that distinct regions of Ex1 may affect the LBD cleft closure to differing extents, depending on which AMPAR subunit is present. The $WRT_{64\text{-}66}$ mutant increased KA/Glu ratio only weakly compared with TARPless GluA2. As mentioned above, due to its key position for Ex1 structure, this mutation may exert its effects through disruption of that structure, as well as through direct removal of AMPAR/TARP interaction.

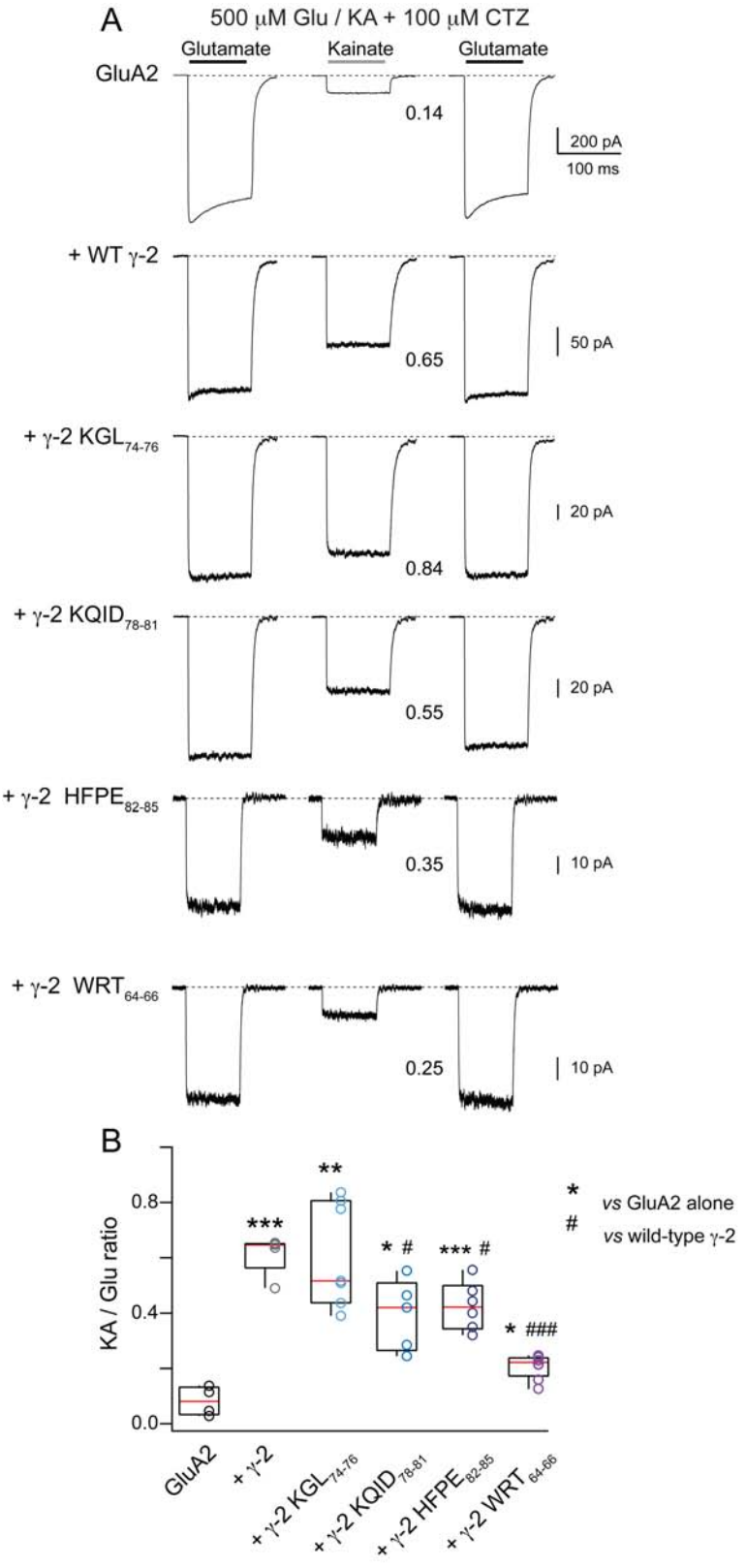

Figure 3.14: Ex1 mutants increased kainate efficacy (relative to glutamate) compared with GluA2 alone, but with the exception of $KGL_{74\text{-}76}$, were less effective than wt γ-2.

Figure 3.14 continued: (**A**) Mean responses from representative patches showing the initial response to 500 μM Glu (left), followed by 500 μM KA (middle) and a second response to Glu (right). Both Glu and KA were supplemented with 100 μM CTZ to limit desensitization. (**B**) Box and whisker plot of the KA/Glu response ratios (measured as a ratio of the steady-state responses in CTZ). The box shows the 25-75 percentile, while the whiskers are the 10-90 percentile. Individual data points are overlaid on the plot (open circles). One-way ANOVA showed a significant overall effect of γ-2 variants co-expressed with GluA2 on KA/Glu response ratio ($F_{(5,\ 11.65)}$ = 38.36 , P= 7.62 $\times$ 10^{-7}). Asterisks mark significant difference compared with GluA2 alone ($*$ P< 0.05, $**$ P< 0.01. $***$ P< 0.001; Welch t-test), while hashes mark significant difference compared with GluA2 + wt γ-2 ($\#$ P< 0.05, $\#\#\#$ P< 0.001; Welch t-test).

3.4 Discussion

The Ex1 region of TARPs is a known AMPAR interaction domain (Tomita et al., 2005; Cho et al., 2007; Milstein and Nicoll, 2009). The individual mutations in Ex1 that we examined affected different measures of TARP efficacy to varying extents, suggesting that specific regions of Ex1 are involved in modulating different AMPAR biophysical properties. In addition, the fact that the effects of a given Ex1 mutation often differed between GluA1 and GluA2 subunits, suggests that the interaction between Ex1 of TARPs and the AMPAR pore-forming subunits may exhibit some interesting subunit specificity.

All of the γ-2 mutants examined gave responses that were more rectifying (greater degree of block by intracellular spermine) than those seen when GluA1 was co-expressed with wt γ-2. In other words, the Ex1 mutants were less effective than wt stragazin at relieving polyamine block. Ca^{2+}-permeability of AMPARs and block by polyamines are determined by the presence of a neutral glutamine (Q) residue at the Q/R site located in the pore region of each of the AMPAR subunits that assemble to form the tetrameric receptor. The presence of edited (arginine, R form) GluA2 subunit within the receptor renders AMPARs Ca^{2+}-impermeable and no longer susceptible to block by polyamines (Bowie and Mayer, 1995; Kamboj et al., 1995; Koh et al., 1995).

The presence of γ-2 is known to greatly reduce polyamine block of CP-AMPARs (Soto et al., 2007), an effect mediated in part by the proximal part of the γ-2 C-tail (Soto et al., 2014). However deletion of the C-terminus appeared insufficient to completely abolish the γ-2-mediated relief of spermine block (Soto et al., 2014). It is thus of interest, that in the study presented here, all three Ex1 mutants co-expressed with GluA1 showed rectification intermediate between GluA1 alone and GluA1 + wt γ-2. On the other hand, when Ex1 mutants were co-expressed with GluA2, the mutants $KGL_{74\text{-}76}$ and $KQID_{78\text{-}81}$ reduced GluA2 spermine block to the same extent as wt γ-2, while the mutants $HFPE_{82\text{-}85}$ and $WRT_{64\text{-}66}$ were significantly less efficient than wt γ-2.

With either GluA1 or GluA2, the *I-V* relationships for the Ex1 mutants were almost identical to the *I-V* for wt γ-2 at negative membrane potentials and any differences were observed only at positive membrane potentials. This could suggest that while the Ex1 region of TARPs does not play a role in regulating spermine binding to the AMPAR channel pore, it may affect the permeation of spermine through the AMPAR channel at positive potentials. Thus, it appears that both extracellular and intracellular (Soto et al., 2014) regions of the TARP are required for regulation of AMPAR

rectification.

γ-2 has been reported to increase mean single-channel conductance of AMPARs (Soto et al., 2009; Jackson et al., 2011; Shelley et al., 2012; Coombs et al., 2012; Zhang et al., 2014). None of the mutations in Ex1 affected the ability of γ-2 to increase GluA2 single-channel conductance. Together with only a partial effect of Ex1 mutants on rectification, these results suggest that other regions of the TARP, such as TM2 (Tomita et al., 2005) may also play an important role in modulating AMPAR properties, particularly those related to ion permeation, where the effect of the TARP may result from AMPAR/TARP interactions within the channel pore region (Soto et al., 2014).

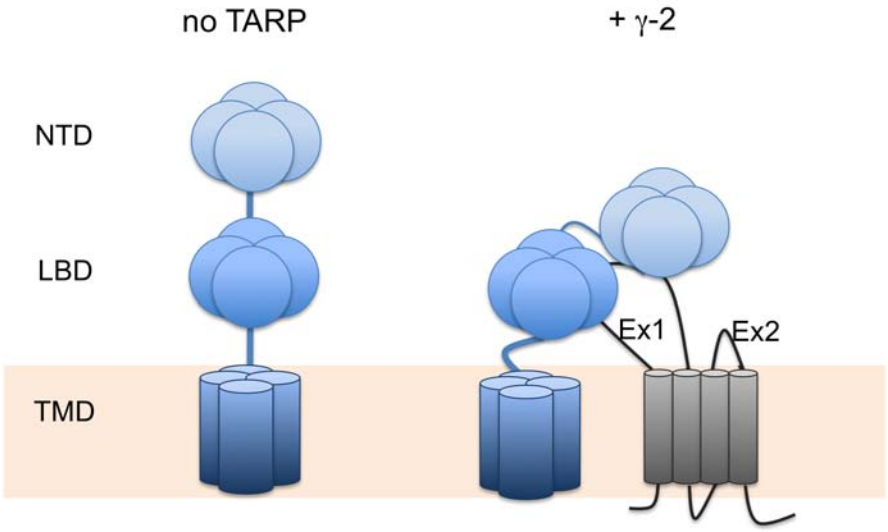

Figure 3.15: Ex1 of γ-2 may contact both the NTD and LBD of GluA2 and wedge between these two domains. Proposed relative arrangement of GluA2 domains in the absence of TARP (left) and in complex with γ-2 (right). When the AMPAR co-assembles with the TARP, the Ex1 of γ-2 contacts both the NTD and the LBD of GluA2 and wedges between the two domains, altering their relative position. AMPAR domains: NTD: N-terminal domain, LBD: ligand-binding domain, TMD: transmembrane domain. TARP regions: Ex1: first extracellular loop, Ex2: second extracellular loop.

The fact that different mutations in Ex1 affected GluA1 and GluA2 rectification differently, may suggest that the interaction is subunit-specific, which may result from structural differences in the arrangement of the Ex1 region in different AMPAR/TARP complexes. Regulation of deactivation kinetics also differed between GluA1 and GluA2. While wt γ-2 and all of the Ex1 mutants significantly increased the time constant of

deactivation of GluA1 AMPARs, the deactivation of homomeric GluA2Q receptors was unchanged by the presence of wt γ-2 or any of the Ex1 mutants. GluA2 has previously been reported to be only weakly sensitive to γ-2 -mediated modulation of deactivation and a complete lack of sensitivity was observed with GluA3 (Suzuki et al., 2008). This again suggests that the interaction between Ex1 of TARPs and the AMPAR exhibits subunit-dependent properties. It would be thus of interest to obtain structural data on γ-2 interaction with GluA1.

A number of other functional properties of AMPARs, including desensitization kinetics, the extent of desensitization, channel open probability and the relative efficacy of kainate also differed between individual Ex1 mutants, and (within the same mutant) between co-expression with GluA1 and GluA2. However, at all times the Ex1 mutants retained some TARP-like properties, suggesting that none of the mutations alone was sufficient to completely abolish TARP interaction with either GluA1 or GluA2. The impact of the $WRT_{64\text{-}66}$ mutation on the multiple functional properties of GluA2 was the most consistent and most profound amongst all the Ex1 mutants. This specific mutation targets a region highly conserved in the CACNG family, and may disrupt the secondary structure of Ex1 due to its location in the proximity of the double cysteine (residues 67-68, Fig. 3.2).

Structural differences between different AMPAR subunits may add to the diversity of functional effects observed here. While the regions of Ex1 we have investigated are known to interact with both LBD and NTD of GluA2, the relative affinities of the different Ex1 regions for the two AMPAR domains are not the same. Previously published data suggest that partial agonist efficacy is regulated by the LBD only (Jin et al., 2003). Thus disruption of γ-2 interaction with the LBD of AMPAR could explain the reduced kainate efficacy seen with the Ex1 mutants. The role of the NTD in the regulation of AMPAR properties by TARPs is less clear. The NTD has been reported to affect AMPAR assembly (Rossmann et al., 2011). However, it is known that AMPARs lacking the NTD remain functional (see Pasternack et al. 2002). The role of the NTD in AMPAR/TARP complex function is investigated further in the next Chapter.

The fact that Ex1 contains both NTD and LBD interaction patches may imply substantial reconfigurations of the AMPAR upon TARP interaction. Based on the structural and functional data obtained so far, the proposed structure of the AMPAR/TARP complex is that the Ex1 of γ-2 interacts with both NTD and LBD of GluA2 and wedges between these two domains (see Fig. 3.15). The AMPAR interaction region spans a substantial part of Ex1, which could explain the incomplete loss of TARP-like properties by the Ex1 mutants. However, peptide arrays utilize linear peptides, lacking secondary or tertiary structure. It is thus not possible to deduce which of these in-

teractions occur when a full-length TARP forms a complex with an AMPAR tetramer. Further structural data would therefore be necessary to determine the physiological importance of the interactions described here.

4

Experimental Chapter 2: The role of the N-terminal domain of GluA2 in AMPAR/TARP interaction

4.1 Summary

The data shown in Experimental Chapter 1 (Chapter 3) suggested that the extracellular domains of γ-2 (Ex1 and Ex2) interact with both the N-terminal domain (NTD) and the ligand-biding domain (LBD) of GluA2Q. This Chapter expands on these findings to explore the specific role of GluA2Q NTD in AMPAR/TARP interaction. Part of the work described here was carried out in collaboration with Ingo Greger and colleagues (MRC LMB Cambridge). Our collaborators set out to investigate the specific single amino acid residues in Ex1 of γ-2 that are responsible for its binding to the NTD of GluA2Q. They designed both deletion and alanine (Ala) substitution peptide arrays spanning the Ex1 of γ-2 and identified three residues which interact strongly with the GluA2Q NTD. They then generated mutants of γ-2, where the residues identified with the peptide arrays were substituted with Ala. In addition to disrupting γ-2/NTD interaction by mutating the relevant residues on γ-2 Ex1, our collaborators also designed a GluA2Q construct lacking its NTD (GluA2Q$\triangle$NTD), thus disrupting the γ-2/NTD interaction from the AMPAR side. We co-expressed the relevant γ-2 Ex1 mutants with wt or $\triangle$NTD GluA2Q and investigated the effect of disrupting TARP/NTD interaction on a number of AMPAR functional properties, including deactivation and desensitization kinetics, steady-state current fraction, rectification, mean single-channel conductance and KA/Glu ratio.

4.2 Introduction

The NTD of AMPARs spans the first ∼400 amino acids of the receptor immediately following the signal peptide, which targets the AMPAR to the membrane and is later cleaved off by proteolysis. At its C-terminal end, the NTD is connected to the LBD via a flexible ∼16 amino acid linker (Sobolevsky et al., 2009). The NTD layer of AMPARs forms a clamshell composed of two distinct lobes (Jin et al., 2009), rendering a structure similar to that proposed for kainate receptor NTD (Kumar et al., 2009) and the NTD of NMDARs. The clamshell of the AMPAR NTD appears to be dynamic and the movements within the NTD layer are similar to those seen in NMDARs (Dutta et al., 2012). In NMDARs, the NTD is the site of action for allosteric modulators, which can increase NMDAR activity by promoting clamshell cleft opening (Gielen et al., 2009) or reduce the activity through cleft closure (Karakas et al., 2009). In contrast with the NMDAR NTD, no ligands for the AMPAR NTD have been identified to date. Despite some sequence similarity to the mGluR LBD and the bacterial periplasmic leucine/isoleucine/valine-binding protein (LIVBP) (O'Hara et al., 1993; Paas, 1998), the AMPAR NTD is thought to lack an amino acid binding site (Jin et al., 2009); however, a putative ligand-binding site within the AMPAR NTD has been reported (Sukumaran et al., 2011).

The NTD of AMPARs is thought to provide the specificity needed for correct AMPAR assembly. Early biochemical studies used chimeras with kainate receptors to show that the NTD is critical for the assembly of AMPAR subunits with each other, as assessed by Co-IP (Leuschner and Hoch, 1999). However, it was later revealed that other domains, such as the LBD and the TMs are also important for the assembly of functional channels (Ayalon and Stern-Bach, 2001). This is reflected in the fact that within the AMPAR tetramer, subunit-subunit dimers are different in the NTD and LBD layers (Sobolevsky et al., 2009), supporting the view that the NTD alone is insufficient to drive the formation of functional AMPAR tetramers. Therefore, the NTD is thought to mediate the initial assembly of AMPAR subunits into dimers. The isolated NTDs of GluA1 and GluA2 were shown to form tight homomeric dimers in solution (Jin et al., 2009). However, dimerisation of GluA3 homomers is not favoured and the remaining AMPAR subunits preferentially heteromerize with the critical GluA2 subunit at the dimer level, a process also mediated by the NTD (Rossmann et al., 2011). The NTD of AMPARs appears therefore to govern the initial dimerisation of AMPAR subunits, defining the final stoichiometry of AMPARs. It thus plays a major role in determination of several AMPAR biophysical properties, such as inward rectification, which is lacking in GluA2R-containing AMPAR heteromers.

Roles of the NTD, other than those in AMPAR assembly, have been poorly charac-

Figure 4.1: Mutations introduced into γ-2 Ex1 to disrupt interaction with the NTD of GluA2. Two mutations were introduced into Ex1 of γ-2 to disrupt interactions with GluA2 NTD detected using peptide arrays. These included: the single residue mutant R_{65} substitued with Ala, and a triple Ala substitution mutant $R_{65}NF_{72\text{-}73}$, in which apart from the R_{65}, two additional NTD binding sites at N_{72} and F_{73} were also disrupted. Note that the constructs were generated by members of the Greger lab.

terised. Recombinant AMPARs lacking the NTD are functional (Pasternack et al., 2002) and differ only subtly from wt AMPARs. Although the NTD is located $\sim$60 angstrom away from the plane of the plasma membrane, and is thus thought to be beyond the reach of the assiociated TARP, our data suggest that GluA2 NTD interacts with stargazin via the TARP extracellular domain (Experimental Chapter 1). In support of our findings, structural data showed that glutamate-sensitive dynamic rearrangements of the NTD layer can been observed in native (Nakagawa et al., 2005), but not recombinantly expressed AMPARs (Tichelaar et al., 2004; Midgett et al., 2012). The major difference between these studies is that native AMPARs were strongly associated with TARPs (Nakagawa et al., 2005), while the recombinant receptors in the two studies mentioned above lacked these auxiliary subunits.

NTD deletion has been previously reported to affect neither the γ-2-mediated facilitation of trafficking, nor the increase in desensitization τ_w (Bedoukian et al., 2006). However, the data presented in that study showed only that the TARP can still affect GluA2 properties when the NTD is deleted from the AMPAR, and lacked the comparison to a wt receptor. It thus did not permit comment on the relative magnitude of the 'TARP effect' in the absence and presence of the NTD. In order to shed some light on the role of the NTD in the function of AMPAR/TARP complexes, our collaborators

used peptide arrays to identify specific single residues on the Ex1 of γ-2 which interact with the NTD of GluA2. They then generated two γ-2 mutants in which the interaction with AMPAR NTD was disrupted, due to substitution of the amino acids important for this interaction with Ala residues (the singly-substituted R_{65} and the triple Ala mutant $R_{65}NF_{72\text{-}73}$, Fig. 4.1). We co-expressed these γ-2 mutants with wt GluA2Q or GluA2Q lacking the N-terminal domain (GluA2Q ΔNTD, see Fig. 4.2), in order to investigate the effects of the complete disruption of TARP-NTD interactions. We then investigated how disrupting these interactions between the GluA2 NTD and γ-2 affects a number of functional AMPAR properties, including deactivation and desensitization τ_w, steady-state current, rectification, mean single-channel conductance (estimated from NSFA) and the relative efficacy of the partial agonist kainate.

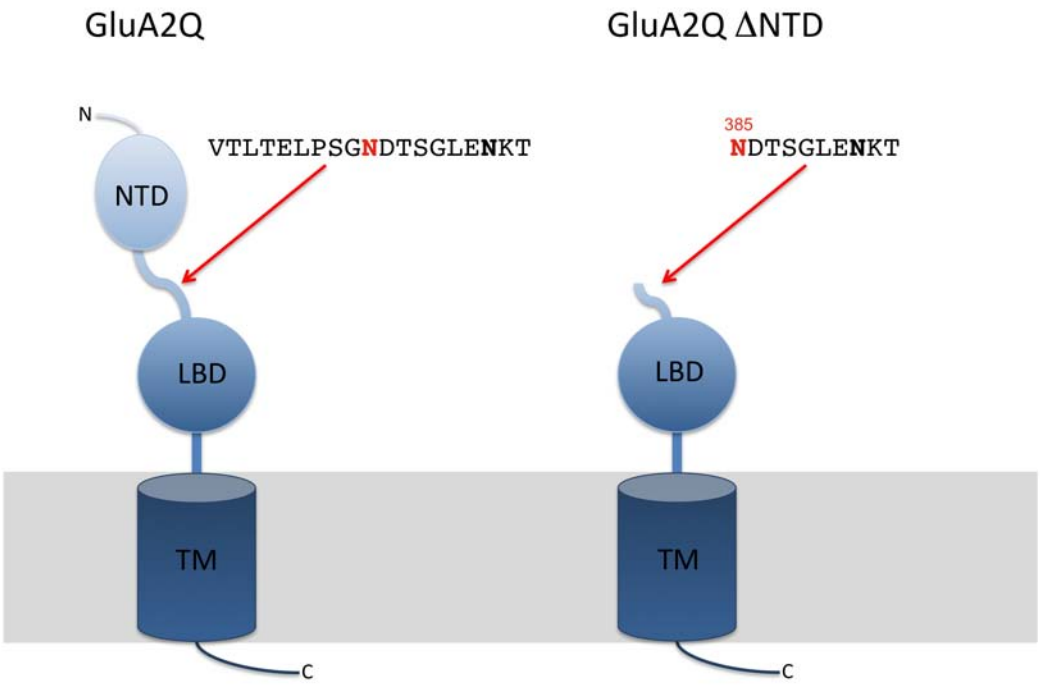

Figure 4.2: The GluA2Q ΔNTD construct was used to ensure complete disruption of TARP-NTD interactions. In comparison with wt GluA2Q (left), GluA2Q ΔNTD (right) lacked the whole N-terminal domain and a substantial part of the NTD-LBD linker (deletion up to N_{385} within the linker, signal peptide not included in the count). Linker truncation was introduced to minimise any non-specific effects arising from abnormal interactions of the flexible, unstructured linker in the absence of the NTD. Note: The signal peptide was also removed in the GluA2Q ΔNTD construct and replaced with the following sequence: MGILPSPGMPALLSLVSLLSVLLMGCVAETG, which resulted from its insertion into the pHLsec vector (Aricescu et al., 2006). An N-terminal HA tag (YPYDVPDYA) was also introduced immediately after the signal sequence. Note that the construct was generated by members of the Greger lab.

4.3 Results

4.3.1 Identification of residues important for interaction between the NTD of GluA2 and the Ex1 of γ-2

Our collaborators used two distinct types of peptide array to identify the single amino acid residues responsible for γ-2 binding to the NTD of GluA2. Both arrays contained peptides from the central part of stragazin Ex1, which appears to interact with the NTD as suggested by our earlier data (see Experimental Chapter 1, Fig. 3.2 on page 70.) The first array (Fig. 4.3, panel A) was an Ala substitution array, in which single naturally occurring residues within the γ-2 Ex1 were sequentially replaced by Ala residues with the increasing peptide count. The second array was a deletion array (Fig. 4.3, panel B), where single amino acid residues were sequentially deleted from the γ-2 Ex1. Both arrays were probed with the NTD of GluA2, leading to the identification of three residues crucial for binding of γ-2 to the NTD: R_{65}, N_{72} and F_{73}. The R_{65} residue appeared to interact very strongly with the NTD, which could be observed in both the Ala substitution and the deletion array. In the Ala substitution array (Fig. 4.3, panel A) R_{65} was substituted with Ala in peptide 3, resulting in the loss of GluA2 NTD binding. This result was confirmed in the deletion array (Fig. 4.3, panel B) where R_{65} was deleted in peptide 14 which showed almost no binding to the NTD of GluA2.

The residues N_{72} and F_{73} were not substituted with Ala in panel A, but were removed in the deletion array (Fig. 4.3, panel B). In peptides 5 and 6 N_{72} and F_{73} were sequentially deleted, resulting in a reduced binding to the NTD of GluA2, as judged from the signal intensity being lower than for the preceding peptide (peptide 4). The residues identified as important for binding to the NTD were again confirmed in peptide 23 of the deletion array, which lacked R_{65} on its N-terminal end and F_{73} on its C-terminal end and showed almost no binding to the NTD. As the strongest decrease in NTD binding throughout these experiments was observed with disruption of R_{65}, it is likely that the lack of binding seen in peptide 23 was mainly caused by deletion of that residue rather than the F_{73}.

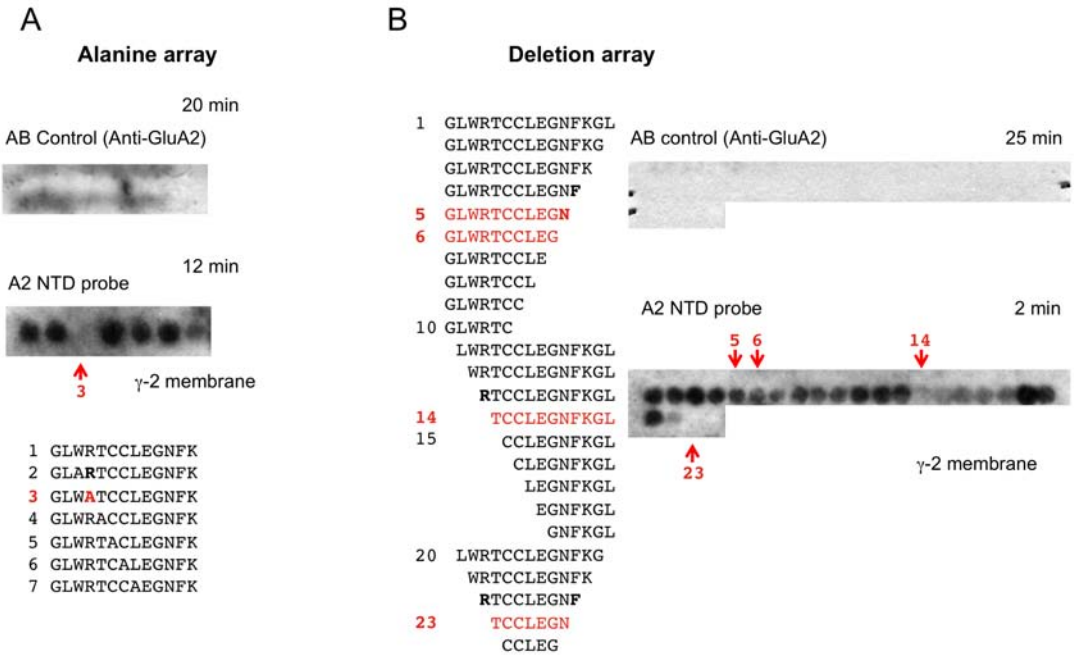

Figure 4.3: Peptide arrays were used to map contacts between the NTD of GluA2Q and the central part of γ-2 Ex1. (**A**) Alanine substitution array containing peptides from the central part of the γ-2 Ex1 loop probed with the NTD of GluA2. The array contained a series of 13-mer peptides, with peptide 1 being the control peptide (wt γ-2 sequence from G_{62} to K_{74}) and the following peptides containing a single residue Ala substitution starting at W_{64} in peptide 2 and shifting with each peptide by 1 residue towards the C-terminal end of the Ex1 loop. Top panel: Non-specific signal, resulting from direct anti-GluA2 antibody binding to the membrane. The membrane was exposed for 20 minutes. Lower panel: the same membrane was exposed to the rat GluA2 NTD and probed with rabbit anti-GluA2 antibody (Alomone, 1:250) followed by a HRP-conjugated anti-rabbit antibody (Pierce, 1:1500). The membrane was exposed for 12 minutes. Peptide 3, which identified the R_{65} residue is indicated by a red arrow. The sequences of all of the peptides are shown below the array. In peptide 3 sequence the Ala residue used to substitute R_{65} is shown in red.

Figure 4.3 continued: (**B**) Deletion array containing a series of variable length peptides from the central part of γ-2 Ex1. Peptide 1 was the control peptide with γ-2 sequence from G_{62} to L_{76}. Compared to peptide 1 (control), peptides 2-10 contained a single residue deletion at the C-terminal end, shifting by 1 residue from the preceding peptide. Peptides 11-19 contained an analogous deletion at the N-terminal end. In peptides 20-24 there was a two-residue shift in length from the preceding peptide (starting again from peptide 1 as the control), with one residue deleted at the N-terminal end and one at the C-terminal end. Top panel: Non-specific signal, resulting from direct anti-GluA2 antibody binding to the membrane. The membrane was exposed for 25 minutes. Lower panel: the same membrane was exposed to the rat GluA2 NTD and probed with rabbit anti-GluA2 antibody (Alomone, 1:250) followed by a HRP-conjugated anti-rabbit antibody (Pierce, 1:1500). The membrane was exposed for 2 minutes. Peptides 5 and 6, which identified the N_{72} and F_{73} residues, as well as peptides 14 and 23 which identified the R_{65} residue are indicated by red arrows above and below the array. The sequence of all the peptides is shown next to the array, with peptides 5, 6, 14 and 23 in red and the key deleted residues highlighted in bold. (**Note:**) All work that lead to the generation of this figure was conducted by members of the Greger lab. The methods used to generate the arrays shown here were the same as those shown before in Fig. 3.2 on page 70 in Experimental Chapter 1.

The data from the peptide arrays therefore suggest that the primary residue responsible for binding of γ-2 Ex1 to the NTD of GluA2 is the R_{65}, while the residues N_{72} and F_{73} play an auxiliary role, supporting and strengthening the TARP/NTD interaction. As mentioned above, based on the results of this peptide array, our collaborators generated two γ-2 Ex1 Ala substitution mutants, the single R_{65} mutant and a triple $R_{65}NF_{72\text{-}73}$ mutant, with the former removing the main NTD interaction site, and the triple mutant removing both the primary site of interaction and the two auxiliary ones. It is however worth noting, that while the biochemical data strongly supports the importance of the R_{65} residue for NTD binding, it is less clear how important for NTD binding the residues N_{72} and F_{73} are. This is due to the fact, that the result from both the Ala substitution array and the deletion array were very clear for R_{65}, while on the other hand, N_{72} and F_{73} were not mutated in the Ala substitution array and were identified only in the deletion array, where other factors, such as peptide length could affect the binding.

4.3.2 Deletion of the N-terminal domain slows GluA2 deactivation

We expressed homomeric wt and $\triangle$NTD GluA2Q AMPARs either alone, with wt γ-2 or with the γ-2 mutants: R_{65} and $R_{65}NF_{72\text{-}73}$ and examined the effect that perturbation of γ-2/NTD interaction had on the time constant of GluA2 deactivation (τ_w). Deactivation was examined by fitting the decay of the current responses to 1 ms applications of 10

mM Glu at -60 mV. We were particularly interested if TARP-dependent changes in AMPAR properties were affected by disruption of γ-2 interactions with the NTD (i.e. in a statistically significant interaction evident from two-way ANOVA).

As seen in Fig. 4.4, when GluA2Q deactivation was examined, we found that in the absence of the NTD the deactivation time constant was significantly prolonged ($F_{(1, 42)}$= 18.305, P = 1.0644 $\times$ 10^{-4}). There was, however, no significant overall effect of the TARP ($F_{(3, 42)}$= 2.7509, P= 0.0545) and no statistically significant interaction between the effect NTD and that of the TARP ($F_{(3, 42)}$= 0.4456, P= 0.7217). Deactivation time constant was similar for TARPless wt GluA2 (0.57 $\pm$ 0.05 ms) and for the same receptor TARPed with γ-2 (0.99 $\pm$ 0.21 ms), R_{65} (0.65 $\pm$ 0.08 ms) and $R_{65}NF_{72\text{-}73}$ (0.52 $\pm$ 0.09 ms). In the absence of the GluA2 NTD the time constant of deactivation was prolonged, both for the TARPless $\triangle$NTD GluA2 (1.02 $\pm$ 0.21) and for $\triangle$NTD GluA2 TARPed with wt γ-2 (1.34 $\pm$ 0.17 ms) or the R_{65} (0.86 $\pm$ 0.10 ms) and $R_{65}NF_{72\text{-}73}$ (0.91 $\pm$ 0.05 ms) mutants. There was a slight trend towards an increase in deactivation time constant in the presence of wt γ-2, but that was non-significant for both wt and $\triangle$NTD GluA2. Indeed, subsequent pairwise comparisons revealed no significant differences between the individual groups, as shown in Table 4.1.

The non-significant main effect of TARP on GluA2 deactivation time constant contrasts with the data shown in Experimental Chapter 1, where we found a slight overall increase in the time constant of GluA2Q deactivation in the presence of the TARP. However, it is worth noting that the data in Experimental Chapter 1 were examined using a one-way ANOVA, while the analysis of the data shown here involved a two-way ANOVA. Thus, the discrepancy can likely be attributed to the lower power of the more complex statistical test used here.

Test No.	**Test pair**			***P*-value**
1	GluA2wt	*vs.*	GluA2$\triangle$NTD	0.85
2	GluA2wt	*vs.*	GluA2wt + γ-2	0.85
3	GluA2wt	*vs.*	GluA2wt + R_{65}	1.00
4	GluA2wt	*vs.*	GluA2wt + $R_{65}NF_{72\text{-}73}$	1.00
5	GluA2wt + γ-2	*vs.*	GluA2wt + R_{65}	1.00
6	GluA2wt + γ-2	*vs.*	GluA2wt + $R_{65}NF_{72\text{-}73}$	0.85
7	GluA2$\triangle$NTD	*vs.*	GluA2$\triangle$NTD + γ-2	1.00
8	GluA2$\triangle$NTD	*vs.*	GluA2$\triangle$NTD + R_{65}	1.00
9	GluA2$\triangle$NTD	*vs.*	GluA2$\triangle$NTD + $R_{65}NF_{72\text{-}73}$	1.00
10	GluA2$\triangle$NTD + γ-2	*vs.*	GluA2$\triangle$NTD + R_{65}	0.48
11	GluA2$\triangle$NTD + γ-2	*vs.*	GluA2$\triangle$NTD + $R_{65}NF_{72\text{-}73}$	0.59

Table 4.1: Disruption of interactions with GluA2 NTD produced no significant differences in deactivation time constant from the controls.

The slowing of GluA2(flip) deactivation upon NTD deletion has been reported previ-

ously (Bedoukian et al., 2006) and was robustly reproduced in this study. It is, however, interesting that neither of the two mutations in γ-2 was capable of reproducing the effect on GluA2 deactivation seen with the NTD removal. Thus, it is possible that removal of the NTD affects the conformation of the AMPAR itself, prolonging channel deactivation, an effect independent of the interactions with the associated TARP.

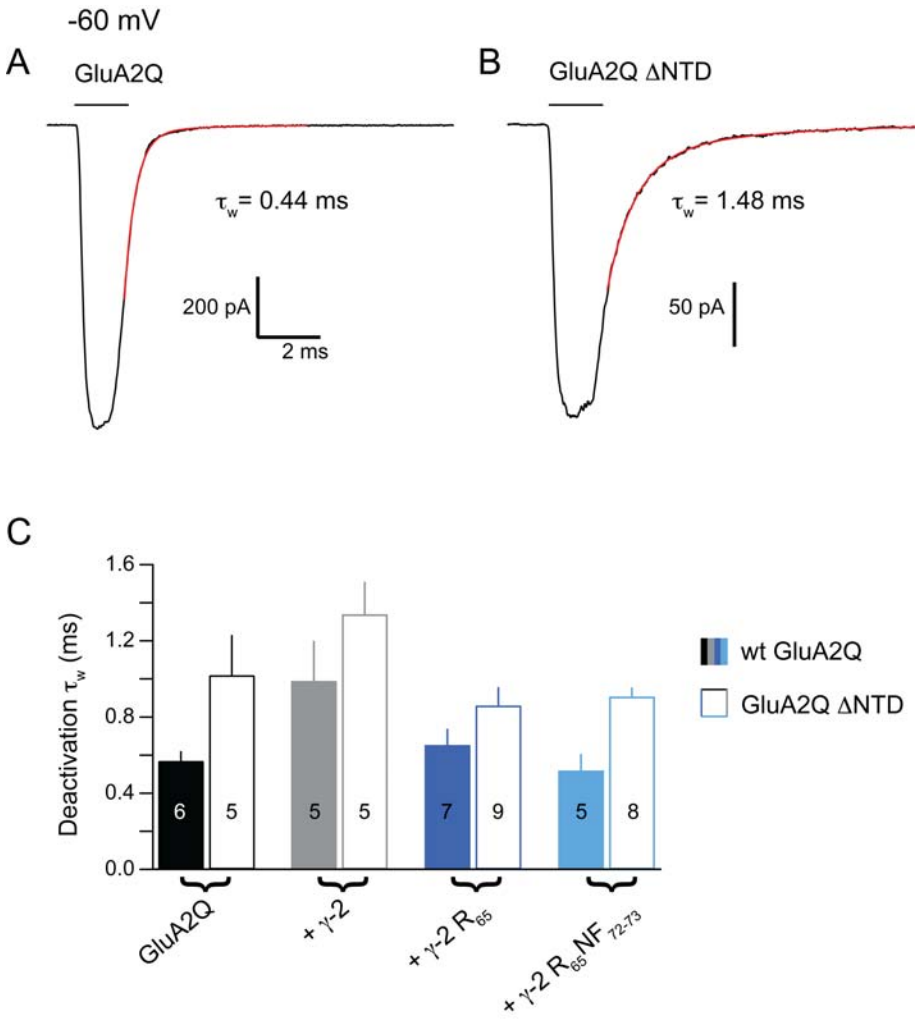

Figure 4.4: Deletion of the NTD slowed the time constant of GluA2 deactivation.
(**A**) Average response to a 1 ms pulse of 10 mM Glu from a representative patch expressing TARPless wt GluA2Q receptors. Individual sweeps were aligned at the 20% rise before averaging. The horizontal bar marks the duration of Glu application. Deactivation τ_w for this patch is indicated on the graph. (**B**) As for A, but for a patch expressing TARPless ΔNTD GluA2Q (**C**) Histogram showing τ_w of deactivation for each of the AMPAR/TARP variants. Bars denote the SEM and the *n* numbers for each group are indicated at the bottom of the histogram. Closed bars indicate wt GluA2Q, open bars indicate ΔNTD GluA2Q. Two-way ANOVA showed a significant main effect of the NTD on GluA2 deactivation ($F_{(1, 42)}$= 18.305, P = 1.0644 $\times$ 10^{-4}), a non-significant main effect of the TARP ($F_{(3, 42)}$= 2.7509, P= 0.0545) and a non-significant interaction ($F_{(3, 42)}$= 0.4456, P= 0.7217). There were no significant pairwise tests.

4.3.3 γ-2 slows GluA2 desensitization in an NTD-independent manner

A number of previous studies reported a slowing of AMPAR desensitization upon γ-2 co-expression (see for instance Tomita et al. 2005; Priel et al. 2005). In order to assess if the γ-2-mediated slowing of GluA2 desensitization requires the TARP to interact with the NTD, we examined the responses to 100 ms applications of 10 mM Glu at -60 mV and compared the weighted time constant of desensitization, τ_w (see Fig. 4.5C). We found that, overall, TARP co-expression resulted in a slowing of GluA2 desensitization ($F_{(3, 87)}$= 24.875, P= 1.0284 $\times$ 10^{-11}). Deletion of the NTD also resulted in a slowing of GluA2 desensitization ($F_{(1, 87)}$= 27.1923, P= 1.2302 $\times$ 10^{-6}). The effect of the TARP, however, was independent of that of the NTD, resulting in a statistically non-significant interaction ($F_{(3, 87)}$= 0.5155, P= 0.6727). The data shown here suggest that the magnitude of the TARP-dependent slowing of desensitization is similar in the presence and the absence of the GluA2 NTD. Thus, it appears that the interaction of γ-2 with the NTD is unlikely to participate in the slowing of AMPAR desensitization by the associated TARP.

Subsequent pairwise test (see Table 4.2) showed that wt γ-2 significantly prolonged wt GluA2 desensitization (10.17 $\pm$ 0.78 ms) compared with the TARPless receptor (4.93 $\pm$ 0.29 ms). This effect was retained in the absence of the NTD (ΔNTD GluA2 + γ-2: 12.42 $\pm$ 0.43 ms *vs.* 7.79 $\pm$ 1.00 ms for TARPless ΔNTD GluA2), in agreement with a previous study by Bedoukian et al. (2006), which also showed that γ-2 prolongs desensitization of GluA2 AMPARs lacking the NTD. We found, that the R_{65} and $R_{65}NF_{72\text{-}73}$ mutants also acted as TARPs, prolonging the desensitization of both wt GluA2 (9.83 $\pm$ 1.16 ms and 8.60 $\pm$ 0.82 ms for R_{65} and $R_{65}NF_{72\text{-}73}$ respectively) and ΔNTD GluA2 (14.25 $\pm$ 1.62 ms and 12.30 $\pm$ 0.63 ms for R_{65} and $R_{65}NF_{72\text{-}73}$ respectively). None of the mutants acted differently from wt γ-2 and they did not appear to mimic the effect of NTD deletion when co-expressed with wt GluA2. Thus, it appears that point mutations which disrupt TARP interactions with the NTD have a different effect on AMPAR gating than does deletion of the whole N-terminal domain. This implies that TARP interaction with the NTD may be involved in TARP-dependent slowing of AMPAR desensitization, and also suggests that the NTD may play a TARP-independent modulatory role in AMPAR gating.

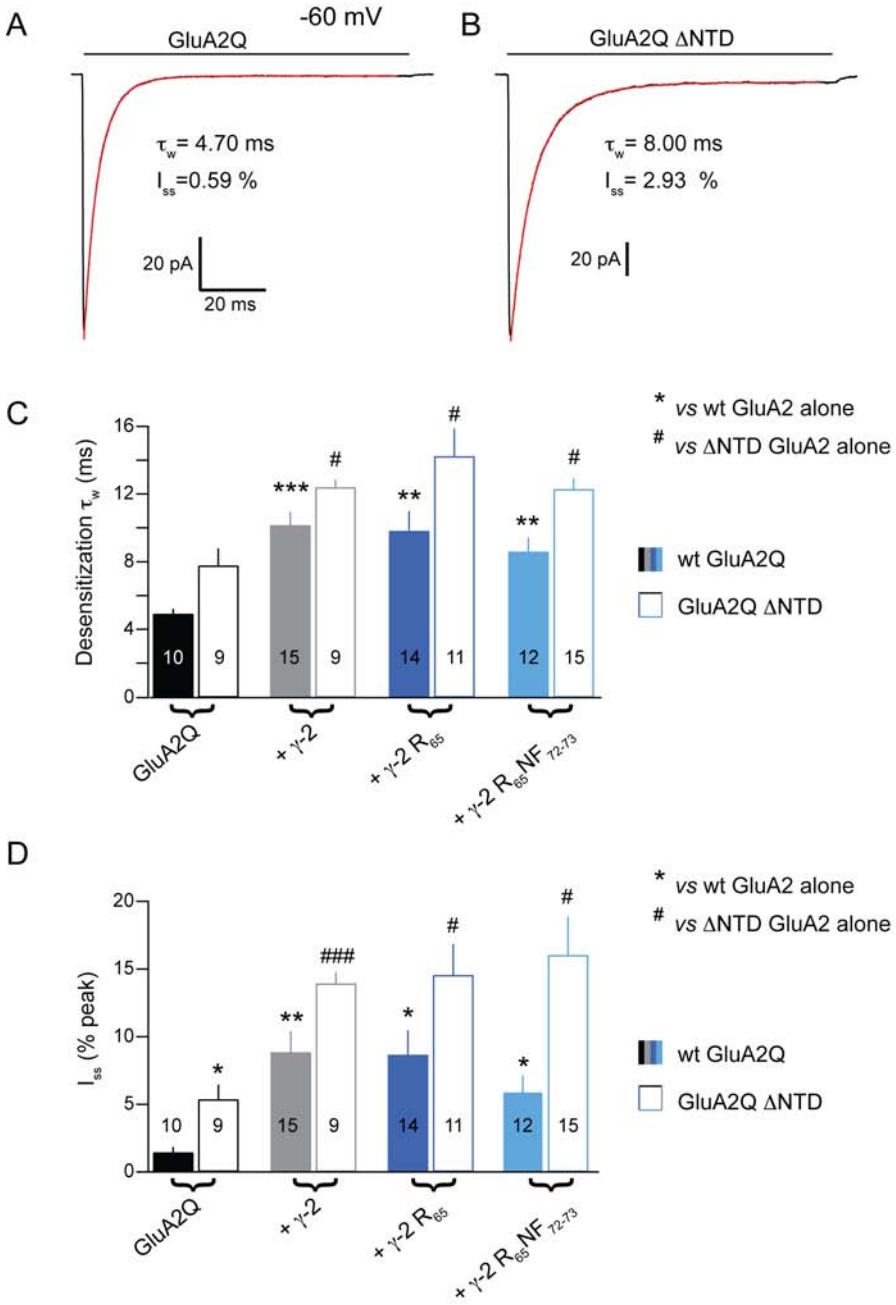

Figure 4.5: γ-2 mediated slowing of GluA2 desensitization was independent of the TARP interaction with the NTD.

(**A**) Average response to a 100 ms pulse of 10 mM Glu from a representative patch expressing TARPless wt GluA2Q receptors. Individual sweeps were aligned at the 20% rise before averaging. The horizontal bar marks the duration of Glu application. Desensitization τ_w and the I_{ss} for this patch are indicated on the graph. (**B**) As for A, but for a patch expressing TARPless ΔNTD GluA2Q (**C**) Histogram showing τ_w of desensitization for each of the AMPAR/TARP variants. Bars denote the SEM and the *n* numbers for each group are indicated at the bottom of the histogram. Closed bars indicate wt GluA2Q, open bars indicate ΔNTD GluA2Q. Two-way ANOVA showed a significant main effect of the NTD on GluA2 desensitization ($F_{(1, 87)}$= 27.1923, P = 1.2302 $\times$ 10^{-6}), a significant main effect of the TARP ($F_{(3, 87)}$= 24.875 P= 1.0284 $\times$ 10^{-11}) and a non-significant interaction ($F_{(3, 87)}$= 0.5155, P= 0.6727).

Figure 4.5 continued: (**D**) Histogram showing the steady-state current (I_{ss}), calculated as % peak current amplitude, for each of the AMPAR/TARP variants. Bars denote the SEM and the *n* numbers for each group are indicated at the bottom of the histogram. Closed bars indicate wt GluA2Q, open bars indicate ΔNTD GluA2Q. Two-way ANOVA showed a significant main effect of the NTD on GluA2 steady-state current percentage ($F_{(1, 87)}$= 28.6368, P = 6.9931 $\times$ 10^{-7}), a significant main effect of the TARP ($F_{(3, 87)}$= 25.9212 P= 4.5016 $\times$ 10^{-12}) and a non-significant interaction ($F_{(3, 87)}$= 1.1439, P= 0.336). For pairwise tests shown in panels C and D, asterisks mark significant difference *vs.* TARPless wt GluA2 ($*$ P< 0.05, $**$ P< 0.01 and $***$ P< 0.001; Welch *t*-test), while hashes mark significant difference *vs.* TARPless ΔNTD GluA2 (# P< 0.05, # # # P< 0.001; Welch *t*-test).

Test No.	Test pair			*P*-value
1	GluA2wt	*vs.*	GluA2ΔNTD	0.11
2	GluA2wt	*vs.*	GluA2wt + γ-2	8.102 $\times$ 10^{-5}
3	GluA2wt	*vs.*	GluA2wt + R_{65}	0.0095
4	GluA2wt	*vs.*	GluA2wt + $R_{65}NF_{72\text{-}73}$	0.0095
5	GluA2wt + γ-2	*vs.*	GluA2wt + R_{65}	1.00
6	GluA2wt + γ-2	*vs.*	GluA2wt + $R_{65}NF_{72\text{-}73}$	0.72
7	GluA2ΔNTD	*vs.*	GluA2ΔNTD + γ-2	0.011
8	GluA2ΔNTD	*vs.*	GluA2ΔNTD + R_{65}	0.022
9	GluA2ΔNTD	*vs.*	GluA2ΔNTD + $R_{65}NF_{72\text{-}73}$	0.013
10	GluA2ΔNTD + γ-2	*vs.*	GluA2ΔNTD + R_{65}	0.89
11	GluA2ΔNTD + γ-2	*vs.*	GluA2ΔNTD + $R_{65}NF_{72\text{-}73}$	1.00

Table 4.2: Wt γ-2 as well as the γ-2 mutants prolonged GluA2 desensitization time constant both in the presence and in the absence of the NTD.

As shown in Fig 4.5D, in addition to investigating the effect of disrupting TARP/NTD interactions on GluA2 desensitization kinetics, we also examined how disrupting these interactions affects the percentage of the steady-state current (I_{ss}). Overall, TARP co-expression increased the steady-state current percentage significantly ($F_{(3, 87)}$= 25.9212, P= 4.5016 $\times$ 10^{-12}). As seen in panel D Fig. 4.5, wt γ-2 increased the steady-state current fraction of wt GluA2 (wt GluA2 + γ-2 8.86 $\pm$ 1.53 % *vs.* 1.46 $\pm$ 0.40 % for TARPless wt GluA2), as well as ΔNTD GluA2 (ΔNTD GluA2 + γ-2 13.95 $\pm$ 0.81 % *vs.* 5.38 $\pm$ 1.07 % for TARPless Δ NTD GluA2). R_{65} and $R_{65}NF_{72\text{-}73}$ also increased the steady-state current fraction of full-length GluA2 (8.67 $\pm$ 1.80 % and 5.93 $\pm$ 1.21 % for R_{65} and $R_{65}NF_{72\text{-}73}$ respectively) and of GluA2 lacking the NTD (14.57 $\pm$ 2.29 % and 16.04 $\pm$ 2.84 % for R_{65} and $R_{65}NF_{72\text{-}73}$ respectively) and were not significantly different from wt γ-2 (see Table 4.3).

Overall, deletion of the NTD also increased the percentage of the steady-state current ($F_{(1, 87)}$= 28.6368, P= 6.9931 $\times$ 10^{-7}). This was evident even in the absence of the TARP, when the steady-state currents from TARPless GluA2 wt and GluA2

Test No.	Test pair			*P*-value
1	GluA2wt	*vs.*	GluA2ΔNTD	0.032
2	GluA2wt	*vs.*	GluA2wt + γ-2	0.0026
3	GluA2wt	*vs.*	GluA2wt + R_{65}	0.014
4	GluA2wt	*vs.*	GluA2wt + $R_{65}NF_{72\text{-}73}$	0.023
5	GluA2wt + γ-2	*vs.*	GluA2wt + R_{65}	1.00
6	GluA2wt + γ-2	*vs.*	GluA2wt + $R_{65}NF_{72\text{-}73}$	0.59
7	GluA2ΔNTD	*vs.*	GluA2ΔNTD + γ-2	0.00014
8	GluA2ΔNTD	*vs.*	GluA2ΔNTD + R_{65}	0.020
9	GluA2ΔNTD	*vs.*	GluA2ΔNTD + $R_{65}NF_{72\text{-}73}$	0.020
10	GluA2ΔNTD + γ-2	*vs.*	GluA2ΔNTD + R_{65}	1.00
11	GluA2ΔNTD + γ-2	*vs.*	GluA2ΔNTD + $R_{65}NF_{72\text{-}73}$	1.00

Table 4.3: γ-2 increased GluA2 steady-state current even when the interactions with the NTD were disrupted.

ΔNTD were compared (see panel D Fig. 4.5 and Table 4.3). There was, however, no statistically significant interaction between the effects of TARP and the NTD when the steady-state current was examined ($F_{(3,\ 87)}$= 1.1439, P= 0.336), suggesting that the TARP-mediated increase in steady-state current fraction was independent of the presence of the NTD, and, conversely, that deletion of the NTD resulted in an increase in steady-state current irrespective of TARP co-expression. Thus, it appears that although the NTD modulated AMPAR steady-state current, that modulation did not require TARP association. In addition, the increase in steady-state current mediated by γ-2 still occurred when the NTD was absent, or when the TARP/NTD interaction was disrupted by mutations in Ex1 of γ-2.

4.3.4 γ-2 co-expression partially relieves polyamine block of GluA2 regardless of the presence of the NTD

The Q form of GluA2 used in this Chapter is Ca^{2+}-permeable (Burnashev et al., 1992a). At positive membrane potentials, CP-AMPARs are blocked by endogenous intracellular polyamines, however, the block is partially relieved by γ-2 (Soto et al., 2007). The susceptibility of wt and ΔNTD GluA2Q to block by 100 μM intracellular spermine was assessed by stepping the membrane voltage from -100 mV to +60 mV in 10 mV increments and applying a 1 ms pulse of 10 mM Glu at each voltage. The peak currents at all voltages were normalised to the peak at -100 mV and plotted against the membrane potential to obtain the *I-V* plots, from which rectification index (RI) was quantified as the ratio of slope conductance at positive and negative membrane voltages.

Our results agreed with the previous study by Soto et al. (2007) and with the re-

sults shown in Experimental Chapter 1 of this Thesis, in that TARP co-expression relieved spermine block of GluA2Q, resulting in a significantly higher rectification index in the presence of the TARP ($F_{(3, 47)}$= 102.5631, P= 1.2251 $\times$ 10^{-20}). As shown in Fig. 4.6 and Table 4.4, wt γ-2 (RI= 0.318 $\pm$ 0.035) as well as R_{65} (0.305 $\pm$ 0.035) and $R_{65}NF_{72\text{-}73}$ (0.298 $\pm$ 0.043) relieved polyamine block compared with TARPless wt GluA2 (0.094 $\pm$ 0.022). The γ-2-mediated relief of spermine block was also evident when the ΔNTD GluA2 was used. All three variants of γ-2 reduced the degree of spermine block when co-expressed with ΔNTD GluA2. The RI was similar for wt γ-2 (0.351 $\pm$ 0.003), R_{65} (0.286 $\pm$ 0.025) and $R_{65}NF_{72\text{-}73}$ (0.332 $\pm$ 0.045) and was, in all three cases, significantly different from that seen with TARPless ΔNTD GluA2 (0.075 $\pm$ 0.015). The results are summarised in Fig. 4.6 and Table 4.4.

Test No.	Test pair			*P*-value
1	GluA2wt	*vs.*	GluA2ΔNTD	1.00
2	GluA2wt	*vs.*	GluA2wt + γ-2	0.0035
3	GluA2wt	*vs.*	GluA2wt + R_{65}	0.0032
4	GluA2wt	*vs.*	GluA2wt + $R_{65}NF_{72\text{-}73}$	0.013
5	GluA2wt + γ-2	*vs.*	GluA2wt + R_{65}	1.00
6	GluA2wt + γ-2	*vs.*	GluA2wt + $R_{65}NF_{72\text{-}73}$	1.00
7	GluA2ΔNTD	*vs.*	GluA2ΔNTD + γ-2	0.00028
8	GluA2ΔNTD	*vs.*	GluA2ΔNTD + R_{65}	0.00015
9	GluA2ΔNTD	*vs.*	GluA2ΔNTD + $R_{65}NF_{72\text{-}73}$	0.0029
10	GluA2ΔNTD + γ-2	*vs.*	GluA2ΔNTD + R_{65}	0.17
11	GluA2ΔNTD + γ-2	*vs.*	GluA2ΔNTD + $R_{65}NF_{72\text{-}73}$	1.00

Table 4.4: γ-2 as well as the R_{65} and $R_{65}NF_{72\text{-}73}$ mutants relieved spermine block of wt and Δ NTD GluA2.

Unlike association with TARP, deletion of the N-terminal domain no had overall effect on GluA2 rectification ($F_{(1, 47)}$= 0.0022, P= 0.9626) and there was no statistically significant interaction between the effect of TARP and that of the NTD ($F_{(3, 47)}$= 0.528, P= 0.6653).

Thus, it appears that the NTD of AMPARs does not play a role in the modulation of polyamine block. Polyamines are blockers of the AMPAR channel, while the NTD is the domain most distal from the channel pore and thus unlikely to directly contribute to polyamine binding. The results shown here suggest that this domain also lacks any indirect, allosteric effect on spermine binding or permeation. Furthermore, the two Ex1 mutants examined here, R_{65} and $R_{65}NF_{72\text{-}73}$, unlike many of the mutants investigated in Experimental Chapter 1, did not show a reduced ability to relieve spermine block compared with wt γ-2. Thus it appears that the three residues in Ex1 that interact strongly with the NTD do not contribute to the regulation of rectification by γ-2. Furthermore, this implies that the impaired relief of spermine block seen with some of the Ex1 mutants in Experimental Chapter 1 likely resulted from disruption of γ-2 interactions with AMPAR domains other than the NTD.

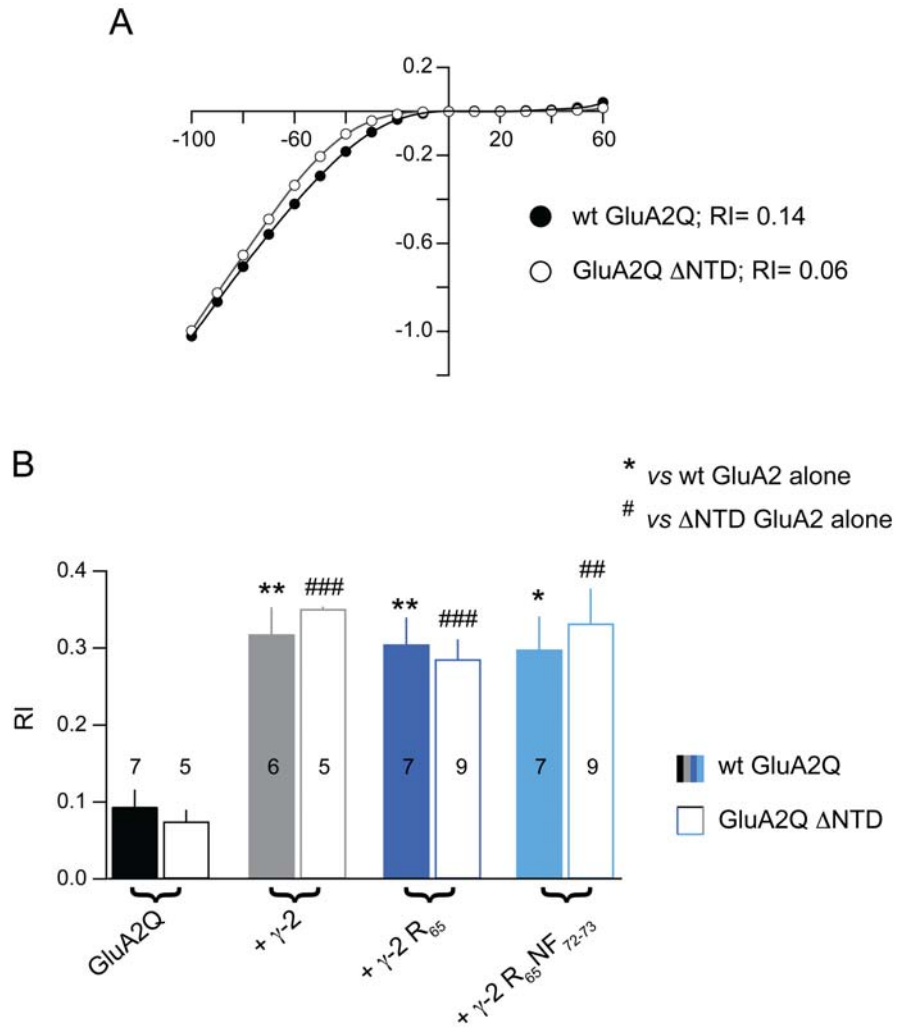

Figure 4.6: TARP co-expression relieved spermine block regardless of the presence of GluA2 NTD.

(**A**) Peak *I-V* plots for from individual representative patches for TARPless wt GluA2 (closed circles) and TARPless ΔNTD GluA2 (open circles). The peak currents at each voltage were normalised to the peak at -100 mV, plotted against the membrane potential and fitted with a 9th order polynomial. The RI values for the representative patches are shown on the graph. (**B**) Histogram showing RI for each of the AMPAR/TARP variants. Bars denote the SEM and the *n* numbers for each group are indicated on the histogram. Closed bars indicate wt GluA2Q, open bars indicate ΔNTD GluA2Q. Two-way ANOVA showed a non-significant main effect of the NTD on GluA2 RI ($F_{(1,\,47)}$= 0.0022, P = 0.9626), a significant main effect of the TARP ($F_{(3,\,47)}$= 102.563, P= 1.2251 $\times$ 10^{-20}) and a non-significant interaction ($F_{(3,\,47)}$= 0.528, P= 0.6653). For pairwise tests, asterisks mark significant difference *vs.* TARPless wt GluA2 ($*$ P< 0.05, $**$ P< 0.01; Welch *t*-test), while hashes mark significant difference *vs.* TARPless ΔNTD GluA2 ($\#\,\#$ P< 0.01, $\#\,\#\,\#$ P< 0.001; Welch *t*-test).

4.3.5 γ-2 co-expression and NTD deletion have opposing, but independent effects on GluA2 mean single-channel conductance

TARP co-expression has been shown to increase AMPAR single-channel conductance (see for instance Soto et al. 2009; Jackson et al. 2011; Shelley et al. 2012).

In this study, we used NSFA to investigate if the γ-2-dependent increase in mean single-channel conductance of GluA2 depends on the interactions of this TARP with the NTD of GluA2. Mean single-channel conductance of wt γ-2 as well as the R_{65} and $R_{65}NF_{72\text{-}73}$ mutants co-expressed with wt GluA2 or GluA2 $\triangle$NTD was estimated by fitting the parabolic NSFA function (2.6, Materials and Methods) to the current responses generated by 100 ms applications of 10 mM Glu at -60 mV. The data are shown in Fig. 4.7 and the statistical tests are listed in Table 4.5. Similar to the results shown in Experimental Chapter 1, in the present study TARP co-expression significantly increased GluA2 mean single-channel conductance ($F_{(3,\ 52)}$= 24.59, P= 4.8187 $\times$ 10^{-10}). Indeed, co-expression of γ-2 (37.02 $\pm$ 2.27 pS) as well as the R_{65} (30.65 $\pm$ 1.94 pS) and $R_{65}NF_{72\text{-}73}$ (35.66 $\pm$ 2.39 pS) mutants increased mean single-channel conductance compared with TARPless wt GluA2 (21.95 $\pm$ 1.00 pS). Thus, the data shown here agree with previously published studies reporting an increase in AMPAR mean single-channel conductance upon TARP co-expression.

Test No.	**Test pair**			***P*-value**
1	GluA2wt	*vs.*	GluA2$\triangle$NTD	0.017
2	GluA2wt	*vs.*	GluA2wt + γ-2	0.00036
3	GluA2wt	*vs.*	GluA2wt + R_{65}	0.019
4	GluA2wt	*vs.*	GluA2wt + $R_{65}NF_{72\text{-}73}$	0.019
5	GluA2wt + γ-2	*vs.*	GluA2wt + R_{65}	0.19
6	GluA2wt + γ-2	*vs.*	GluA2wt + $R_{65}NF_{72\text{-}73}$	0.69
7	GluA2$\triangle$NTD	*vs.*	GluA2$\triangle$NTD + γ-2	0.0497
8	GluA2$\triangle$NTD	*vs.*	GluA2$\triangle$NTD + R_{65}	0.040
9	GluA2$\triangle$NTD	*vs.*	GluA2$\triangle$NTD + $R_{65}NF_{72\text{-}73}$	0.015
10	GluA2$\triangle$NTD + γ-2	*vs.*	GluA2$\triangle$NTD + R_{65}	0.38
11	GluA2$\triangle$NTD + γ-2	*vs.*	GluA2$\triangle$NTD + $R_{65}NF_{72\text{-}73}$	0.61

Table 4.5: γ-2 variants increased mean-single channel conductance of wt and $\triangle$NTD GluA2 receptors.

By contrast, deletion of the NTD resulted in an overall reduction in mean-single channel conductance ($F_{(1,\ 52)}$= 33.9134, P= 3.6527 $\times$ 10^{-7}). This was seen with the TARPless $\triangle$NTD GluA2 receptors (15.88 $\pm$ 1.17 pS) as well as with the $\triangle$NTD GluA2 co-expressed with γ-2 (22.93 $\pm$ 2.00 pS) and the $R_{65}NF_{72\text{-}73}$ mutant (25.86 $\pm$ 1.85 pS), but was less pronounced with the R_{65} mutant (29.22 $\pm$ 3.17 pS). The interaction between the effect of TARP and that of the NTD was statistically non-significant ($F_{(3,\ 52)}$= 2.5799, P= 0.0634), suggesting that the magnitude of the TARP-mediated increase in mean single-channel conductance is similar in the presence and in the absence of the NTD. Thus, it appears that the effects of γ-2 co-expression and NTD deletion on GluA2 mean-single channel conductance are opposing, but independent, and that TARP interactions with the NTD are unlikely to play a role in the TARP-mediated increase in mean-single channel conductance.

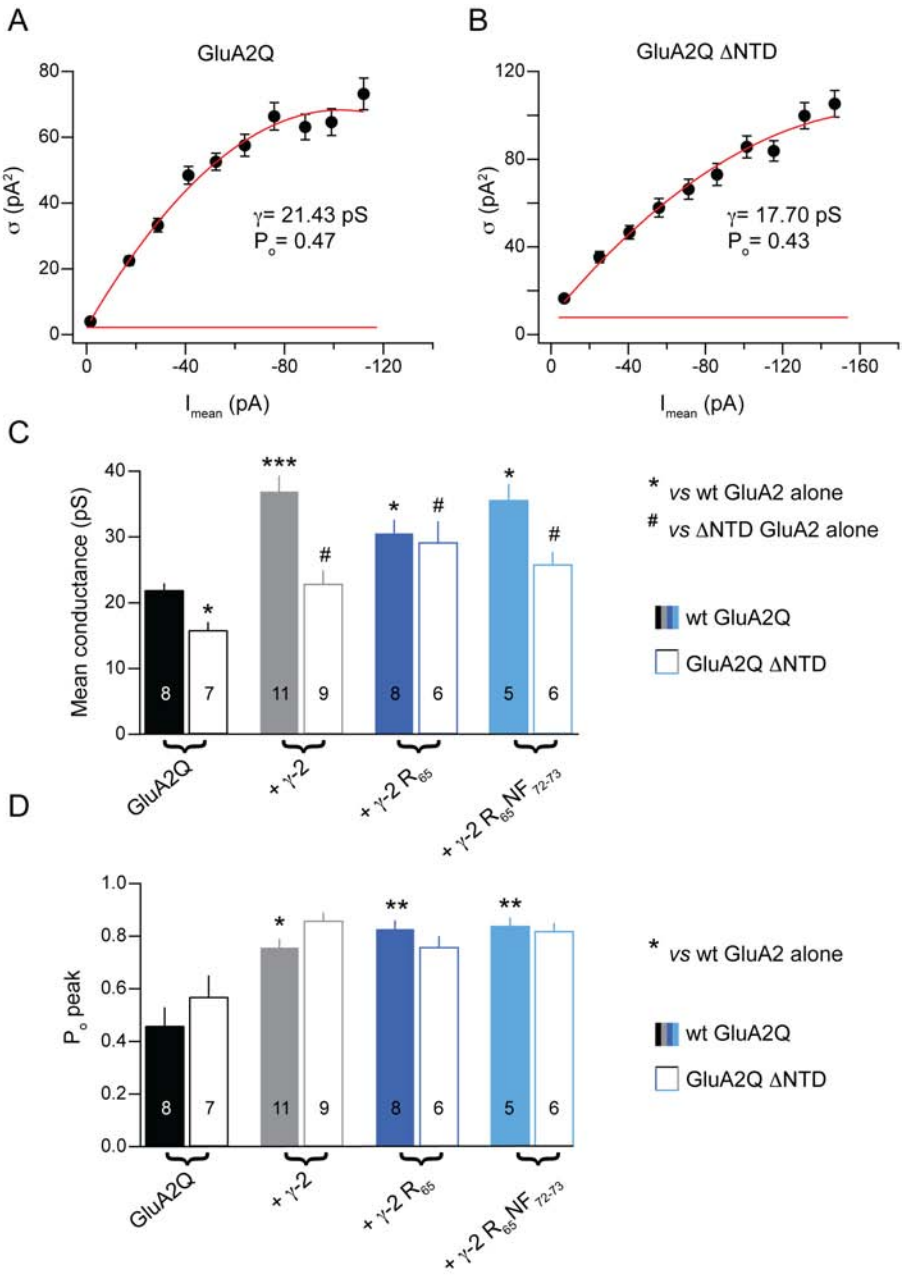

Figure 4.7: Co-expression of wt γ-2 as well as the R_{65} and $R_{65}NF_{72\text{-}73}$ mutants increased mean single-channel conductance of wt and ΔNTD GluA2. (**A**) NSFA fit to the average current from an example patch expressing TARPless wt GluA2. Current variance was plotted against mean current. The red horizontal line indicates the σ_b level and the red line through the points shows the parabolic NSFA fit to equation 2.6. The mean single-channel conductance (γ) and peak open probability (P_o) values for this patch are shown on the graph. (**B**) As for A, but for a patch expressing TARPless ΔNTD GluA2. (**C**) Histogram showing the mean single-channel conductance for each of the AMPAR/TARP variants. Bars denote the SEM and the *n* numbers for each group are indicated at the bottom of the histogram. Closed bars indicate wt GluA2Q, open bars indicate ΔNTD GluA2Q. Two-way ANOVA showed a significant main effect of the NTD on GluA2 mean single-channel conductance ($F_{(1, 52)}$= 33.9134, P = 3.6527 $\times$ 10^{-7}), a significant main effect of the TARP ($F_{(3, 52)}$= 24.59 P= 4.8187 $\times$ 10^{-10}) and a non-significant interaction ($F_{(3, 52)}$= 2.5799, P= 0.0634).

Figure 4.7 continued: (**D**) Histogram showing the peak P_o for each of the AMPAR/TARP variants. Bars denote the SEM and the *n* numbers for each group are indicated at the bottom of the histogram. Closed bars indicate wt GluA2Q, open bars indicate ΔNTD GluA2Q. Two-way ANOVA showed a non-significant main effect of the NTD on GluA2 peak P_o ($F_{(1, 52)}$= 0.6795, P = 0.4135), a significant main effect of the TARP ($F_{(3, 52)}$= 10.6052 P= 1.5066 $\times$ 10^{-5}) and a non-significant interaction ($F_{(3, 52)}$= 2.36, P= 0.0821). For pairwise tests shown in panels C and D, asterisks mark significant difference *vs.* TARPless wt GluA2 ($*$ P< 0.05, $**$ P< 0.01 and $***$ P< 0.001; Welch *t*-test), while hashes mark significant difference *vs.* TARPless ΔNTD GluA2 ($\#$ P< 0.05; Welch *t*-test).

In addition to providing information about the mean single-channel conductance, NSFA also renders an estimate of the peak open probability (4.7D). γ-2 has previously been reported to increase peak P_o of GluA2 (Soto et al., 2009). Similarly, in this study we found that, overall, P_o was significantly higher in the presence of the TARP ($F_{(3, 52)}$= 10.6052, P= 1.5066 $\times$ 10^{-5}). Indeed, compared with TARPless wt GluA2 (0.46 $\pm$ 0.07), P_o was increased upon co-expression with wt γ-2 (0.76 $\pm$ 0.03) as well as with the R_{65} (0.83 $\pm$ 0.03) and $R_{65}NF_{72\text{-}73}$ (0.84 $\pm$ 0.03) mutants. Thus, it appears that the residues substituted with Ala in these Ex1 mutants do not contribute to the γ-2-mediated increase in peak P_o of GluA2.

Test No.	Test pair			*P*-value
1	GluA2wt	*vs.*	GluA2ΔNTD	0.60
2	GluA2wt	*vs.*	GluA2wt + γ-2	0.016
3	GluA2wt	*vs.*	GluA2wt + R_{65}	0.0048
4	GluA2wt	*vs.*	GluA2wt + $R_{65}NF_{72\text{-}73}$	0.0042
5	GluA2wt + γ-2	*vs.*	GluA2wt + R_{65}	0.55
6	GluA2wt + γ-2	*vs.*	GluA2wt + $R_{65}NF_{72\text{-}73}$	0.39
7	GluA2ΔNTD	*vs.*	GluA2ΔNTD + γ-2	0.072
8	GluA2ΔNTD	*vs.*	GluA2ΔNTD + R_{65}	0.33
9	GluA2ΔNTD	*vs.*	GluA2ΔNTD + $R_{65}NF_{72\text{-}73}$	0.14
10	GluA2ΔNTD + γ-2	*vs.*	GluA2ΔNTD + R_{65}	0.39
11	GluA2ΔNTD + γ-2	*vs.*	GluA2ΔNTD + $R_{65}NF_{72\text{-}73}$	0.60

Table 4.6: All three γ-2 variants significantly increased peak P_o of wt GluA2, but not GluA2 ΔNTD.

In the absence of the GluA2 NTD, there was also a slight trend towards an increased P_o when ΔNTD GluA2 AMPARs were co-expressed with γ-2 (0.86 $\pm$ 0.03 *vs.* 0.57 $\pm$ 0.08 for TARPless ΔNTD GluA2) and the two mutants (0.76 $\pm$ 0.04 and 0.82 $\pm$ 0.03 for R_{65} and $R_{65}NF_{72\text{-}73}$ respectively), however, the individual combinations were not significantly different from ΔNTD GluA2 alone (see Table 4.6). Deletion of the NTD itself lacked an effect on GluA2 P_o ($F_{(1, 52)}$= 0.6795, P= 0.4135) and there was no statistically significant interaction between the effects of the NTD and the TARP ($F_{(3, 52)}$= 2.36, P= 0.0821). Thus, it appears that the interaction between γ-2 and

the NTD of GluA2 is not required for an increase in P_o upon co-expression of the TARP.

4.3.6 γ-2 increases relative kainate efficacy independently of its interaction with the NTD of GluA2

γ-2 has reproducibly been shown to increase the relative efficacy of the partial agonist kainate (see for instance Turetsky et al. 2005; Tomita et al. 2005 and Experimental Chapter 1 of this Thesis). In the current study, we were particularly interested if γ-2 interactions with the NTD of GluA2 play a role in the modulation of KA/Glu ratio by this TARP. The responses to KA and Glu were obtained by exposing the patch to 100 ms pulses of 500 μM Glu, then 500 μM KA and again to Glu (both agonists were supplemented with 100 μM CTZ to reduce AMPAR desensitization). KA/Glu ratio was calculated as the ratio of the steady-state response to KA and the average of the steady-state responses to Glu (before and after KA application).

Overall, TARP co-expression significantly increased KA/Glu ratio ($F_{(3, 60)}$= 358.9669, P= 2.8699 $\times$ 10^{-38}). When compared with TARPless wt GluA2 (0.029 $\pm$ 0.006), co-expression of γ-2 (0.65 $\pm$ 0.033) as well as the mutants R_{65} (0.58 $\pm$ 0.034) and $R_{65}NF_{72\text{-}73}$ (0.52 $\pm$ 0.044) resulted in a significantly higher KA/Glu ratio (see Fig. 4.8 and Table 4.7). The two Ex1 mutants increased KA/Glu ratio to the same levels as wt γ-2, which suggests that the mutated residues in Ex1 are unlikely to contribute to the γ-2-mediated increase in relative KA efficacy.

Test No.	Test pair			*P*-value
1	GluA2wt	*vs.*	GluA2ΔNTD	0.17
2	GluA2wt	*vs.*	GluA2wt + γ-2	1.344 $\times$ 10^{-6}
3	GluA2wt	*vs.*	GluA2wt + R_{65}	3.291 $\times$ 10^{-7}
4	GluA2wt	*vs.*	GluA2wt + $R_{65}NF_{72\text{-}73}$	3.289 $\times$ 10^{-6}
5	GluA2wt + γ-2	*vs.*	GluA2wt + R_{65}	0.17
6	GluA2wt + γ-2	*vs.*	GluA2wt + $R_{65}NF_{72\text{-}73}$	0.12
7	GluA2ΔNTD	*vs.*	GluA2ΔNTD + γ-2	3.291 $\times$ 10^{-7}
8	GluA2ΔNTD	*vs.*	GluA2ΔNTD + R_{65}	3.027 $\times$ 10^{-8}
9	GluA2ΔNTD	*vs.*	GluA2ΔNTD + $R_{65}NF_{72\text{-}73}$	6.796 $\times$ 10^{-6}
10	GluA2ΔNTD + γ-2	*vs.*	GluA2ΔNTD + R_{65}	0.17
11	GluA2ΔNTD + γ-2	*vs.*	GluA2ΔNTD + $R_{65}NF_{72\text{-}73}$	0.17

Table 4.7: γ-2 as well as the mutants R_{65} and $R_{65}NF_{72\text{-}73}$ increased KA/Glu ratio when co-expressed with wt GluA2 or with GluA2 ΔNTD..

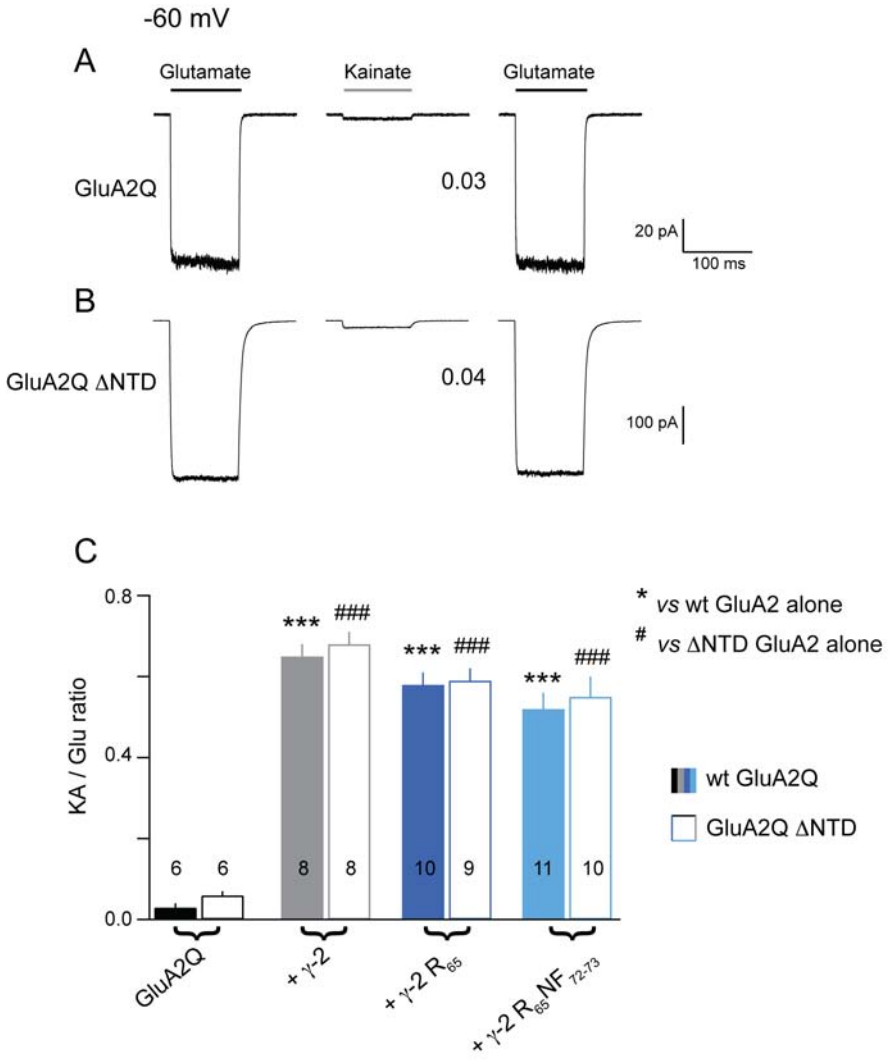

Figure 4.8: KA/Glu ratio of wt and △ NTD GluA2 was significantly increased in the presence of γ-2 or the R_{65} and $R_{65}NF_{72\text{-}73}$ mutants. (**A**) Mean responses from representative patches showing the initial response to 500 μM Glu (left), followed by 500 μM KA (middle) and a recovery of response to Glu (right). Both Glu and KA were supplemented with 100 μM CTZ to limit desensitization. (**B**) As for A, but for a patch expressing TARPless ΔNTD GluA2. (**C**) Histogram showing the KA/Glu ratio for each of the AMPAR/TARP variants. Bars denote the SEM and the *n* numbers for each group are indicated at the bottom of the histogram. Closed bars indicate wt GluA2Q, open bars indicate ΔNTD GluA2Q. Two-way ANOVA showed a significant main effect of the NTD on KA/Glu ratio ($F_{(1,\,60)}$= 5.1105, P = 0.0274), a significant main effect of the TARP ($F_{(3,\,60)}$= 358.9669 P= 2.8699 $\times$ 10^{-38}) and a non-significant interaction ($F_{(3,\,60)}$= 0.1146, P= 0.9512).

In the absence of the GluA2 NTD, co expression of wt γ-2 (0.68 $\pm$ 0.034) as well as R_{65} (0.59 $\pm$ 0.028) or $R_{65}NF_{72\text{-}73}$ (0.55 $\pm$ 0.047) also lead to a significant increase in KA/Glu ratio compared with TARPless $\triangle$NTD GluA2 (0.065 $\pm$ 0.014). This agrees with a previous study by Tomita et al. (2007), which showed that γ-2 increased KA/Glu ratio when GluA1 lacking the NTD was used. Interestingly, deletion of the NTD slightly, but significantly increased KA/Glu ratio across all of the tested combinations ($F_{(1, 60)}$= 5.1105, P= 0.0274), however, this effect was independent of that mediated by TARP co-expression, resulting in a statistically non-significant interaction ($F_{(3, 60)}$= 0.1146, P= 0.9512).

The ability to increase KA/Glu ratio was retained by the Ex1 mutants in which residues interacting strongly with the NTD were substituted with Ala. In addition, γ-2 was still able to increase KA/Glu ratio when $\triangle$NTD rather than wt GluA2 was used. Thus, it appears that TARP/NTD interaction is not required for the increase in KA/Glu ratio upon TARP co-expression. However, a small but significant increase in KA/Glu ratio upon NTD deletion was observed with both TARPless and TARPed receptors, suggesting that the NTD itself may play a role in modulation of kainate efficacy. Since the efficacy of partial agonists has been shown to be determined by the degree of the LBD cleft closure (Jin et al., 2003), it is possible that the effect of NTD deletion is an allosteric one, i.e. that the LBD cleft closes more efficiently when the NTD is absent, which results in increased KA/Glu ratio.

4.4 Discussion

The results described in this Chapter suggest that AMPARs lacking their NTD are functional, which agrees with previously published studies (Pasternack et al., 2002; Bedoukian et al., 2006). Similar to the results of Pasternack et al. (2002) obtained with GluA4, we found that deletion of the NTD increased the desensitization time constant of GluA2. In addition, GluA2 deactivation was also prolonged in the absence of the NTD, in agreement with the previous report by Bedoukian et al. (2006). Thus, it appears that the NTD plays a somewhat 'inhibitory' role in AMPAR gating, limiting the charge transfer through these receptors. Since the NTD is the most sequence-diverse domain of the AMPAR, it is possible that this diversity contributes to shaping the synaptic responses mediated by different AMPAR subtypes. However, a comparison of the role of the NTD in other AMPAR subunits would be required for a more detailed conclusion.

Furthermore, we found interesting effects of the NTD deletion on AMPAR properties that are though to be primarily mediated by other receptor domains. Mean single-channel conductance was found to be reduced in the absence of the NTD. The methods used in this study did not allow us to investigate whether this reduction in mean-single channel conductance reflects a reduction in the conductance level as such, or a shift towards the occupancy of lower conductance states (of this multiple conductance channel) in the absence of the NTD. It is unclear how deletion of the NTD could affect ion conduction through the AMPAR channel pore, if this was indeed the mechanism for the reduction in mean single-channel conductance observed in the absence of the NTD. Furthermore, GluA2 block by spermine, which also binds within the channel pore is unaffected by NTD deletion, suggesting that rather than affecting the pore region through a currently unknown mechanism, the NTD may stabilise certain AMPAR conformations, which correspond to higher conductance states. Thus, the reduced mean single-channel conductance in the absence of the NTD may be better explained by preferential openings to lower conductance states. However, this is only a speculation which cannot be resolved using the data shown here. Single-channel recordings, which were not performed in this study, could give more insight into the detailed mechanism of this phenomenon.

Another interesting result was the small, albeit significant increase in KA/Glu ratio upon NTD deletion. As mentioned above, the lower efficacy of partial agonists on AMPARs is thought to result from the LBD cleft closing to a lesser extend than when a full agonist is bound (Jin et al., 2003). It is thus possible, that the slight increase in KA/Glu ratio observed upon NTD deletion reflects a higher degree of the LBD cleft closure, due to less constraints being imposed on this domain in the absence of the

NTD.

In agreement with previous studies we found that γ-2 can efficiently modulate a number of functional properties of AMPARs lacking the NTD, such as desensitization (Bedoukian et al., 2006) and KA/Glu ratio (Tomita et al., 2007). We were particularly interested to determine if the magnitude of "TARP effect" is different in the absence of the NTD, which would suggest that interactions between γ-2 and the NTD of GluA2 contribute to the modulation of AMPAR properties by this TARP. Our results, however, revealed no statistically significant interactions between the effect of TARP and the NTD, i.e. the results suggest that the magnitude of TARP effect is generally similar for wt and $\triangle$NTD GluA2. Furthermore, the two Ex1 mutants, R_{65} and $R_{65}NF_{72\text{-}73}$, in which regions of strong interaction with the NTD were disrupted, showed no difference from wt γ-2 when the TARP effects on different AMPAR properties were examined. Thus, it appears that these particular residues do not contribute to TARP-mediated modulation of AMPAR function. In summary, the results shown here suggest that the reduced ability of some of the Ex1 mutants shown in Experimental Chapter 1 to modulate AMPAR properties results from disruption of γ-2 interactions with AMPAR domains which are distinct from the NTD.

The results described in this Chapter allow us to gain further insight into the role of the NTD in AMPAR function, but also suggest that this domain plays little role in TARP-mediated modulation of these receptors. This is surprising, given the extensive NTD contacts revealed by the peptide arrays shown here and in Experimental Chapter 1. It is possible, that the NTD plays a more structural role in supporting the TARP/AMPAR interaction, consistent with the model in which the Ex1 of TARPs wedges between the NTD and LBD of the AMPAR and brings the two domains closer together. Furthermore, since the NTD of native AMPARs is though to contribute to extensive contacts with binding partners located within the synapse (O'Brien et al., 1999; Saglietti et al., 2007; Sia et al., 2007), it would be interesting to investigate how NTD deletion and/or the mutations in Ex1 of γ-2 employed in this Chapter would affect the properties of AMPARs in a native system. It is possible, that a more pronounced role for the TARP/NTD interaction could emerge in the presence of other synaptic proteins, which could potentially affect this interaction.

5

Experimental Chapter 3: TARP stoichiometry affects functional properties of AMPARs

5.1 Summary

The experiments described in this Chapter were designed to provide further insight into the mechanisms of TARP/AMPAR interaction. In the former Experimental Chapters, we identified certain regions of the AMPAR that interact with γ-2. The experiments described below have focused on AMPAR/TARP complexes as a whole. Specifically, we have tried to relate TARP stoichiometry to functional properties of AMPARs. By using tandem constructs of AMPR subunits covalently linked to TARPs, we have been able to control TARP stoichiometry. We then designed experiments to investigate how AMPAR properties change with γ-2 stoichiometry. The parameters examined included: AMPAR deactivation and desensitization kinetics, the fraction of the steady-state current, the rate of AMPAR recovery from desensitization, and the mean single-channel conductance.

In addition, we explored the possibility that AMPARs may simultaneously be complexed with two different TARPs, γ-2 (Type Ia TARP) and γ-7 (Type II TARP). Since these two TARPs differ in their CNQX sensitivity, we used this pharmacological feature to investigate the TARP phenotype of AMPARs that contained two different TARPs.

5.2 Introduction

The stoichiometry of AMPAR/TARP complexes, i.e. the number of TARPs that assemble within a complex consisting of auxiliary subunits and the basic AMPAR tetramer, is suggested to vary between different types of neurons and affect biophysical and pharmacological properties of AMPARs (Shi et al., 2009). From experiments using BN-PAGE, the TARP stoichiometry of heterologously expressed AMPARs has also been suggested to vary in a way that depends on the amount of γ-2 available (Kim et al., 2010). A recent study (Hastie et al., 2013), attempted to directly measure the number of TARP molecules associated with an AMPAR by tagging the TARP with GFP and counting the number of bleaching steps required to completely bleach the fluorescence of GFP spots co-localised with mCherry-tagged GluA1. The study by Hastie et al. (2013) suggested that a GluA1 tetramer may be associated with up to 4 molecules of TARPs γ-2 and γ-3, but only one or two molecules of TARP γ-4.

Evidence for variable TARP stoichiometry in native systems is indirect and comes mostly from electrophysiological studies. Kainate efficacy was shown to vary depending on TARP stoichiometry in a heterologous expression system (Shi et al., 2009). This pharmacological tool was used to investigate TARP stoichiometry in two distinct subtypes of hippocampal neurons, with TARP stoichiometry apparently saturated (4 TARPs per AMPAR) in CA1 pyramidal cells but not in dentate granule cells. Another recent study suggested that the number of γ-8 or γ-7 molecules in the AMPAR complex affects the potentiation of kainate currents by cyclothiazide (CTZ) (Gill et al., 2011), however the physiological relevance of these findings is unclear (Herring et al., 2013). Currently available studies thus suggests that some of the AMPAR properties vary depending on the number of associated TARP molecules. However, the amount of information on AMPAR stoichiometry available in literature is limited, and there is no clear consensus.

The aim of this Chapter was to investigate the influence of TARP stoichiometry on AMPAR properties by using a fixed TARP stoichiometry of 0, 2 or 4 γ-2 molecules per AMPAR. To achieve this, we used tandem AMPAR/TARP constructs, where the N-terminus of the TARP was covalently attached to the C-terminus of the AMPAR via a 9-amino acid linker (see Fig. 5.1 A). Heteromeric GluA1/2 AMPARs were used (see Fig. 5.1 B), so that a linear *I-V* relationship indicated that the appropriate stoichiometry had been achieved. To investigate which AMPAR properties vary with γ-2 stoichiometry, we used outside-out patches pulled from transiently transfected tsA201 cells. The properties examined included: AMPAR deactivation and desensitization kinetics, the fraction of steady-state current, the rate recovery from desensitization and the mean single-channel conductance.

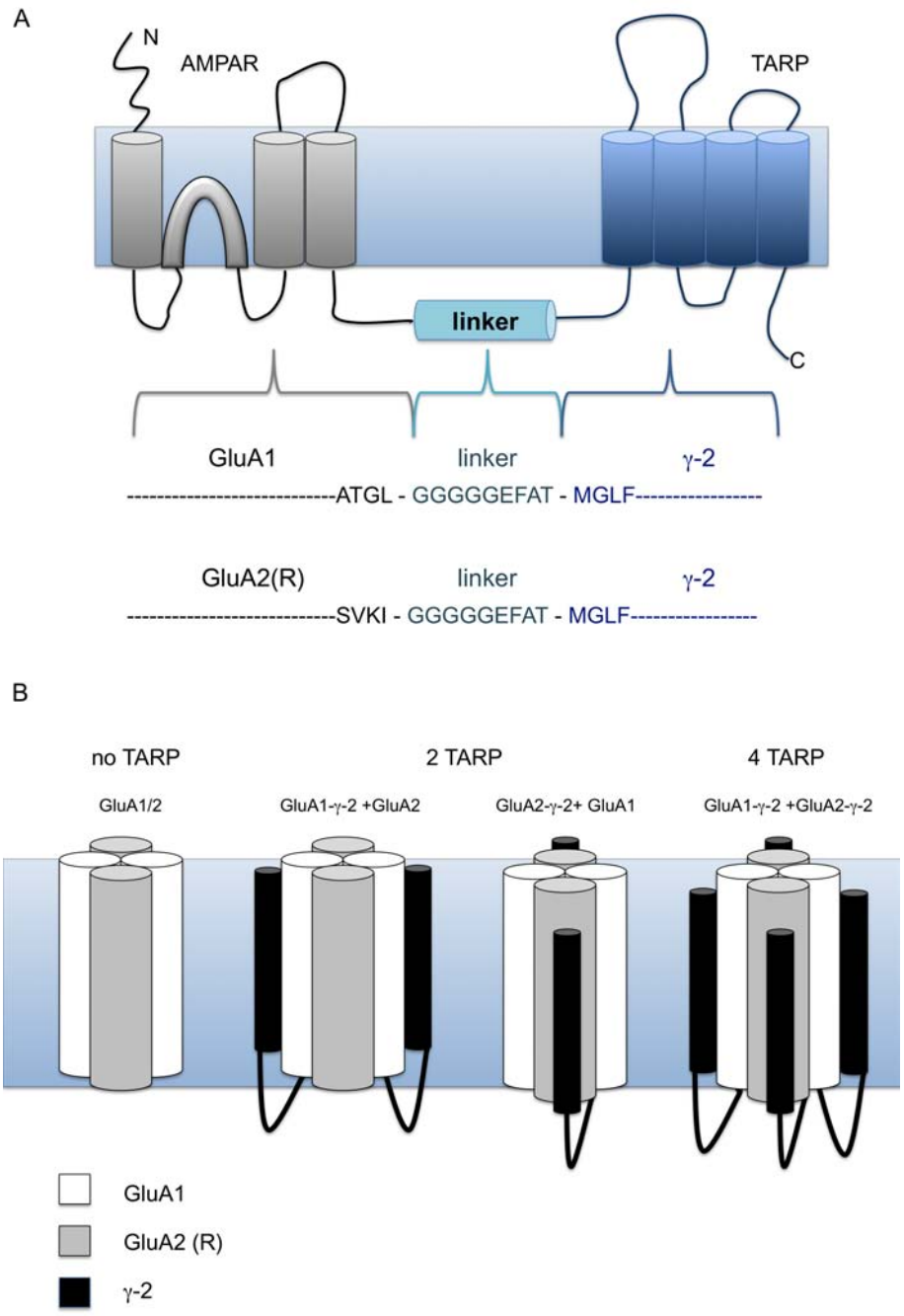

Figure 5.1: Fixed γ-2 stoichiometry was achieved using tandem AMPAR-TARP constructs. (**A**) Schematic representation of an AMPAR-TARP tandem. The AMPAR (GluA1 or GluA2R) part of the protein is coloured in grey, the linker is represented by a light blue box and located intracellularly and the γ-2 part of the protein is coloured in blue. Linker peptide sequences are shown at the bottom, preceded by the C-terminal sequence of the AMPAR subunit and followed by the N-terminal sequence of the TARP (as indicated by the coloured brackets). The GluA1-γ-2 and the GluA2-γ-2 tandems shared the same 9-amino acid liker sequence. (**B**) The three TARP stoichiometries investigated in this Chapter resulted in four possible permutations of the transfected constructs. From left to right: 0 TARP stoichiometry was achieved by co-transfecting GluA1 and GluA2R subunits. The 2 TARP stoichiometry was achieved in two different ways: by co-expressing the GluA1-γ-2 tandem with GluA2 or, conversely, by co-expressing the GluA2-γ-2 tandem with GluA1. Finally, the 4 TARP stoichiometry was achieved by co-expressing the two tandems together (GluA1-γ-2 and GluA2-γ-2).

Previous studies on TARP stoichiometry used mainly two TARPs, γ-2 and γ-8, albeit not in combination with the same AMPAR. Experiments reported in literature, which employed mass spectrometry (Schwenk et al., 2012) and imaging (Hastie et al., 2013) predicted a variable stoichiometry of up to 4 γ-2 molecules per AMPAR. We therefore investigated whether in receptors occupied by only two γ-2 molecules, the other two putative sites may be available to bind another TARP. γ-2 and γ-7 are both abundant in the cerebellum and previous studies have suggested that these two TARPs may co-assemble in the same AMPAR/TARP complexes (Kato et al., 2007; Studniarczyk et al., 2013). We thus chose to investigate GluA2/3 heteromeric receptors associated simultaneously with γ-2 and γ-7.

γ-2 and γ-7 belong to two different classes of TARPs and regulate AMPARs differentially. A previous study from our lab has shown that CNQX blocks but does not activate γ-7-associated native and recombinant receptors (Bats et al., 2012), while it is a partial agonist at γ-2-associated AMPARs (Menuz et al., 2007; Bats et al., 2012). As whole-cell CNQX currents, should be relatively easy to detect if present, this differential sensitivity of the two TARPs to CNQX was chosen to probe the TARP phenotype of AMPARs associated simultaneously with γ-2 and γ-7.

To investigate whether one of the TARPs is dominant in AMPARs that contain both γ-2 and γ-7, or whether both TARPs co-modulate AMPAR properties, we used tandem AMPAR-TARP constructs to express receptors containing simultaneously both γ-2 and γ-7, as shown in Fig. 5.2. Similar to the experiment described for γ-2 above, we used heteromeric (GluA2/3) AMPARs, so that a linear *I-V* relationship indicated that the desired TARP stoichiometry had been achieved. In addition, to minimize the influence of GluA3 homomers on the whole-cell currents recorded, cells were held at +40 mV.

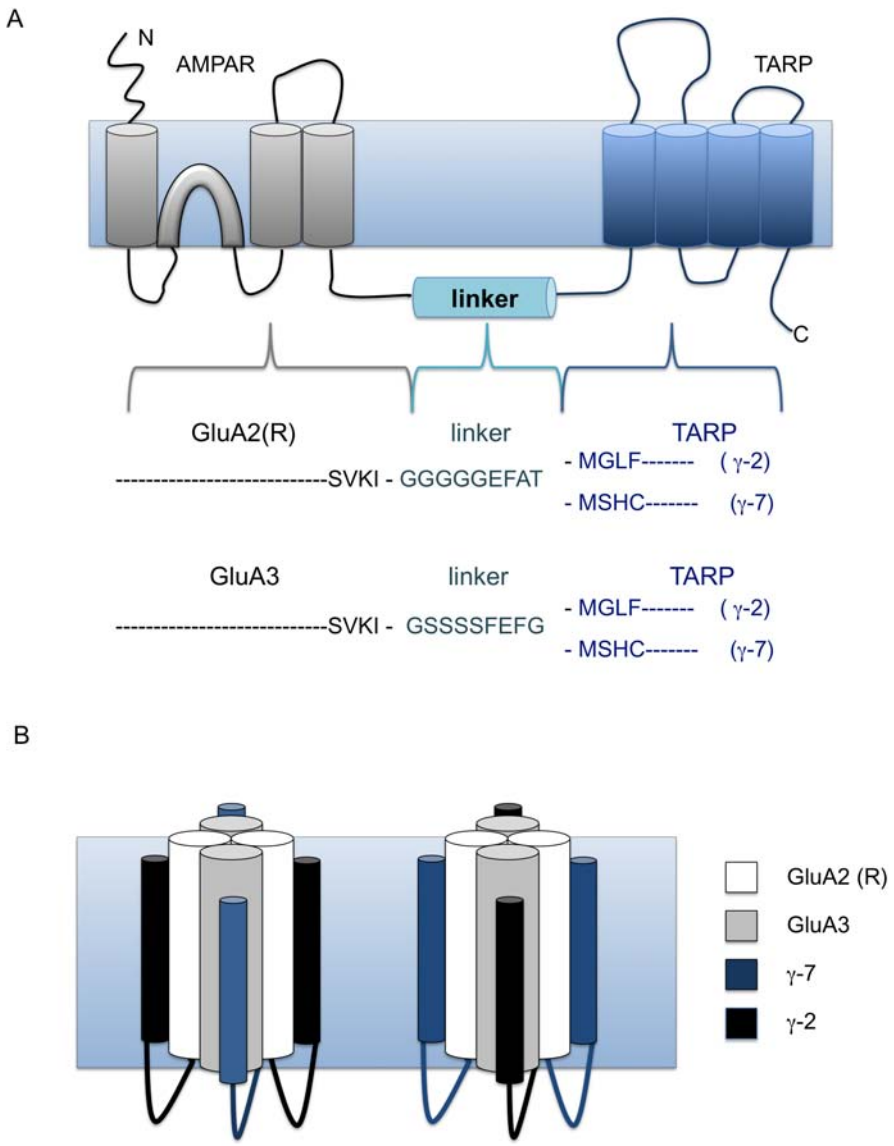

Figure 5.2: Tandem AMPAR-TARP constructs were used to ensure co-assembly of γ-2 and γ-7 in the same AMPAR complex. (**A**) Schematic of the tandem AMPAR-TARP constructs used for experiments on two-TARP containing AMPARs. The AMPAR (GluA2R or GluA3) part of the protein is coloured in grey, the intracellular linker is represented as a light blue box and the TARP (γ-2 or γ-7) part of the protein is coloured in blue. Linker peptide sequences are shown at the bottom, preceded by the C-terminal sequence of the AMPAR subunit and followed by the N-terminal sequence of the TARP (as indicated by the coloured brackets). Note that although the lengths of the linkers used in GluA2 and GluA3 tandems are the same, their sequences vary. (**B**) Schematic representation of an AMPAR/TARP complex containing two different TARPs: γ-2 and γ-7. Due to the use of heteromeric AMPARs, linear *I-V* relationship indicated successful co-assembly. Left: GluA3-γ-7 tandem construct assembled with a GluA2(R)-γ-2 tandem. Right: The converse combination, GluA3-γ-2 tandem construct assembled with GluA2-γ-7 tandem.

5.3 Results

5.3.1 Rectification was used to assess the assembly of tandem constructs into AMPAR/TARP complexes with defined TARP stoichiometry

In order to assess how efficiently tandem AMPAR-TARP constructs assembled into functional receptors, we measured the rectification index (RI) of AMPAR currents in patches. RI was measured as the ratio of peak Glu responses at -60 and +60 mV, as shown in panel A, Fig. 5.3. A linear *I-V* relationship indicated that most assemblies were GluA2-containing heteromers, and thus indicated a TARP stoichiometry of 0, 2 or 4, as described above. TARPless AMPARs have been reported to preferentially form heteromeric rather than homomeric assemblies (Mansour et al., 2001). In the data set presented here TARPless AMPAR subunits also formed mainly heteromeric assemblies as judged from their RI (0.566 $\pm$ 0.042, n= 47); however, some variability in RI was observed (see panel B, Fig 5.3).

Similarly to the TARPless controls, AMPARs formed from tandem AMPAR-TARP constructs showed varying degrees of rectification. The RI of the fully TARPed (4 TARP stoichiometry) GluA1/2 AMPARs (mean RI = 0.653 $\pm$ 0.027, n= 44; panel E Fig. 5.3) was not significantly different from the TARPless control shown in Fig. 5.3 panel B (P= 0.084). The large scatter in both cases suggested a mixture of patches with Ca^{2+}-permeable and impermeable AMPARs. However, both 2 TARP-containing AMPAR combinations showed a significant difference in RI from TARPless controls (for GluA1-γ-2 + GluA2, panel C Fig. 5.3: mean RI= 0.808 $\pm$ 0.010, n= 76, P= 2.22 $\times$ 10^{-6}; for GluA2-γ-2 + GluA1, panel D Fig. 5.3: mean RI = 0.234 $\pm$ 0.035, n= 26, P= 2.2 $\times$ 10^{-7}). The 2 TARP-containing combinations were also different from the fully TARPed receptors (GluA1-γ-2 + GluA2: P= 4.40 $\times$ 10^{-6} and GluA2-γ-2 + GluA1: P< 1 $\times$ 10^{-8}).

Comparison of the RI distribution histograms in panels C and D of Figure 5.3 suggests that receptors containing two γ-2 molecules assembled well (i.e. formed heteromers) when γ-2 was tethered to GluA1 (panel C) but not when it was tethered to GluA2 (panel D) . There was a significant difference in RI between these two variants of 2 TARP stoichiometry (P< 1 $\times$ 10^{-8}), suggesting that in the presence of the GluA2-γ-2 tandem, GluA1 formed mostly homomeric AMPARs. It is thus possible, that the constraints imposed by covalently tethering the TARP affect the ability of γ-2 to efficiently traffic AMPARs to the cell surface and that this is most pronounced for the GluA2 subunit, which in its R form has been suggested to be largely retained in the ER (Greger et al., 2002, 2003).

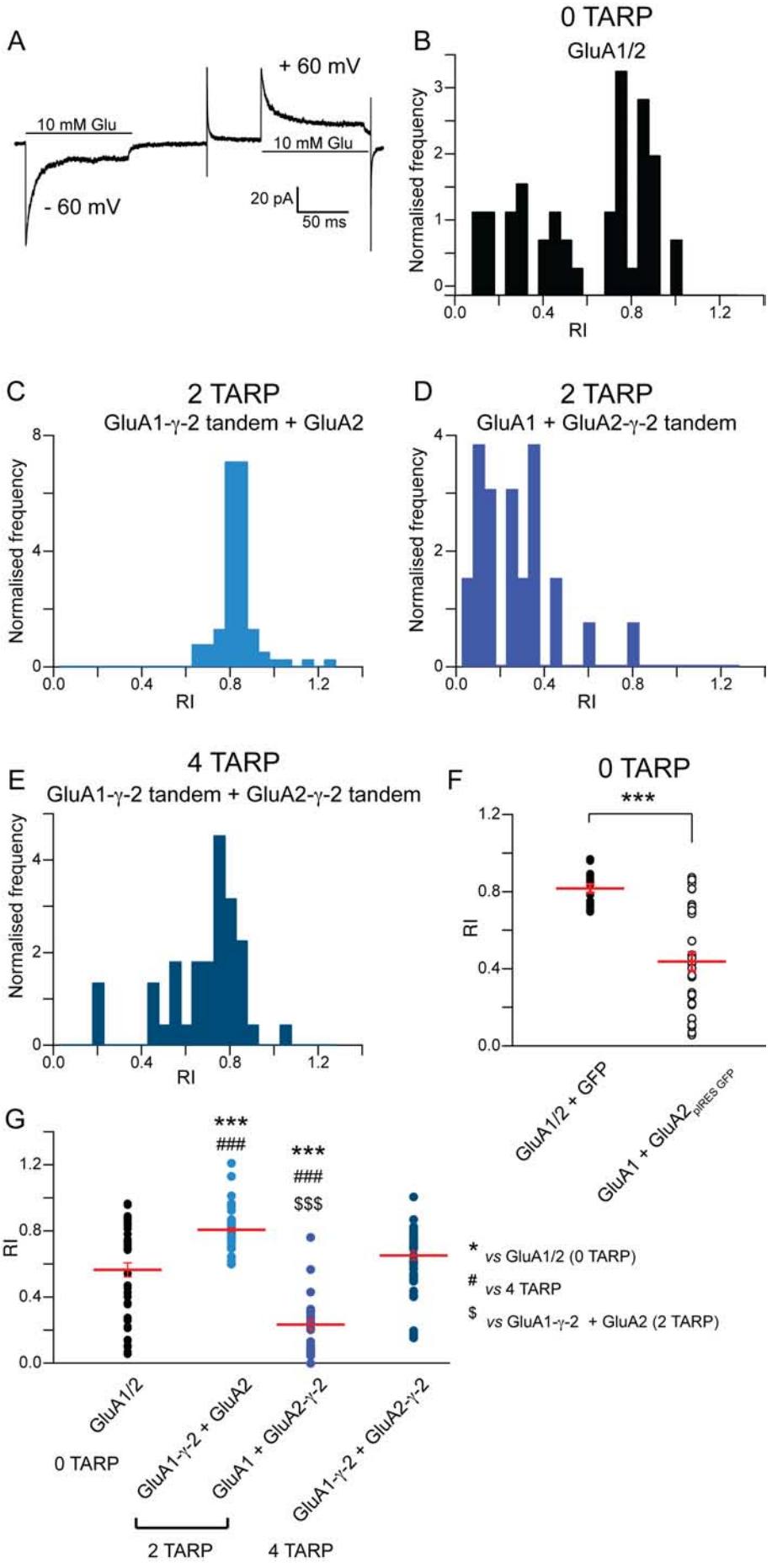

Figure 5.3: Rectification index served as a measure of tandem construct assembly into AMPAR/TARP complexes of defined TARP stoichiometry.

Figure 5.3 continued: (**A**) A representative average trace illustrating the protocol used to obtain RI. A 100 ms pulse of 10 mM Glu (indicated by the black bar on top of the figure) was applied while the patch was held at -60 mV. The patch was then stepped to +60 mV and another 100 ms pulse of 10 mM Glu was applied. The RI was measured as the ratio of peak amplitudes at +60 and -60 mV. (**B**) Frequency histogram of RIs from patches pulled from cells transfected with TARPless GluA1/2 (n= 47). The count was normalised to probability density. (**C-E**) As for B, but for GluA1-γ-2 + GluA2 (2 TARP, n= 76), GluA2-γ-2 + GluA1 (2 TARP, n= 26) and GluA1-γ-2 + GluA2-γ-2 (4 TARP, n= 44), respectively. (**F**) TARPless GluA1/2 control patches from panel B subdivided into two groups based on the vector used for the GluA2 subunit during transfection. The RI values for the individual patches are shown as closed circles for GluA1 + GluA2 + GFP co-transfection as 3 separate plasmids (left column) and as open circles for the GluA1 co-transfection with GluA2(R) in the pIRES-EGFP vector. The triple asterisk above the graph indicates a significant difference in RI between the two groups (P= 1.133×10^{-8}, Welch two-sample t-test). (**G**) RIs for all of the stoichiometry groups investigated here. The RI values for the individual patches are shown as closed circles. The red horizontal lines represent the mean RI for each condition and the vertical bars show the SEM. One-way ANOVA showed an overall significant difference in RI between the groups ($F_{(3,\ 67.94)}$ = 91.87 , P= 7.36×10^{-24}). Asterisks mark significant difference *vs.* TARPless GluA1/2 ($***$ P< 0.001; Welch t-test), hashes mark significant difference *vs.* the fully TARPed GluA1-γ-2 + GluA2-γ-2 receptors (### P< 0.001; Welch t-test). while dollar signs mark significant difference *vs.* GluA1-γ-2 + GluA2 ($$$ P< 0.001; Welch t-test).

In summary, a large variability in RI was observed in this data set, reflecting varying degrees of assembly of GluA2-containing heteromers. The process of AMPAR heteromerization is mediated mainly through the NTD of AMPARs (Rossmann et al., 2011), and it is the C terminus of AMPAR that is modified by TARP association in the tandem construct. It is therefore unclear if the use of tandems affected heteromerization directly. Another possibility is, that despite the efforts to optimize transfections to facilitate heteromeric assembly by varying the GluA1:GluA2 transfection ratio (see Materials and Methods), there was a difference in protein expression levels between the vectors used for transfection, which affected the ability of tandem constructs to assemble. Some dependence of rectification on the expression vector was observed in TARPless controls (see panel F, Fig. 5.3), where the mean RI for GluA1/2 co-expression with 60 ng GFP as 3 separate constructs was 0.81 $\pm$ 0.02 (n= 16), while co-expression of GluA1 with GluA2(R) in pIRES-EGFP rendered currents with a significantly lower RI (0.44 $\pm$ 0.05, n= 31, P= 1.133×10^{-8}, Welch two-sample t-test). Note that protein expression (surface or total) for the different constructs was not quantified.

In order to compare all four AMPAR/TARP combinations shown in Fig. 5.1 B, we decided to record all responses at +40 mV in the presence of 100 μM intracellular sper-

mine. This approach was based on previous studies suggesting that at this holding potential all TARPless and the vast majority of TARPed Ca^{2+}-permeable GluA1 homomers are blocked (Soto et al., 2007). Thus under these conditions, the majority of receptors still conducting are expected to be GluA1/2 heteromers. We also assumed that relatively few GluA2(R) homomers would form, as previous studies suggested that edited GluA2 is mostly retained in the ER (Greger et al., 2002, 2003).

Where possible, currents were also examined at -80 mV. For the -80 mV recordings, patches with an RI of 0.7 or more were analysed. The GluA1 + GluA2-γ-2 version of the 2 TARP stoichiometry was therefore not included in the -80 mV analysis. Thus, the 2 TARP stoichiometry at -80 mV is represented only by the GluA1-γ-2 + GluA2 combination. For +40 mV, data were included regardless of patch RI, resulting in the 2 TARP stoichiometry being achieved in two different ways, either by the use of a GluA1-γ-2 tandem or by the use of GluA2-γ-2 tandem (as shown above in Fig. 5.1 B).

5.3.2 Deactivation time constant of GluA1/2 was slowed only when all subunits were TARPed

Deactivation of heteromeric GluA1/2 AMPARs with a defined γ-2 stoichiometry was measured by fitting the decay of current responses to 1 ms Glu pulses, as described previously. It is worth noting that currents from several of the patches that expressed fully-TARPed (GluA1-γ-2 + GluA2-γ-2) AMPARs required fitting to a triple exponential, due to the presence of a prominent slow component. This was evident at both +40 mV (5 out of 8 patches) and -80 mV (4 out of 8 patches).

At +40 mV (Fig. 5.4), deactivation τ_w was significantly prolonged compared with TARPless AMPARs only when GluA1/2 AMPARs were TARPed with four γ-2 molecules. τ_w was increased almost $\sim$6-fold (from 1.073 $\pm$ 0.139 ms for TARPless GluA1/2 to 5.949 $\pm$ 1.013 ms for 4 TARPs; P= 0.011). Neither version of the 2 TARP stoichiometry increased GluA1/2 deactivation time constant (τ_w of currents from GluA1-γ-2 tandem + GluA2: 1.067 $\pm$ 0.069 ms; P= 1.00; GluA2-γ-2 tandem + GluA1: 1.046 $\pm$ 0.070 ms; P= 1.00). The two versions of 2 TARP stoichiometry were not significantly different from each other (P= 1.00) and were both significantly different from the fully TARPed receptors (GluA1-γ-2 tandem + GluA2: P= 0.011; GluA2-γ-2 tandem + GluA1: P= 0.011).

Deactivation time constant showed a similar pattern of dependence on γ-2 stoichiometry when the currents were recorded at -80 mV (Fig. 5.5). GluA1/2 receptors fully

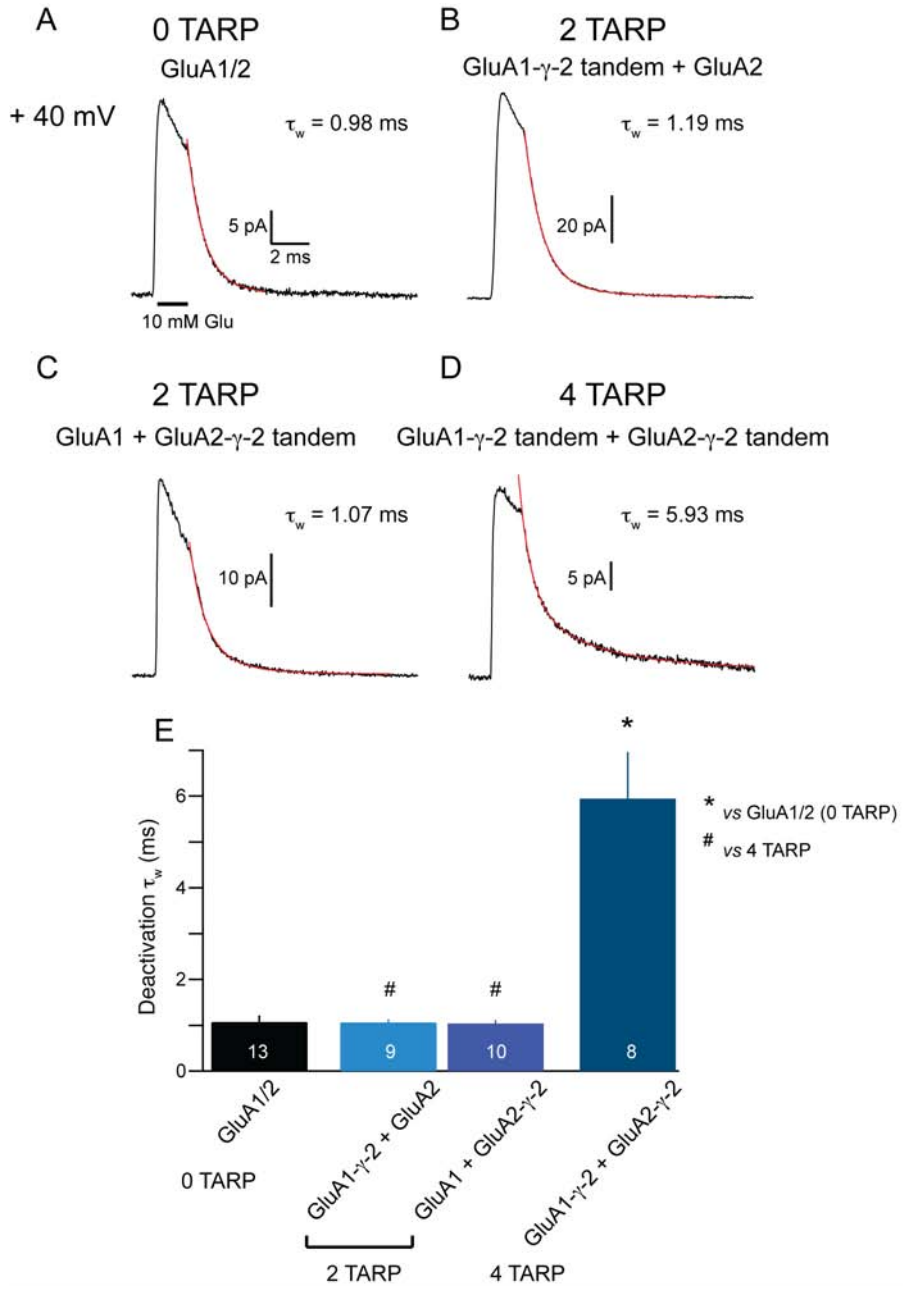

Figure 5.4: Deactivation of GluA1/2 AMPARs varied with γ-2 stoichiometry when the patches were held at +40 mV. (**A**) Average response to a 1 ms pulse of 10 mM Glu from a representative patch expressing TARPless GluA1/2 receptors. Individual sweeps were aligned at the 20% rise before averaging. The horizontal bar marks the duration of Glu application. Deactivation τ_w for this patch is indicated on the graph. (**B-D**) As for A, but for patches expressing GluA1-γ-2 + GluA2 (2 TARP), GluA2-γ-2 + GluA1 (2 TARP) and GluA1-γ-2 + GluA2-γ-2 (4 TARP) respectively. (**E**) Histogram showing τ_w of deactivation for each of the TARP stoichiometry variants. Bars denote the SEM and the *n* numbers for each group are indicated in white at the bottom of the histogram. One-way ANOVA showed a significant effect of γ-2 stoichiometry on GluA1/2 deactivation ($F_{(3,\ 17.78)} = 7.24$, $P = 0.0022$). For pairwise tests, asterisks mark significant difference *vs.* GluA1/2 alone ($*$ $P < 0.05$; Welch *t*-test), while hashes mark significant difference *vs.* GluA1-γ-2 + GluA2-γ-2 (4 TARP) ($\#$ $P < 0.05$; Welch *t*-test).

TARPed with γ-2 showed a significantly slower deactivation time when compared with TARPless controls (2.577 $\pm$ 0.458 ms *vs.* 0.776 $\pm$ 0.059 ms; P= 0.017). In contrast, GluA1/2 AMPARs TARPed with only 2 molecules of γ-2 did not display prolonged deactivation compared with TARPless AMPARs (0.862 $\pm$ 0.061 ms; P= 0.319). The presence of only 2 TARPs was significantly less efficient at slowing deactivation than the presence of 4 TARPs (P= 0.017).

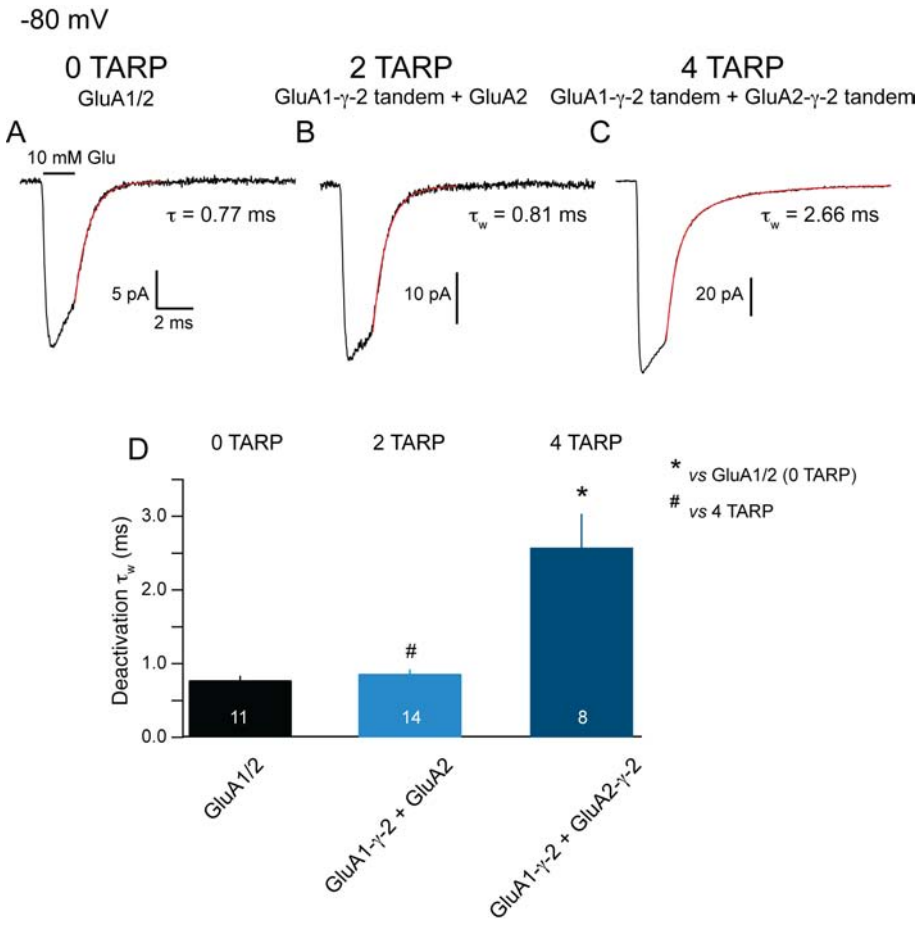

Figure 5.5: Deactivation of GluA1/2 AMPARs varied with γ-2 stoichiometry when the patches were held at -80 mV. (**A**) Average response to a 1 ms pulse of 10 mM Glu from a representative patch expressing TARPless GluA1/2 receptors. Individual sweeps were aligned at the 20% rise before averaging. The horizontal bar marks the duration of Glu application. Deactivation τ_w for this patch is indicated on the graph. (**B-C**) As for A, but for patches expressing GluA1-γ-2 + GluA2 (2 TARP) and GluA1-γ-2 + GluA2-γ-2 (4 TARP) respectively. (**D**) Histogram showing τ_w of deactivation for each of the TARP stoichiometry variants. Bars denote the SEM and the *n* numbers for each group are indicated in white at the bottom of the histogram. One-way ANOVA showed a significant effect of γ-2 stoichiometry on GluA1/2 deactivation ($F_{(2,\ 14.4)}$ = 7.49, P= 0.0059). For pairwise tests, asterisks mark significant difference *vs.* GluA1/2 alone ($*$ P< 0.05; Welch *t*-test), while hashes mark significant difference *vs.* GluA1-γ-2 + GluA2-γ-2 (4 TARP) ($\#$ P< 0.05; Welch *t*-test).

These results suggest that deactivation of AMPARs varies with TARP stoichiometry both at positive and negative holding potentials. If such differences occur in native

receptors, variability in TARP stoichiometry could affect the decay of EPSCs. A similar observation has been reported previously. Cerebellar granule cells from *stargazer* +/- mice, which have been suggested to have a reduced TARP stoichiometry, displayed a significantly faster mEPSC decay compared with wt. On the contrary, overexpression of γ-2 in *stg* granule cells prolonged mEPSC decay compared to wt (Milstein et al., 2007). This difference could likely reflect accelerated AMPAR deactivation.

5.3.3 TARP stoichiometry determines AMPAR desensitization

The effect of γ-2 stoichiometry on the time course and extent of AMPAR desensitization was examined at both +40 mV and -80 mV holding potentials. As described previously, the responses to desensitizing (100 ms) pulses of 10 mM Glu were fitted with a double exponential, allowing the desensitization time constant, τ_w, and the percentage of steady-state current (I_{ss}) to be extracted from the fit. These parameters were used as measures of desensitization time course and extent respectively.

At +40 mV both the desensitization τ_w and the I_{ss} showed a similar pattern of dependence on γ-2 stoichiometry (see Fig. 5.6). Desensitization τ_w was significantly slowed compared with TARPless GluA1/2 AMPARs when receptors were TARPed with four γ-2 molecules (10.813 $\pm$ 0.739 ms *vs.* 7.029 $\pm$ 0.676 ms, P= 0.0036). Similarly, fully TARPed receptors showed a significantly larger I_{ss} than TARPless controls (22.471 $\pm$ 1.748 % *vs.* 4.141 $\pm$ 1.344 %, P= 2.5 $\times$ 10^{-7}).

Both variants of AMPARs TARPed with only two molecules of γ-2 showed no effect on either desensitization τ_w or the I_{ss} when compared with TARPless controls (GluA1-γ-2 + GluA2: τ_w= 6.886 $\pm$ 0.321 ms P= 0.85 and I_{ss}= 3.923 $\pm$ 0.677 P= 1.00; GluA2-γ-2 + GluA1: τ_w= 5.706 $\pm$ 0.501 ms P= 0.254 and I_{ss}= 4.001 $\pm$ 1.476 P= 1.00). The two variants of 2 TARP stoichiometry did not differ from each other in desensitization τ_w (P= 0.187) or the I_{ss} (P= 1.00). Furthermore, they both were significantly less efficient than fully TARPed receptors at slowing desensitization τ_w (GluA1-γ-2 + GluA2: P= 0.0013; GluA2-γ-2 + GluA1: P= 1.23 $\times$ 10^{-4}) and had a significantly lower I_{ss} than the AMPARs containing 4 γ-2 molecules (GluA1-γ-2 + GluA2: P= 8.3 $\times$ 10^{-7}; GluA2-γ-2 + GluA1: P= 4.9 $\times$ 10^{-7}).

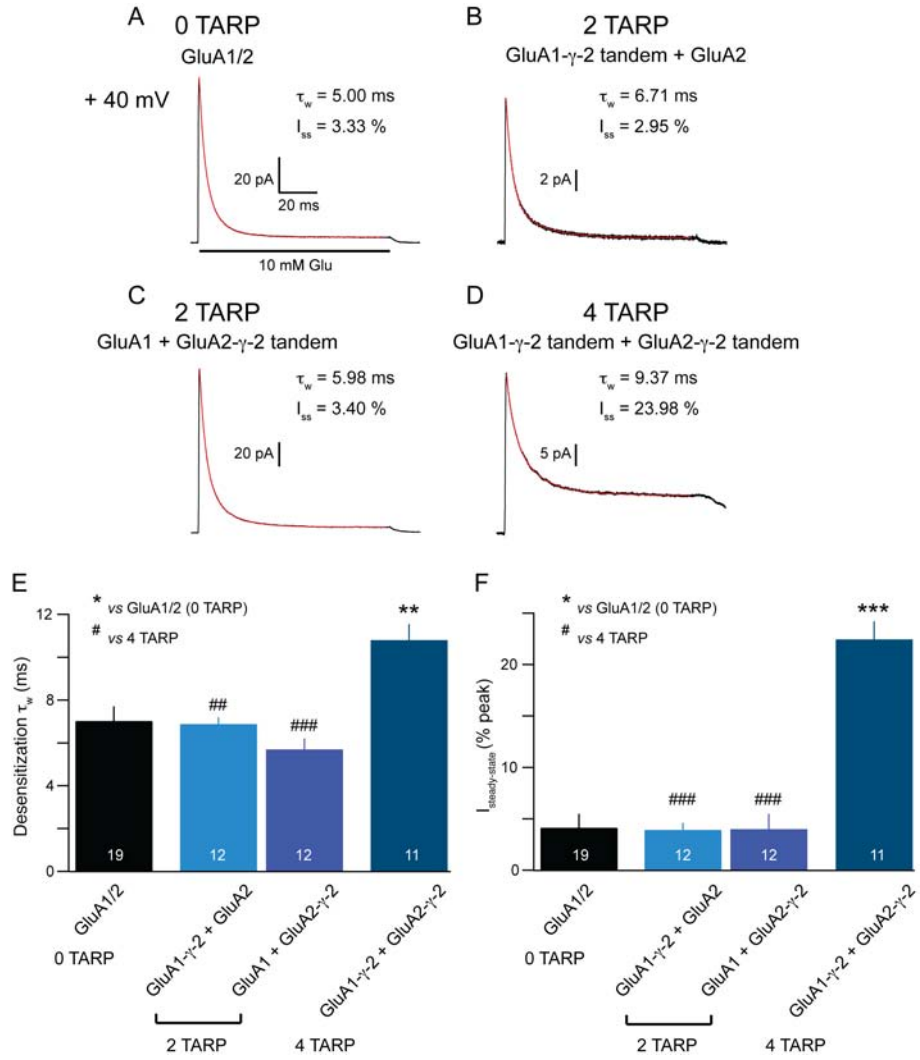

Figure 5.6: γ-2 stoichiometry affected the time course and extent of AMPAR desensitization at +40 mV. (**A**) Average response to a 100 ms pulse of 10 mM Glu from a representative patch expressing TARPless GluA1/2 receptors. Individual sweeps were aligned at the 20% rise before averaging. The horizontal bar marks the duration of Glu application. Desensitization τ_w and the I_{ss} for this patch are indicated on the graph. (**B-D**) As for A, but for patches expressing GluA1-γ-2 + GluA2 (2 TARP), GluA2-γ-2 + GluA1 (2 TARP) and GluA1-γ-2 + GluA2-γ-2 (4 TARP) respectively. (**E**) Histogram showing τ_w of desensitization for each of the TARP stoichiometry variants. Bars denote the SEM and the *n* numbers for each group are indicated in white at the bottom of the histogram. One-way ANOVA showed a significant effect of γ-2 stoichiometry on GluA1/2 desensitization τ_w ($F_{(3,\ 25.48)}$ = 10.58, P= 1.06 $\times$ 10^{-4}). (**F**) Histogram showing the % of steady-state current for each of the TARP stoichiometry variants. Bars denote the SEM and the *n* numbers for each group are indicated in white at the bottom of the histogram. One-way ANOVA showed a significant effect of γ-2 stoichiometry on GluA1/2 steady-state current percentage ($F_{(3,\ 24.55)}$ = 32.13, P= 1.16 $\times$ 10^{-8}). For pairwise tests shown in panels **E** and **F**, asterisks mark significant difference *vs.* GluA1/2 alone ($**$ P< 0.01, $***$ P< 0.001; Welch *t*-test), while hashes mark significant difference *vs.* GluA1-γ-2 + GluA2-γ-2 (4 TARP) (## P< 0.01, ### P< 0.001; Welch *t*-test).

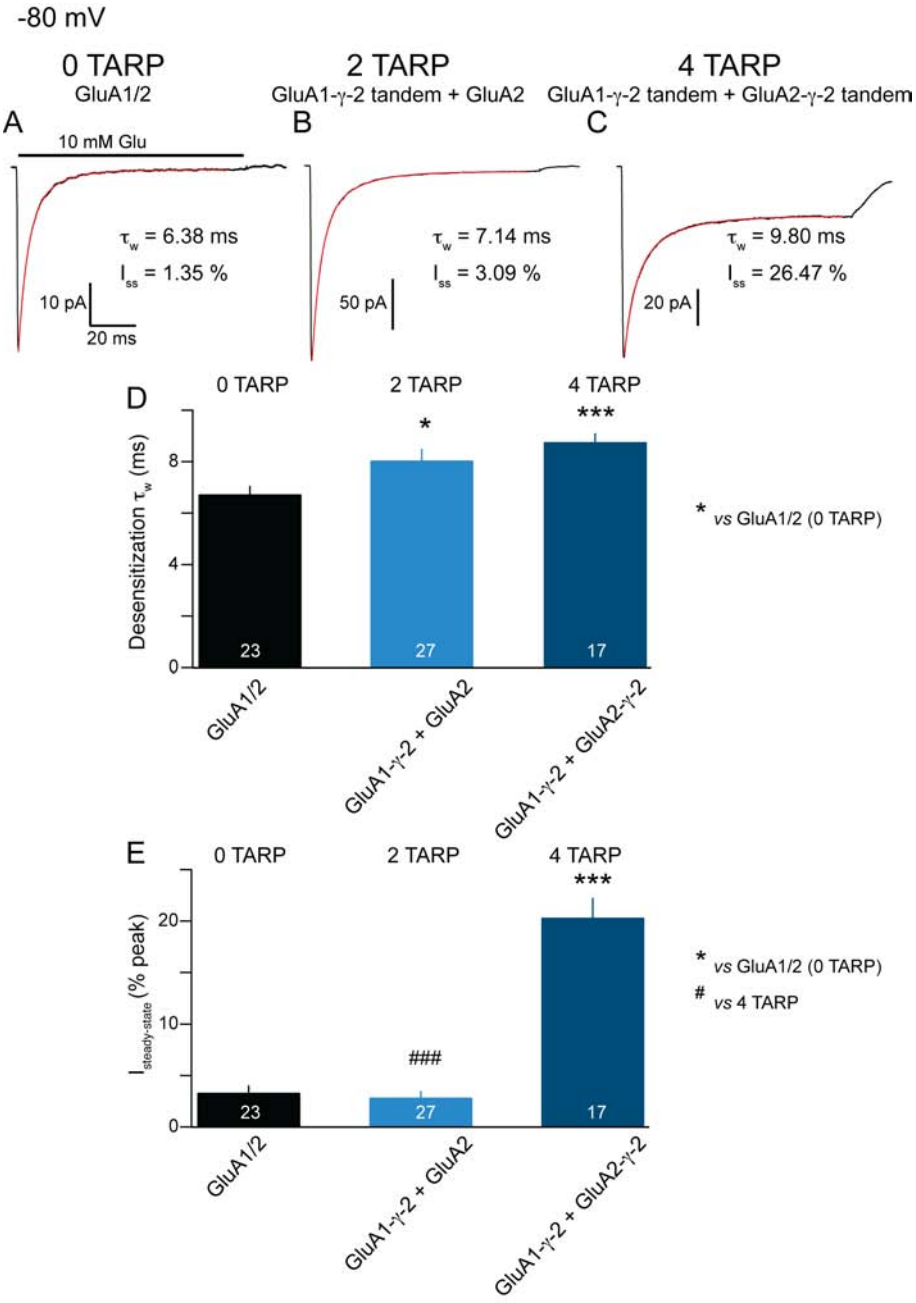

Figure 5.7: The time course and extent of desensitization were differentially affected by γ-2 stoichiometry at -80 mV. (**A**) Average response to a 100 ms pulse of 10 mM Glu from a representative patch expressing TARPless GluA1/2 receptors. Individual sweeps were aligned at the 20% rise before averaging. The horizontal bar marks the duration of Glu application. Desensitization τ_w and the I_{ss} for this patch are indicated on the graph. (**B-C**) As for A, but for patches expressing GluA1-γ-2 + GluA2 (2 TARP) and GluA1-γ-2 + GluA2-γ-2 (4 TARP) respectively. (**D**) Histogram showing τ_w of desensitization for each of the TARP stoichiometry variants. Bars denote the SEM and the *n* numbers for each group are indicated in white at the bottom of the histogram. One-way ANOVA showed a significant effect of γ-2 stoichiometry on GluA1/2 desensitization ($F_{(2,\ 41.66)}$ = 9.28, P= 4.63 $\times$ 10^{-4}). (**E**) Histogram showing the % of steady-state current for each of the TARP stoichiometry variants. Bars denote the SEM and the *n* numbers for each group are indicated in white at the bottom of the histogram. One-way ANOVA showed a significant effect of γ-2 stoichiometry on GluA1/2 steady-state current percentage ($F_{(2,\ 33.51)}$ = 38.23, P= 2.25 $\times$ 10^{-9}).

Figure 5.7 continued: For pairwise tests shown in panels **D** and **E**, asterisks mark significant difference *vs.* GluA1/2 alone ($*$ P< 0.05, $***$ P< 0.001; Welch t-test), while hashes mark significant difference *vs.* GluA1-γ-2 + GluA2-γ-2 (4 TARP) (### P< 0.001; Welch t-test).

At the holding potential of -80 mV (see Fig. 5.7), the I_{ss} showed a similar pattern of dependence on γ-2 stoichiometry as at +40 mV, while desensitization τ_w was affected differently. Desensitization τ_w was significantly slowed compared with TARPless controls (6.741 $\pm$ 0.326 ms) both by the presence of two γ-2 molecules (8.056 $\pm$ 0.444 ms, P= 0.042) and by the presence of four γ-2 molecules (8.765 $\pm$ 0.342 ms, P= 3.83 $\times$ 10^{-4}). Thus, at -80 mV partially TARPed receptors (2 TARP stoichiometry) appeared to be as effective as their fully TARPed counterparts at slowing desensitization τ_w (P= 0.213).

In contrast, the I_{ss} at -80 mV was significantly increased only when GluA1/2 AMPARs were fully TARPed (20.356 $\pm$ 1.903 % *vs.* 3.337 $\pm$ 0.694 %; P= 1.1 $\times$ 10^{-7}) and not partially TARPed (2.873 $\pm$ 0.628 % P= 0.62). The percentage of steady-state current in AMPARs TARPed with two molecules of γ-2 was significantly less than in those TARPed with four molecules of γ-2 (P= 1.1 $\times$ 10^{-7}).

5.3.4 The effect of TARP stoichiometry on AMPAR recovery from desensitization

Recovery from desensitization was measured using a paired pulse protocol (a desensitizing 100 ms pulse was followed by a 10 ms pulse, both of 10 mM Glu) with increasing interpulse interval. The data for each patch were fitted to a Hodgkin-Huxley-type function (Carbone and Plested, 2012), allowing t_{50} (the time needed for the second peak to recover to 50 % of the first peak) to be obtained from the fit.

At the positive holding potential of +40 mV (Fig. 5.8), t_{50} for fully TARPed GluA1/2 receptors was significantly briefer than for TARPless controls (19.138 $\pm$ 4.057 ms *vs.* 41.033 $\pm$ 2.916 ms, P= 0.0029). By contrast, partially TARPed AMPARs showed no significant speeding in their recovery from desensitization (GluA1-γ-2 + GluA2: 36.536 $\pm$ 4.186 ms P= 0.89; GluA2-γ-2 + GluA1: 35.479 $\pm$ 4.239 ms P= 0.89). Furthermore, the two variants of 2 TARP stoichiometry showed no significant difference in their t_{50} values from each other (P= 0.89) or from the fully TARPed GluA1/2 AMPARs (GluA1-γ-2 + GluA2: P= 0.051; GluA2-γ-2 + GluA1: P= 0.053).

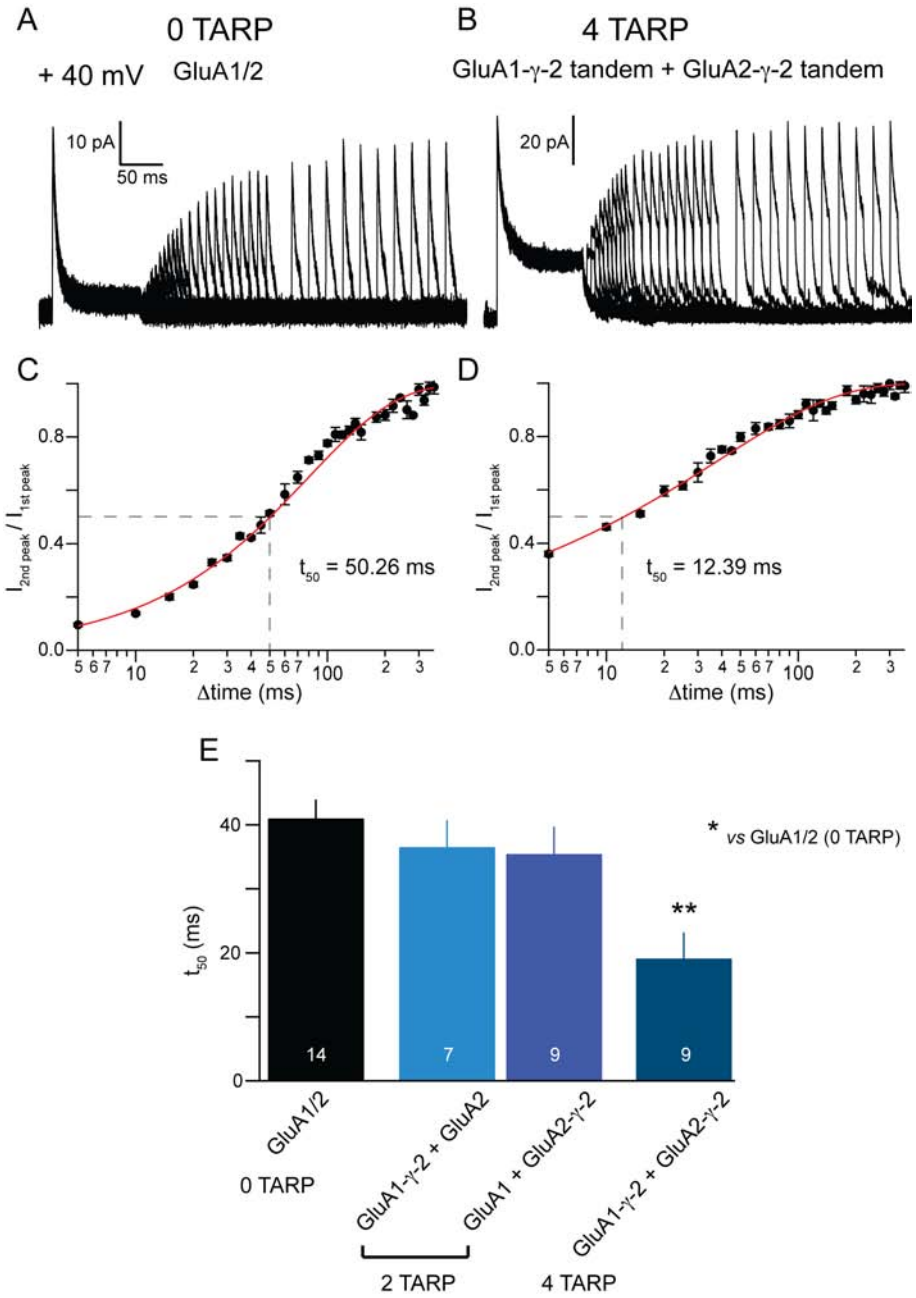

Figure 5.8: Fully TARPed AMPARs showed a significantly faster recovery from desensitization at +40 mV than TARPless controls. (**A**) Record of recovery from desensitization from a representative patch expressing TARPless GluA1/2 receptors. The average responses at each interpulse interval were aligned at the 20 % rise of the first peak and overlaid. (**B**) As for A, but for a patch expressing GluA1-γ-2 + GluA2-γ-2 (4 TARP). (**C**) Hodgkin-Huxley-type fit to the example TARPless GluA1/2 patch shown in panel A. The amplitude of the second peak as fraction of the amplitude of the first peak was plotted on a linear scale against the interpulse interval (logarithmic scale). t_{50} for this patch is indicated by the dashed line and displayed on the graph. (**D**) As for C, but for a patch expressing GluA1-γ-2 + GluA2-γ-2 (4 TARP) (same patch as in panel B). (**D**) Histogram showing t_{50} for each of the TARP stoichiometry variants. Bars denote the SEM and the *n* numbers for each group are indicated in white at the bottom of the histogram. One-way ANOVA showed a significant effect of γ-2 stoichiometry on GluA1/2 recovery from desensitization ($F_{(3,\ 16.95)}$ = 6.07, P= 0.0053). For pairwise tests, asterisks mark significant difference *vs.* GluA1/2 alone ($**$ P< 0.01; Welch t-test).

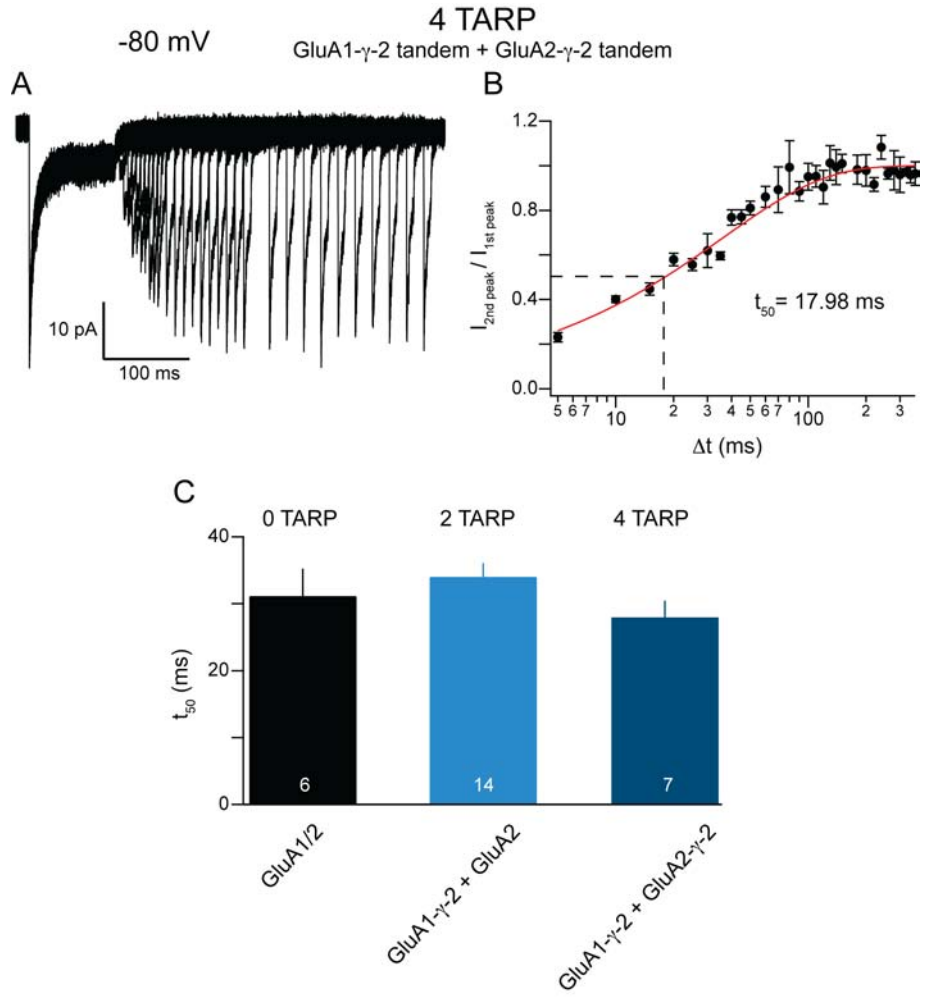

Figure 5.9: γ-2 stoichiometry had no effect on GluA1/2 recovery from desensitization at -80 mV. (**A**) Record of recovery from desensitization from a representative patch expressing GluA1-γ-2 + GluA2-γ-2 (4 TARP). The average responses at each interpulse interval were aligned at the 20 % rise of the first peak and overlaid. (**B**) Hodgkin-Huxley-type fit to the example fully TARPed patch shown in panel A. The amplitude of the second peak as fraction of the amplitude of the first peak was plotted on a linear scale against the interpulse interval (logarithmic scale). t_{50} for this patch is indicated by the dashed line and displayed on the graph. (**C**) Histogram showing t_{50} for each of the TARP stoichiometry variants. Bars denote the SEM and the *n* numbers for each group are indicated in white at the bottom of the histogram. One-way ANOVA showed no significant effect of γ-2 stoichiometry on GluA1/2 recovery from desensitization ($F_{(2,\ 11.16)}$ = 1.68, P= 0.231).

At the -80 mV holding potential t_{50} was similar across TARP stoichiometries: TARP-less GluA1/2: 31.163 $\pm$ 4.074 ms; GluA1-γ-2 + GluA2 (2 TARP): 34.008 $\pm$ 2.046 ms and GluA1-γ-2 + GluA2-γ-2 (4 TARP): 27.965 $\pm$ 2.471 ms. Thus we did not detect any overall effect of γ-2 stoichiometry on recovery from desensitization at -80 mV (see Fig. 5.9).

The results shown above suggest that the effect of γ-2 on GluA1/2 recovery from desensitization may depend on both TARP stoichiometry and the holding potential, so

that the effect of γ-2 on GluA1/2 recovery from desensitization is more pronounced at positive membrane potentials. By contrast, previous studies on GluA1 receptors (Priel et al., 2005), suggested that γ-2 speeds GluA1 recovery from desensitisation at the negative holding potential of -60 mV. However, Priel et al. (2005) used a different way of quantifying recovery from desensitization: measured recovery time constant from a single exponential fit, rather than the t_{50} obtained here from a Hodgkin-Huxley-type fit. Thus, the differences in experimental methods could contribute to the discrepancy between our findings and those of Priel et al. (2005). However, given that in our recently published study, co-expression of γ-2 did not accelerate the recovery from desensitization of either GluA2 or GluA3 (Cais et al., 2014), it is possible that the accelerated recovery from desensitization upon γ-2 co-assembly is a feature specific to GluA1 and does not apply to heteromeric GluA1/2 AMPARs.

5.3.5 Attempts to estimate single-channel conductance using NSFA provided some insight into the assembly of AMPARs with different γ-2 stoichiometries

As co assembly of AMPARs with TARPs is known to increase mean-single channel conductance (Tomita et al., 2005; Shelley et al., 2012; Soto et al., 2007, 2009; Jackson et al., 2011), we were also interested to determine how γ-2 stoichiometryinfluenced this parameter. NSFA was applied to currents evoked by 100 ms applications of 10 mM Glu. For TARPless GluA1/2 AMPARs, NSFA provided parabolic fits to the data points both at +40 mV (Fig. 5.10 panel A) and -80 mV (Fig. 5.11 panel A). It was, however, more difficult to apply NSFA to data obtained from the tandem AMPAR-γ-2 constructs. The low apparent P_o, particularly of the GluA1-γ-2 tandem + GluA2 (2 TARP) combination at +40 mV (Fig. 5.10 panel B), meant it was not possible to obtain a realistic estimate of the number of channels (very high estimates of N were obtained). This suggested that rather than fitting a parabolic function, a straight line could be fitted to the first 3 data points, giving only a conductance estimate. In addition, upon the analysis of the currents from fully TARPed AMPARs, it became evident that NSFA cannot be successfully applied to data from patches co-expressing GluA1-γ-2 and GluA2-γ-2 tandems.

At both +40 mV (Fig. 5.10 panel D) and -80 mV (Fig. 5.11 panel C) the average current variance *vs.* mean current plots for AMPARs TRAPed with 4 γ-2 molecules failed to ass through the origin, suggesting the presence of a a component that added some current, but little or no variance. When individual patches for the 4 TARP combination were examined, the parabolic fit (constrained to go through the origin) was often visibly shallower than the data points or the software used was unable to fit a

parabolic relationship to the data points (fitting failed). A similar phenomenon had previously been observed in the lab for GluA2(R) homomeric AMPARs TARPed with γ-2. These receptors were shown to activate a mixture of low and high conductance channels. This resulted in a shift of the current-variance plots from the origin, as the low conductance openings added current but almost no variance (Dr Ian Coombs, unpublished data).

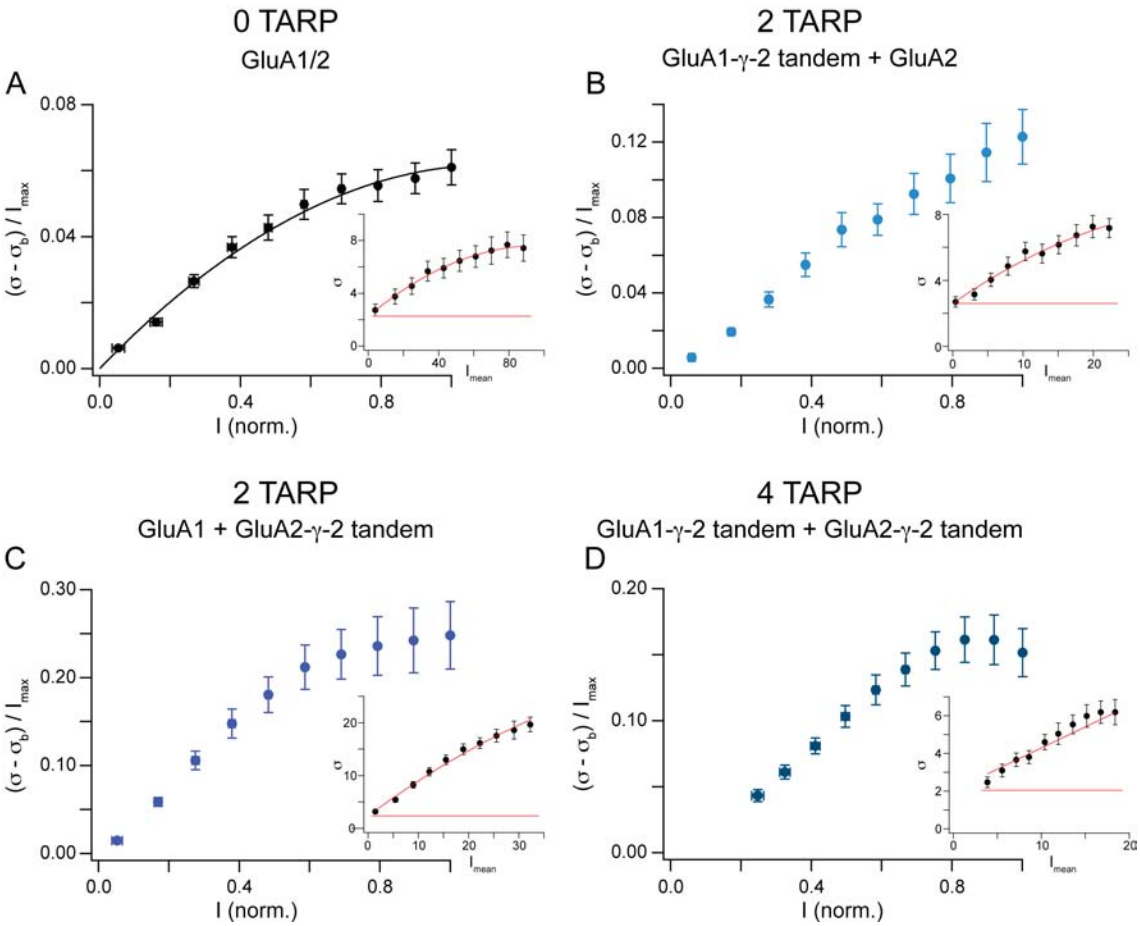

Figure 5.10: At +40 mV, the current variance *vs.* mean current plot for fully TARPed GluA1/2 AMPARs was shifted from the origin. (**A**) Average (*n*=15) normalised current-variance relationship for TARPless GluA1/2. Mean current (x-axis) was normalised to the peak (1st bin). Variance was also normalised to the peak current after subtracting σ_b. Vertical and horizontal error bars on the data points indicate the variance and mean current SEM respectively. The black line shows the parabolic NSFA fit to equation 2.6 on page 61 (weighted by the SEM). The σ_b parameter of the fit was constrained to 0. Inset: NSFA fit to the average current from an example TARPless GluA1/2 patch. Current variance was plotted against mean current. The red horizontal line indicates the σ_b level and the red line through the points shows the parabolic NSFA fit to equation 2.6. (**B-D**) As for A, but for GluA1-γ-2 tandem + GluA2 (2 TARP, *n*= 10), GluA2-γ-2 tandem + GluA1 (2 TARP, *n*= 12) and GluA1-γ-2 tandem + GluA2-γ-2 tandem (4 TARP, *n*= 11) respectively. Fitting to equation 2.6 was not performed for these groups, as explained in the text.

Since the 4 TARP stoichiometry in this data set was achieved by co-expressing the GluA2(R)-γ-2 tandem with the GluA1-γ-2 tandem, it is possible that these patches contained a mixed population of AMPARs: the fully TARPed GluA1/2 heteromers (GluA1-γ-2 tandem + GluA2(R)-γ-2 tandem), as well as a proportion of homomers of the GluA1-γ-2 tandem and of the GluA2(R)-γ-2 tandem. The existence of the two populations of homomers might be suggested by low RI (see Fig. 5.3), as GluA1-γ-2 homomers would be Ca^{2+}-permeable and thus rectifying. It is also suggested by the NSFA characteristics which are similar to those of GluA2(R) + γ-2 homomers.

The NSFA results shown above could thus be explained by the presence of a small population of GluA2(R)-γ-2 tandem homomers. Another possibility, however, is that like the TARPed GluA2(R) homomers, fully TARPed GluA1/2 heteromers also give rise to a population of low and high conductance openings. In order to distinguish between these two hypotheses we designed an additional experiment, using the polyamine channel blocker Philantotoxin-74 (PhTx-74).

PhTx-74 is a use- and voltage-dependent blocker of the AMPAR ion channel pore, which blocks both Ca^{2+}-permeable and Ca^{2+}-impermeable AMPARs, albeit with different affinities (Kromann et al., 2002; Nilsen and England, 2007; Poulsen et al., 2014a). Recent studies showed that although TARPs increase the sensitivity of AMPARs to extracellularly applied polyamines (Jackson et al., 2011), 1 mM PhTx-74 should be sufficient to non-selectively block GluA1 homomers as well as GluA1/2 heteromers in the presence of γ-2, leaving unblocked only γ-2-TARPed GluA2(R) homomers, which are relatively insensitive to this blocker (Poulsen et al., 2014a).

Thus, if the fully TARPed receptors were blocked by 1 mM PhTx-74, this would suggest that few GluA2R-γ-2 homomers formed and thus GluA1/2 heteromers were giving rise to a mix of high and low conductance openings. On the other hand, the presence of a fraction of current insensitive to PhTx-74 would suggest formation of GluA2R-γ-2 tandem homomers.

As shown in Fig. 5.12 panel B, the steady-state current from Ca^{2+}-permeable GluA1-γ-2 tandem receptors evoked by co-application of Glu and CTZ was almost completely blocked by PhTx-74 during the duration of the 100 ms pulse. This pattern of response was observed in all patches for this condition (n= 5).

In contrast, the fully TARPed Ca^{2+}-impermeable GluA1-γ-2 tandem + GluA2-γ-2 tandem receptors displayed a proportion of steady-state current that was insensitive to PhTx-74 (panel D, Fig. 5.12). This response pattern was observed in all patches for this condition (n= 4). The large steady-state current seen in panel D likely indi-

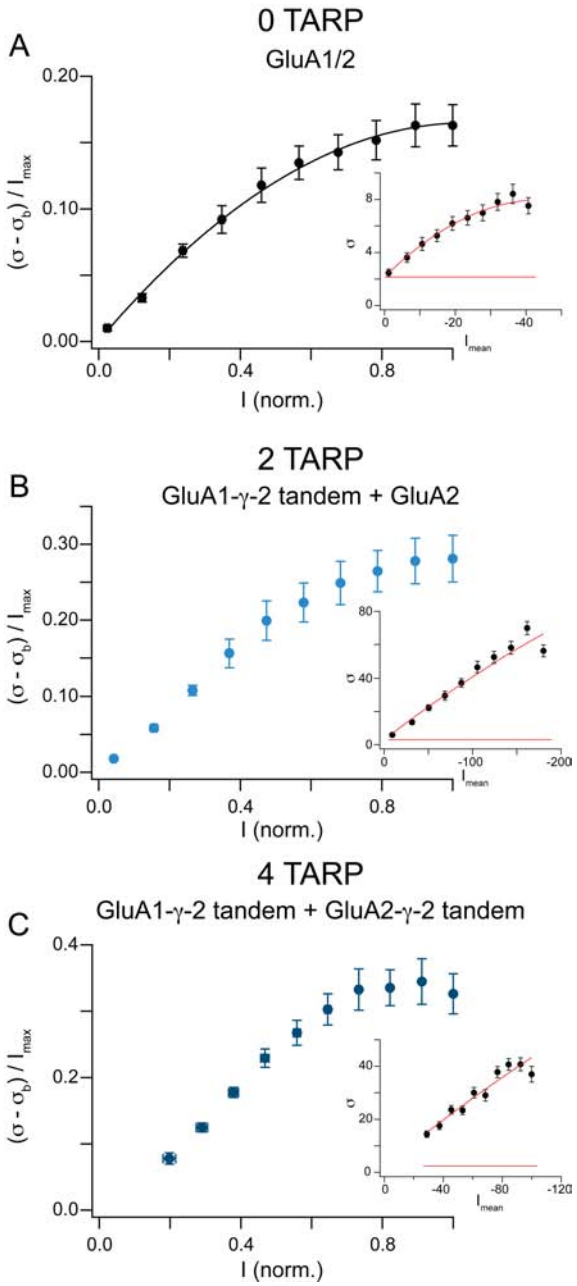

Figure 5.11: At -80mV the average current variance *vs.* mean current plot for fully TARPed GluA1/2 AMPARs showed similar characteristics as at +40 mV. (**A**) Average (n=11) normalised current-variance relationship for TARPless GluA1/2. Mean current (x-axis) was normalised to the peak (1st bin). Variance was also normalised to the peak current after subtracting σ_b. Vertical and horizontal error bars on the data points indicate the variance and mean current SEM respectively. The black line shows the parabolic NSFA fit to equation 2.6 on page 61 (weighted by the SEM). The σ_b parameter of the fit was constrained to 0. Inset: NSFA fit to the average current from an example TARPless GluA1/2 patch. Current variance was plotted against mean current. The red horizontal line indicates the σ_b level and the red line through the points shows the parabolic NSFA fit to equation 2.6. (**B-C**) As for A, but for GluA1-γ-2 tandem + GluA2 (2 TARP, n= 16) and GluA1-γ-2 tandem + GluA2-γ-2 tandem (4 TARP, n= 12) respectively. Fitting to equation 2.6 was not performed for these groups, as described in the text.

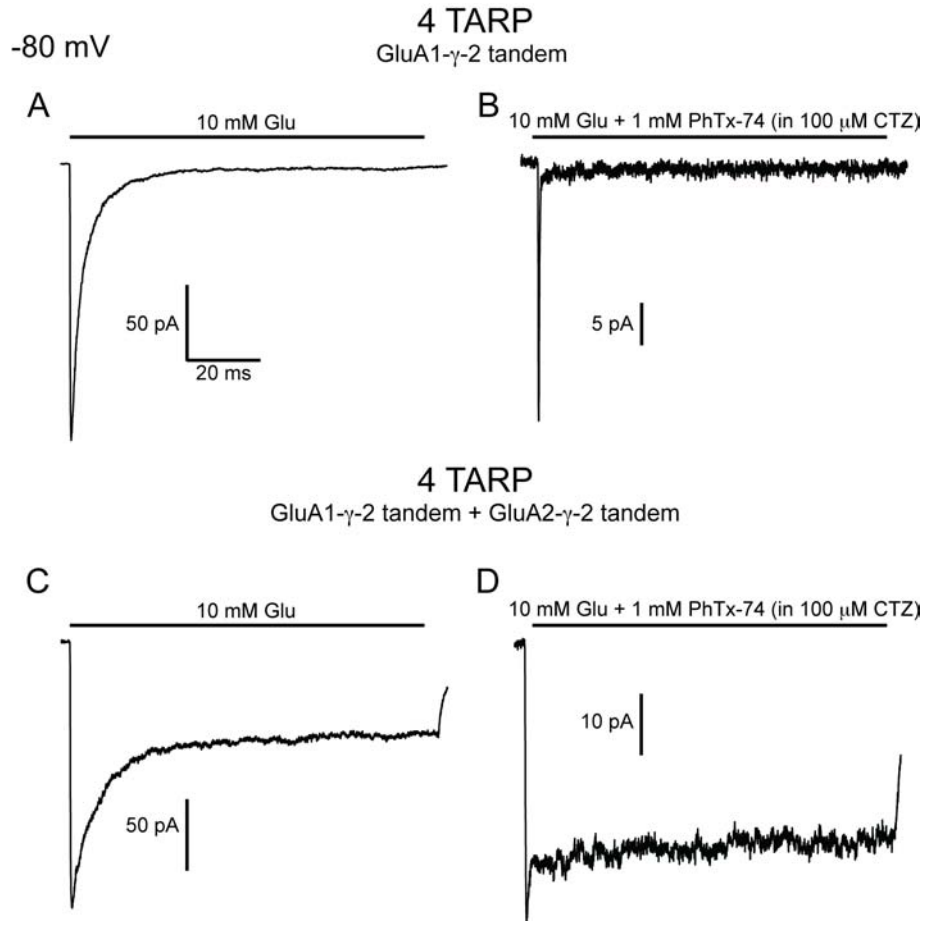

Figure 5.12: Response to 1 mM PhTx-74 did not exclude the possibility that the fully-TARPed GluA1/2 AMPARs do not heteromerize completely, forming a population of GluA2(R)-γ-2 tandem homomers. (**A**) Average response to a 100 ms pulse of 10 mM Glu from a representative patch expressing fully TARPed Ca^{2+}-permeable GluA1-γ-2 receptors. Individual sweeps were aligned at the 20% rise before averaging. The horizontal bar marks the duration of Glu application. (**B**) Average response from the same patch as in panel A. The patch was constantly exposed to 100 μM CTZ and rapidly jumped into 10 mM Glu + 1 mM PhTx-74 (100 ms pulse, duration marked by the horizontal bar). Individual sweeps were aligned at the 20% rise before averaging. (**C**) and (**D**) as for A and B respectively, but for a patch expressing the heteromeric combination of tandems: GluA1-γ-2 and GluA2(R)-γ-2.

cated the presence of GluA2R-γ-2 homomers that are insensitive to PhTx-74. However, the experimental design did not allow us to quantitatively estimate the fraction of GluA2(R)-γ-2 homomers.

The results of the experiment involving PhTx-74 block suggest that the patches co-expressing the GluA1-γ-2 and GluA2-γ-2 tandems contained a mixture of heteromers and GluA2(R)-γ-2 homomers. In addition, it appears that some GluA1-γ-2 homomers also formed, as the RI values (calculated as in Fig. 5.3) for the four patches expressing GluA1-γ-2 tandem + GluA2-γ-2 tandem, for which PhTx-74 block was examined, ranged from 0.68 to 0.82. Therefore, it is possible that GluA1/2 heteromeric AMPARs

fully TARPed with γ-2 have a limited ability to assemble and that a proportion of homomeric receptors forms under these conditions.

5.3.6 AMPARs that contain more than one type of TARP are functional

TARP stoichiometry has mostly been considered in terms of the number of molecules of a single type of TARP per AMPAR. The co-assembly of more than one TARP subtype in an AMPAR complex is a different aspect of TARP stoichiometry. Previous studies suggest that TARPs γ-2 and γ-7 might co-assemble with the same receptor (Kato et al., 2007; Studniarczyk et al., 2013). However this possibility has not been directly investigated and it is not known whether such receptors are functional.

The experiments described below were designed to address this issue, and if these receptors were functional, to investigate their properties. A previous study from our lab showed that unlike AMPARs TARPed with γ-2, those TARPed with γ-7 are CNQX-insensitive (Bats et al., 2012). Thus, we decided to examine CNQX pharmacology of AMPARs TARPed simultaneously with γ-2 and γ-7. We used tandem AMPAR constructs and heteromeric GluA2/3 AMPARs to ensure a fixed stoichiometry of the receptors investigated (see Fig. 5.2). GluA2/3 heteromers as well as TARPs γ-2 and γ-7 are present in the cerebellar stellate cells (Fukaya et al., 2005; Soto et al., 2007; Bats et al., 2012). In addition, a recent study by Studniarczyk et al. (2013) showed that γ-2 and γ-7 co-precipitate from cerebellar lysates. Thus, we decided to focus specifically on the combination of GluA2/3 AMPARs with γ-2 and γ-7. 10 μM CNQX was used as previously published (Bats et al., 2012).

Receptors containing both γ-2 and γ-7 (two possible permutations: GluA2(R)-γ-2 + GluA3-γ-7 and the converse: GluA2(R)-γ-7 + GluA3-γ-2) were compared with GluA2/3 AMPARs that were either TARPless or in which all subunits were TARPed with γ-2 or with γ-7. In each cell, the current evoked by CNQX was quantified as a percentage of Glu-evoked current (see Materials and Methods). Isolated tsA201 cells were clamped at +40 mV to minimise the contribution of GluA3 homomers to the currents recorded. In addition, cells with RI < 0.7 (or those cells for which no RI measure was obtained) were excluded from the analysis. The agonist application method was validated using GluA4 + γ-2, an AMPAR/TARP combination that had previously been reported to respond to CNQX (Bats et al., 2012). We obtained CNQX-evoked currents (data not shown) in 4 out of 4 cells examined (V_h= -40 or -80 mV, in the presence of 100 μM intracellular spermine).

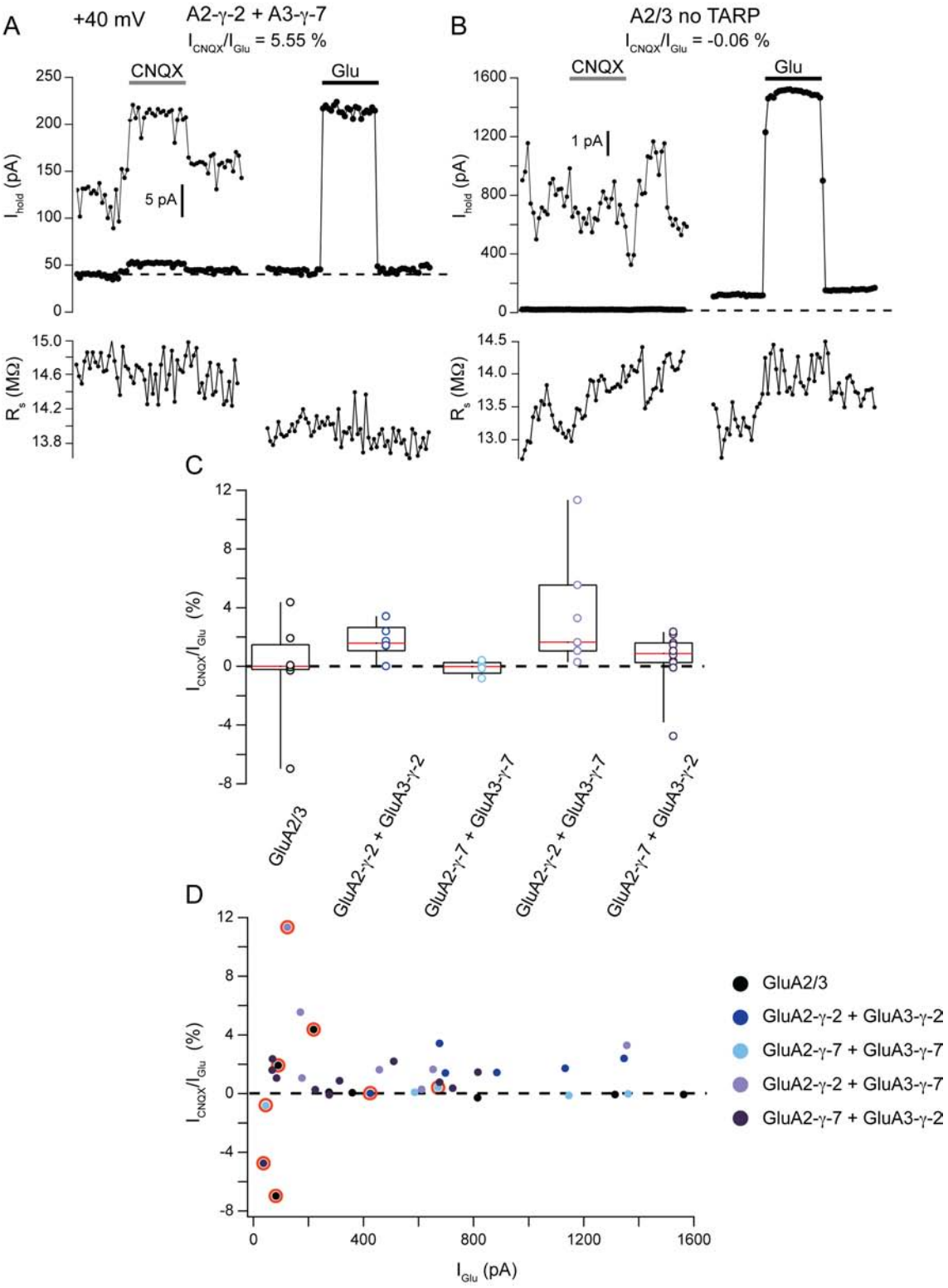

Figure 5.13: CNQX is a partial agonist on AMPARs simultaneously TARPed with both γ-2 and γ-7. (**A**) Top panel: The change in whole-cell holding current (I_{hold}) in response to CNQX (10 μM) and Glu (50 μM) for a representative cell expressing GluA2-γ-2 and GluA3-γ-7. The cell was constantly exposed to 50 μM CTZ. Holding current is plotted (on the y-axis) against sweep number. The dashed line represents the initial I_{hold} level (in control before CNQX application). Each dot represents the I_{hold} measurement for a single sweep. Applications of CNQX and Glu are of equal duration (20 sweeps) and are indicated on top of the graph by a grey and black line respectively.

Figure 5.13 continued: The gap between the CNQX and Glu applications represents the wash-out period (not shown) in which the solutions in both lines of the application tool were exchanged. CNQX/Glu ratio for that cell is shown above the trace. Inset: CNQX application (with control being applied before and after) shown on a smaller current scale (indicated by the scale bar). Each dot represents the I_{hold} measurement for a single sweep. Bottom panel: Series resistance corresponding to the current trace shown in the top panel. Each dot represents the R_s measure for a single sweep. (**B**) As in A, but for a representative cell expressing TARPless GluA2/3. Note that no response to CNQX could be observed. (**C**) Box and whisker plot of the CNQX to Glu response ratios (whole-cell steady-state responses in CTZ; CNQX current is expressed as % Glu current) for GluA2/3 (n= 8), GluA2(R)-γ-2+GluA3-γ-2 (n= 6), GluA2(R)-γ-7+GluA3-γ-7 (n= 5), GluA2(R)-γ-2+GluA3-γ-7 (n= 7) and GluA2(R)-γ-7+GluA3-γ-2 (n= 11). The box shows the 25-75 percentile, while the whiskers are the 10-90 percentile. Individual data points are overlaid on the plot (open circles). The dashed line shows the 0 level. One-way ANOVA showed a significant overall effect of the different TARP combinations on the CNQX to Glu response ratio ($F_{(4,\ 14.64)}$ = 4.08 , P= 0.0202). (**D**) Plot of CNQX/Glu ratio against the Glu current amplitude for all the cells. Outliers are circled in red (the outlier point is that located in the center of the red circle). Outliers were calculated as points outside 1.5 $\times$ IQR (inter-quantile range). Note that most of the outliers occur at low I_{Glu} amplitudes (< 400 pA). This suggests that in some cells with relatively small currents, noise produced by baseline fluctuations could affect the CNQX/Glu ratio measurement.

Furthermore, as expected no CNQX current was observed in cells transfected with TARPless GluA2/3 (I_{CNQX}/I_{Glu} = -0.116 $\pm$ 1.130 %). Similarly, receptors fully TARPed with γ-7 showed no response to CNQX (-0.088 $\pm$ 0.203 %), supporting the view that AMPAR TARPed with γ-7 are CNQX-insensitive (Bats et al., 2012). However, as the earlier study used native AMPARs (in cerebellar stellate cells) and recombinant AMPARs co-expressed with γ-7, it was unclear whether the lack of CNQX sensitivity was a property of γ-7 or whether it resulted, for example, from γ-7 stoichiometry being different from that of γ-2. AMPARs investigated in the experiments shown above were fully TARPed (4 TARP molecules per AMPAR), which suggest that, even at 4 TARP stoichiometry, γ-7 conveys a lack of CNQX sensitivity on AMPARs.

By contrast, AMPARs fully TARPed with γ-2 responded to CNQX (1.736 $\pm$ 0.463 %), as did those TARPed with two γ-2 molecules and two γ-7 molecules (GluA2-γ-2 + GluA3-γ-7: 3.542 $\pm$ 1.454 % ; GluA2-γ-7 + GluA3-γ-2: 0.558 $\pm$ 0.579 %). However, the large degree of scatter seen in the data set and the fact that multiple statistical tests were performed simultaneously (with appropriate P-value corrections) resulted in no significant differences between the individual groups, despite an overall significant effect of the different TARP variants on CNQX/Glu ratio. The statistical tests performed to test between the individual groups are listed in Table 5.1.

Test No.	Test pair	*P*-value
1	GluA2/3 *vs.* GluA2-γ-2 + GluA3-γ-2	0.81
2	GluA2/3 *vs.* GluA2-γ-7 + GluA3-γ-7	1.00
3	GluA2/3 *vs.* GluA2-γ-2 + GluA3-γ-7	0.57
4	GluA2/3 *vs.* GluA2-γ-7 + GluA3-γ-2	1.00
5	GluA2-γ-2 + GluA3-γ-2 *vs.* GluA2-γ-7 + GluA3-γ-7	0.091
6	GluA2-γ-2 + GluA3-γ-2 *vs.* GluA2-γ-2 + GluA3-γ-7	1.00
7	GluA2-γ-2 + GluA3-γ-2 *vs.* GluA2-γ-7 + GluA3-γ-2	0.80
8	GluA2-γ-7 + GluA3-γ-7 *vs.* GluA2-γ-2 + GluA3-γ-7	0.42
9	GluA2-γ-7 + GluA3-γ-7 *vs.* GluA2-γ-7 + GluA3-γ-2	1.00
10	GluA2-γ-2 + GluA3-γ-7 *vs.* GluA2-γ-7 + GluA3-γ-2	0.65

Table 5.1: Individual TARP combinations did not differ in CNQX/Glu ratio.

A notable observation from the experiments described above is that the CNQX-evoked currents generally represented only a small fraction of the Glu-evoked currents. Several factors could contribute to the relatively low CNQX/Glu ratios observed in this study. Sensitivity to CNQX of AMPAR subunits TARPed with γ-2 appears to vary (Bats et al., 2012), with GluA3 and GluA1 showing smaller CNQX/Glu ratios than GluA4. No data on GluA2(R) seemed to be available in literature, presumably due to poor expression of these receptors (Greger et al., 2002, 2003). From the experiments described above it, appeared that GluA2/3 heteromers show relatively small responses to CNQX, in line with the previous study by Bats et al. (2012) suggesting that GluA3-containing AMPARs have limited CNQX sensitivity when TARPed with γ-2.

Previous studies reporting CNQX-evoked currents used negative holding potentials and large driving forces (-70 mV, Menuz et al. 2007 and -80 mV, Bats et al. 2012), while here the cells were held at +40 mV. Thus it is possible that in some cells, we failed to detect CNQX-evoked current due to the small driving force resulting in a low current amplitude. Indeed, in the data set shown here CNQX-evoked currents rarely exceeded 20 pA in amplitude and were only a small fraction of Glu-evoked currents. As shown in Fig. 5.13 panel D, most of the outliers were cells in which the Glu current amplitude was small. It is thus possible, that in some cells agonist-unrelated fluctuations in I_{hold} affected the measurement of CNQX-evoked current. On the other hand, in cells expressing CNQX-insensitive AMPARs, baseline fluctuations during CNQX application would have a larger effect on the CNQX/Glu ratio measurement when the Glu current was small, resulting in data points often falling further away from the zero line than for larger Glu currents. Thus, it would be of interest to perform similar experiments in a high-expression system, such as *Xenopus laevis* oocytes, which could provide means to more accurately quantify the dependence of CNQX-evoked current on TARP stoichiometry.

5.4 Discussion

TARP stoichiometry is an aspect of TARP function which to date has been given relatively little attention. Previous studies suggest that several properties of AMPARs vary with TARP stoichiometry. Kainate efficacy (relative to glutamate) has been shown to increase proportionally to the stoichiometry of TARPs γ-2 and γ-8 (Shi et al., 2009). A study by Milstein et al. (2007) suggested that in comparison with wt, granule cells from *stg* heterozygous mice showed a speeding of mEPSC decay time and a reduction in kainate potency. It is controversial whether γ-2 stoichiometry is reduced in *stg* heterozygotes, since the ratio of kainate to AMPA responses in these cells has been reported not to differ from that seen in wt granule cells (Kim et al., 2010). However, overexpression of γ-2 in cerebellar granule cells from *stg* mice produced an increase in mEPSC decay time and kainate potency relative to wild-type (Milstein et al., 2007), so that when more TARP became available an increase in mEPSC decay time was observed. This may suggest that the stoichiometry of γ-2 is normally not saturated in cerebellar granule cells, allowing γ-2 overexpression in wt cells to affect mEPSC properties. In our study, both deactivation and desensitization of AMPARs appeared to depend on γ-2 stoichiometry. Since deactivation and desensitization are thought to contribute to mEPSC decay, our findings support those previously presented in literature, which suggested that gating of AMPARs is influenced by TARP stoichiometry.

Our findings suggest that some AMPAR parameters may depend both on TARP stoichiometry and on the holding potential. The inclusion of both 2 and 4 γ-2 molecules prolonged AMPAR desensitization when the currents were examined at -80 mV. However, at +40 mV, fully TARPed, but not partially TARPed receptors showed a slowing of desensitization compared with TARPless GluA1/2 AMPARs. This suggests that partially TARPed AMPARs may prolong desensitization when the cell membrane potential is negative, but not when it is depolarised. Thus, charge transfer through these receptors may be limited at depolarised membrane voltages, which could affect synaptic transmission. It is worth noting, however, that fully TARPed AMPARs showed a slowing of desensitization regardless of whether V_m was positive or negative. This may imply that some effects of TARP stoichiometry in native receptors could be influenced by neuronal activity.

In summary, our findings suggest that a number of AMPAR functional properties are modified by γ-2 stoichiometry. This could reflect an additive effect of the consecutive γ-2 molecules assembled, or could result from the occupation of two types of non-equivalent TARP binding sites (Schwenk et al., 2012), as shown schematically in Fig. 5.14. These two types of binding sites could result from the AMPAR symmetry at the

LBD level observed in the GluA2 crystal structure (Sobolevsky et al., 2009). Irrespective of the molecular mechanism, however, it appears that TARP stoichiometry may provide a mean for modulating native AMPAR responses. Thus, neurons may have, as of yet unknown, mechanisms for controlling TARP stoichiometry.

The ratio of responses to KA and Glu has been previously reported to be a sensitive measure of TARP stoichiometry (Shi et al., 2009; Gill et al., 2011). Together with biochemical assays, the amplitude of kainate-evoked current was used in a study by Kim et al. (2010) to suggest that in a recombinant system the stoichiometry of γ-2 increases when more TARP becomes available. Thus, it appears that in recombinant system the amount of available TARP controls stoichiometry. By contrast, the control of TARP stoichiometry in neurons appears to be more complex. Previous reports suggest that the stoichiometry of TARP γ-8 varies between hippocampal cell types (Shi et al., 2009) and that cerebellar Purkinje cells contain two molecules of TARP γ-7 per AMPAR (Gill et al., 2011). This could suggest, that in neurons, one or more mechanisms for controlling TARP stoichiometry applies. TARP stoichiometry on native AMPARs could potentially be controlled by simultaneous co-assembly of TARPs and other auxiliary subunits with the same AMPAR (Kato et al., 2010a; Gill et al., 2011), however the detailed mechanism appears unclear (Herring et al., 2013).

An interesting finding has arisen from our experiments on PhTx-74 block of fully TARPed GluA1/2 heteromers. The incomplete block of these receptors by PhTx-74 suggest that their ability to assemble may be limited, possibly resulting in simultaneous formation of heteromers as well as GluA1 and GluA2(R) homomers. This limited assembly could result from the use of tandem constructs, but could also suggest a correlation between TARP stoichiometry and AMPAR assembly, i.e. that fully TARPed AMPARs form homomers more readily than partially TARPed ones. Thus it is possible that AMPAR composition may depend on TARP stoichiometry. However, a number of additional experiments would be necessary to gain further insight into the effect of TARP stoichiometry on AMPAR assembly.

Native gel western blotting coupled with tagging of one of the tandem constructs used here could allow separation of the putative receptor populations by molecular weight. Thus, it could be possible to investigate whether three separate populations of receptors indeed form upon co-transfection of the GluA1-γ-2 tandem with the GluA2(R)-γ-2 tandem and, if so, what the relative contribution of each of these AMPAR populations is. These additional biochemical experiments would also help to clarify our findings and differentiate clearly between those effects observed in these study that were produced by altering TARP stoichiometry and those that could have arisen from contamination of the fully-TARPed receptor population by GluA1-γ-2 homomers and GluA2(R)-γ-2 homomers.

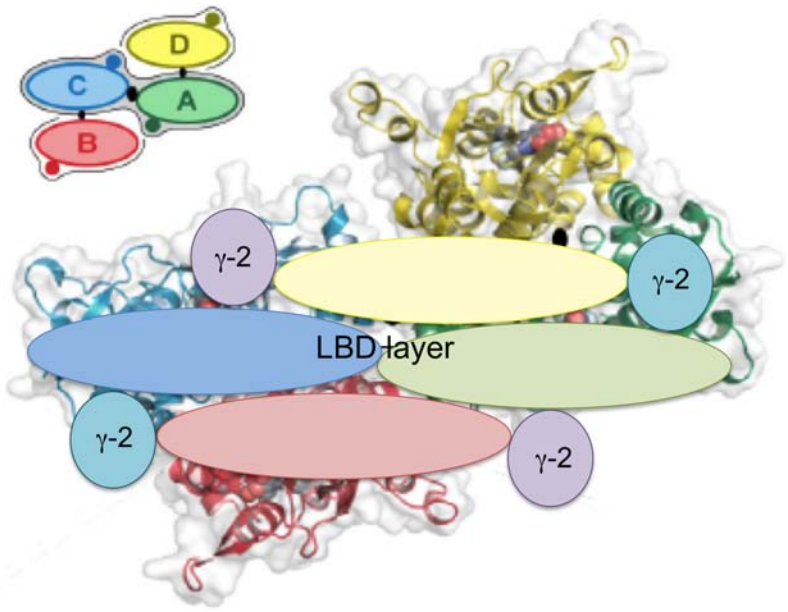

Figure 5.14: Schematic representation of the four γ-2 binding sites at the level of AMPAR LBD layer. The schematic representation of the AMPAR tetramer co-assembled with four TARPs is overlaid on the cross-section of AMPAR taken at the LBD level (adapted from Sobolevsky et al. 2009). Note that, as suggested by Schwenk et al. (2012), given the LBD symmetry the γ-2 binding sites could form two equivalent pairs (marked purple and blue), rather than all being equivalent.

In addition to investigating the effect of γ-2 stoichiometry on AMPAR properties, we also used tandem constructs to co-express TARPs γ-2 and γ-7 in the same AMPAR complex. AMPARs TARPed with two different TARPs simultaneously formed functional channels, a finding which has no been reported previously. Furthermore, CNQX currents were detected in cells transfected with GluA2/3 AMPARs co-assembled with γ-2 or both γ-7 and γ-2, suggesting that two molecules of γ-2 per AMPAR are sufficient to convey CNQX sensitivity on AMPARs, even when the other two TARP binding sites are occupied by a CNQX-insensitive TARP. Thus it is possible that in the cerebellum, TARPs γ-2 and γ-7 co-assemble with the same AMPARs to modify their properties, in line with the previous report of the two TARPs co-precipitating from cerebellar lysates (Studniarczyk et al., 2013). In addition, we have confirmed previous results from our lab showing that AMPAR association with TARP γ-7 fails to convert CNQX from an antagonist to a partial antagonist (Bats et al., 2012), and, by fixing the stoichiometry of γ-7, we showed that the lack of CNQX sensitivity conveyed upon AMPARs is a property of γ-7 that is independent of stoichiometry.

The experiments described in this Chapter suggest that both the number of TARP molecules associated with an AMPAR and simultaneous co-assembly of more than one TARP subtype could shape AMPAR properties. However, TARPs are not the only auxiliary AMPAR subunits known. In addition to the relatively well-studied CNIH proteins (Schwenk et al., 2009; Kato et al., 2010a; Gill et al., 2011; Coombs et al., 2012; Herring et al., 2013), a number of other AMPAR auxiliary subunits have been identified (von Engelhardt et al., 2010; Schwenk et al., 2012). Even for the best studied of these, there is limited data available on the location of their binding site on the AMPAR tetramer, or the co-assembly in the same complexes as TARP family members. Thus, a complex network of AMPAR interacting partners emerges, with AMPAR synaptic responses likely to be shaped by all the associated auxiliary proteins in ways which are still poorly understood. However, as most native AMPARs are though to co-assemble with TARPs, the number and nature of TARP molecules associated with the AMPAR complex remains an important factor determining the properties of native AMPAR responses.

6

General Discussion

The experiments described in this Thesis aimed to provide insight into the molecular mechanisms underlying AMPAR interaction with their auxiliary subunits, TARPs. We focused mostly on the prototypical TARP γ-2. In the first two Experimental Chapters we investigated regions of interaction within the extracellular domains of γ-2 and the AMPAR, that had been identified by our collaborators using peptide arrays.

In Experimental Chapter 1 (Chapter 3) we focused specifically on the first extracellular loop of γ-2 (Ex1), which has previously been reported to contribute to TARP interaction with the AMPAR (Tomita et al., 2005; Cho et al., 2007; Milstein et al., 2007; Milstein and Nicoll, 2009). We compared the ability of wt γ-2 and several γ-2 mutants to modulate functional properties of GluA1 and GluA2Q AMPARs. All of the mutants contained either Ala substitutions or deletions of 3-4 amino acids, which resulted in disruption of specific regions of interaction between Ex1 of γ-2 and the AMPAR. The mutants showed an impaired ability to modulate AMPAR function, when compared to wt γ-2. However, they differed in their specific effects on the various AMPAR properties and often behaved differently depending on whether they were co-expressed with GluA1 or with GluA2Q. Thus, the data presented in Experimental Chapter 1 suggested that different regions of Ex1 modulate distinct AMPAR properties and, furthermore, that this interaction may be AMPAR subunit-specific. It is, however, worth noting that all of the Ex1 mutants still acted as TARPs, affecting numerous AMPAR properties, some to the same extent as wt γ-2. This further supports the view that Ex1 is not the only domain that binds to the AMPAR (Tomita et al., 2005), and highlights the importance of other domains of γ-2 for AMPAR/TARP interaction.

The $WRT_{64\text{-}66}$ mutation had the most profound and most consistent effect on the ability of γ-2 to modulate AMPARs. This mutation affected the tip region of Ex1, close to the two cysteines, which are though to participate in maintenance of Ex1 struc-

ture. Furthermore, the $HFPE_{82\text{-}85}$ deletion showed multiple effects on the properties of AMPARs examined, despite this region being present in array peptides that were both positive and negative for AMPAR binding, suggesting that the effects of this mutation may be produced by the shortened length of Ex1. Thus, it appears that a specific conformation of Ex1 is important for the modulation of AMPAR properties by γ-2, suggesting a specific arrangement of Ex1 in AMPAR/TARP complexes. Based on our structural and functional data, we hypothesise that in an AMPAR/TARP complex the Ex1 of γ-2 is located between the NTD and the LBD of the AMPAR and interacts with both domains to bring them closer together. However, since our structural data come from peptide arrays which use linear peptides rather than whole proteins with a defined structure, it remains unclear which interactions occur when the complete TARP and AMPAR assemble together. Some interaction regions identified by the peptide array may not be available for AMPAR binding in native receptors. Thus, further structural data would be required to reveal the detailed molecular arrangement of the AMPAR/TARP complex.

Supported by structural and functional data, our hypothesis concerning the position of Ex1 between the NTD and the LBD within the AMPAR/TARP complex suggests a multifaceted interaction of Ex1 with these two distinct domains of the AMPAR. In contrast with the LBD, the role of the AMPAR NTD has been given relatively little attention to date. Although previous studies have shown that AMPARs can still function in the absence of their NTD (Pasternack et al., 2002) and that AMPAR modulation by γ-2 is retained in these receptors (Bedoukian et al., 2006), we were interested if the NTD contributes *functionally* to the modulation of AMPAR properties by γ-2.

The data presented in Experimental Chapter 2 (Chapter 4) suggest that the NTD of GluA2 has a number of modulatory roles in receptor function. The absence of the NTD resulted in prolonged deactivation and desensitization of both TARPless and TARPed GluA2, suggesting an 'inhibitory' effect of this domain on GluA2 gating. By contrast, mean single-channel conductance was reduced when the NTD was lacking, which suggests that the NTD may stabilise higher conductance states of the AMPAR, an effect which could arise for instance from the NTD stabilising ligand binding. However, our data suggest that NTD deletion does not affect the function of the associated TARP. This suggests, that the interactions between the NTD and the TARP identified using peptide arrays have little influence on TARP-mediated modulation of AMPAR function. However, these interactions may play a more structural role, given that the proposed arrangement of the TARP between the NTD and the LBD would require substantial repositioning of the NTD. This structural role may be especially important in native systems, where the NTD of AMPARs have been shown to interact with a variety of synaptic partners (O'Brien et al., 1999; Saglietti et al., 2007; Sia et al.,

2007). It is currently unclear if Ex1 of TARPs might also interact with synaptic partners present in the cleft. Since a role for TARPs in dendritic growth has been reported (Hamad et al., 2014), it would be interesting to investigate whether, together with the AMPAR NTD, the Ex1 of TARPs may contribute to interactions with extracellular synaptic structures.

In Experimental Chapter 3 (Chapter 5) of this Thesis, we described experiments that were designed to add a broader context to the detailed molecular study described in the first two Experimental Chapters. We investigated the properties of AMPAR/TARP complexes as a whole, in particular with relation to TARP stoichiometry. By employing AMPAR-TARP tandem constructs, covalently linking the two proteins, we were able to express AMPAR/TARP complexes with a defined γ-2 stoichiometry of 0, 2 or 4 TARP molecules. We found that a number of functional AMPAR properties, such as gating kinetics and the fraction of the steady-state current, vary with γ-2 stoichiometry. This agrees with previous studies that have suggested that TARP stoichiometry affects AMPAR function (Shi et al., 2009; Gill et al., 2011). Indeed, the stoichiometry of native AMPARs has been proposed to vary (Shi et al., 2009) and this variability may contribute to the diversity of AMPAR-mediated synaptic transmission. Furthermore, we found that at negative membrane potentials, GluA1/2 AMPARs showed prolonged desensitization time constant when the receptors contained only two molecules of γ-2. Thus, these 'partially TARPed' receptors could be important for shaping high-frequency responses at synapses where desensitization contributes to EPSC decay.

We have also considered the possibility that two distinct TARP subtypes may co-assemble within the same AMPAR complex. TARPs γ-2 and γ-7 have been shown to co-precipitate from cerebellar lysates (Studniarczyk et al., 2013). However, it was unclear whether this reflected co-assembly of the two different TARPs with the same AMPAR, or the presence of distinct AMPARs linked together via synaptic scaffolding proteins. We thus used tandem AMPAR/TARP complexes to express receptors TARPed simultaneously with γ-2 and γ-7 to decide if these were functional.

Furthermore, we investigated the ability of CNQX to activate these AMPARs, since TARPs γ-2 and γ-7 differ in their ability to convert CNQX into a partial agonist (Bats et al., 2012). AMPARs containing both γ-2 and γ-7 were found to respond to CNQX, suggesting that, in this respect, γ-2 dominates over γ-7. Thus, our results suggest that when type I and type II TARPs co-assemble within the same AMPAR complex, they produce functional receptors.

Given that the molecular weight of a native AMPAR complex as seen on BN PAGE is

more than 669 kDa (Vandenberghe et al., 2005b), which largely exceeds the molecular weight that can be deduced for an AMPAR tetramer (a subunit is $\sim$100 kDa in molecular weight, as reported by Rogers et al., 1991), it is possible that a number of auxiliary AMPAR subunits, including TARPs, may be associated in a single complex with native receptors. In light of the recent discoveries identifying a number of other AMPAR auxiliary subunits (Schwenk et al., 2009; von Engelhardt et al., 2010; Shanks et al., 2012; Schwenk et al., 2012), it appears that the co-assembly of two different TARPs within the same complex, as well as the co-assembly of TARPs with other auxiliary subunits proposed by Schwenk et al. (2012) could potentially increase the diversity of AMPARs involved in fast excitatory transmission in the CNS. Indeed, as suggested by Schwenk et al. (2012), AMPARs may form multimeric complexes with an apparent molecular mass of 0.6-1 MDa, where the tetrameric receptor forms the core of the complex with various auxiliary subunits in the periphery.

References

Abouda, H., Hizem, Y., Gargouri, A., Depienne, C., Bouteiller, D., Riant, F., Tournier-Lasserve, E., Gourfinkel-An, I., LeGuern, E. and Gouider, R. (2010). Familial form of typical childhood absence epilepsy in a consanguineous context. Epilepsia *51*, 1889–93.

Ahmed, A. H. and Oswald, R. E. (2010). Piracetam defines a new binding site for allosteric modulators of α-amino-3-hydroxy-5-methyl-4-isoxazole-propionic acid (AMPA) receptors. J Med Chem *53*, 2197–203.

Aricescu, A. R., Lu, W. and Jones, E. Y. (2006). A time- and cost-efficient system for high-level protein production in mammalian cells. Acta Crystallogr D Biol Crystallogr *62*, 1243–50.

Armstrong, N. and Gouaux, E. (2000). Mechanisms for activation and antagonism of an AMPA-sensitive glutamate receptor: crystal structures of the GluR2 ligand binding core. Neuron *28*, 165–81.

Armstrong, N., Mayer, M. and Gouaux, E. (2003). Tuning activation of the AMPA-sensitive GluR2 ion channel by genetic adjustment of agonist-induced conformational changes. Proc Natl Acad Sci USA *100*, 5736–41.

Armstrong, N., Sun, Y., Chen, G. Q. and Gouaux, E. (1998). Structure of a glutamate-receptor ligand-binding core in complex with kainate. Nature *395*, 913–7.

Ascher, P. and Nowak, L. (1988). The role of divalent cations in the N-methyl-D-aspartate responses of mouse central neurones in culture. J Physiol (Lond) *399*, 247–66.

Ayalon, G. and Stern-Bach, Y. (2001). Functional assembly of AMPA and kainate receptors is mediated by several discrete protein-protein interactions. Neuron *31*, 103–13.

Balannik, V., Menniti, F. S., Paternain, A. V., Lerma, J. and Stern-Bach, Y. (2005). Molecular mechanism of AMPA receptor noncompetitive antagonism. Neuron *48*, 279–88.

Banke, T. G., Bowie, D., Lee, H., Huganir, R. L., Schousboe, A. and Traynelis, S. F. (2000). Control of GluR1 AMPA receptor function by cAMP-dependent protein kinase. J Neurosci *20*, 89–102.

Barrionuevo, G., Schottler, F. and Lynch, G. (1980). The effects of repetitive low frequency stimulation on control and "potentiated" synaptic responses in the hippocampus. Life Sci *27*, 2385–91.

Barry, M. F. and Ziff, E. B. (2002). Receptor trafficking and the plasticity of excitatory synapses. Current Opinion in Neurobiology *12*, 279–86.

Bats, C., Groc, L. and Choquet, D. (2007). The interaction between Stargazin and PSD-95 regulates AMPA receptor surface trafficking. Neuron *53*, 719–34.

Bats, C., Soto, D., Studniarczyk, D., Farrant, M. and Cull-Candy, S. G. (2012). Channel properties reveal differential expression of TARPed and TARPless AMPARs in stargazer neurons. Nat Neurosci *15*, 853–61.

Bedoukian, M. A., Weeks, A. M. and Partin, K. M. (2006). Different domains of the AMPA receptor direct stargazin-mediated trafficking and stargazin-mediated modulation of kinetics. J Biol Chem *281*, 23908–21.

Beneyto, M. and Meador-Woodruff, J. H. (2006). Lamina-specific abnormalities of AMPA receptor trafficking and signaling molecule transcripts in the prefrontal cortex in schizophrenia. Synapse *60*, 585–98.

Bettler, B., Boulter, J., Hermans-Borgmeyer, I., O'Shea-Greenfield, A., Deneris, E. S., Moll, C., Borgmeyer, U., Hollmann, M. and Heinemann, S. (1990). Cloning of a novel glutamate receptor subunit, GluR5: expression in the nervous system during development. Neuron *5*, 583–95.

Bettler, B., Egebjerg, J., Sharma, G., Pecht, G., Hermans-Borgmeyer, I., Moll, C., Stevens, C. F. and Heinemann, S. (1992). Cloning of a putative glutamate receptor: a low affinity kainate-binding subunit. Neuron *8*, 257–65.

Bliss, T. V. and Collingridge, G. L. (1993). A synaptic model of memory: long-term potentiation in the hippocampus. Nature *361*, 31–9.

Bliss, T. V. and Gardner-Medwin, A. R. (1973). Long-lasting potentiation of synaptic transmission in the dentate area of the unanaestetized rabbit following stimulation of the perforant path. J Physiol (Lond) *232*, 357–74.

Bliss, T. V. and Lomo, T. (1973). Long-lasting potentiation of synaptic transmission in the dentate area of the anaesthetized rabbit following stimulation of the perforant path. J Physiol (Lond) *232*, 331–56.

Boehm, J., Kang, M.-G., Johnson, R. C., Esteban, J., Huganir, R. L. and Malinow,

R. (2006). Synaptic incorporation of AMPA receptors during LTP is controlled by a PKC phosphorylation site on GluR1. Neuron *51*, 213–25.

Boudkkazi, S., Brechet, A., Schwenk, J. and Fakler, B. (2014). Cornichon2 dictates the time course of excitatory transmission at individual hippocampal synapses. Neuron *82*, 848–58.

Boulter, J., Hollmann, M., O'Shea-Greenfield, A., Hartley, M., Deneris, E., Maron, C. and Heinemann, S. (1990). Molecular cloning and functional expression of glutamate receptor subunit genes. Science *249*, 1033–7.

Bowie, D., Lange, G. D. and Mayer, M. L. (1998). Activity-dependent modulation of glutamate receptors by polyamines. J Neurosci *18*, 8175–85.

Bowie, D. and Mayer, M. L. (1995). Inward rectification of both AMPA and kainate subtype glutamate receptors generated by polyamine-mediated ion channel block. Neuron *15*, 453–62.

Brickley, S. G., Farrant, M., Swanson, G. T. and Cull-Candy, S. G. (2001). CNQX increases GABA-mediated synaptic transmission in the cerebellum by an AMPA/kainate receptor-independent mechanism. Neuropharmacology *41*, 730–6.

Brusa, R., Zimmermann, F., Koh, D. S., Feldmeyer, D., Gass, P., Seeburg, P. H. and Sprengel, R. (1995). Early-onset epilepsy and postnatal lethality associated with an editing-deficient GluR-B allele in mice. Science *270*, 1677–80.

Burnashev, N., Monyer, H., Seeburg, P. H. and Sakmann, B. (1992a). Divalent ion permeability of AMPA receptor channels is dominated by the edited form of a single subunit. Neuron *8*, 189–98.

Burnashev, N., Schoepfer, R., Monyer, H., Ruppersberg, J. P., Günther, W., Seeburg, P. H. and Sakmann, B. (1992b). Control by asparagine residues of calcium permeability and magnesium blockade in the NMDA receptor. Science *257*, 1415–9.

Cais, O., Herguedas, B., Krol, K., Cull-Candy, S. G., Farrant, M. and Greger, I. H. (2014). Mapping the interaction sites between AMPA receptors and TARPs reveals a role for the receptor N-terminal domain in channel gating. Cell Rep *9*, 728–40.

Carbone, A. L. and Plested, A. J. R. (2012). Coupled control of desensitization and gating by the ligand binding domain of glutamate receptors. Neuron *74*, 845–57.

Chen, G. Q., Cui, C., Mayer, M. L. and Gouaux, E. (1999). Functional characterization of a potassium-selective prokaryotic glutamate receptor. Nature *402*, 817–21.

Chen, L., Chetkovich, D. M., Petralia, R. S., Sweeney, N. T., Kawasaki, Y., Wenthold, R. J., Bredt, D. S. and Nicoll, R. A. (2000). Stargazin regulates synaptic targeting of AMPA receptors by two distinct mechanisms. Nature *408*, 936–43.

Chen, L., El-Husseini, A., Tomita, S., Bredt, D. S. and Nicoll, R. A. (2003). Stargazin differentially controls the trafficking of α-amino-3-hydroxyl-5-methyl-4-isoxazolepropionate and kainate receptors. Mol Pharmacol *64*, 703–6.

Chen, R.-S., Deng, T.-C., Garcia, T., Sellers, Z. M. and Best, P. M. (2007). Calcium channel Îş subunits: a functionally diverse protein family. Cell Biochem Biophys *47*, 178–186.

Chetkovich, D. M., Chen, L., Stocker, T. J., Nicoll, R. A. and Bredt, D. S. (2002). Phosphorylation of the postsynaptic density-95 (PSD-95)/discs large/zona occludens-1 binding site of stargazin regulates binding to PSD-95 and synaptic targeting of AMPA receptors. J Neurosci *22*, 5791–6.

Cho, C.-H., St-Gelais, F., Zhang, W., Tomita, S. and Howe, J. R. (2007). Two families of TARP isoforms that have distinct effects on the kinetic properties of AMPA receptors and synaptic currents. Neuron *55*, 890–904.

Choi, J., Ko, J., Park, E., Lee, J.-R., Yoon, J., Lim, S. and Kim, E. (2002). Phosphorylation of stargazin by protein kinase A regulates its interaction with PSD-95. J Biol Chem *277*, 12359–63.

Chu, P. J., Robertson, H. M. and Best, P. M. (2001). Calcium channel γ subunits provide insights into the evolution of this gene family. Gene *280*, 37–48.

Clayton, A., Siebold, C., Gilbert, R. J. C., Sutton, G. C., Harlos, K., McIlhinney, R. A. J., Jones, E. Y. and Aricescu, A. R. (2009). Crystal structure of the GluR2 amino-terminal domain provides insights into the architecture and assembly of ionotropic glutamate receptors. J Mol Biol *392*, 1125–32.

Cokić, B. and Stein, V. (2008). Stargazin modulates AMPA receptor antagonism. Neuropharmacology *54*, 1062–70.

Coleman, S. K., Moykkynen, T., Cai, C., Ossowski, L. V., Kuismanen, E., Korpi, E. R. and Keinanen, K. (2006). Isoform-Specific Early Trafficking of AMPA Receptor Flip and Flop Variants. J Neurosci *26*, 11220–11229.

Coleman, S. K., Möykkynen, T., Hinkkuri, S., Vaahtera, L., Korpi, E. R., Pentikäinen, O. T. and Keinänen, K. (2010). Ligand-binding domain determines endoplasmic reticulum exit of AMPA receptors. Journal of Biological Chemistry *285*, 36032–9.

Collingridge, G. L., Herron, C. E. and Lester, R. A. (1988). Synaptic activation of N-methyl-D-aspartate receptors in the Schaffer collateral-commissural pathway of rat hippocampus. The Journal of Physiology *399*, 283–300.

Collingridge, G. L., Kehl, S. J. and McLennan, H. (1983). Excitatory amino acids in synaptic transmission in the Schaffer collateral-commissural pathway of the rat hippocampus. J Physiol (Lond) *334*, 33–46.

Collingridge, G. L., Olsen, R. W., Peters, J. and Spedding, M. (2009). A nomenclature for ligand-gated ion channels. Neuropharmacology *56*, 2–5.

Conti, F., Neumcke, B., Nonner, W. and Stämpfli, R. (1980). Conductance fluctuations from the inactivation process of sodium channels in myelinated nerve fibres. The Journal of Physiology *308*, 217–39.

Coombs, I. D., Soto, D., Zonouzi, M., Renzi, M., Shelley, C., Farrant, M. and Cull-Candy, S. G. (2012). Cornichons modify channel properties of recombinant and glial AMPA receptors. J Neurosci *32*, 9796–804.

Cull-Candy, S. G. and Leszkiewicz, D. N. (2004). Role of distinct NMDA receptor subtypes at central synapses. Sci STKE *2004*, re16.

Cull-Candy, S. G. and Usowicz, M. M. (1987). Multiple-conductance channels activated by excitatory amino acids in cerebellar neurons. Nature *325*, 525–8.

Das, S., Sasaki, Y. F., Rothe, T., Premkumar, L. S., Takasu, M., Crandall, J. E., Dikkes, P., Conner, D. A., Rayudu, P. V., Cheung, W., Chen, H. S., Lipton, S. A. and Nakanishi, N. (1998). Increased NMDA current and spine density in mice lacking the NMDA receptor subunit NR3A. Nature *393*, 377–81.

Delgado, J. Y., Coba, M., Anderson, C. N. G., Thompson, K. R., Gray, E. E., Heusner, C. L., Martin, K. C., Grant, S. G. N. and O'Dell, T. J. (2007). NMDA receptor activation dephosphorylates AMPA receptor glutamate receptor 1 subunits at threonine 840. J Neurosci *27*, 13210–21.

Deng, F., Price, M. G., Davis, C. F., Mori, M. and Burgess, D. L. (2006). Stargazin and other transmembrane AMPA receptor regulating proteins interact with synaptic scaffolding protein MAGI-2 in brain. J Neurosci *26*, 7875–84.

Derkach, V., Barria, A. and Soderling, T. R. (1999). Ca^{2+}/calmodulin-kinase II enhances channel conductance of α-amino-3-hydroxy-5-methyl-4-isoxazolepropionate type glutamate receptors. Proc Natl Acad Sci USA *96*, 3269–74.

Dev, K. K., Nishimune, A., Henley, J. M. and Nakanishi, S. (1999). The protein kinase C α binding protein PICK1 interacts with short but not long form alternative splice variants of AMPA receptor subunits. Neuropharmacology *38*, 635–44.

Din, N., Ahmad, I., Haq, I. U., Elahi, S., Hoessli, D. C. and Shakoori, A. R. (2010). The function of GluR1 and GluR2 in cerebellar and hippocampal LTP and LTD is regulated by interplay of phosphorylation and O-GlcNAc modification. J Cell Biochem *109*, 585–97.

Dong, H., O'Brien, R. J., Fung, E. T., Lanahan, A. A., Worley, P. F. and Huganir, R. L. (1997). GRIP: a synaptic PDZ domain-containing protein that interacts with AMPA

receptors. Nature *386*, 279–84.

Dong, H., Zhang, P., Song, I., Petralia, R. S., Liao, D. and Huganir, R. L. (1999). Characterization of the glutamate receptor-interacting proteins GRIP1 and GRIP2. J Neurosci *19*, 6930–41.

Dong, H. and Zhou, H.-X. (2011). Atomistic mechanism for the activation and desensitization of an AMPA-subtype glutamate receptor. Nat Commun *2*, 354.

Doyle, D. A., Cabral, J. M., Pfuetzner, R. A., Kuo, A., Gulbis, J. M., Cohen, S. L., Chait, B. T. and MacKinnon, R. (1998). The structure of the potassium channel: molecular basis of K^+ conduction and selectivity. Science *280*, 69–77.

Drummond, J. B., Tucholski, J., Haroutunian, V. and Meador-Woodruff, J. H. (2013). Transmembrane AMPA receptor regulatory protein (TARP) dysregulation in anterior cingulate cortex in schizophrenia. Schizophr Res *147*, 32–8.

Dutta, A., Shrivastava, I. H., Sukumaran, M., Greger, I. H. and Bahar, I. (2012). Comparative dynamics of NMDA- and AMPA-glutamate receptor N-terminal domains. Structure *20*, 1838–49.

Egebjerg, J., Bettler, B., Hermans-Borgmeyer, I. and Heinemann, S. (1991). Cloning of a cDNA for a glutamate receptor subunit activated by kainate but not AMPA. Nature *351*, 745–8.

El-Husseini, A. E.-D., Schnell, E., Dakoji, S., Sweeney, N., Zhou, Q., Prange, O., Gauthier-Campbell, C., Aguilera-Moreno, A., Nicoll, R. A. and Bredt, D. S. (2002). Synaptic strength regulated by palmitate cycling on PSD-95. Cell *108*, 849–63.

Esteban, J. A., Shi, S.-H., Wilson, C., Nuriya, M., Huganir, R. L. and Malinow, R. (2003). PKA phosphorylation of AMPA receptor subunits controls synaptic trafficking underlying plasticity. Nat Neurosci *6*, 136–43.

Everett, K. V., Chioza, B., Aicardi, J., Aschauer, H., Brouwer, O., Callenbach, P., Covanis, A., Dulac, O., Eeg-Olofsson, O., Feucht, M., Friis, M., Goutieres, F., Guerrini, R., Heils, A., Kjeldsen, M., Lehesjoki, A.-E., Makoff, A., Nabbout, R., Olsson, I., Sander, T., Sirén, A., McKeigue, P., Robinson, R., Taske, N., Rees, M. and Gardiner, M. (2007). Linkage and association analysis of CACNG3 in childhood absence epilepsy. Eur J Hum Genet *15*, 463–72.

Everts, I., Villmann, C. and Hollmann, M. (1997). N-Glycosylation is not a prerequisite for glutamate receptor function but Is essential for lectin modulation. Mol Pharmacol *52*, 861–73.

Fu, A. K. Y., Hung, K.-W., Fu, W.-Y., Shen, C., Chen, Y., Xia, J., Lai, K.-O. and Ip, N. Y. (2011). APC(Cdh1) mediates EphA4-dependent downregulation of AMPA receptors in homeostatic plasticity. Nat Neurosci *14*, 181–9.

Fukaya, M., Yamazaki, M., Sakimura, K. and Watanabe, M. (2005). Spatial diversity in gene expression for VDCCγ subunit family in developing and adult mouse brains. Neurosci Res *53*, 376–83.

Gahring, L., Carlson, N. G., Meyer, E. L. and Rogers, S. W. (2001). Granzyme B proteolysis of a neuronal glutamate receptor generates an autoantigen and is modulated by glycosylation. J Immunol *166*, 1433–8.

Gallo, V., Upson, L. M., Hayes, W. P., Vyklicky, L., Winters, C. A. and Buonanno, A. (1992). Molecular cloning and development analysis of a new glutamate receptor subunit isoform in cerebellum. J Neurosci *12*, 1010–23.

Gebhardt, C. and Cull-Candy, S. G. (2006). Influence of agonist concentration on AMPA and kainate channels in CA1 pyramidal cells in rat hippocampal slices. The Journal of Physiology *573*, 371–94.

Geiger, J. R., Melcher, T., Koh, D. S., Sakmann, B., Seeburg, P. H., Jonas, P. and Monyer, H. (1995). Relative abundance of subunit mRNAs determines gating and Ca^{2+} permeability of AMPA receptors in principal neurons and interneurons in rat CNS. Neuron *15*, 193–204.

Gielen, M., Retchless, B. S., Mony, L., Johnson, J. W. and Paoletti, P. (2009). Mechanism of differential control of NMDA receptor activity by NR2 subunits. Nature *459*, 703–7.

Gill, M. B., Kato, A. S., Roberts, M. F., Yu, H., Wang, H., Tomita, S. and Bredt, D. S. (2011). Cornichon-2 modulates AMPA receptor-transmembrane AMPA receptor regulatory protein assembly to dictate gating and pharmacology. J Neurosci *31*, 6928–38.

Glitsch, M. and Marty, A. (1999). Presynaptic effects of NMDA in cerebellar Purkinje cells and interneurons. J Neurosci *19*, 511–9.

Greger, I. H., Akamine, P., Khatri, L. and Ziff, E. B. (2006). Developmentally regulated, combinatorial RNA processing modulates AMPA receptor biogenesis. Neuron *51*, 85–97.

Greger, I. H., Khatri, L., Kong, X. and Ziff, E. B. (2003). AMPA receptor tetramerization is mediated by Q/R editing. Neuron *40*, 763–74.

Greger, I. H., Khatri, L. and Ziff, E. B. (2002). RNA editing at arg607 controls AMPA receptor exit from the endoplasmic reticulum. Neuron *34*, 759–72.

Hamad, M. I. K., Jack, A., Klatt, O., Lorkowski, M., Strasdeit, T., Kott, S., Sager, C., Hollmann, M. and Wahle, P. (2014). Type I TARPs promote dendritic growth of early postnatal neocortical pyramidal cells in organotypic cultures. Development *141*, 1737–48.

Hanley, J. G. (2014). Subunit-specific trafficking mechanisms regulating the synaptic expression of Ca^{2+}-permeable AMPA receptors. Semin Cell Dev Biol *27*, 14–22.

Hanley, J. G., Khatri, L., Hanson, P. I. and Ziff, E. B. (2002). NSF ATPase and α-/β-SNAPs disassemble the AMPA receptor-PICK1 complex. Neuron *34*, 53–67.

Hansen, J. P., Chen, R.-S., Larsen, J. K., Chu, P.-J., Janes, D. M., Weis, K. E. and Best, P. M. (2004). Calcium channel γ6 subunits are unique modulators of low voltage-activated (Cav3.1) calcium current. J Mol Cell Cardiol *37*, 1147–58.

Hashimoto, K., Fukaya, M., Qiao, X., Sakimura, K., Watanabe, M. and Kano, M. (1999). Impairment of AMPA receptor function in cerebellar granule cells of ataxic mutant mouse stargazer. J Neurosci *19*, 6027–36.

Hastie, P., Ulbrich, M. H., Wang, H.-L., Arant, R. J., Lau, A. G., Zhang, Z., Isacoff, E. Y. and Chen, L. (2013). AMPA receptor/TARP stoichiometry visualized by single-molecule subunit counting. Proc Natl Acad Sci USA *110*, 5163–8.

Hayashi, T. and Huganir, R. L. (2004). Tyrosine phosphorylation and regulation of the AMPA receptor by SRC family tyrosine kinases. J Neurosci *24*, 6152–60.

Hayashi, T., Rumbaugh, G. and Huganir, R. L. (2005). Differential regulation of AMPA receptor subunit trafficking by palmitoylation of two distinct sites. Neuron *47*, 709–23.

Hayashi, Y., Shi, S. H., Esteban, J. A., Piccini, A., Poncer, J. C. and Malinow, R. (2000). Driving AMPA receptors into synapses by LTP and CaMKII: requirement for GluR1 and PDZ domain interaction. Science *287*, 2262–7.

Henley, J. M., Barker, E. A. and Glebov, O. O. (2011). Routes, destinations and delays: recent advances in AMPA receptor trafficking. Trends in Neurosciences *34*, 258–68.

Herb, A., Burnashev, N., Werner, P., Sakmann, B., Wisden, W. and Seeburg, P. H. (1992). The KA-2 subunit of excitatory amino acid receptors shows widespread expression in brain and forms ion channels with distantly related subunits. Neuron *8*, 775–85.

Herring, B. E., Shi, Y., Suh, Y. H., Zheng, C.-Y., Blankenship, S. M., Roche, K. W. and Nicoll, R. A. (2013). Cornichon proteins determine the subunit composition of synaptic AMPA receptors. Neuron *77*, 1083–96.

Hideyama, T., Yamashita, T., Suzuki, T., Tsuji, S., Higuchi, M., Seeburg, P. H., Takahashi, R., Misawa, H. and Kwak, S. (2010). Induced loss of ADAR2 engenders slow death of motor neurons from Q/R site-unedited GluR2. J Neurosci *30*, 11917–25.

Higuchi, M., Maas, S., Single, F. N., Hartner, J., Rozov, A., Burnashev, N., Feldmeyer,

D., Sprengel, R. and Seeburg, P. H. (2000). Point mutation in an AMPA receptor gene rescues lethality in mice deficient in the RNA-editing enzyme ADAR2. Nature *406*, 78–81.

Hogner, A., Greenwood, J. R., Liljefors, T., Lunn, M.-L., Egebjerg, J., Larsen, I. K., Gouaux, E. and Kastrup, J. S. (2003). Competitive antagonism of AMPA receptors by ligands of different classes: crystal structure of ATPO bound to the GluR2 ligand-binding core, in comparison with DNQX. J. Med. Chem. *46*, 214–21.

Hogner, A., Kastrup, J. S., Jin, R., Liljefors, T., Mayer, M. L., Egebjerg, J., Larsen, I. K. and Gouaux, E. (2002). Structural basis for AMPA receptor activation and ligand selectivity: crystal structures of five agonist complexes with the GluR2 ligand-binding core. J Mol Biol *322*, 93–109.

Hollmann, M. and Heinemann, S. (1994). Cloned glutamate receptors. Annu Rev Neurosci *17*, 31–108.

Hollmann, M., Maron, C. and Heinemann, S. (1994). N-glycosylation site tagging suggests a three transmembrane domain topology for the glutamate receptor GluR1. Neuron *13*, 1331–43.

Hollmann, M., O'Shea-Greenfield, A., Rogers, S. W. and Heinemann, S. (1989). Cloning by functional expression of a member of the glutamate receptor family. Nature *342*, 643–8.

Huh, K. H. and Wenthold, R. J. (1999). Turnover analysis of glutamate receptors identifies a rapidly degraded pool of the N-methyl-D-aspartate receptor subunit, NR1, in cultured cerebellar granule cells. J Biol Chem *274*, 151–7.

Hullebroeck, M. F. and Hampson, D. R. (1992). Characterization of the oligosaccharide side chains on kainate binding proteins and AMPA receptors. Brain Res *590*, 187–92.

Jackson, A. C., Milstein, A. D., Soto, D., Farrant, M., Cull-Candy, S. G. and Nicoll, R. A. (2011). Probing TARP modulation of AMPA receptor conductance with polyamine toxins. J Neurosci *31*, 7511–20.

Jackson, A. C. and Nicoll, R. A. (2011). The expanding social network of ionotropic glutamate receptors: TARPs and other transmembrane auxiliary subunits. Neuron *70*, 178–99.

Jay, S. D., Ellis, S. B., McCue, A. F., Williams, M. E., Vedvick, T. S., Harpold, M. M. and Campbell, K. P. (1990). Primary structure of the gamma subunit of the DHP-sensitive calcium channel from skeletal muscle. Science *248*, 490–2.

Jin, R., Banke, T. G., Mayer, M. L., Traynelis, S. F. and Gouaux, E. (2003). Structural basis for partial agonist action at ionotropic glutamate receptors. Nat Neurosci *6*,

803–10.

Jin, R., Clark, S., Weeks, A. M., Dudman, J. T., Gouaux, E. and Partin, K. M. (2005). Mechanism of positive allosteric modulators acting on AMPA receptors. J Neurosci *25*, 9027–36.

Jin, R. and Gouaux, E. (2003). Probing the function, conformational plasticity, and dimer-dimer contacts of the GluR2 ligand-binding core: studies of 5-substituted willardiines and GluR2 S1S2 in the crystal. Biochemistry *42*, 5201–13.

Jin, R., Horning, M., Mayer, M. L. and Gouaux, E. (2002). Mechanism of activation and selectivity in a ligand-gated ion channel: structural and functional studies of GluR2 and quisqualate. Biochemistry *41*, 15635–43.

Jin, R., Singh, S. K., Gu, S., Furukawa, H., Sobolevsky, A. I., Zhou, J., Jin, Y. and Gouaux, E. (2009). Crystal structure and association behaviour of the GluR2 amino-terminal domain. EMBO J *28*, 1812–23.

Johansen, T. H., Chaudhary, A. and Verdoorn, T. A. (1995). Interactions among GYKI-52466, cyclothiazide, and aniracetam at recombinant AMPA and kainate receptors. Mol Pharmacol *48*, 946–55.

Kamboj, S. K., Swanson, G. T. and Cull-Candy, S. G. (1995). Intracellular spermine confers rectification on rat calcium-permeable AMPA and kainate receptors. The Journal of Physiology *486 (Pt 2)*, 297–303.

Kandel, E. R. (1997). Genes, synapses, and long-term memory. J Cell Physiol *173*, 124–5.

Kanno, T., Yaguchi, T., Nagata, T., Mukasa, T. and Nishizaki, T. (2010). Regulation of AMPA receptor trafficking by O-glycosylation. Neurochem Res *35*, 782–8.

Karakas, E., Simorowski, N. and Furukawa, H. (2009). Structure of the zinc-bound amino-terminal domain of the NMDA receptor NR2B subunit. EMBO J *28*, 3910–20.

Kasper, C., Lunn, M.-L., Liljefors, T., Gouaux, E., Egebjerg, J. and Kastrup, J. S. (2002). GluR2 ligand-binding core complexes: importance of the isoxazolol moiety and 5-substituent for the binding mode of AMPA-type agonists. FEBS Lett *531*, 173–8.

Kato, A. S., Gill, M. B., Ho, M. T., Yu, H., Tu, Y., Siuda, E. R., Wang, H., Qian, Y.-W., Nisenbaum, E. S., Tomita, S. and Bredt, D. S. (2010a). Hippocampal AMPA receptor gating controlled by both TARP and cornichon proteins. Neuron *68*, 1082–96.

Kato, A. S., Gill, M. B., Yu, H., Nisenbaum, E. S. and Bredt, D. S. (2010b). TARPs differentially decorate AMPA receptors to specify neuropharmacology. Trends Neu-

rosci *33*, 241–8.

Kato, A. S., Siuda, E. R., Nisenbaum, E. S. and Bredt, D. S. (2008). AMPA receptor subunit-specific regulation by a distinct family of type II TARPs. Neuron *59*, 986–96.

Kato, A. S., Zhou, W., Milstein, A. D., Knierman, M. D., Siuda, E. R., Dotzlaf, J. E., Yu, H., Hale, J. E., Nisenbaum, E. S., Nicoll, R. A. and Bredt, D. S. (2007). New transmembrane AMPA receptor regulatory protein isoform, γ-7, differentially regulates AMPA receptors. J Neurosci *27*, 4969–77.

Keinänen, K., Wisden, W., Sommer, B., Werner, P., Herb, A., Verdoorn, T. A., Sakmann, B. and Seeburg, P. H. (1990). A family of AMPA-selective glutamate receptors. Science *249*, 556–60.

Kelly, L., Farrant, M. and Cull-Candy, S. G. (2009). Synaptic mGluR activation drives plasticity of calcium-permeable AMPA receptors. Nat Neurosci *12*, 593–601.

Kim, C. H., Chung, H. J., Lee, H. K. and Huganir, R. L. (2001). Interaction of the AMPA receptor subunit GluR2/3 with PDZ domains regulates hippocampal long-term depression. Proc Natl Acad Sci USA *98*, 11725–30.

Kim, K. S., Yan, D. and Tomita, S. (2010). Assembly and stoichiometry of the AMPA receptor and transmembrane AMPA receptor regulatory protein complex. J Neurosci *30*, 1064–72.

Kinney, G. A., Overstreet, L. S. and Slater, N. T. (1997). Prolonged physiological entrapment of glutamate in the synaptic cleft of cerebellar unipolar brush cells. J Neurophysiol *78*, 1320–33.

Knight, H. M., Maclean, A., Irfan, M., Naeem, F., Cass, S., Pickard, B. S., Muir, W. J., Blackwood, D. H. R. and Ayub, M. (2008). Homozygosity mapping in a family presenting with schizophrenia, epilepsy and hearing impairment. Eur J Hum Genet *16*, 750–8.

Koh, D. S., Burnashev, N. and Jonas, P. (1995). Block of native Ca^{2+}-permeable AMPA receptors in rat brain by intracellular polyamines generates double rectification. The Journal of Physiology *486 (Pt 2)*, 305–12.

Köhler, M., Kornau, H. C. and Seeburg, P. H. (1994). The organization of the gene for the functionally dominant α-amino-3-hydroxy-5-methylisoxazole-4-propionic acid receptor subunit GluR-B. J Biol Chem *269*, 17367–70.

Kolleker, A., Zhu, J. J., Schupp, B. J., Qin, Y., Mack, V., Borchardt, T., Köhr, G., Malinow, R., Seeburg, P. H. and Osten, P. (2003). Glutamatergic plasticity by synaptic delivery of GluR-B(long)-containing AMPA receptors. Neuron *40*, 1199–212.

Komander, D. and Rape, M. (2012). The ubiquitin code. Annu Rev Biochem *81*,

203–29.

Körber, C., Werner, M., Hoffmann, J., Sager, C., Tietze, M., Schmid, S. M., Kott, S. and Hollmann, M. (2007). Stargazin interaction with α-amino-3-hydroxy-5-methyl-4-isoxazole propionate (AMPA) receptors is critically dependent on the amino acid at the narrow constriction of the ion channel. J Biol Chem *282*, 18758–66.

Kott, S., Sager, C., Tapken, D., Werner, M. and Hollmann, M. (2009). Comparative analysis of the pharmacology of GluR1 in complex with transmembrane AMPA receptor regulatory proteins γ2, γ3, γ4, and γ8. Neuroscience *158*, 78–88.

Kott, S., Werner, M., Körber, C. and Hollmann, M. (2007). Electrophysiological properties of AMPA receptors are differentially modulated depending on the associated member of the TARP family. J Neurosci *27*, 3780–9.

Kristensen, A. S., Jenkins, M. A., Banke, T. G., Schousboe, A., Makino, Y., Johnson, R. C., Huganir, R. and Traynelis, S. F. (2011). Mechanism of Ca^{2+}/calmodulin-dependent kinase II regulation of AMPA receptor gating. Nat Neurosci *14*, 727–35.

Kromann, H., Krikstolaityte, S., Andersen, A. J., Andersen, K., Krogsgaard-Larsen, P., Jaroszewski, J. W., Egebjerg, J. and Strømgaard, K. (2002). Solid-phase synthesis of polyamine toxin analogues: potent and selective antagonists of Ca^{2+}-permeable AMPA receptors. J Med Chem *45*, 5745–54.

Kumar, J., Schuck, P., Jin, R. and Mayer, M. L. (2009). The N-terminal domain of GluR6-subtype glutamate receptor ion channels. Nat Struct Mol Biol *16*, 631–8.

Kutsuwada, T., Kashiwabuchi, N., Mori, H., Sakimura, K., Kushiya, E., Araki, K., Meguro, H., Masaki, H., Kumanishi, T. and Arakawa, M. (1992). Molecular diversity of the NMDA receptor channel. Nature *358*, 36–41.

Lau, A. Y. and Roux, B. (2007). The free energy landscapes governing conformational changes in a glutamate receptor ligand-binding domain. Structure *15*, 1203–14.

Lau, A. Y. and Roux, B. (2012). The hidden energetics of ligand binding and activation in a glutamate receptor. Nature Publishing Group *18*, 283–287.

Lee, H. K., Barbarosie, M., Kameyama, K., Bear, M. F. and Huganir, R. L. (2000). Regulation of distinct AMPA receptor phosphorylation sites during bidirectional synaptic plasticity. Nature *405*, 955–9.

Lee, H.-K., Takamiya, K., Kameyama, K., He, K., Yu, S., Rossetti, L., Wilen, D. and Huganir, R. L. (2007). Identification and characterization of a novel phosphorylation site on the GluR1 subunit of AMPA receptors. Mol Cell Neurosci *36*, 86–94.

Leonard, A. S., Davare, M. A., Horne, M. C., Garner, C. C. and Hell, J. W. (1998). SAP97 is associated with the α-amino-3-hydroxy-5-methylisoxazole-4-propionic

acid receptor GluR1 subunit. J Biol Chem *273*, 19518–24.

Lerma, J. (2006). Kainate receptor physiology. Curr Opin Pharmacol *6*, 89–97.

Letts, V. A., Felix, R., Biddlecome, G. H., Arikkath, J., Mahaffey, C. L., Valenzuela, A., Bartlett, F. S., Mori, Y., Campbell, K. P. and Frankel, W. N. (1998). The mouse stargazer gene encodes a neuronal Ca^{2+}-channel γ subunit. Nat Genet *19*, 340–7.

Leuschner, W. D. and Hoch, W. (1999). Subtype-specific Assembly of α -Amino-3-hydroxy-5-methyl-4-isoxazole Propionic Acid Receptor Subunits Is Mediated by Their N-terminal Domains. Journal of Biological Chemistry *274*, 16907–16916.

Lin, D.-T., Makino, Y., Sharma, K., Hayashi, T., Neve, R., Takamiya, K. and Huganir, R. L. (2009). Regulation of AMPA receptor extrasynaptic insertion by 4.1N, phosphorylation and palmitoylation. Nat Neurosci *12*, 879–87.

Liu, S. J. and Cull-Candy, S. G. (2005). Subunit interaction with PICK and GRIP controls Ca^{2+} permeability of AMPARs at cerebellar synapses. Nat Neurosci *8*, 768–75.

Liu, Y.-L., Fann, C. S.-J., Liu, C.-M., Chen, W. J., Wu, J.-Y., Hung, S.-I., Chen, C.-H., Jou, Y.-S., Liu, S.-K., Hwang, T.-J., Hsieh, M. H., Chang, C. C., Yang, W.-C., Lin, J.-J., Chou, F. H.-C., Faraone, S. V., Tsuang, M. T. and Hwu, H.-G. (2008). RASD2, MYH9, and CACNG2 genes at chromosome 22q12 associated with the subgroup of schizophrenia with non-deficit in sustained attention and executive function. Biol Psychiatry *64*, 789–96.

Lomeli, H., Mosbacher, J., Melcher, T., Höger, T., Geiger, J. R., Kuner, T., Monyer, H., Higuchi, M., Bach, A. and Seeburg, P. H. (1994). Control of kinetic properties of AMPA receptor channels by nuclear RNA editing. Science *266*, 1709–13.

Lomeli, H., Sprengel, R., Laurie, D. J., Köhr, G., Herb, A., Seeburg, P. H. and Wisden, W. (1993). The rat delta-1 and delta-2 subunits extend the excitatory amino acid receptor family. FEBS Lett *315*, 318–22.

Long, S. B., Campbell, E. B. and Mackinnon, R. (2005). Crystal structure of a mammalian voltage-dependent Shaker family K^+ channel. Science *309*, 897–903.

Lunn, M.-L., Hogner, A., Stensbøl, T. B., Gouaux, E., Egebjerg, J. and Kastrup, J. S. (2003). Three-dimensional structure of the ligand-binding core of GluR2 in complex with the agonist (S)-ATPA: implications for receptor subunit selectivity. J. Med. Chem. *46*, 872–5.

Lynch, G., Larson, J., Kelso, S., Barrionuevo, G. and Schottler, F. (1983). Intracellular injections of EGTA block induction of hippocampal long-term potentiation. Nature *305*, 719–21.

Maas, S., Patt, S., Schrey, M. and Rich, A. (2001). Underediting of glutamate receptor GluR-B mRNA in malignant gliomas. Proc Natl Acad Sci USA *98*, 14687–92.

Maccaferri, G. and Dingledine, R. (2002). Complex effects of CNQX on CA1 interneurons of the developing rat hippocampus. Neuropharmacology *43*, 523–9.

Malinow, R. and Malenka, R. C. (2002). AMPA receptor trafficking and synaptic plasticity. Annu Rev Neurosci *25*, 103–26.

Mammen, A. L., Kameyama, K., Roche, K. W. and Huganir, R. L. (1997). Phosphorylation of the α-amino-3-hydroxy-5-methylisoxazole4-propionic acid receptor GluR1 subunit by calcium/calmodulin-dependent kinase II. J Biol Chem *272*, 32528–33.

Mansour, M., Nagarajan, N., Nehring, R. B., Clements, J. D. and Rosenmund, C. (2001). Heteromeric AMPA receptors assemble with a preferred subunit stoichiometry and spatial arrangement. Neuron *32*, 841–53.

Mayer, M. L., Olson, R. and Gouaux, E. (2001). Mechanisms for ligand binding to GluR0 ion channels: crystal structures of the glutamate and serine complexes and a closed apo state. J Mol Biol *311*, 815–36.

Mayer, M. L. and Westbrook, G. L. (1987). Permeation and block of N-methyl-D-aspartic acid receptor channels by divalent cations in mouse cultured central neurones. The Journal of Physiology *394*, 501–27.

Melcher, T., Maas, S., Herb, A., Sprengel, R., Seeburg, P. H. and Higuchi, M. (1996). A mammalian RNA editing enzyme. Nature *379*, 460–4.

Menuz, K., Stroud, R. M., Nicoll, R. A. and Hays, F. A. (2007). TARP auxiliary subunits switch AMPA receptor antagonists into partial agonists. Science *318*, 815–7.

Meyerson, J. R., Kumar, J., Chittori, S., Rao, P., Pierson, J., Bartesaghi, A., Mayer, M. L. and Subramaniam, S. (2014). Structural mechanism of glutamate receptor activation and desensitization. Nature *514*, 328–34.

Midgett, C. R., Gill, A. and Madden, D. R. (2012). Domain architecture of a calcium-permeable AMPA receptor in a ligand-free conformation. Front Mol Neurosci *4*, 56.

Milstein, A. D. and Nicoll, R. A. (2009). TARP modulation of synaptic AMPA receptor trafficking and gating depends on multiple intracellular domains. Proc Natl Acad Sci USA *106*, 11348–51.

Milstein, A. D., Zhou, W., Karimzadegan, S., Bredt, D. S. and Nicoll, R. A. (2007). TARP subtypes differentially and dose-dependently control synaptic AMPA receptor gating. Neuron *55*, 905–18.

Monyer, H., Sprengel, R., Schoepfer, R., Herb, A., Higuchi, M., Lomeli, H., Burnashev, N., Sakmann, B. and Seeburg, P. H. (1992). Heteromeric NMDA receptors: molecular and functional distinction of subtypes. Science *256*, 1217–21.

Morimoto-Tomita, M., Zhang, W., Straub, C., Cho, C.-H., Kim, K. S., Howe, J. R. and Tomita, S. (2009). Autoinactivation of neuronal AMPA receptors via glutamate-regulated TARP interaction. Neuron *61*, 101–12.

Morita, K., Furuse, M., Fujimoto, K. and Tsukita, S. (1999). Claudin multigene family encoding four-transmembrane domain protein components of tight junction strands. Proc Natl Acad Sci USA *96*, 511–6.

Moriyoshi, K., Masu, M., Ishii, T., Shigemoto, R., Mizuno, N. and Nakanishi, S. (1991). Molecular cloning and characterization of the rat NMDA receptor. Nature *354*, 31–7.

Mosbacher, J., Schoepfer, R., Monyer, H., Burnashev, N., Seeburg, P. H. and Ruppersberg, J. P. (1994). A molecular determinant for submillisecond desensitization in glutamate receptors. Science *266*, 1059–62.

Nakagawa, T., Cheng, Y., Ramm, E., Sheng, M. and Walz, T. (2005). Structure and different conformational states of native AMPA receptor complexes. Nature *433*, 545–9.

Nakanishi, N., Shneider, N. A. and Axel, R. (1990). A family of glutamate receptor genes: evidence for the formation of heteromultimeric receptors with distinct channel properties. Neuron *5*, 569–81.

Ng, D., Pitcher, G. M., Szilard, R. K., Sertié, A., Kanisek, M., Clapcote, S. J., Lipina, T., Kalia, L. V., Joo, D., McKerlie, C., Cortez, M., Roder, J. C., Salter, M. W. and McInnes, R. R. (2009). Neto1 is a novel CUB-domain NMDA receptor-interacting protein required for synaptic plasticity and learning. PLoS Biol *7*, e41.

Nilsen, A. and England, P. M. (2007). A subtype-selective, use-dependent inhibitor of native AMPA receptors. J Am Chem Soc *129*, 4902–3.

Nissenbaum, J., Devor, M., Seltzer, Z., Gebauer, M., Michaelis, M., Tal, M., Dorfman, R., Abitbul-Yarkoni, M., Lu, Y., Elahipanah, T., delCanho, S., Minert, A., Fried, K., Persson, A.-K., Shpigler, H., Shabo, E., Yakir, B., Pisanté, A. and Darvasi, A. (2010). Susceptibility to chronic pain following nerve injury is genetically affected by CACNG2. Genome Res *20*, 1180–90.

Nowak, L., Bregestovski, P., Ascher, P., Herbet, A. and Prochiantz, A. (1984). Magnesium gates glutamate-activated channels in mouse central neurones. Nature *307*, 462–5.

O'Brien, R. J., Xu, D., Petralia, R. S., Steward, O., Huganir, R. L. and Worley, P.

(1999). Synaptic clustering of AMPA receptors by the extracellular immediate-early gene product Narp. Neuron *23*, 309–23.

Oh, M. C. and Derkach, V. A. (2005). Dominant role of the GluR2 subunit in regulation of AMPA receptors by CaMKII. Nat Neurosci *8*, 853–4.

Oh, M. C., Derkach, V. A., Guire, E. S. and Soderling, T. R. (2006). Extrasynaptic membrane trafficking regulated by GluR1 serine 845 phosphorylation primes AMPA receptors for long-term potentiation. J Biol Chem *281*, 752–8.

O'Hara, P. J., Sheppard, P. O., Thøgersen, H., Venezia, D., Haldeman, B. A., McGrane, V., Houamed, K. M., Thomsen, C., Gilbert, T. L. and Mulvihill, E. R. (1993). The ligand-binding domain in metabotropic glutamate receptors is related to bacterial periplasmic binding proteins. Neuron *11*, 41–52.

Opazo, P., Labrecque, S., Tigaret, C. M., Frouin, A., Wiseman, P. W., Koninck, P. D. and Choquet, D. (2010). CaMKII triggers the diffusional trapping of surface AMPARs through phosphorylation of stargazin. Neuron *67*, 239–52.

Osten, P., Khatri, L., Perez, J. L., Köhr, G., Giese, G., Daly, C., Schulz, T. W., Wensky, A., Lee, L. M. and Ziff, E. B. (2000). Mutagenesis reveals a role for ABP/GRIP binding to GluR2 in synaptic surface accumulation of the AMPA receptor. Neuron *27*, 313–25.

Paas, Y. (1998). The macro- and microarchitectures of the ligand-binding domain of glutamate receptors. Trends Neurosci *21*, 117–25.

Pachernegg, S., Strutz-Seebohm, N. and Hollmann, M. (2012). GluN3 subunit-containing NMDA receptors: not just one-trick ponies. Trends Neurosci *35*, 240–9.

Partin, K. M., Bowie, D. and Mayer, M. L. (1995). Structural determinants of allosteric regulation in alternatively spliced AMPA receptors. Neuron *14*, 833–43.

Partin, K. M., Fleck, M. W. and Mayer, M. L. (1996). AMPA receptor flip/flop mutants affecting deactivation, desensitization, and modulation by cyclothiazide, aniracetam, and thiocyanate. J Neurosci *16*, 6634–47.

Partin, K. M., Patneau, D. K. and Mayer, M. L. (1994). Cyclothiazide differentially modulates desensitization of alpha-amino-3-hydroxy-5-methyl-4-isoxazolepropionic acid receptor splice variants. Mol Pharmacol *46*, 129–38.

Pasternack, A., Coleman, S. K., Jouppila, A., Mottershead, D. G., Lindfors, M., Pasternack, M. and Keinänen, K. (2002). Alpha-amino-3-hydroxy-5-methyl-4-isoxazolepropionic acid (AMPA) receptor channels lacking the N-terminal domain. J Biol Chem *277*, 49662–7.

Patneau, D. K. and Mayer, M. L. (1991). Kinetic analysis of interactions between

kainate and AMPA: evidence for activation of a single receptor in mouse hippocampal neurons. Neuron *6*, 785–98.

Perez-Otano, I., Schulteis, C. T., Contractor, A., Lipton, S. A., Trimmer, J. S., Sucher, N. J. and Heinemann, S. F. (2001). Assembly with the NR1 subunit is required for surface expression of NR3A-containing NMDA receptors. J Neurosci *21*, 1228–37.

Plant, K., Plant, K., Pelkey, K. A., Pelkey, K. A., Bortolotto, Z. A., Bortolotto, Z. A., Morita, D., Morita, D., Terashima, A., Terashima, A., McBain, C. J., McBain, C. J., Collingridge, G. L., Collingridge, G. L., Isaac, J. T. R. and Isaac, J. T. R. (2006). Transient incorporation of native GluR2-lacking AMPA receptors during hippocampal long-term potentiation. Nature Neuroscience *9*, 602.

Plested, A. J. R. and Mayer, M. L. (2009). AMPA receptor ligand binding domain mobility revealed by functional cross linking. J Neurosci *29*, 11912–23.

Poulsen, M. H., Lucas, S., Strømgaard, K. and Kristensen, A. S. (2014a). Evaluation of PhTX-74 as subtype-selective inhibitor of GluA2-containing AMPA receptors. Molecular Pharmacology *85*, 261–8.

Poulsen, M. H., Lucas, S., Strømgaard, K. and Kristensen, A. S. (2014b). Inhibition of AMPA Receptors by Polyamine Toxins is Regulated by Agonist Efficacy and Stargazin. Neurochem Res *39*, 1906–13.

Price, M. G., Davis, C. F., Deng, F. and Burgess, D. L. (2005). The α-amino-3-hydroxyl-5-methyl-4-isoxazolepropionate receptor trafficking regulator "stargazin" is related to the claudin family of proteins by Its ability to mediate cell-cell adhesion. J Biol Chem *280*, 19711–20.

Priel, A., Kolleker, A., Ayalon, G., Gillor, M., Osten, P. and Stern-Bach, Y. (2005). Stargazin reduces desensitization and slows deactivation of the AMPA-type glutamate receptors. Journal of Neuroscience *25*, 2682–6.

Raman, I. M. and Trussell, L. O. (1992). The kinetics of the response to glutamate and kainate in neurons of the avian cochlear nucleus. Neuron *9*, 173–86.

Roche, K. W., O'Brien, R. J., Mammen, A. L., Bernhardt, J. and Huganir, R. L. (1996). Characterization of multiple phosphorylation sites on the AMPA receptor GluR1 subunit. Neuron *16*, 1179–88.

Rogers, S. W., Hughes, T. E., Hollmann, M., Gasic, G. P., Deneris, E. S. and Heinemann, S. (1991). The characterization and localization of the glutamate receptor subunit GluR1 in the rat brain. J Neurosci *11*, 2713–24.

Rosenmund, C., Stern-Bach, Y. and Stevens, C. F. (1998). The tetrameric structure of a glutamate receptor channel. Science *280*, 1596–9.

Rossmann, M., Sukumaran, M., Penn, A. C., Veprintsev, D. B., Babu, M. M. and Greger, I. H. (2011). Subunit-selective N-terminal domain associations organize the formation of AMPA receptor heteromers. EMBO J *30*, 959–71.

Rozov, A., Zilberter, Y., Wollmuth, L. P. and Burnashev, N. (1998). Facilitation of currents through rat Ca^{2+}-permeable AMPA receptor channels by activity-dependent relief from polyamine block. The Journal of Physiology *511 (Pt 2)*, 361–77.

Ruknudin, A., Song, M. J. and Sachs, F. (1991). The ultrastructure of patch-clamped membranes: a study using high voltage electron microscopy. J Cell Biol *112*, 125–34.

Saglietti, L., Dequidt, C., Kamieniarz, K., Rousset, M.-C., Valnegri, P., Thoumine, O., Beretta, F., Fagni, L., Choquet, D., Sala, C., Sheng, M. and Passafaro, M. (2007). Extracellular interactions between GluR2 and N-cadherin in spine regulation. Neuron *54*, 461–77.

Sainlos, M., Tigaret, C., Poujol, C., Olivier, N. B., Bard, L., Breillat, C., Thiolon, K., Choquet, D. and Imperiali, B. (2011). Biomimetic divalent ligands for the acute disruption of synaptic AMPAR stabilization. Nat Chem Biol *7*, 81–91.

Schnell, E., Sizemore, M., Karimzadegan, S., Chen, L., Bredt, D. S. and Nicoll, R. A. (2002). Direct interactions between PSD-95 and stargazin control synaptic AMPA receptor number. Proc Natl Acad Sci USA *99*, 13902–7.

Schober, D. A., Gill, M. B., Yu, H., Gernert, D. L., Jeffries, M. W., Ornstein, P. L., Kato, A. S., Felder, C. C. and Bredt, D. S. (2011). Transmembrane AMPA receptor regulatory proteins and cornichon-2 allosterically regulate AMPA receptor antagonists and potentiators. Journal of Biological Chemistry *286*, 13134–42.

Scholz, R., Berberich, S., Rathgeber, L., Kolleker, A., Köhr, G. and Kornau, H.-C. (2010). AMPA receptor signaling through BRAG2 and Arf6 critical for long-term synaptic depression. Neuron *66*, 768–80.

Schorge, S. and Colquhoun, D. (2003). Studies of NMDA receptor function and stoichiometry with truncated and tandem subunits. J Neurosci *23*, 1151–8.

Schwarz, L. A., Hall, B. J. and Patrick, G. N. (2010). Activity-dependent ubiquitination of GluA1 mediates a distinct AMPA receptor endocytosis and sorting pathway. J Neurosci *30*, 16718–29.

Schwenk, J., Harmel, N., Brechet, A., Zolles, G., Berkefeld, H., Müller, C. S., Bildl, W., Baehrens, D., Hüber, B., Kulik, A., Klöcker, N., Schulte, U. and Fakler, B. (2012). High-resolution proteomics unravel architecture and molecular diversity of native AMPA receptor complexes. Neuron *74*, 621–33.

Schwenk, J., Harmel, N., Zolles, G., Bildl, W., Kulik, A., Heimrich, B., Chisaka, O.,

Jonas, P., Schulte, U., Fakler, B. and Klocker, N. (2009). Functional Proteomics Identify Cornichon Proteins as Auxiliary Subunits of AMPA Receptors. Science *323*, 1313–1319.

Scoville, W. B. and Milner, B. (1957). Loss of recent memory after bilateral hippocampal lesions. J Neurol Neurosurg Psychiatr *20*, 11–21.

Seidenman, K. J., Steinberg, J. P., Huganir, R. and Malinow, R. (2003). Glutamate receptor subunit 2 Serine 880 phosphorylation modulates synaptic transmission and mediates plasticity in CA1 pyramidal cells. J Neurosci *23*, 9220–8.

Sekiguchi, M., Fleck, M. W., Mayer, M. L., Takeo, J., Chiba, Y., Yamashita, S. and Wada, K. (1997). A novel allosteric potentiator of AMPA receptors: 4–2-(phenylsulfonylamino)ethylthio–2,6-difluoro-phenoxyaceta mide. J Neurosci *17*, 5760–71.

Selvakumar, B., Huganir, R. L. and Snyder, S. H. (2009). S-nitrosylation of stargazin regulates surface expression of AMPA-glutamate neurotransmitter receptors. Proc Natl Acad Sci USA *106*, 16440–5.

Semenov, A., Möykkynen, T., Coleman, S. K., Korpi, E. R. and Keinänen, K. (2012). Autoinactivation of the stargazin-AMPA receptor complex: subunit-dependency and independence from physical dissociation. PLoS ONE *7*, e49282.

Shanks, N. F., Maruo, T., Farina, A. N., Ellisman, M. H. and Nakagawa, T. (2010). Contribution of the global subunit structure and stargazin on the maturation of AMPA receptors. J Neurosci *30*, 2728–40.

Shanks, N. F., Savas, J. N., Maruo, T., Cais, O., Hirao, A., Oe, S., Ghosh, A., Noda, Y., Greger, I. H., Yates, J. R. and Nakagawa, T. (2012). Differences in AMPA and kainate receptor interactomes facilitate identification of AMPA receptor auxiliary subunit GSG1L. Cell Rep *1*, 590–8.

Shelley, C., Farrant, M. and Cull-Candy, S. G. (2012). TARP-associated AMPA receptors display an increased maximum channel conductance and multiple kinetically distinct open states. The Journal of Physiology *590*, 5723–38.

Sheng, M. and Sala, C. (2001). PDZ domains and the organization of supramolecular complexes. Annu Rev Neurosci *24*, 1–29.

Shi, S., Hayashi, Y., Esteban, J. A. and Malinow, R. (2001). Subunit-specific rules governing AMPA receptor trafficking to synapses in hippocampal pyramidal neurons. Cell *105*, 331–43.

Shi, Y., Lu, W., Milstein, A. D. and Nicoll, R. A. (2009). The stoichiometry of AMPA receptors and TARPs varies by neuronal cell type. Neuron *62*, 633–40.

Shi, Y., Suh, Y. H., Milstein, A. D., Isozaki, K., Schmid, S. M., Roche, K. W. and Nicoll, R. A. (2010). Functional comparison of the effects of TARPs and cornichons on AMPA receptor trafficking and gating. Proc Natl Acad Sci USA *107*, 16315–9.

Sia, G.-M., Béïque, J.-C., Rumbaugh, G., Cho, R., Worley, P. F. and Huganir, R. L. (2007). Interaction of the N-terminal domain of the AMPA receptor GluR4 subunit with the neuronal pentraxin NP1 mediates GluR4 synaptic recruitment. Neuron *55*, 87–102.

Sigworth, F. J. (1980). The variance of sodium current fluctuations at the node of Ranvier. The Journal of Physiology *307*, 97–129.

Silberberg, G., Levit, A., Collier, D., Clair, D. S., Munro, J., Kerwin, R. W., Tondo, L., Floris, G., Breen, G. and Navon, R. (2008). Stargazin involvement with bipolar disorder and response to lithium treatment. Pharmacogenet Genomics *18*, 403–12.

Smith, T. C. and Howe, J. R. (2000). Concentration-dependent substate behavior of native AMPA receptors. Nat Neurosci *3*, 992–7.

Sobolevsky, A. I., Rosconi, M. P. and Gouaux, E. (2009). X-ray structure, symmetry and mechanism of an AMPA-subtype glutamate receptor. Nature *462*, 745–56.

Sommer, B., Keinänen, K., Verdoorn, T. A., Wisden, W., Burnashev, N., Herb, A., Köhler, M., Takagi, T., Sakmann, B. and Seeburg, P. H. (1990). Flip and flop: a cell-specific functional switch in glutamate-operated channels of the CNS. Science *249*, 1580–5.

Sommer, B., Köhler, M., Sprengel, R. and Seeburg, P. H. (1991). RNA editing in brain controls a determinant of ion flow in glutamate-gated channels. Cell *67*, 11–9.

Song, I. and Huganir, R. L. (2002). Regulation of AMPA receptors during synaptic plasticity. Trends Neurosci *25*, 578–88.

Song, I., Kamboj, S., Xia, J., Dong, H., Liao, D. and Huganir, R. L. (1998). Interaction of the N-ethylmaleimide-sensitive factor with AMPA receptors. Neuron *21*, 393–400.

Soto, D., Coombs, I. D., Gratacòs-Batlle, E., Farrant, M. and Cull-Candy, S. G. (2014). Molecular Mechanisms Contributing to TARP Regulation of Channel Conductance and Polyamine Block of Calcium-Permeable AMPA Receptors. J Neurosci *34*, 11673–83.

Soto, D., Coombs, I. D., Kelly, L., Farrant, M. and Cull-Candy, S. G. (2007). Stargazin attenuates intracellular polyamine block of calcium-permeable AMPA receptors. Nat Neurosci *10*, 1260–7.

Soto, D., Coombs, I. D., Renzi, M., Zonouzi, M., Farrant, M. and Cull-Candy, S. G. (2009). Selective regulation of long-form calcium-permeable AMPA receptors by an atypical TARP, γ-5. Nat Neurosci *12*, 277–85.

Standley, S. and Baudry, M. (2000). The role of glycosylation in ionotropic glutamate receptor ligand binding, function, and trafficking. Cell Mol Life Sci *57*, 1508–16.

Stäubli, U., Perez, Y., Xu, F. B., Rogers, G., Ingvar, M., Stone-Elander, S. and Lynch, G. (1994). Centrally active modulators of glutamate receptors facilitate the induction of long-term potentiation in vivo. Proc Natl Acad Sci USA *91*, 11158–62.

Stein, E. L. A. and Chetkovich, D. M. (2010). Regulation of stargazin synaptic trafficking by C-terminal PDZ ligand phosphorylation in bidirectional synaptic plasticity. J Neurochem *113*, 42–53.

Stern-Bach, Y., Bettler, B., Hartley, M., Sheppard, P. O., O'Hara, P. J. and Heinemann, S. F. (1994). Agonist selectivity of glutamate receptors is specified by two domains structurally related to bacterial amino acid-binding proteins. Neuron *13*, 1345–57.

Stern-Bach, Y., Russo, S., Neuman, M. and Rosenmund, C. (1998). A point mutation in the glutamate binding site blocks desensitization of AMPA receptors. Neuron *21*, 907–18.

Straub, C., Hunt, D. L., Yamasaki, M., Kim, K. S., Watanabe, M., Castillo, P. E. and Tomita, S. (2011). Distinct functions of kainate receptors in the brain are determined by the auxiliary subunit Neto1. Nat Neurosci *14*, 866–73.

Straub, C. and Tomita, S. (2012). The regulation of glutamate receptor trafficking and function by TARPs and other transmembrane auxiliary subunits. Current Opinion in Neurobiology *22*, 488–95.

Studniarczyk, D., Coombs, I., Cull-Candy, S. G. and Farrant, M. (2013). TARP Îş-7 selectively enhances synaptic expression of calcium-permeable AMPARs. Nat Neurosci *16*, 1266–74.

Suchyna, T. M., Markin, V. S. and Sachs, F. (2009). Biophysics and Structure of the Patch and the Gigaseal. Biophysj *97*, 738–747.

Sukumaran, M., Rossmann, M., Shrivastava, I., Dutta, A., Bahar, I. and Greger, I. H. (2011). Dynamics and allosteric potential of the AMPA receptor N-terminal domain. EMBO J *30*, 972–82.

Sumioka, A., Yan, D. and Tomita, S. (2010). TARP phosphorylation regulates synaptic AMPA receptors through lipid bilayers. Neuron *66*, 755–67.

Sun, Y., Olson, R., Horning, M., Armstrong, N., Mayer, M. and Gouaux, E. (2002). Mechanism of glutamate receptor desensitization. Nature *417*, 245–53.

Suzuki, E., Kessler, M. and Arai, A. C. (2008). The fast kinetics of AMPA GluR3 receptors is selectively modulated by the TARPs γ4 and γ8. Mol Cell Neurosci *38*, 117–23.

Swanson, G. T., Kamboj, S. K. and Cull-Candy, S. G. (1997). Single-channel properties of recombinant AMPA receptors depend on RNA editing, splice variation, and subunit composition. J Neurosci *17*, 58–69.

Tang, M., Pelkey, K. A., Ng, D., Ivakine, E., McBain, C. J., Salter, M. W. and McInnes, R. R. (2011). Neto1 is an auxiliary subunit of native synaptic kainate receptors. J Neurosci *31*, 10009–18.

Thomas, G. M., Lin, D.-T., Nuriya, M. and Huganir, R. L. (2008). Rapid and bidirectional regulation of AMPA receptor phosphorylation and trafficking by JNK. EMBO J *27*, 361–72.

Tichelaar, W., Safferling, M., Keinänen, K., Stark, H. and Madden, D. R. (2004). The Three-dimensional Structure of an Ionotropic Glutamate Receptor Reveals a Dimer-of-dimers Assembly. J Mol Biol *344*, 435–42.

Tomita, S. (2010). Regulation of ionotropic glutamate receptors by their auxiliary subunits. Physiology (Bethesda) *25*, 41–9.

Tomita, S., Adesnik, H., Sekiguchi, M., Zhang, W., Wada, K., Howe, J. R., Nicoll, R. A. and Bredt, D. S. (2005). Stargazin modulates AMPA receptor gating and trafficking by distinct domains. Nature *435*, 1052–8.

Tomita, S., Chen, L., Kawasaki, Y., Petralia, R. S., Wenthold, R. J., Nicoll, R. A. and Bredt, D. S. (2003). Functional studies and distribution define a family of transmembrane AMPA receptor regulatory proteins. J Cell Biol *161*, 805–16.

Tomita, S., Fukata, M., Nicoll, R. A. and Bredt, D. S. (2004). Dynamic interaction of stargazin-like TARPs with cycling AMPA receptors at synapses. Science *303*, 1508–11.

Tomita, S., Sekiguchi, M., Wada, K., Nicoll, R. A. and Bredt, D. S. (2006). Stargazin controls the pharmacology of AMPA receptor potentiators. Proc Natl Acad Sci USA *103*, 10064–7.

Tomita, S., Shenoy, A., Fukata, Y., Nicoll, R. A. and Bredt, D. S. (2007). Stargazin interacts functionally with the AMPA receptor glutamate-binding module. Neuropharmacology *52*, 87–91.

Tomita, S., Stein, V., Stocker, T. J., Nicoll, R. A. and Bredt, D. S. (2005). Bidirectional synaptic plasticity regulated by phosphorylation of stargazin-like TARPs. Neuron *45*, 269–77.

Tovar, K. R. and Westbrook, G. L. (1999). The incorporation of NMDA receptors with a distinct subunit composition at nascent hippocampal synapses in vitro. J Neurosci *19*, 4180–8.

Traynelis, S. F., Wollmuth, L. P., McBain, C. J., Menniti, F. S., Vance, K. M., Ogden, K. K., Hansen, K. B., Yuan, H., Myers, S. J. and Dingledine, R. (2010). Glutamate receptor ion channels: structure, regulation, and function. Pharmacological Reviews *62*, 405–96.

Turetsky, D., Garringer, E. and Patneau, D. K. (2005). Stargazin modulates native AMPA receptor functional properties by two distinct mechanisms. J Neurosci *25*, 7438–48.

Vandenberghe, W., Nicoll, R. A. and Bredt, D. S. (2005a). Interaction with the unfolded protein response reveals a role for stargazin in biosynthetic AMPA receptor transport. J Neurosci *25*, 1095–102.

Vandenberghe, W., Nicoll, R. A. and Bredt, D. S. (2005b). Stargazin is an AMPA receptor auxiliary subunit. Proc Natl Acad Sci USA *102*, 485–90.

Vlachová, V., Vyklický, L., Vyklický, L. and Vyskocil, F. (1987). The action of excitatory amino acids on chick spinal cord neurones in culture. J Physiol (Lond) *386*, 425–38.

von Engelhardt, J., Mack, V., Sprengel, R., Kavenstock, N., Li, K. W., Stern-Bach, Y., Smit, A. B., Seeburg, P. H. and Monyer, H. (2010). CKAMP44: a brain-specific protein attenuating short-term synaptic plasticity in the dentate gyrus. Science *327*, 1518–22.

Waegemans, T., Wilsher, C. R., Danniau, A., Ferris, S. H., Kurz, A. and Winblad, B. (2002). Clinical efficacy of piracetam in cognitive impairment: a meta-analysis. Dement Geriatr Cogn Disord *13*, 217–24.

Wollmuth, L. P. and Sobolevsky, A. I. (2004). Structure and gating of the glutamate receptor ion channel. Trends Neurosci *27*, 321–8.

Wyeth, M. S., Pelkey, K. A., Petralia, R. S., Salter, M. W., McInnes, R. R. and McBain, C. J. (2014). Neto auxiliary protein interactions regulate kainate and NMDA receptor subunit localization at mossy fiber-CA3 pyramidal cell synapses. J Neurosci *34*, 622–8.

Wyllie, D. J., Traynelis, S. F. and Cull-Candy, S. G. (1993). Evidence for more than one type of non-NMDA receptor in outside-out patches from cerebellar granule cells of the rat. The Journal of Physiology *463*, 193–226.

Xia, H., von Zastrow, M. and Malenka, R. C. (2002). A novel anterograde trafficking signal present in the N-terminal extracellular domain of ionotropic glutamate recep-

tors. J Biol Chem *277*, 47765–9.

Xia, J., Zhang, X., Staudinger, J. and Huganir, R. L. (1999). Clustering of AMPA receptors by the synaptic PDZ domain-containing protein PICK1. Neuron *22*, 179–87.

Yamada, K. A. and Tang, C. M. (1993). Benzothiadiazides inhibit rapid glutamate receptor desensitization and enhance glutamatergic synaptic currents. J Neurosci *13*, 3904–15.

Yamazaki, M., Ohno-Shosaku, T., Fukaya, M., Kano, M., Watanabe, M. and Sakimura, K. (2004). A novel action of stargazin as an enhancer of AMPA receptor activity. Neurosci Res *50*, 369–74.

Yang, J. H., Sklar, P., Axel, R. and Maniatis, T. (1995). Editing of glutamate receptor subunit B pre-mRNA in vitro by site-specific deamination of adenosine. Nature *374*, 77–81.

Yelshansky, M. V., Sobolevsky, A. I., Jatzke, C. and Wollmuth, L. P. (2004). Block of AMPA receptor desensitization by a point mutation outside the ligand-binding domain. J Neurosci *24*, 4728–36.

Zhang, W., Devi, S. P. S., Tomita, S. and Howe, J. R. (2014). Auxiliary proteins promote modal gating of AMPA- and kainate-type glutamate receptors. Eur J Neurosci *39*, 1138–47.

Zuber, B., Nikonenko, I., Klauser, P., Muller, D. and Dubochet, J. (2005). The mammalian central nervous synaptic cleft contains a high density of periodically organized complexes. Proc Natl Acad Sci USA *102*, 19192–7.

Zuo, J., Jager, P. L. D., Takahashi, K. A., Jiang, W., Linden, D. J. and Heintz, N. (1997). Neurodegeneration in Lurcher mice caused by mutation in $\delta 2$ glutamate receptor gene. Nature *388*, 769–73.